

**DEVELOPMENT OF AN IMPEDIMETRIC BIOSENSOR USING A  
NON-ANTIBODY BASED BIOLOGICAL RECOGNITION  
MOLECULE**

**Monika Raina**

Submitted in accordance with the requirements for  
The degree of Doctor of philosophy



**UNIVERSITY OF LEEDS**

The University of Leeds

School of Electronic and Electrical Engineering

October, 2013

The candidate confirms that the work submitted is her own and that appropriate credit has been given where reference has been made to the work of others. This copy has been supplied on the understanding that it is copyright material and that no quotation from the thesis may be published without proper acknowledgement.

This copy has been supplied on the understanding that it is copyright material and that no quotation from the thesis may be published without proper acknowledgement.

*Assertion of moral rights (optional):*

The right of Monika Raina to be identified as Author of this work has been asserted by her in accordance with the Copyright, Designs and Patents Act 1988.

© 2013The University of Leeds and Monika Raina

## Acknowledgements

I would like to express my sincere and deep gratitude for my supervisors Prof. Christoph Wälti and Prof. Alexander Giles Davies. I cannot imagine getting through this project, not to mention this thesis without their continued help, suggestions and encouragement. Their patience has been incredible.

I would also like to thank Dr. Steve Johnson for his insightful suggestions. They proved helpful during the evolution of my project.

I would like to thank all the current and former members of Bioelectronics Laboratory: Rajan, Vidhya, Dominika, Richard, Dave, Mike, Irene, Alban, Devesh, Minde, William, Andy, Sybilla and Mark for all their incredible support, as well as jokes and good humour that they brought to the laboratory. It made the day all the more enjoyable and the work more fun.

My acknowledgements would not be complete without mentioning the help of colleagues from the Astbury Centre for Structural Molecular Biology at the University of Leeds, where I performed a significant amount of my work. I would like to thank Prof. Michael McPherson, Sarah Deacon, Christian Tiede, Darren Tomlinson and Ian Manfield who supported me with my research through their suggestions and feedback during our many productive meetings. Thank you all very much. Your help, support, encouragement and suggestions during the course of this work have been invaluable.

Finally, I would like to thank my dear family and friends for their unconditional love, support and good wishes.

## Abstract

The molecular recognition layer generally immobilised on the active interface of a biosensor is one of the key factors in governing the biosensor's performance, and in particular its sensitivity and selectivity. The aim of this thesis was to investigate a novel non-immunoglobulin-based recognition molecule as the capture molecule for electrochemical biosensors with the aim to improve sensitivity and specificity of label-free biosensing.

To understand the characteristics of the biomolecular layer of a biosensor formed from the non-immunoglobulin-based recognition molecule, the Adhiron scaffold developed at the University of Leeds was used as the model system. The Adhiron scaffold consists of one  $\alpha$ -helix, four  $\beta$ -sheets, and three variable regions. The three variable regions comprise two surface-exposed loops and the N-terminus of the protein. Adhiron-based binders against a well-characterised antibody, the anti-myc tag antibody, were selected using phage-display and used as a model system for this study. The phage-display library was constructed by inserting randomised peptides into the three variable regions of the Adhiron scaffold. The best performing binder, selected from the ten Adhiron myc binders panned from a phage display screen against polyclonal anti-myc tag antibodies, myc binder 2, was chosen as the biological recognition molecules for the development of an electrochemical impedimetric biosensor.

Cloning of the Adhiron binders in pET-11(a) expression vector, optimisation of expression and purification of the binders, was carried out and the binders were obtained in soluble form. Adhiron myc binder 2, which showed the best binding against monoclonal anti-myc tag antibodies, showed a high thermal stability of 85° C, with well-defined  $\alpha$ -helical and  $\beta$ -sheet structures. This binder was thoroughly characterised further before being used as a recognition molecule of an electrochemical biosensor.

An electrochemical Adhiron-based myc binder 2 sensor was fabricated to detect monoclonal anti-myc tag antibodies over a range of concentrations. The Adhiron myc binder 2 based EIS biosensor comprised a highly sensitive insulating layer formed by a self-assembled monolayer of carboxylic acid terminated alkylthiol-PEG

onto which Adhiron myc binder 2 was grafted. The sensing mechanism was based on the change in phase of the electrochemical impedance measured at 0.1 Hz observed upon binding of monoclonal anti-myc tag antibodies onto the sensor. Monoclonal anti-myc tag antibodies were detected down to a concentration of less than 100 pM, over a range from 0.1–200 nM anti-myc tag antibodies. These findings demonstrated for the first time the successful use of Adhiron-based antibody-mimetics as recognition molecules in label-free biosensors.

To improve the sensitivity of the Adhiron-based electrochemical biosensor, and potentially to modulate the sensitivity *in situ*, the performance of the sensor at different electrochemical DC-biases was investigated. The sensitivity of the sensor was observed to increase with increasing DC bias applied to the sensor surface. This sensitivity modulation was demonstrated to be reversible, therefore opening up a range of opportunities for future label-free biosensor architectures.

## List of Abbreviations

<b>m</b>	Metre
<b>s</b>	Second
<b>g</b>	Gram
<b>mg</b>	Milligram
<b>µg</b>	Microgram
<b>mL</b>	Millilitre
<b>µL</b>	Microlitre
<b>V</b>	Volt
<b>mV</b>	Millivolt
<b>°C</b>	Degree celsius
<b>min</b>	Minute
<b>M</b>	Molar
<b>µM</b>	Micromolar
<b>nM</b>	Nanomolar
<b>pM</b>	Picomolar
<b>fmol</b>	Femtomolar
<b>Hz</b>	Hertz
<b>mHz</b>	Millihertz
<b>kHz</b>	Kilohertz
<b>kDa</b>	Kilodalton
<b>BP</b>	Base pair
<b>Hr</b>	Hour
<b>M.W</b>	Molecular weight
<b>vs.</b>	Versus
<b>RPM</b>	Rotations per minute
<b>Deg</b>	Degree

**Amino Acids Representation**

<b>One letter code</b>	<b>Three letter code</b>	<b>Amino acid</b>
A	Ala	Alanine
C	Cys	Cysteine
D	Asp	Asparatic Acid
E	Glu	Glutamic Acid
F	Phe	Phenylalanine
G	Gly	Glycine
H	His	Histidine
I	Ile	Isoleucine
K	Lys	Lysine
L	Leu	Leucine
M	Met	Methionine
N	Asn	Asparagine
P	Pro	Proline
Q	Gln	Glutamine
R	Arg	Arginine
S	Ser	Serine
T	Thr	Threonine
V	Val	Valine
W	Trp	Tryptophan
Y	Tyr	Tyrosine

## Table of Contents

<b>Acknowledgements.....</b>	<b>iii</b>
<b>Abstract.....</b>	<b>iv</b>
<b>List of Abbreviations.....</b>	<b>vi</b>
<b>Amino Acids Representation .....</b>	<b>vii</b>
<b>Table of Contents .....</b>	<b>viii</b>
<b>List of Figures.....</b>	<b>xi</b>
<b>Chapter 1. Introduction.....</b>	<b>15</b>
1.1. Biomarkers .....	15
1.2. Biosensors .....	17
1.2.1. Transducers .....	17
1.2.2. Biological recognition molecules .....	18
1.3. Summary of the project.....	21
1.4. Organisation of the thesis .....	22
1.4.1. Chapter 2 .....	22
1.4.2. Chapter 3 .....	22
1.4.3. Chapter 4 .....	22
1.4.4. Chapter 5 .....	23
1.4.5. Chapter 6 .....	23
1.4.6. Chapter 7 .....	23
<b>Chapter 2. Literature review .....</b>	<b>24</b>
2.1. Biomarkers .....	24
2.2. Biosensors .....	27
2.2.1. Biological recognition molecules .....	27
2.2.2. Transducers .....	39
<b>Chapter 3. Background and techniques .....</b>	<b>46</b>
3.1. Background .....	46
3.1.1. Prokaryotic gene expression .....	46
3.1.2. Gene regulation system – Operon .....	47
3.1.3. Recombinant DNA technology .....	50
3.1.4. Recombinant protein expression.....	53
3.1.5. Proteins .....	54
3.1.6. Antibodies .....	56

3.1.7. Phage Display Library .....	58
3.2. Techniques.....	65
3.2.1. Electrophoretic techniques.....	65
3.2.2. Spectrophotometry.....	71
3.2.3. Circular Dichroism (CD) .....	72
3.2.4. Differential scanning calorimetry (DSC).....	74
3.2.5. Surface plasmon resonance (SPR).....	76
3.2.6. Electrochemistry.....	78
<b>Chapter 4. Development of a novel non-antibody based recognition molecule .....</b>	<b>85</b>
4.1. Introduction .....	85
4.2. Materials and methods.....	89
4.2.1. Materials.....	89
4.2.2. Techniques.....	93
4.3. Results .....	101
4.3.1. Generation of Adhiron based library by BSTG.....	101
4.3.2. Selection of Adhiron myc binders.....	104
4.3.3. Cloning .....	104
4.3.4. Optimisation of expression of Adhiron based binders.....	112
4.3.5. Expression of Adhiron myc binders .....	117
4.3.6. Purification of Adhiron myc binders .....	121
4.3.7. Dialysis of purified Adhiron myc binders .....	126
4.3.8. Characterisation .....	127
4.4. Discussion.....	129
<b>Chapter 5. Fabrication of an impedimetric biosensor based of a non- antibody recognition protein –Adhiron myc binder 2 .....</b>	<b>131</b>
5.1. Introduction .....	131
5.1.1. Electrochemical impedance spectroscopy .....	131
5.2. Materials.....	135
5.3. Methods .....	135
5.3.1. Surface Plasmon Resonance.....	135
5.3.2. ELISA.....	136
5.3.3. Electrochemical impedance spectroscopy .....	136
5.4. Results .....	138
5.4.1. ELISA.....	138
5.4.2. Surface plasmon resonance .....	140

5.4.3. Electrochemical impedance spectroscopy .....	143
5.4.4. Discussion .....	156
<b>Chapter 6. Voltage induced modulation of the sensitivity of the impedimetric biosensor .....</b>	<b>157</b>
6.1. Introduction .....	157
6.2. Materials .....	161
6.3. Methods .....	161
6.4. Results .....	162
6.4.1. Applying different voltages to the SAM .....	162
Conclusion .....	179
<b>Chapter 7. Conclusions.....</b>	<b>181</b>
<b>References .....</b>	<b>185</b>
<b>Appendix.....</b>	<b>203</b>

## List of Figures

Figure 1-1 Schematic representation of the constituents of a biosensor. ....	17
Figure 2-1 The flow of genetic information.....	25
Figure 2-2 Shows a schematic diagram comparing an antibody with a peptide aptamer. ....	35
Figure 3-1 Schematic representation of the <i>lac</i> operon in <i>E. coli</i> . ....	49
Figure 3-2 Schematic representation of a cloning vector. ....	51
Figure 3-3 Restriction digestion and ligation of foreign DNA and vector to generate a recombinant vector.....	52
Figure 3-4 Primary structure of a protein.....	55
Figure 3-5 Secondary, tertiary and quaternary structure of protein. ....	56
Figure 3-6 Basic structure of an antibody (immunoglobulin). ....	57
Figure 3-7 Filamentous bacteriophage M13. ....	59
Figure 3-8 Life cycle of bacteriophage.....	60
Figure 3-9 Shows the vector map of pBSTG1 Adh phagemid. ....	63
Figure 3-10 Phage selection using Biopanning. ....	64
Figure 3-11 Schematic representation of different types of ELISA.....	70
Figure 3-12 Circular dichroism spectra.....	73
Figure 3-13 Differential scanning calorimetry. ....	76
Figure 3-14 Surface plasma resonance.....	77
Figure 3-15 Schematic of electrochemical cell.....	79
Figure 3-16 Shows a double junction electrode with a built in reference electrode. ....	80
Figure 3-17 Cyclic voltametry. ....	82
Figure 3-18 The Nyquist plot and the Bode plot.....	84
Figure 4-1 Amino acid sequence of Adhiron92 scaffold with secondary structure elements. ....	87
Figure 4-2 X-ray crystal structure of Adhiron 92 scaffold. ....	87
Figure 4-3 Schematic representation of pET-11(a) adhiron myc binder 2 plasmid.....	90
Figure 4-4 ELISA to show binding of Adhiron myc binders.....	103
Figure 4-5 The sequences of the 20 Adhiron myc binders. ....	103

Figure 4-6 The sequence alignment of the ten selected Adhiron myc binders. ....	104
Figure 4-7 Gel electrophoresis of Adhiron binders from plasmid.....	105
Figure 4-8 A schematic of incorporating <i>Not</i> 1 and <i>Nhe</i> 1 restriction sites into pET- 11(a) vector.....	107
Figure 4-9 Colony PCR. ....	109
Figure 4-10 Vector pET-11(Ad).....	110
Figure 4-11 Gel electrophoresis for Adhiron myc binder inserts. ....	111
Figure 4-12 Shows the schematic of incorporating Adhiron myc binders into the pET-11(Ad) vector. ....	112
Figure 4-13 Dot blot for optimising expression of Adhiron binders. ..	113
Figure 4-14 Western blotting to detect expression of Adhiron GST B4.....	114
Figure 4-15 Purification of Adhiron GST B4 grown in different autoinduction media. ....	116
Figure 4-16 SDS PAGE of Adhiron GST B4 after dialysis in 10 mM PBS (pH 7.2).....	117
Figure 4-17 SDS PAGE of Adhiron myc binder 1,2,4 and 18.....	118
Figure 4-18 Western blot of total cell lysates and soluble fractions of Adhiron myc binder 1, 4, 2 and 18. ....	119
Figure 4-19 SDS PAGE of total soluble fraction and cell lysate of Adhiron myc binder 5, 7, 13 and 17.....	120
Figure 4-20 Western blot of soluble fractions and the cell lysates of Adhiron myc binder 5, 7, 13 and 17. ....	121
Figure 4-21 Purification of Adhiron myc binder 1, 2, 4 and 18.....	122
Figure 4-22 Purification of Adhiron myc binder 5, 7, 13 and 17.....	124
Figure 4-23 Purificaiton of Adhiron myc binder 11 and 20.....	125
Figure 4-24 SDS PAGE of Adhiron scaffold, Adhiron GST B4 binder and ten Adhiron myc binders. ....	126
Figure 4-25 Circular dichroism of Adhiron myc binders. ....	127
Figure 4-26 Differential scanning calorimetry of lysozyme, Adhiron myc binder 2 and Adhiron scaffold. ....	129
Figure 5-1. ELISA on Adhiron myc binders, Adhiron scaffold and GST B4 binder. ....	139
Figure 5-2 Sequence alignment of Adhiron myc binders with myc epitope. ....	140
Figure 5-3 Activation of carboxylic group using EDC-NHS chemistry. ....	141
Figure 5-4 Surface Plasmon resonance sensograms of Adhiron myc binder 2, Adhiron scaffold and Adhiron myc binder 4. ....	142

Figure 5-5. Cyclic voltametry on bare gold and gold grafted with self assembled monolayer. ....	144
Figure 5-6. Absolute impedance vs. frequency of various surfaces. ....	145
Figure 5-7. Phase vs. frequency of different surfaces. ....	146
Figure 5-8. Phase vs. Frequency of surface in 10 mM PBS (pH 7.2). ..	148
Figure 5-9. Comparison of surface stability in buffer before and after 200 mV potential tuning. ....	150
Figure 5-10. Phase vs. Frequency before and after immobilisation of 10 µg/ml of Adhiron myc binder 2. ....	151
Figure 5-11. response of the sensor surface towards different concentration of monoclonal anti myc tag antibodies. ....	152
Figure 5-12. Cumulative addition of different concentrations of monoclonal anti-myc tag antibodies. ....	154
Figure 5-13. The working of Adhiron myc binder 2 based impedimetric biosensor. ....	155
Figure 6-1. Schematic representation of potential induced defects in SAM. ....	160
Figure 6-2. Phase vs. Frequency at different DC biases applied to the SAM immobilised gold surface. ....	163
Figure 6-3. Absolute impedance change with respect to frequency at different DC biases. ....	164
Figure 6-4 Reversibility in defects caused by potential change, checked at 0 V and 0.1 V applied to the surface against reference (Ag/AgCl). ....	165
Figure 6-5 Reversibility in defects caused by potential change, checked at five different voltages applied to the surface against reference (Ag/AgCl). ....	166
Figure 6-6 Reversibility in defects caused by potential change, checked at six different voltages applied to the surface against reference (Ag/AgCl). ....	167
Figure 6-7 Phase vs. Frequency measured at different potentials after incubating the SAM surface with Adhiron myc binder 2. ....	168
Figure 6-8 Change in phase ( $\Delta\phi$ ) measured at 0.1 Hz after incubating the sensor surface in different concentrations of monoclonal anti myc tag anti bodies at different voltages applied to the surface. ....	169
Figure 6-9 Regeneration of sensor surface on incubating in 10 mM PBS, pH 7.2. ....	170
Figure 6-10 Change in phase vs. Frequency before and after incubation of 10 µg/ml of Adhiron IL8 binder. ....	171

<b>Figure 6-11 Stability check of the SAM immobilised surface at different potentials.....</b>	<b>172</b>
<b>Figure 6-12 Response of the Adhiron IL8 biosensors to different concentrations of the IL8 protein at different potentials.....</b>	<b>175</b>
<b>Figure 6-13 Inter-sensor variation in response of the Adhiron IL8 biosensor to the IL8 protein.....</b>	<b>176</b>
<b>Figure 6-14 Response of IL8 biosensor to IL8 protein on a surface subjected to different potentials.....</b>	<b>178</b>

## Chapter 1. Introduction

Enormous resources are dedicated to the treatment of some of today's most prevalent diseases because of their high mortality and morbidity rate and associated high healthcare costs. These include diabetes, cardiovascular disease and cancer. Each year cardiovascular disease (CVD) causes over 4 million deaths in Europe of which 1.9 million are in the European Union (EU) (Nichols *et al.*, 2012). In the European Union, the estimated expense related to cardiovascular diseases has been around €196 billion annually. Furthermore, there were an estimated 3.45 million new cases of cancer (excluding non-melanoma skin cancer) and 1.75 million deaths from cancer in Europe in 2012 (Ferlay *et al.*, 2013). According to a study done by the international diabetes federation, 35 million adults were reported to be suffering from diabetes (both type 1 and type 2) in 2011 in Europe, and this number is predicted to increase by 23%, to 43 million, by 2030 (Whiting *et al.*, 2011). In Europe the overall estimated cost for the treatment and management of diabetes is estimated to be €89 billion annually (Freitag, 2012).

The high mortality rate and scale of expenditure related to a particular disease could be reduced significantly by early and reliable diagnosis of the disease, through enabling, early intervention. Delays in diagnosis and thus delays in treatment can increase the health complications associated with the disease as well as increase the healthcare costs. The prerequisites to address the challenge of early diagnostics require the detection of even very small changes in the body, that are indicative of a particular disease or the onset thereof. Arguably, a very promising route is the measurement of biomarkers in body fluids.

### 1.1. Biomarkers

In general a biomarker is a physiological or pathological measurable object, which is related to a particular disease, and any change, increase or decrease, in concentration can be indicative of a particular disease. For example, micro RNAs form a class of small non-coding RNAs that control gene expression in cells. Their abnormal expression can initiate human diseases like cancer. Increased expression of a microRNA called miR-21 has been reported in case of breast cancer cell lines that can be used to predict breast cancer (Iorio *et al.*, 2005). However, genes govern the

production of proteins, and genetic mutations cause modifications in the protein signaling pathway that can lead to differential expression of a protein in a cell *i.e.* over-expressed or modified as a consequence of the disease. The level of gene expression (m-RNA transcripts) and the protein expression cannot be reliably correlated therefore it becomes more feasible to detect the differentially expressed proteins, which can be used as biomarkers to indicate a diseased state (see section 2.1). For example, the differentially expressed protein high sensitivity CRP (hs-CRP) has emerged as a major cardiovascular biomarker (Calabrò *et al.*, 2009).

Currently, the early detection of diseases using different biomarkers is carried out using various diagnostic techniques. Most of the diagnostic techniques use labelled biological recognition molecules or analytes and are based on Enzyme-Linked Immunosorbent Assay (ELISA). ELISA is a solid phase immunoassay technique used in clinical laboratories to detect biomarkers in the blood or other body fluids of a patient using a biological recognition molecule. Antibodies are used as the biological recognition molecules in ELISA that bind specifically to the biomarkers in the sample of body fluids. In order to detect the biomarkers, either a primary antibody (that recognises a specific biomarker), conjugated to an enzyme is used for direct detection or a secondary antibody conjugated to an enzyme is used that binds to the primary antibody. The binding is detected using an enzyme catalysed light emitting reaction (chemiluminescence). Various strategies of antibody immobilisation and signal amplification are used for detection of antibodies and antigens (see section 3.2.1.4).

Although these techniques can measure a wide range of analytes like hormones, antibodies, enzymes etc and can be performed in centralised laboratories, they are not well suited for fast and convenient *in vitro* diagnostics. Transportation of sample to the laboratory, pre-treatment, measurement and then return of the data to the patient is time consuming and expensive. Moreover the highly automated, high throughput machines required in the centralised laboratories lead to stupendous expenditure, in particular in terms of maintenance, as well as technical assistance. One of the aims of biosensor development is to move clinical analysis from centralised laboratories to the doctor's clinic or even to a patient's home to make detection tools easier to handle, cheaper and convenient to use.

To enable early detection of disease through the detection of small deviations of protein biomarker concentrations from the normal levels expected for a healthy person, an analytical device that offers a fast, reliable response with high sensitivity and is cost efficient and simple to use, is required in the field of clinical diagnostics.

## 1.2. Biosensors

Clinical diagnostics is one of the most progressive as well as demanding field where new technologies that offer better specificity and sensitivity, are sought constantly. The analytical devices employed to detect the presence of biomarkers for clinical diagnostics are generally referred to as biosensors. Biosensors are trying to move clinical analysis from centralised laboratories to the doctor's clinic or the patient's home to make detection tools easier to handle, cheaper and convenient to use. A recent definition of a biosensor by Newman *et al.* (2004) defines a biosensor as 'a compact analytical device incorporating a biological or biologically-derived sensing element either integrated within or intimately associated with a physicochemical transducer'.

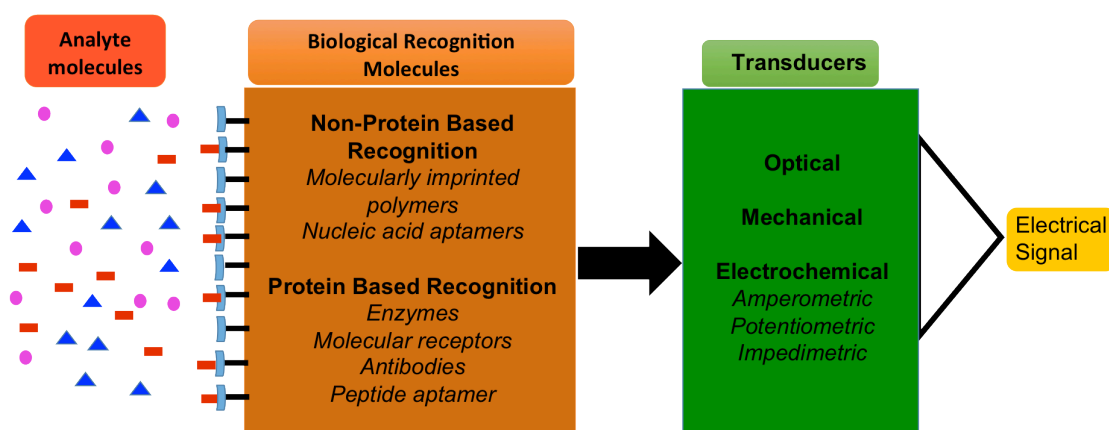


**Figure 1-1 Schematic representation of the constituents of a biosensor.**

The molecular recognition layer binds the analyte molecules (extreme left) and the signal transducer converts the binding event into an electrical signal.

The biological component of a biosensor is the recognition molecule that binds the target molecule. In electronic biosensors, the binding of the target molecule to the biological component leads to a change of the environment of the sensor which is then converted into an electrical signal by a transducer.

### 1.2.1. Transducers

The main types of transducers used commercially and in research laboratories are optical, mechanical and electrochemical.

Optical biosensors are based on the change in absorbance (Hulko *et al.*, 2011) or luminescence (Holst and Grunwald, 2001) in the environment of the biosensor that

takes place in UV / infrared or visible spectral regions of light. Optical biosensing is most commonly done using an enzyme-based assay (ELISA) where fluorescence-tagged antibodies are used to detect the binding of a biological recognition molecule to the analyte.

Mechanical biosensors are based on the detection of change in the mechanical properties of a surface due to binding of analyte molecules to the recognition layer e.g. measuring change in stress on a cantilever surface that is immobilised with biological recognition molecules (Datar *et al.*, 2009) or change in the acoustic properties of the surface e.g. measuring shift in resonance frequency of the sensing surface on binding of the analyte molecules (Chaste *et al.*, 2012).

Electrochemical biosensors are based on measuring the electrical properties of a surface onto which a biological recognition layer is immobilised. The interaction of the analyte with the biological recognition molecules is detected by the change in current (amperometric response) (Cass *et al.*, 1984), voltage (potentiometric response) (Yamamoto *et al.*, 1980) or impedance (impedimetric response) (Zhang *et al.*, 2013).

### **1.2.2. Biological recognition molecules**

The majority of the effort devoted to the development of biosensors has been focussed on improving the signal transduction feature of the biosensors to make them more efficient for clinical diagnostics. Most of the aspects required for the development of an efficient biosensor from the point of care prospective are expected to be addressable *via* engineering of the electronics, but the performance of the biosensor is also dependent on the biological component. Moreover to understand the behaviour of a biosensor it is important to understand the characteristics and behaviour of the molecular component of the biosensor.

This thesis aims at improving the performance of biosensors through the engineering of biological recognition layer for an electrochemical biosensor. The interaction of the analyte with the biological recognition molecule determines the sensitivity, specificity and ultimately the limit of detection of the biosensor. These characteristics have significant consequences when clinical samples are used where the biological analytes are sometimes present only in pg/mL concentration or less. The engineering of biorecognition layer can be useful to modify important structural or conformational features that have a major impact on the working of a biosensor affecting its sensitivity, selectivity and non-specific binding. Furthermore, the stability of the biological recognition layer plays a vital role in the shelf life of a biosensor. As the

biological layer is also susceptible to degradation, the use of a biosensor in different environmental conditions is determined by the conditions suitable for the storage of the biological component. Various classes of recognition molecules have been explored to constitute the molecular component of biosensors.

In the course of development of biosensors, enzymes had been the initial tools used as biological recognition elements. Glucose biosensors are probably the most studied and commercially most important biosensors for monitoring glucose levels in diabetic patients. They exploit the catalytic activity as well as the specificity of the enzyme glucose oxidase as biological recognition element.

Another class of recognition molecules is formed by antibodies. Antibodies or immunoglobulins are protein molecules produced by the immune system (body's self defence mechanism) when the immune cells encounter a foreign molecule or antigen. It is a complex Y-shaped multi domain complex consisting of two identical polypeptides - heavy chain and two identical polypeptides - light chains, which are held together by glycosylation and disulphide linkages. Antibodies interact with specific sites on an antigen molecule termed the antibody epitopes (see section 3.1.6). The specificity and selectivity of antibodies has been widely exploited for forming the biological recognition molecules for the detection of various biomarkers.

Although they are currently the most widely used biological recognition molecules in state-of-the-art biosensors, the complex structure of antibodies is a limitation in their application on different biosensing platforms giving rise to problems like irreversible denaturation, poor shelf-life (Colas, 2008). Furthermore, post-translational modifications are required to maintain the structural domains of antibody (glycosylation and disulphide bonding), which makes the expression of antibodies difficult in bacterial hosts.

In order to overcome the limitations associated with antibodies alternatives to antibodies have been explored. Smaller yet functional forms of antibodies called antibody fragments have been used such as scFv (single-chain Fv fragments). Although they can be expressed in bacterial cells, their stability in the reducing bacterial environment is reduced as the disulphide bonds are not formed (Wörn and Plückthun, 2001).

The constraints encountered in case of antibody based biological recognition molecules have led to non-antibody-based and even non-protein-based recognition molecules. A class of molecules based on nucleic acid, DNA and RNA, called nucleic acid aptamers have been used for the recognition of biological molecules. These recognition molecules are single stranded DNA or RNA molecules that bind to target

molecules like amino acids, peptides and proteins (Jayasena, 1999). The selection of the aptamers is done using a technique called Systematic Evolution of Ligands by Exponential enrichment (SELEX), wherein the nucleic acid aptamers against different targets are selected from a random pool of oligonucleotides (Tuerk and Gold, 1990). A drawback of RNA aptamers is that they are prone to nuclease degradation unlike DNA aptamers that are more resistant to nuclease degradation. Moreover the synthesis of chemically modified RNA oligonucleotides that are nuclease resistant is an expensive process.

A different class of non-antibody based recognition molecules that can mimic antibodies for binding different targets called peptide aptamers have been developed. Peptide aptamers are based on well-defined protein scaffolds that present peptides designed to allow an interaction with a biological target molecule. They do not require disulphide bonds or glycosylation for their stability and therefore can be expressed in bacterial cells.

Some of the scaffolds exploited so far are affibodies (Nord *et al.*, 1997), Kunitz domains (Dennis and Lazarus, 1994b), anticalins (Skerra, 2008), DARPinS (Stumpp *et al.*, 2008), scaffolds based on Thioredoxin A (Lu *et al.*, 1995; Colas *et al.*, 1996),  $\beta$ -lactamase based scaffold (Legendre *et al.*, 2002), fibronectins (Koide *et al.*, 1998) and stefin A triple mutant (Woodman *et al.*, 2005).

The small size, robustness and flexibility to structural modifications in order to bind a desired target molecule makes these engineered protein scaffolds promising in the field of biosensing (Colas, 2008; Song *et al.*, 2011).

A novel scaffold called Adhiron based on consensus protein design was developed by the McPherson group at the Astbury Centre for the structural molecular biology at the University of Leeds. Adhiron is discussed briefly in the following section.

#### **1.2.2.1. Adhiron scaffold**

The Adhiron scaffold was engineered on the basis of a consensus sequence of plant-derived phytocystatins (Tiede *et al.*, 2014). Consensus design strategy helps to engineer proteins based on multiple sequence alignment, and thus the designed proteins are structurally more robust than their counterparts (Main *et al.*, 2003). This makes the scaffold suitable to present various peptides against different targets. Adhiron is structurally compact with four-strand anti-parallel  $\beta$ -sheet core and a central helical structure. Two variable regions and an N-terminus site of the scaffold form the peptide insertion sites.

Adhiron based binders presenting different peptide sequences were selected against anti-myc tag antibodies through phage display library. The binding of anti-myc tag antibodies against c myc epitope (EQKLISEEDL) has been well studied (Evan *et al.*, 1985) and myc tag was therefore chosen as a proof of concept system to study adhirons as recognition molecules in biosensors.

### **1.3. Summary of the project**

To develop a biological recognition layer based on the best Adhiron myc binder against monoclonal anti myc tag antibodies, ten Adhiron myc binders were chosen from the binders obtained from the phage display by the BSTG group (Bioscreening Technology Group, Biomedical and Health Research Centre, University of Leeds).

The ten binders were cloned into an expression vector, expressed, purified and characterised. The best binder was chosen to form the biomolecular layer of a transducer surface.

Amongst the various transducers discussed above it was important to choose an electronic transducer that has properties suitable for point-of-care diagnostics. From the point of care diagnostics a biosensor should not require any pre-treatment of sample, give a fast response and should be amenable to miniaturisation. Electrochemical impedance spectroscopy, an electrochemical based label-free detection of analytes seems to have potential to build a point-of-care biosensor. EIS is an electrochemical technique used to measure impedance of a surface by measuring the response against the applied AC signal. Impedance biosensors can be miniaturised using microfabricated arrays that can detect multiple analytes at the same time, or a single analyte on different electrodes. Such promising characteristics of EIS based biosensing platform can be used for the point-of-care application.

After choosing the best Adhiron myc binder to form the biological recognition layer, EIS was used to create a biosensor for the detection of monoclonal anti-myc tag antibodies. The impedimetric biosensor employing a well-characterised biological recognition layer of Adhiron binders against monoclonal anti-myc tag antibodies was developed and used as proof-of-principle for the working of a biosensing system.

This thesis discusses the various strategies developed in order to overcome a range of limitations faced during the development of the system. The results of the myc biosensor were then taken forward to investigate the interesting phenomenon of

modulating the sensitivity of an Adhiron based biosensor by applying different electrochemical DC biases. This approach shows great potential to tune dynamically the sensitivity and dynamic range of a label-free sensing system. This thesis discusses the development of impedimetric biosensor, its limitations and how they can be overcome.

## **1.4. Organisation of the thesis**

### **1.4.1. Chapter 2**

Chapter 2 contains a literature review that gives an account of the foundation of biosensors and their application in the field of diagnostics. It discusses the development of different biological recognition molecules against various biomarkers along with their integration with different sensing platforms with the advent of growing technology. It discusses the different types of biosensors by segregating a biosensor into the biological recognition molecule and the transducer. It describes the use of integrating an antibody mimetic probe with an impedimetric transducer as a promising tool to create a label-free, multiplexed, miniaturised biosensor.

### **1.4.2. Chapter 3**

Describes the background of various techniques and introduces the terminologies used in this work that are important to understand the context of the following chapters.

### **1.4.3. Chapter 4**

This chapter describes the cloning, expression and purification of the adhiron based anti myc antibody binders. It also describes the characterisation of the binders using circular dichroism (CD), differential scanning calorimetry (DSC) and enzyme linked immunosorbent assay (ELISA). Furthermore, it illustrates the three-dimensional structure, thermal stability of the adhiron scaffold, as well as the effect of inserting different peptides into the variable regions.

#### **1.4.4. Chapter 5**

Chapter 5 describes the development of a myc-biosensor as a proof-of-concept for using Adhiron binders in label-free electronic biosensor. The chapter details the design, surface chemistry and electrochemical detection of the monoclonal anti-myc antibodies. The chapter explains the various issues experienced during the development of the biosensor, as well as the strategies adopted to overcome these impediments. The various important observations and conclusions drawn in this chapter have been implemented in demonstrating a concept based on change in sensitivity using DC voltage bias in the following chapter.

#### **1.4.5. Chapter 6**

During the fabrication of the EIS based biosensor, it was found that the application of different electrochemical DC biases can be exploited to modulate the sensitivity of the biosensor. This is discussed in detail in this chapter.

#### **1.4.6. Chapter 7**

This chapter summarises the findings of the thesis and discusses their impact on the research field of biosensors. It also discusses the potential future directions of this work.

## Chapter 2. Literature review

Disease diagnosis has been an indispensable step in clinical healthcare to identify diseases and thus intervene for the improvement of the individual. Early detection can help to reduce the overall healthcare costs of taking care of the patient in the later stages of the ailment.

The early medical diagnosis was primarily based on observations of clinical symptoms that would describe dysfunctions in the digestive tract, blood circulation, liver and spleen. The practice of examining the body fluids for the detection of a disease also became significant after Hippocratic doctrine of humoral pathology that recognised disorders in the body fluids as the cause of all diseases (Berger, 1999).

During 17th century the invention of the microscope opened new ways to investigate disease causing organisms. Later new advanced diagnostic tools such as high-magnification microscope, X-ray, chemical and bacteriological detections started invading the field of clinical diagnosis.

The organisms responsible for tuberculosis, cholera, typhoid, and diphtheria were isolated in the 1880s. A number of laboratory tests were introduced to detect these diseases e.g. the Wasserman test for syphilis was introduced in 1906 after spirochete was identified as the organism responsible for the disease (Wassermann and Bruck, 1906). These advancements reduced the dependence of clinicians on the observation-based opinions, and the detection of diseases was based on the level of biomarkers in the patient's samples.

### 2.1. Biomarkers

Biomarkers are defined as “cellular, biochemical or molecular alterations that are measurable in biological media such as human tissues, cells, or fluids” (Hulka and Wilcosky, 1988). It is a vital tool for detection, diagnosis and treatment of a disease.

In 1949 Pauling and his colleagues discovered that sickle cell anaemia was caused due to a single amino acid change at the  $\beta$ -globin chain and coined the term molecular disease (Pauling *et al.*, 1949). Later the molecular basis of various other genetic diseases like  $\beta$ -thalassemia (Orkin *et al.*, 1983) and phenylketonurea (Chakraborty *et al.*, 1987) was also studied.

In the year 2001 with the advent of Human Genome Project, the complete sequencing of human DNA (3 billion base pairs) was unravelled (Venter *et al.*, 2001). With this major breakthrough in the field of molecular diagnostics, along with the high throughput molecular techniques, many genetic mutations were linked to a genetic disease. These mutations were characteristic of a particular pathogenic infection or the outcome of a genetic disorder, and thus biomarkers for the corresponding diseases.

As the molecular alterations were occurring much earlier than the first sign of physiological or clinical symptoms were noticeable, the nucleic acid (RNA / DNA) based technology became important part of diagnosis.

Although genome sequencing has helped to discover diagnostically relevant biomarkers, the genetic information gives only a glimpse of what may occur. The information provided by the sequencing of the genome needs to be associated with the genetic products. The genetic information is transcribed into messenger RNA (mRNA) molecules, which are then translated into polypeptide chains. These polypeptide chains undergo post-translational modifications to form mature protein products (Figure 2-1).

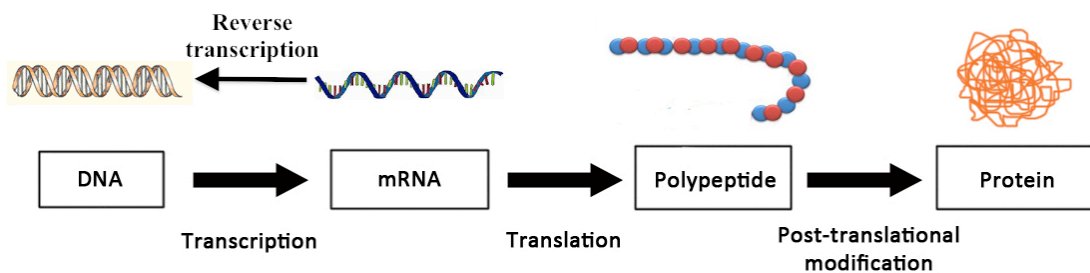


**Figure 2-1 The flow of genetic information.**

Shows the flow of genetic information from genome to proteome through the transcription of DNA into mRNA (messenger RNA) or *vice versa* (reverse transcription) and translation of m-RNA into a polypeptide chain of aminoacids. The mature protein is formed after the post-translational modifications.

The overall cellular function of a cell can be interrogated in principle by the direct measurement of the level of protein expression. There is a poor correlation between the mRNA transcripts and the protein level in the cell and therefore the biochemical state of the cell cannot be directly related to mRNA levels (Gygi *et al.*, 1999; Anderson and Seilhamer, 1997; Greenbaum *et al.*, 2003). This requires the direct

analysis of proteins and identifying protein biomarkers and the difference in their level of expression in a diseased and a healthy cell. Protein based biomarkers also enhance the understanding of biochemical changes that occur during the progression of the disease and thus can help in the efficient treatment.

With the advent of proteomics that refers to the study of structure and function of proteins, high throughput techniques have been used to analyse large number of proteins in parallel. 2D PAGE (two dimensional polyacrylamide gel electrophoresis) has been used to identify tumour associated antigens (TAA) as potential biomarkers in hepatocellular carcinoma (Yau *et al.*, 2013). In 2D PAGE, protein samples are resolved on the basis of their isoelectric points as well as molecular weights and visualised using different staining techniques.

Various protein biomarkers associated with clinical dysfunctions have been discovered like interleukin-6 (IL-6) and tumor necrosis factor- $\alpha$  (TNF- $\alpha$ ) against autoimmune disorders (Castro and Gourley, 2010). The detection of these biomarkers in the patient's body fluid can reduce the mortality rate, as well as guide the physicians through the treatment of these diseases. These protein biomarkers are present in the readily available body fluids like serum, urine or saliva.

Although the convergence of proteomics and genomics has resulted in the discovery of a wide range of biomarkers against various types of diseases, the detection of these biomarkers in the biological fluids demands the development of analytical devices. These analytical devices are referred to as biosensors.

## 2.2. Biosensors

A biosensor consists of a biological recognition layer immobilised on to a transducer surface. The binding of analyte molecules or biomarkers to the recognition layer causes changes in the vicinity of the sensor surface, which is converted into an electrical signal by the transducer (see Figure 1-1 section 1.2).

The following section discusses the various types of biosensors based on the different types of biological recognition molecules and transducers.

### 2.2.1. Biological recognition molecules

The biological recognition molecules form a critical part of the biosensing devices in sensing the analyte molecules.

Historically, important enzyme-based assays that rely upon the use of enzymes for sensing still remain commercially important e.g. glucose biosensors based on Gox (Glucose oxidase) has been the most widely used glucose sensor for monitoring glucose level by diabetic patients (MediSense Inc).

On the other hand, non-enzyme based recognition molecules called bio-affinity based recognition molecules rely upon binding interaction of biological recognition molecules to the specific analytes. The use of affinity-based biosensing has increased dramatically. The most widely used technique in biosensing called ELISA is based on the affinity of antibodies to various analytes (see section 3.2.1.4). The antibody based sensors or immunosensors have been designed for monitoring various vital biomarkers, such as human chorionic gonadotropin (hCG) which is an important diagnostic marker in pregnancy test and is detected by anti-hCG antibodies (Canfield *et al.*, 1987).

Although antibodies are the most widely used biorecognition molecules because of their specificity towards the target molecules, their complex structure having four polypeptide chains, disulphide bonds and involvement of glycosylation (post-translational modification) make it difficult to produce antibodies in bacterial hosts. With advances in technology, artificial recognition elements or biomimics such as nucleic acid aptamers, peptides, protein aptamers and molecularly imprinted polymers (MIPs) have been developed in the laboratories to allow improved stability and reproducibility in biosensing.

Biological recognition molecules are classified as non-protein based and protein based recognition molecules. The following section describes the two categories of biological recognition molecules.

#### **2.2.1.1. Non-protein based capture molecules**

##### ***Molecularly Imprinted Polymers (MIP)***

“The molecular imprinting technique can be defined as the formation of specific nano-sized cavities by means of template-directed synthesis” (Zhang *et al.*, 2006).

One of the greatest advantages of the artificial receptors over the naturally occurring ones is the freedom of molecular design. There are two methods of fabricating molecularly imprinted polymers (Wulff, 2002). One is based on non-covalent interaction such as hydrogen bonds, electrostatic interactions, hydrophobic interactions and van der Waals forces. The appropriate monomers bearing the desired functionality are introduced into the polymers by copolymerization in presence of the crosslinkers through intermolecular interactions. The other is covalent molecular imprinting in which the monomer mixture contains functional monomers that conjugate with the template through covalent bonds. In both cases, after the removal of the template an imprint containing the binding sites corresponding to the target molecules are obtained (Arshady and Mosbach, 1981).

There are potential advantages of imprinted polymers such as the robustness of the polymer and the flexibility to incorporate desired functional monomers in the polymer.

Molecular imprinting has been used effectively to create capture molecules for small molecules such as drugs, pesticides and explosive markers (Vasapollo *et al.*, 2011). Although imprinting of proteins has been reported (Venton and Gudipati, 1995; Chou *et al.*, 2005) but it is much constrained by the dynamic nature of protein molecules. Because of the three dimensional structure of proteins, the functional groups responsible for the binding to the analyte, are located at different positions on the polypeptide chain (Wulff, 2002). This makes it difficult to use a protein as a template for molecular imprinting.

Another problem related to molecular imprinting of proteins has been the solubility issue. Most of the molecular imprinting takes place in presence of non-polar solvents. This can lead to destabilization and denaturation of the proteins. In order to lower the effect of organic solvents a hydrophilic crosslinker N,N'-methylene bisacrylamide

(MBAA) was used to prepare protein imprinted hydrogels (Kimhi and Bianco-Peled, 2007).

### ***Nucleic acid Aptamers***

Nucleic acid aptamers are single stranded DNA or RNA molecules that can bind to other biomolecules. They are selected from a random pool of oligonucleotides by a process called Systematic Evolution of Ligands by Exponential enrichment (SELEX) (Tuerk and Gold, 1990; Ellington and Szostak, 1990). SELEX method is conceptually based on the ability of the selected oligonucleotides to bind to various target molecules. The process involves a number of randomised oligonucleotides that have a complexity based on the number of oligonucleotide positions present in the linear oligomers. The oligonucleotide library pool is incubated with the target of interest. The bound sequences are separated from the rest of the pool using different elution methods. The eluted oligonucleotides are further amplified by polymerase chain reaction (PCR) so as to obtain an enriched library of oligonucleotides that specifically bind the target. PCR is a widely used to amplify the desired segment of DNA using an enzyme called DNA polymerase (Bartlett and Stirling, 2003).

In the aptamer selection technology, the binding affinity and specificity of an aptamer can further be improved by doing a round of second selection using a biased library. The biased library comprises of variants of the primary aptamer that were not present in the first round of SELEX. Therefore as an *in vitro* process the selection of improved aptamers against their targets becomes more feasible unlike in case of *in vivo* methods for producing antibodies.

The ability of single stranded nucleic acids to fold into complex structures is a source of functional diversity that can be used to bind many biologically relevant markers (Patel *et al.*, 1997; Harada and Frankel, 1995).

With the advent of SELEX various aptamers have been developed against important clinical targets where these aptamers act as inhibitors. An antagonist aptamer of von Willebrand Factor (vWF) was developed as a novel antithrombotic agent for use in patients with acute coronary syndromes (Gilbert *et al.*, 2007). Two synthetic aptamers were identified that bind to prostate cancer cells *via* the prostate specific membrane antigen (PSMA) (Lupold *et al.*, 2002). Aptamers that bind E-selectin, expressed in endothelial cell surface of vessels during inflammation, have also been developed (Mann *et al.*, 2010). RNA aptamers targeted against various cell surface markers have

been used to deliver siRNA (small interfering RNA) as a therapeutic agent through RNA interference (Chu *et al.*, 2006).

The biosensors based on nucleic acid aptamers are designed using different strategies. For example, the conformational change of aptamers upon binding has been used in the detection of platelet-derived growth factor (PDGF). DNA aptamer modified with methylene blue at one end is tethered to the gold electrode from the other end. It remains in an unfolded state when PDGF is absent that keeps methylene blue far from the electrode surface. On binding to the target, PDGF, the aptamer undergoes conformational change and the distance between the electrode and methylene blue decreases. This increases the electron transfer with an increase in current (Lai *et al.*, 2006).

The easy synthesis and desired functionalisation of the nucleic acid aptamers elaborates the use of different immobilisation chemistries in biosensors. Despite many advances very few aptamers have been identified that bind specific protein post-translational modifications. This is because the aptamers are selected through *in vitro* screening against recombinant proteins, which either lack the post-translational modification or misfold in the *in vitro* conditions. Thus the selected aptamer can lack the recognition for a post translationally modified target protein in the biological sample (Mann *et al.*, 2010).

### **2.2.1.2. Protein Based Recognition Molecules**

#### ***Enzymes***

Enzymes are proteins that catalyse specific chemical reactions without being consumed in the process. The three-dimensional structure of an enzyme formed by the folding of the polypeptide chain consists of a binding site that interacts with the substrate to form an enzyme substrate complex. The specificity of the enzymes towards their substrate is the major characteristic exploited widely in the enzyme-based biosensors. The enzymatic reactions are accompanied by the production or consumption of various species such as gases (CO<sub>2</sub>, NH<sub>3</sub>, O<sub>2</sub>) that can be detected optically or electrochemically (Moreno-Bondi *et al.*, 1990).

The first generation enzyme based sensors such as those developed by Clarke, were based on immobilisation of the enzyme on an ion selective electrode and the production or consumption of specific ions was monitored (Clark and Lyons, 1962). The major drawback in these enzyme-based sensors was that during the analysis of real samples, detection of products was interfered by ions or dissolved gases in the

biological samples. This led to the incorporation of an artificial mediator and the commercial launch of the first biosensor by research groups in Oxford and Cranfield (Cass *et al.*, 1984). It was based on electron mediated transfer mechanism using glucose oxidase enzyme and ferrocene. Ferrocene (Fc) was used as an electron transfer mediator, as it acts as a good electron acceptor. Glucose was converted by glucose oxidase into gluconolactone, which led to glucose oxidase ( $\text{GOX}_{\text{ox}}$ ) to be reduced into  $\text{GOX}_{\text{red}}$ . Ferrocene accepts electrons from  $\text{GOX}_{\text{red}}$  to get reduced and thus diffuses to the electrode where it is reoxidised.

Due to the role of cholesterol in the cardiovascular diseases there has been a focus on the determination of cholesterol level in the blood. For the clinical analysis of cholesterol, its oxidase has been used most frequently. During the interaction of cholesterol oxidase with its substrate, the consumption of oxygen is detected by using a dye whose fluorescence is quenched by molecular oxygen (Trettnak and Wolfbeis, 1990). Enzyme based biosensors have been reported for the detection of uric acid for the diagnosis of inflammatory arthritis or hyperurecemia (Cete *et al.*, 2006).

The major disadvantages with the enzyme-based sensors are related to their operational stability and shelf life and attempts have been made to improve their properties (Chaniotakis, 2004).

Another important limitation of enzyme-based biosensors is that the enzymes can be used as biological recognition molecules only for a limited number of biomarkers. To circumvent this problem, another class of enzymes known as allosteric enzymes have been employed as the recognition molecules in biosensing as they exhibit regulatory catalytic activity. An allosteric enzyme has a receptor site where modulation occurs and an active site where the substrate binds. The receptor site binds to non-substrate molecules that influence the activity of the active site. This influence can be either enhancing or impairing the enzyme activity. Modulation of the allosteric sites by displaying the sensing elements at these sites enables the detection of new targets by the enzyme. *E. coli* alkaline phosphatase has been modulated by inserting an epitope from HIV-1 gp120 protein near the active site of the enzyme to detect anti-gp120 monoclonal antibody (Brennan *et al.*, 1994).

### ***Molecular receptors***

Molecular receptors are membrane proteins that bind specific molecules and undergo a conformational change triggering a cellular response. The signal transduction in the cells is an example of how nature detects the presence of something for the

biochemical changes taking place in the cells. These receptors are generally membrane receptors that trigger responses on binding to hormones, aminoacids, insulin, and neurotransmitters and also to various non-biological species like drugs. The specificity, speed and sensitivity that helps the cells to carry out signal transduction in such a complex environments have inspired the development of biosensors based on such principles. It has led to creating sensors based on structure-switching molecules or receptors, which can be converted into a detectable signal (Plaxco and Soh, 2011).

Biosensor based on apo-riboflavin binding protein was used to detect riboflavin / vitamin B2. It was based on the principle of displacement of riboflavin analogue from the riboflavin receptor molecules (Yao and Rechnitz, 1987).

Protein polymyxin b derived from the cell membrane of *Bacillus polymyxa* was used as a biorecognition molecule to detect a liposaccharide endotoxin (LPS) (James *et al.*, 1996). LPS is an immune stimulant that causes the clinical syndrome called sepsis, an immunological disorder leading to inflammation and blood clotting.

The major drawbacks in the use of protein receptors in biosensing include the difficulty in isolating the multimeric membrane receptor proteins and maintenance of their biological activity on isolation and immobilisation.

### ***Antibodies***

Antibodies are proteins produced by the immune system of an organism in response to foreign antigens. They form the most widely used class of biological recognition molecules in the field of biosensing. The general structure of antibodies consists of a variable region and a constant region (see section 3.1.6). The variable region binds to the target through complementarity-determining region (CDR), whereas the constant region binds the other molecules of immune system. The CDR forms the epitope binding site of an antibody to its target antigen. The diversity of antibodies, their specificity and affinity against different antigens in the immune system, makes them more reliable as biological recognition molecules in the field of diagnostics.

The production of antibodies depends on the *in vivo* immune response elicited by an immunogen called as an antigen. An antigen is recognised as a foreign molecule by the immune system and antibodies are synthesised against that antigen. The antibody recognises a specific region of the antigen called as antibody epitope. Antibodies can be raised against proteins, peptides, nucleic acids or carbohydrates etc.

Depending on the type of specificity of an antibody towards an antigen, antibodies are classified as polyclonal and monoclonal antibodies. Polyclonal antibodies are produced by immunisation of host organisms with immunogens / antigens. The antibodies produced are derived from multiple plasma cells that recognise the same target but different epitopes on the target. Also each polyclonal serum even if produced from the same animal is unique and not reproducible (Bradbury *et al.*, 2003).

With the establishment of monoclonal antibody technology by Köhler and Milstein, cell clones were used that produced monoclonal antibodies more specific to target proteins (Köhler and Milstein, 1975). The use of monoclonal antibodies instead of polyclonal antibodies enhanced specificity and sensitivity of the antibody based assays.

Owing to their high specificity and binding versatility the most commonly used detection method, ELISA, is based on binding of antibodies to different antigens. Antibodies have been used in the detection of cancer biomarkers (Malhotra *et al.*, 2010), bacteria and viruses (Carnes and Wilkins, 2005).

Although antibodies are most commonly used for detecting analyte molecules but due to their complex and large size, they tend to be more fragile which most likely also affects the shelf life and sensitivity when used on a sensing platform (Jayasena, 1999). In order to produce smaller yet functional forms of antibodies, re-engineering of antibodies has been employed. Single-chain Fvs (25 kD) with improved stability have been reported that are engineered by removing the intradomain disulphide bond and applying a reducing redox potential during ribosome display (Jermutus *et al.*, 2001). Furthermore, it was discovered that a part of the humoral immune response of camels and llamas is based on the interaction of the antigens with only one single variable domain of the antibodies called the  $V_H$  (variable heavy chain) domain. The recombinant single domain meets most of the desired properties of small recognition units (Muyldermans, 2001).

Many biomolecular diversity or display technologies like phage display (Hoogenboom and Chames, 2000) and *in vitro* display (FitzGerald, 2000) have been used to select antibodies against specific biomarkers with improved sensitivities due to ability to screen larger recombinant libraries.

In phage display the antibody fragments are fused with the phage coat proteins and the genetic information is encapsulated inside the phage capsid. The displayed antibody fragments are, therefore physically linked to their nucleic acid sequences allowing selection of binding partners in the phage display library (see section 3.1.7). In case of

ribosome display / *in vitro* display the complex of the mRNA, ribosome and nascent antibody is selected against immobilised antigens. The mRNA is isolated from the bound complex and reverse transcribed to cDNA. The nucleotide sequence obtained from the cDNA can then be used for creating better binding antibodies. The other techniques used are yeast two hybrid (Fu *et al.*, 2013) and mRNA display (Fukuda *et al.*, 2006).

An alternative to the antibody based recognition molecules is the use of non-antibody based protein scaffolds called peptide aptamers.

### ***Peptide Aptamers***

Imitating the humoral response, efforts have been made to design antibody-mimicking protein scaffolds that constitute variable peptide regions mimicking the complementarity determining regions (CDR) of antibodies. Such protein scaffolds can be used to present binding functionalities in their variable regions, thus forming biological recognition molecules called peptide aptamers. The less complex and smaller peptide aptamers in comparison with antibodies are promising alternatives in the field of biosensing.

Figure 2-2 shows a schematic representation of comparison between an antibody and a peptide aptamer. The important characteristics that distinguish a peptide aptamer from an antibody are their smaller, less complex structure (formed from a single polypeptide chain) than antibodies (~150 kDa), which impart more stability and longer shelf life to the peptide aptamers (Jayasena, 1999; Song *et al.*, 2011; Colas, 2008). Moreover, peptide aptamers do not require disulphide bonding or posttranslational modifications for maintaining their stability unlike antibodies (Colas, 2008).

Their simple structure can be modified according to the desired features required for changing the sensitivity, non-specific binding and stability of the biological recognition layer in a biosensor.

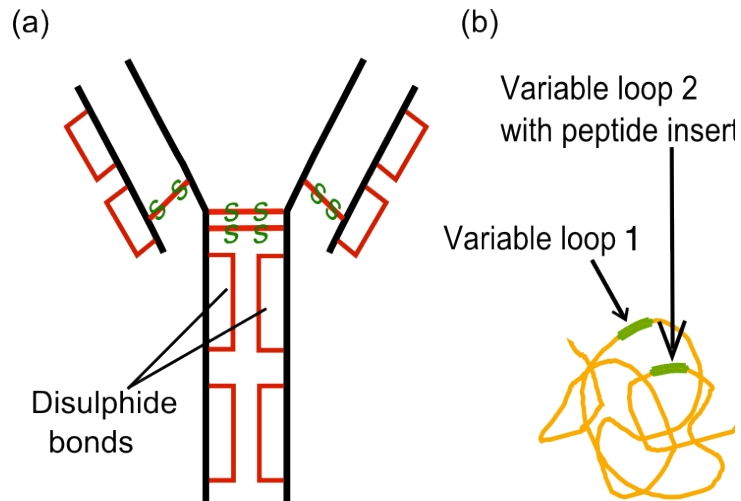


**Figure 2-2 Shows a schematic diagram comparing an antibody with a peptide aptamer.**

(a) An antibody comprising of two identical light chains and two identical heavy chains held together by multiple intrachain and interchain disulphide bonds (b) a protein scaffold (peptide aptamer) comprising of a single polypeptide chain and two variable loops with a constrained peptide in loop 2. Adapted from (Colas, 2008).

In the engineering of peptide aptamers, a protein framework is used to constrain peptides into their variable loops (Figure 2-2(b)). Peptides with both ends attached to a protein framework are called as constrained peptides (CP) and have a preferred conformation. As biological recognition molecules, these constrained peptides possess unique advantages over the flexible peptides with free ends. Linear or unconstrained peptides can take up large number of different conformations through internal rotations (Ladner *et al.*, 1993). Therefore, the analyte molecule can accept the unconstrained polypeptide in one or few conformations due to the favourable van der Waals and other non-covalent interactions. Whereas the constrained peptides with restricted number of free rotations will most likely exhibit different affinity, but more specificity to its analyte as compared to its unconstrained counterpart (Koivunen *et al.*, 1995).

The thermodynamic aspect of the protein conformation is an imperative aspect because the optimal binding site for the ligand should be a perfect complement for the ligand. It should also be rigid, so that the loss of conformational entropy upon binding is minimal (Chia-en *et al.*, 2007).

### *Engineering a peptide aptamer*

For engineering different scaffolds various strategies have been used to improve the various characteristics of the scaffold like stability, recombinant expression yield, solubility (Binz *et al.*, 2005). Once a suitable scaffold is optimised it is modified for the desired ligand binding function. One of the approaches to engineer a binding site is using combinatorial engineering approach in which a random library based on insertion of amino acid sequences is first generated by targeting different positions on the peptide aptamer, e.g. within the variable loops (Koide *et al.*, 1998) or inserting random peptide sequences into the loops (Colas *et al.*, 1996). The mutants with the desired binding specificities are selected using different systems like the yeast two-hybrid system (Young, 1998), filamentous phage display (Smith, 1985) followed by panning in the presence of the ligand. Other techniques used are colony screening assays (Schlehuber *et al.*, 2000), plasmid-binding repressor fusion proteins (Cull *et al.*, 1992), and ‘ribosome display’ (Roberts, 1999).

### *Scaffold based on thioredoxin (TrxA)*

A pioneering work in the development of peptide aptamers against a specific target was done using a scaffold based on thioredoxin A (TrxA) protein (Colas *et al.*, 1996). TrxA which is a small enzyme involved in cytosolic thio-disulphide equilibrium in *E. coli*. It is a highly soluble, rigid protein that can be expressed in large amounts. A short active sequence in the enzyme forms a solvent accessible, disulphide-constrained loop that can be used for insertion of various peptide sequences and will inactivate the enzyme. Colas *et al.* reported the expression of combinatorial library of conformationally constrained 20-residue peptides displayed in the active site loop of *E. coli* trxA scaffold. The binders were selected against human CDK2 using yeast two-hybrid system. Prior to this work, the entire coding sequence of *E. coli* thioredoxin (TrxA) protein was inserted into partially functional flagella on the bacterial cell surface and the active loops of the *E. coli* trxA were replaced by random dodecapeptide sequences (Lu *et al.*, 1995). Selection of variants was done against three murine monoclonal antibodies, that resulted in mapping three different antibody epitopes.

The other most advanced approaches in the field of peptide aptamers comprise of the following.

### *Affibodies*

This protein scaffold is based on the Z-domain of Staphylococcal protein-A (SPA) that binds to the Fc region of immunoglobulin G (Nilsson *et al.*, 1987). (Nord *et al.*, 1997). Z domain consists of repetitive structure consisting of small thermally and proteolytically stable domain. It contains three  $\alpha$ -helices, which are arranged in an antiparallel three-helix bundle. It is well expressed in soluble form in *E. coli* and devoid of disulphide bridges. A combinatorial library was constructed based on the mutagenesis of Fc binding regions of Z domain (Nord *et al.*, 1995). The repertoire of mutagenised Z-domains was used to detect Taq DNA polymerase, human insulin and human apo-lipoprotein A-1 (Andersson *et al.*, 2003; Nord *et al.*, 1997).

### *Kunitz domains*

Kunitz domains are stable proteins with 50-60 amino acid residues (6 cysteine residues) present in various protease inhibitors. They have been engineered to produce high affinity binding molecules using phage display libraries to bind to various proteases (Nixon and Wood, 2006; Dennis and Lazarus, 1994a). Variants of the first Kunitz domain of human lipoprotein-associated coagulation inhibitor (LACI-D1) were displayed on M13 bacteriophage using pIII protein to select high affinity and stable binders against a serine protease called plasmin (Markland *et al.*, 1996).

### *Anticalins*

They are derived from the lipocalins, a small (60 residues), functionally diverse family of proteins containing a conserved  $\beta$ -barrel of 8 anti-parallel  $\beta$ -strands, four variable loops and a C-terminal  $\alpha$ -helix (Schlehuber and Skerra, 2005). The four variable loops at the open end of anticalins (< 20 kDa) can be modified to derive binding sites against different target molecules (Skerra, 2008).

### *DARPin, designed ankyrin repeat domains*

DARPin are based on natural ankyrin repeat proteins, which are one of the major repeat proteins, involved in protein-protein interactions in organisms from various phyla. DARPin (14-18 kDa) are based on a consensus design strategy of ankyrin repeat proteins and consists of well conserved sequences for maintaining the repeat structure and randomised residues for interacting with the target proteins (Kohl *et al.*, 2003; Binz *et al.*, 2004; Binz *et al.*, 2005; Stumpp *et al.*, 2008).

### *Fibronectin type III domain*

Fibronectin type III domain is based on protein fibronectin that is essential for the formation of extracellular matrix and cell-cell interaction. Fibronectin consists of repeats of three types of small domains (I, II and III). Fibronectin type III domain (FN3) belongs to Ig superfamily and consists of variable loops constrained by the  $\beta$ -sandwich structure resembling the CDR region of antibodies. Unlike antibodies FN3 does not contain any disulphide bonds and therefore can be expressed in bacterial hosts. The mutant FN3 was designed using combinatorial engineering and showed conformational stability. The designed mutant FN3 showed binding to a test analyte ubiquitin molecule (Koide *et al.*, 1998).

### *Stefin A triple mutant (STM)*

It is based on a protein called Human stefin A, a member of the cystatin superfamily. Cystatin superfamily consists of reversibly-binding inhibitors of the papain-like cysteine proteinases (Brzin *et al.*, 1983). Stefin A subgroup of this family consists of proteins that are relatively small (100 amino acids), single domain and require no posttranslational modifications (Woodman *et al.*, 2005). Different gene mutations were incorporated in the Stefin A protein scaffold to form a biologically inert protein scaffold called Stefin A triple mutant (STM). The three-dimensional structure of STM consists of an  $\alpha$ -helix,  $\beta$ -sheets with two variable loops for peptide insertions and shows a thermal stability of 81°C (Woodman *et al.*, 2005). Peptide inserts were incorporated into the variable loops of the scaffold to target various analyte molecules *e.g.* a peptide aptamer based on STM has been used to target a cell signalling molecule called cyclin dependent kinase-2 (CDK-2) (Evans *et al.*, 2008). These Stefin based peptide aptamers, now termed as Affimers were used to target an inflammatory biomarker, C-reactive protein (CRP) (Johnson *et al.*, 2012).

### *Repebodies*

A newly designed scaffold named as repebody is based on variable lymphocyte receptors that are non-immunoglobulin antibodies in jawless vertebrates (Lee *et al.*, 2012). Repebodies are composed of leucine-rich repeats each of which has a  $\beta$ -strand-turn- $\alpha$  helix structure. Since they are derived from naturally occurring antibodies composed of repeat units, therefore they are called as repebodies. They showed high level of soluble expression in *E. coli* and displayed high thermal (melting temperature of 85°C) and pH stability (pH range 3-12). A phage display library was constructed to

select receptors with different binding affinities against interleukin-6 (IL6) (Lee *et al.*, 2012).

### 2.2.2. Transducers

The function of a transducer is to gather the analytical information when in contact with the sample detecting the presence of the analyte and produce a signal. In general, one can categorise the different transducers into labelled and label-free system. In labelled systems, the transducer detects the binding of the analyte to the recognition molecule indirectly through detecting the presence of a label which is normally attached to the target. In contrast, in label-free systems, the binding is detected directly without the need for a label. In the following section biosensors based on different transducers are discussed.

#### *Optical Biosensors*

Optical transducers can sense changes in the optical properties of their environment, and hence can detect the binding of analyte to the biological recognition molecules. The optical detection is mainly based on the change in absorbance or luminescence in the vicinity of the transducing surface. Different compounds absorb at different wavelengths of the electromagnetic spectrum depending upon their electronic configuration. Absorbance at a specific wavelength is measured by passing a beam of monochromatic light through the sample and the amount of light absorbed is then proportional to the concentration of the compound in the sample. On the other hand, luminescence is the phenomenon of emission of light when electrons, excited due to absorbance of energy, return from an excited state to the ground state emitting photons, which are detected using a photodetector. Depending upon the state of excitation, the phenomenon of luminescence can further be divided into phosphorescence, fluorescence and chemiluminescence.

In the field of biosensing fluorescence has been one of the most widely used optical properties for detecting and quantifying biomolecules. Many biomolecules have intrinsic fluorescent properties such that they can be used as fluorescent probes. Each fluorophore has a characteristic spectrum depending upon its electronic configuration. For example, a protein called green fluorescent protein (GFP) has been used to detect protein-protein interactions. GFP is obtained from jellyfish *Aequorea victoria*. Recombinant fluorescent proteins have been constructed using GFPs. When the analyte binds to the recombinant protein, it causes conformational change that is

observed in the change in fluorescence of the GFP (Doi and Yanagawa, 1999; Feilmeier *et al.*, 2000).

Other than naturally occurring fluorophores, synthetic fluorophores have been used in protein based or nucleic acid based biosensors. These fluorophores are incorporated into the recognition molecules by modifying specific amino acid residues *e.g.* a glucose biosensor was designed by using *E. coli* based glucose-binding protein with cysteine residues incorporated at specific sites to covalently attached a thiol reactive fluorophore (Marvin and Hellinga, 1998).

Although fluorescence spectroscopy has been widely used in detecting molecular interactions, there are a number of drawbacks. The fluorophores undergo irreversible photodegradation called photobleaching, that decreases the sensitivity of the assays (Greenbaum *et al.*, 2000). Moreover, controlling the number of fluorophores bound to the recognition molecules can affect the quantitative analysis of the analyte binding to the recognition molecules (Cox and Singer, 2004). The fluorophores may lead to conformational changes when covalently bound to a protein which hampers the biologically significant conformation (Ramachandran *et al.*, 2005).

Another commonly used optical sensing method is called chemiluminescence. Chemiluminescence is the emission of light due to a chemical reaction wherein one of the intermediate products is excited to a higher energy level and emits photons while approaching the ground state. This phenomenon is widely used in ELISA based detection assays (see section 3.2.1.4).

In contrast to the use of labelled biosensors that are based on the fluorescence of the biomolecules or the synthetic fluorophores, label-free optical detection of analyte molecules has been developed.

The more recent development of label-free, very sensitive, non-invasive and continuous real time measurements is based on surface plasmon resonance (SPR). SPR is based on detecting the change in refractive index due to binding of the analyte molecules to the biological recognition layer immobilised on to a gold sensor surface (see section 3.2.5). The binding of the molecules can be monitored in real time using very low amounts of compound and the association-dissociation kinetics can also be analysed. The biochemical properties of a domain in tumor repressor protein were investigated using SPR (Deka *et al.*, 1998).

In order to improve the signals obtained from the conventional SPR biosensors, metallic nanostructures that enable an efficient coupling of incident light to plasmon resonance (LSPs / Localized surface plasmons) (Anker *et al.*, 2008). Use of LSPR for

the detection of avian influenza DNA hybridization has improved sensitivity over the conventional SPR (Shin Ae *et al.*, 2010).

Currently, since the miniaturisation of biosensors is in progress, the important constituents of the optical biosensors like the light source and detectors used are still bulky. The integration of the light source, detector and the biorecognition platform becomes a constraint.

### ***Mechanical Biosensors***

Mechanical biosensors are based on the detection of parameters associated with mechanical deformation *e.g.* force, stress (force per cross sectional area) or mechanical waves (acoustics), that is transformed into a suitable output signal.

In case of biosensors based on mechanical deformation biological recognition molecules are, for example, immobilised on one side of a microcantilever. When the analyte binds to the biological recognition layer, it causes a change in the surface strain on the side of the microcantilever containing the biological recognition layer, which leads to a deflection of the microcantilever. The microcantilever deflection is measured by optical or electrical means.

Microfabricated cantilevers functionalised with biological recognition molecules *e.g.* anti-creatine kinase and anti-myoglobin antibodies were used to detect two cardiac biomarkers creatine kinase and myoglobin respectively (Arntz *et al.*, 2003). The detection was based on the optical changes measured when the laser beam is focused on the free end of the cantilever and the deflection in the cantilever is measured by a photodetector.

A microcantilever mechanical sensor based on piezoresistive detection was developed in which the microcantilever was embedded into a polymer (Porter *et al.*, 2003). Piezoelectric change corresponds to change in the electrical resistivity on the surface in response to change in pressure or stress. On binding of analytes to the polymer, the polymer swelled thus changing the surface stress, which was detected by the change in the surface resistance.

The microfabrication process must be controlled to such an extent that the mechanical properties of all the cantilevers fabricated are similar. This is because the microcantilevers are very sensitive to external influences like temperature drift and disturbances during fluid exchange.

Another class of mechanical biosensors is based on the dependence of the resonance frequency of the mechanical system, *i.e.* the frequency at which the surface vibrates with maximum amplitude as compared to other frequencies, on changes of the overall mass of the system. In this type of biosensor, the mechanical structure, *e.g.* a disc, operates as an oscillator. The recognition molecules are immobilised on to the disc surface, which oscillates at resonance frequency. When target molecules bind to the immobilised capture molecules, the mass of the system changes which in turn leads to a change in resonance frequency. This shift in the resonance frequency can be detected and used to quantify the binding of the analyte to the biological recognition layer.

Further, the properties of the propagation of acoustic waves across a surface or through bulk can be exploited for biosensing. Changes in the overall mass of the system lead to changes of the propagation of the acoustic wave. Depending upon where the propagation of the acoustic wave takes place, the sensors are classified as bulk acoustic waves (BAW) sensors and surface acoustic waves (SAW). In BAW based sensors the acoustic wave travels through the bulk of the material. One of the most commonly used mechanical biosensor is the QCM quartz crystal microbalance. QCM is based on BAW based technology. It has been widely used for detecting molecular interactions (Yao *et al.*, 2010). In SAW based sensors the acoustic wave is confined to the surface of the sensor, which increases the sensitivity of the sensor to any change occurring at the surface (Gronewold, 2007).

### ***Electrochemical Biosensors***

Electrochemical biosensors are based on the detection of analytes by measuring the change in the electrochemical properties of the sensor. The electrochemical change can be measured in the form of current (amperometric), voltage (potentiometric) or impedance (impedimetric).

In general electrochemical processes are measured at the electrode-electrolyte interface. It usually requires a working electrode where the biological recognition molecules detect the analyte, a reference electrode that maintains a stable potential and a counter electrode that maintains the flow of current through the working electrode (see section 3.2.6.2). The different types of electrochemical biosensors have been discussed in the following sections.

### *Amperometric Biosensors*

Amperometric biosensors involve the measurement of current at a constant potential resulting from the redox reactions taking place at the electrode surface. Redox reactions involve the loss (oxidation) or gain (reduction) of electrons.

This electrochemical redox reaction taking place at the working electrode generates a measurable amount of current. Amperometric biosensors use redox enzymes to produce oxidation / reduction reactions. The first amperometric sensor was proposed by Clark at the New York Academy of Sciences symposium in 1962. The sensor consisted of the enzyme glucose oxidase trapped close to the surface of platinum electrode that converted glucose into glucuronic acid and hydrogen peroxide in presence of oxygen. The oxygen was reduced at the metal electrode and the flow of current was proportional to the concentration of oxygen in the solution (Clark and Lyons, 1962).

In order to obtain high currents and increased sensitivity in the amperometric biosensors mediators like ferrocene have been used (Cass *et al.*, 1984). Mediators are molecules that help to carry the charge between the active site of the enzyme and the electrode, thus providing a high rate of electron transfer.

Although it is useful to detect analytes by using enzyme-substrate reactions, almost none of the clinically relevant analytes are natural substrates for enzymes. The major challenges in the amperometric biosensors include the enzyme instability, biomolecular interference from endogenous and exogenous species that can undergo reactions with the working electrodes (Lowry and O'Neill, 1992).

### *Potentiometric Biosensors*

Potentiometric biosensors are based on development of a potential at the working electrode compared to the reference electrode when ideally no current flows between the working and the reference electrode. The development of potential is related to the charge accumulated at the electrodes, which can be related to the ionic activity taking place in the electrochemical cell (Malon *et al.*, 2006).

The relationship between the concentration of the ions and the potential can be determined using the Nernst equation as following:

$$E_{\text{cell}} = E_{0\text{cell}} - \frac{RT}{nF} \ln\left(\frac{[I_a]}{[I_c]}\right)$$

$E_{\text{cell}}$  represents the observed cell potential at zero current,  $E_{0\text{cell}}$  is a constant potential contribution to the cell. R, T, n and F represent the universal gas constant (Joules

Kelvin<sup>-1</sup>mole<sup>-1</sup>), the absolute temperature (Kelvin), the charge number of the electrode reaction and the Faraday constant (Coulombs mole<sup>-1</sup>) respectively.  $I_a$ ,  $I_c$  represent the ionic concentration at the anode and the ionic concentration at the cathode respectively.

Nernst equation provides the fundamental basis for the working of most of the potentiometric biosensors. The binding of analyte molecules to the biological recognition layer, immobilised on to a membrane, changes the transmembrane potential due to change in the ionic flux across the membrane. The ionic flux can also be deliberately induced by adding ionic markers to the solution (Ozdemir *et al.*, 2013).

### *Impedimetric Biosensors*

Impedimetric biosensors are based on electrochemical impedance spectroscopy (EIS) and thus also called as EIS based biosensors. EIS is a technique that measures the two components of impedance, the real part is the ohmic or resistive contribution and the imaginary part is the capacitance contribution (see section 3.2.6.4). It is used to measure intrinsic properties of a surface or a process that affects the resistive and the capacitive behaviour of an electrochemical system.

EIS based biosensors are based on the change in the resistive or capacitive properties of materials upon the binding of analyte to the biorecognition molecules at the electrode surface. Based on the component of impedance being measured in an EIS based biosensor they are classified as faradaic and non-faradaic biosensors.

In the faradaic biosensors the response is based on the transfer of the electrons across the interface, and therefore requires a redox probe that needs corresponding DC bias voltage so as to maintain the transfer of electrons from its reduced to its oxidised state. This transfer of electrons can be measured as electron transfer resistance. Faradaic measurements were used to detect thrombin protein using a gold electrode functionalised with a thrombin binding aptamer (Cai *et al.*, 2006). The binding of p53 gene sequence (tumor biomarker) to complementary DNA probes immobilised on to graphite electrodes was detected by measuring the change in faradaic impedance (Marquette *et al.*, 2006). An impedimetric biosensor for the detection of microorganism *B. anthracis*, used in biological warfares was developed using capture probe complementary to target DNA sequence (Kara *et al.*, 2008).

On the the other hand, non-faradaic biosensors do not require a redox probe and are mainly dependent on the change in resistance or capacitance at the interfacial surface formed by the biological recognition molecules and the electrolyte. An impedimetric

biosensor was fabricated wherein polymeric film containing acetylcholine receptors was immobilised on to an interdigitated electrode to detect cholinergic agents (Taylor *et al.*, 1988). The detection was based on the change in electrical properties of the sensing surface (change in conformation of the receptors or change in ionic flux). Later it was observed that the interdigitated electrodes behave like capacitors that store or release charges as the analyte binds to the receptors (Taylor *et al.*, 1991).

In order to improve the sensing platform various methods have been used to immobilise the biological recognition layer on to the substrate. It was observed that the initial capacitance of the sensor surface should be high so as to detect binding of the analyte molecules (see section 3.2.1.4). An ultra thin insulating layer of tantalum oxide was deposited on the electrode surface forming a capacitor, wherein the electrode formed one of the plates of the capacitor and the second plate was formed by the electrolyte at the interface separated by an insulating layer in between (Gebbert *et al.*, 1992). The biological recognition molecules were immobilised on to the insulating layer. The detection of the binding of analyte was measured by the change in capacitance of the sensing layer.

One of the most commonly used insulating layers in the field of biosensing is self assembled monolayer, which are organic molecules consisting of polar head group to attach to the substrate (*e.g.* gold-thiol bond), hydrophobic tail and a functional group at the end of the tail for covalent attachment of biological recognition molecules (Whitesides *et al.*, 2005). An EIS based immunosensor for the detection of protein interferon-gamma (IFN-gamma) was developed by immobilisation of anti IFN-gamma antibodies on self assembled monolayer of acetylcysteine with a detection limit of 0.02 fg/ml (Dijksma *et al.*, 2001). Label-free detection of DNA hybridisation using impedimetric biosensors have been used wherein binding of complementary DNA oligomers to DNA probe molecules have been detected (Tlili *et al.*, 2005).

A capacitive biosensor was fabricated based on the immobilisation of monoclonal antibodies on to SAM formed by thiotic acid on gold surface to detect human chorionic gonadotropin hormone with a detection limit of 0.5 pg/ml (Berggren and Johansson, 1997).

The current trend in biosensors is in creating point-of-care diagnostic methods. The EIS based biosensing is considered as a potential technology for the fabrication of miniaturized biosensors. The label-free detection that avoids the use of complex and expensive pretreatment processes, ease of miniaturisation, cost effectiveness makes the impedimetric biosensors more attractive for the fabrication of multiplex analysis of different targets (Evans *et al.*, 2008).

## **Chapter 3. Background and techniques**

Since the fields of biology, chemistry, electrical engineering, and physics all congregate in biosensors, this chapter is an effort to bring essentially the concepts of biotechnology and electrical engineering together.

### **3.1. Background**

#### **3.1.1. Prokaryotic gene expression**

Gene expression is the process by which the genetic information on the DNA in the form of nucleotide sequence is used to direct the synthesis of proteins required for the sustenance of the cell.

Prokaryotic gene expression is controlled at two basic levels: the DNA is first transcribed into messenger RNA (mRNA) and then the mRNA sequence is translated into the polypeptide chain that forms protein.

As there is no compartmentalisation of the prokaryotic cell (no nucleus) unlike the eukaryotes, the transcription of the DNA and the translation of m-RNA are coupled together. This coupled transcription and translation is required for gene regulation.

##### **3.1.1.1. Transcription**

The prokaryotic transcription is initiated by binding of an enzyme called RNA polymerase to a specialized upstream DNA sequence called promoter. The RNA polymerase “core enzyme” binds to the DNA upstream of the gene in the promoter region, upon binding it is joined by another sub unit called sigma unit and starts unwinding the DNA double helix. It moves along the template strand and synthesises the complementary mRNA by adding nucleotides on the 3' end of the growing strand. At the terminator region that is usually present at the end of the coding sequence, the transcription is stopped and the mRNA molecule is released.

### 3.1.1.2. Translation

During the process of translation the mRNA is read according to the genetic code. A genetic codon is constituted by a group of three base pairs, which specifies a particular amino acid in a protein. The process of translation takes place in a specialised organelle called ribosome, which binds to the mRNA while it is still being transcribed. Ribosome consists of two subunits the large 50S and the small 30S (S for Svedberg unit). Simultaneously more than one ribosome binds to the mRNA forming a complex called polysome or polyribosome.

Initiation of translation involves the assembly of the ribosomal subunits on mRNA along with the first aminoacyl tRNA (the tRNA charged with the first amino acid) and the initiation factors. Elongation of the polypeptide chain takes place with the addition of amino acids to the carboxyl end of the growing chain. Finally, the termination of the chain occurs at the stop codon and the polypeptide chain is released from the ribosomal complex.

### 3.1.2. Gene regulation system – Operon

The bacterial cells are exposed to various environmental changes but most of the cells are able to adjust to these wide ranges of environmental changes. They are able to use their cellular resources in an efficient way by regulating the expression of genes that helps in economical production of various gene products. The simplest form of this regulation can be explained using the operon model.

An operon consist of an uninterrupted, continuous sequences of nucleotides usually clustered together under the same regulatory system. These clustered genes are generally responsible for a particular function like biochemical synthesis or metabolism. The best-studied cluster of such system is a group of three genes *lacZ*, *lacY*, *lacA* constituting the *lac* operon (Figure 3-1). These structural genes are involved in the metabolism of sugar lactose as an energy source in bacteria. This operon is usually off and is turned on only when lactose is present. Therefore, it is called an inducible operon. In case of *lac* operon, the *lac I* gene transcribes a repressor protein. This gene is continuously expressed and the repressor protein binds to the regulatory region called operator. Operator is present close to promoter and therefore,

in presence of the repressor protein, RNA polymerase cannot initiate transcription. When lactose is present in the environment, it enters the cell and gets converted into allolactose. Allolactose binds to repressor and inhibits it from binding the operator. This successful binding of RNA polymerase to the promoter turns the operon on and leads to transcription of all genes resulting in metabolism of lactose (Table 1). When the lactose level drops, less allolactose is present and repressor is active again. Isopropyl  $\beta$ -D-1-thiogalactopyranoside (IPTG) is a molecular mimic of allolactose and can be used to artificially induce the *lac* operon.

### **3.1.2.1. Catabolite repression of *lac* operon in *Escherichia coli*.**

*E. coli* prefers to use glucose over lactose when both of these molecules are present in the environment. Concentration of glucose in the environment inversely regulates the concentration of cyclic AMP (cAMP). Promoter of the *lac* operator has another binding site for the CAP (Catabolite activator protein) and the cyclic AMP (cAMP) shown in Figure 3-1. This complex assists the binding of RNA polymerase to the promoter of *lac* operon. As the amount of glucose increases the cAMP concentration decreases and the operon is turned off. This is called catabolite repression (Table 1).

The choice of right promoters and regulatory mechanisms helps in expression of recombinant proteins in the *E. coli* expression system.

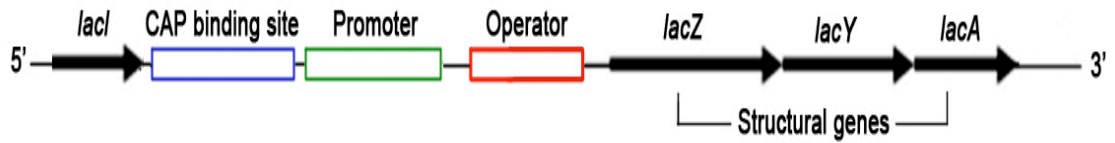


**Figure 3-1 Schematic representation of the *lac* operon in *E. coli*.**

The *lac* operon consists of four genes involved in lactose metabolism, *lacI* transcribes a repressor protein in absence of lactose in the environment, CAP binding site is the target for catabolite repression, promoter is the binding site for the RNA polymerase and the repressor protein produced by the *lacI* binds to the operator. The three structural genes *lacZ*, *lacY* and *lacA* encode for the enzymes  $\beta$ -galactosidase,  $\beta$ -galactoside permease and  $\beta$ -galactoside transacetylase.

Concentration of glucose	Concentration of lactose	Regulatory mechanism	Expression of <i>lac</i> genes
High	Available	CAP, promoter and operator free for binding	On, basal expression of <i>lac</i> genes
High	Unavailable	Repressor protein binds to the Operator	Off, no expression of <i>lac</i> genes
Low	Unavailable	cAMP binds to CAP and repressor protein binds to the operator	Off, no expression of <i>lac</i> genes
Low	Available	cAMP binds to the operator, Allolactose binds to the repressor protein and RNA polymerase binds to the promoter	On, of <i>lac</i> genes strongly expressed

**Table 1- Regulation of *lac* operon under variable concentrations of glucose and lactose.**

### 3.1.3. Recombinant DNA technology

Recombinant DNA technology provides the researcher with the opportunity of manipulating genetic information of an organism by integrating the DNA from different organisms. A DNA molecule obtained *in vitro* by unification of DNA from various sources is referred as a recombinant DNA.

#### 3.1.3.1. Vector

A vector is a recombinant DNA molecule that is used as a vehicle to carry foreign material into a host cell where it can be maintained in a stable condition and can replicate along with the host chromosomal DNA. *E. coli* is the most commonly used host organism because it can be grown easily and economically (Brown, 2001).

Vectors are developed from naturally occurring molecules such as bacterial plasmids. A plasmid is an extra chromosomal element of DNA in bacteria (about 2000-10,000bp). It is a small, covalently closed circular molecule independent of the host chromosome carrying genes that confer resistance to antibiotics, conjugation or metabolism of unusual substrates. Some plasmids are capable of replicating at a high rate in bacteria such as *E. coli* thus they can serve as carriers or vectors to allow replication of recombinant DNAs. Figure 3-2 shows a schematic diagram of a vector.

A vector typically has :

- Genes that confer resistance to antibiotics. One of these genes allows the cells to grow on a media containing an appropriate antibiotic *e.g.* ampicillin and tetracycline. Only the cells containing the antibiotic resistant genes will grow to form colonies.
- The bacterial origin of DNA replication that ensures replication of plasmid with the host cell.
- Restriction sites – Each restriction enzyme used for producing nicks in the DNA has a unique recognition site known as the restriction site. Plasmids are engineered to contain single recognition site for different restriction enzymes that include *Eco* RI, *Bam* HI, *Nhe* I, *Nde* I etc. These enzymes linearise the vector by creating sticky ends or blunt ends that help in ligation of foreign

DNA into the vector backbone. In some vectors many unique restriction sites are clustered into a region called multiple cloning site (MCS), to provide a choice of different restriction enzymes that can be used for manipulation.

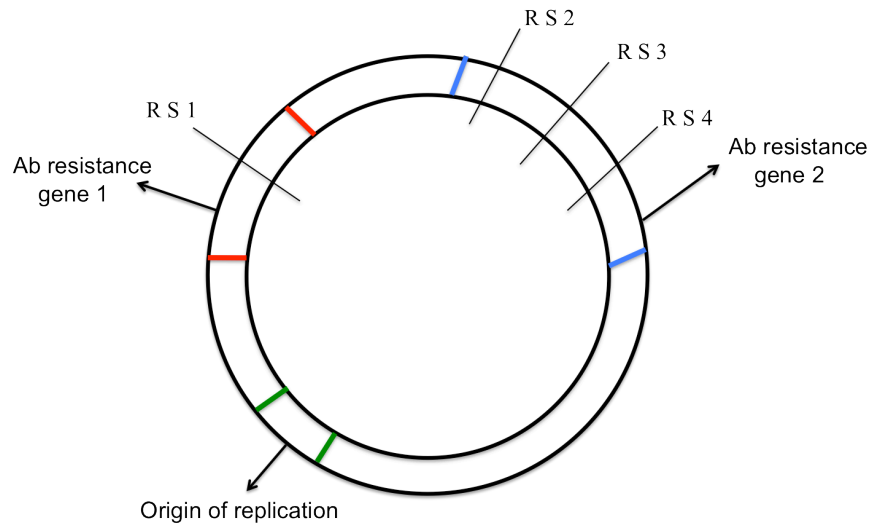


**Figure 3-2 Schematic representation of a cloning vector.**

A cloning vector comprises of the origin of replication, antibiotic (Ab) resistance genes and a number of restriction sites (RS).

### 3.1.3.2. Restriction digestion and ligation

The process of linearising the vector by use of restriction enzymes specific to the restriction sites present in the MCS of the vector is called restriction digestion. The linearised vector is treated with an alkaline phosphatase, this removes the 5' phosphate groups and thus prevents the vector molecule from recircularising. A foreign DNA flanked by the same restriction site can be integrated in the linearised plasmid to form a circular recombinant vector (Figure 3-3). The process of joining two DNA molecules, in this case the linearised vector and the foreign DNA fragment is termed as ligation. The enzyme involved in ligation is called DNA ligase. The two DNAs are incubated together with DNA ligase that seals the nicks (unformed phosphodiester bonds) by catalyzing the formation of phosphodiester bond. The 5'-phosphate of the foreign DNA and the 3'-hydroxyl of the plasmid can still be ligated and the nick will be repaired by the host bacterial system.

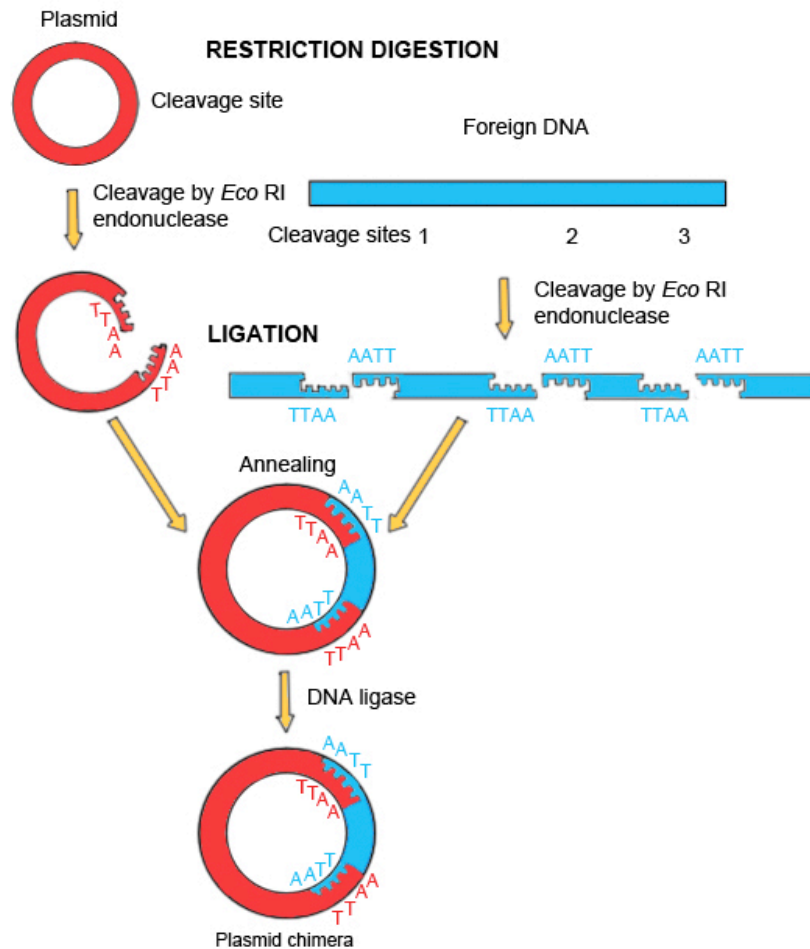


**Figure 3-3 Restriction digestion and ligation of foreign DNA and vector to generate a recombinant vector.**

The vector and the foreign DNA molecule are cleaved using the same restriction endonuclease enzyme (*Eco* RI) to generate the complimentary sticky ends. The foreign DNA molecule is ligated into the linearised vector by DNA ligase enzyme to form the recombinant plasmid. Adapted from (Wolfwikis).

### 3.1.3.3. Transformation

The recombinant vector prepared by ligation of the foreign DNA into the vector backbone is introduced in the host bacterial cell by the process of transformation. The cells are made competent by treating them with calcium at 4°C to make their membranes leaky. This permits entry of foreign DNA into the host cell. These cells can uptake DNA when subjected to a brief increase in temperature called heat shock treatment. Alternatively, electroporation is used where an electric potential is used to drive DNA into the cells.

### 3.1.4. Recombinant protein expression

The expression of a foreign gene ligated into a vector is dependent on regulatory elements surrounding it. The regulatory elements for gene expression in *E. coli* are:

Promoter - the binding site for bacterial polymerase to initiate transcription of the inserted gene.

Terminator- contains signal for the bacterial polymerase to terminate transcription.

Ribosome binding site - a nucleotide sequence recognised by the bacterial ribosome as the point of attachment on the m-RNA.

A foreign gene (eukaryotic / non-bacterial) is surrounded by eukaryotic / non-bacterial regulatory elements that are not recognised by the bacterial system. Thus, the recombinant vector has to be carefully designed by inserting the foreign DNA molecule with its regulatory elements after the regulatory elements of the bacterial system to accomplish expression of the inserted gene in a desired manner. The cloning vectors that can be used to produce recombinant proteins are called expression vectors. One of the popularly used expression vector is pET expression vector.

#### 3.1.4.1. pET expression system

The pET vectors are one of the most well developed cloning and expression systems for recombinant proteins in *E. coli*. It is based on a strong bacteriophage T7 promoter driven system (Studier and Moffatt, 1986; Rosenberg et al., 1987; Studier et al., 1990). T7 phage produces a T7 RNA polymerase that is very specific to the T7 promoter site and thus transcribes genes downstream of the T7 promoter. The gene of interest is downstream of the T7 promoter in the pET vector and the vector is introduced into an *E. coli* strain that has a chromosomal copy of bacteriophage T7 polymerase. T7 promoter is not recognised by the host cell RNA polymerase thus maintaining the gene in a transcriptionally silent state. The T7 polymerase gene is under the control of lacUV5 promoter (Studier and Moffatt, 1986). The lacUV5 promoter is insensitive to cAMP-CAP complex that does not require binding of RNA polymerase to the promoter to initiate transcription (Figure 3-1). Therefore, the protein expression is driven by this mutant promoter even in rich nutrient broth. The

lacUV5 promoter is inducible by IPTG and transcribes T7 RNA polymerase gene, which in turn expresses the target protein.

Using IPTG for the induction of the protein expression under the control of T7 *lac* promoter has many disadvantages. To achieve optimal induction conditions, it needs constant monitoring of the bacterial growth and addition of inducer at the proper stage of growth. Moreover, unintended expression of the proteins can be caused due to small amount of lactose present in the complex media. Therefore, development of non-inducing or auto-inducing media to inhibit undesired induction of the T7 *lac* promoter is essential.

#### **3.1.4.2. Auto induction media**

Autoinducing media (AIM) have been formulated (Studier, 2005) for high level of protein expression without the need of monitoring the cell growth or adding an inducer. AIM is formulated to grow IPTG-inducible expression strains in a defined media based on a mix of carbon sources (generally glucose, lactose and glycerol). The glucose is metabolised preferentially preventing the uptake of lactose. Lactose uptake starts once the glucose concentration drops and  $\beta$ -galactosidase converts lactose to allolactose. Allolactose releases the lac repressor and induces the T7 RNA polymerase expression from lacUV5 promoter in DE3 strains allowing the expression of the target gene.

#### **3.1.5. Proteins**

Proteins form the centre of action in biological processes. Proteins are major active elements in expression of genetic information. An organism's protein composition is the direct expression of its genetic composition. They can work as enzymes catalysing the complex set of chemical reactions that are collectively responsible for the cellular function; or act as chemical messengers known as hormones and are also the receptors for those hormones or as immunoglobulin that form an essential biological defence mechanism in higher organisms.

The structural description of proteins has been traditionally described in terms of four forms: primary, secondary, tertiary and quaternary structure (Voet and Voet, 1995).

The primary structure of a protein, amino acid chain is depicted in Figure 3-4. Amino acids are joined together through the formation of peptide bonds. The pair of linked amino acids is called a dipeptide and a long chain of amino acids is known as polypeptide. Proteins have an N-terminus (containing an amino group) and a C-terminus (containing a carboxylic acid group).

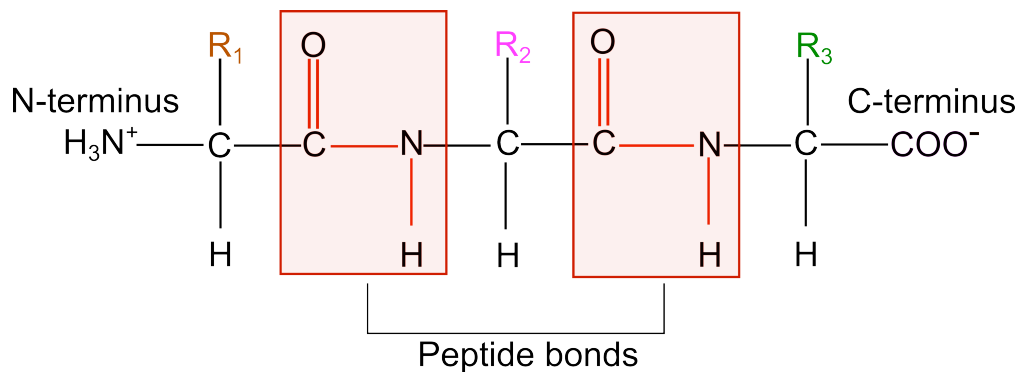


**Figure 3-4 Primary structure of a protein.**

The primary structure of a protein consists of a backbone of amino acids wherein each amino acid comprises of an amine group at one end and a carboxylic group at the other end. Two amino acids are bonded together via a peptide bond between the carboxylic group of one amino acid and amine group of another amino acid. The side residues are designated as R.

The secondary structure is the local spatial arrangement of the polypeptide's backbone. The main elements of the protein secondary structure are the helices and the pleated sheet structures. The helices have chirality *i.e.* they can be either right-handed or a left-handed helix. In the  $\beta$ -pleated sheets the hydrogen bonding takes place between neighbouring polypeptide chains rather than within the same chain as in  $\alpha$ -helix. It comes in two varieties: The anti-parallel  $\beta$ -pleated sheet in which the neighbouring hydrogen bonded polypeptide chains run in opposite directions and the parallel  $\beta$ -pleated sheet in which the hydrogen bonded chains extend in the same direction.  $\beta$ -structure is stabilised by intermolecular hydrogen bonds between  $-\text{NH}$  and  $-\text{CO}$  groups of adjacent polypeptide chains (Figure 3-5(a)). The protein's remaining polypeptide segments have a coil or loop conformation.

Tertiary Structure of a protein is the three dimensional structure of the entire polypeptide chain shown in Figure 3-5(c). It involves the folding of its secondary structural elements, together with the orientation of its side chains. It is constituted by steric relationship between the amino acids located far apart but brought closer by folding. Many proteins are composed of two or more polypeptide chains referred to as subunits, bound through non-covalent interaction or disulphide linkages. The arrangement of the subunits of two or more polypeptide chains forms the quaternary structure shown in Figure 3-5(d). The contact regions between the subunits consist of packed non-polar side chains, hydrogen bonds involving the polypeptide backbones and their side chains, and in some cases interchain disulphide bonds too.

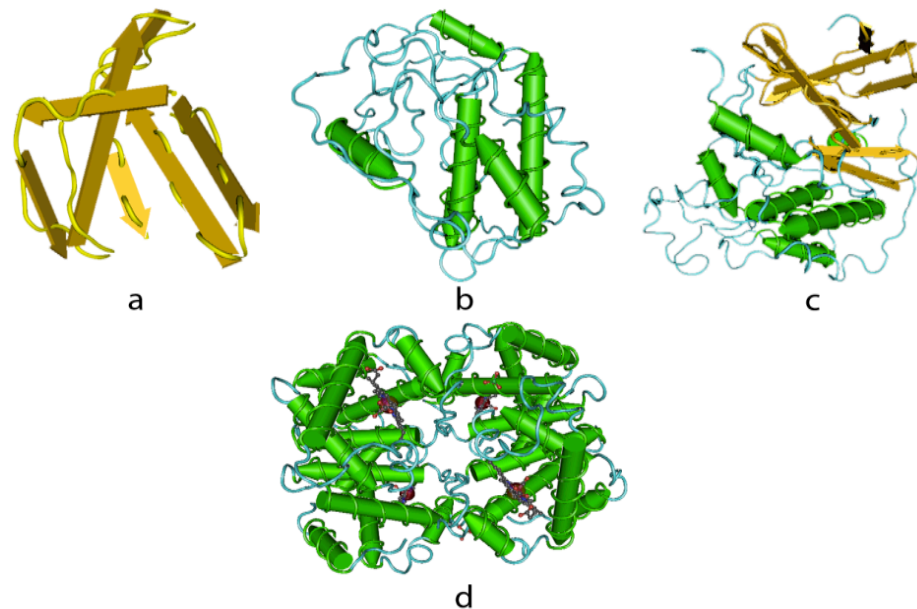


**Figure 3-5 Secondary, tertiary and quaternary structure of protein.**

Structure of Human CDK-2 (Schulze-Gahmen et al., 1996): a)  $\beta$ -sheets, b)  $\alpha$ -helix, c) Tertiary structure and (d) Quaternary structure of Haemoglobin (Safó and Abraham, 2005).

### 3.1.6. Antibodies

Antibody molecules are made up of four peptide chains consisting of two identical light chains (25,000 Da MW) and two identical heavy chains (MW >50,000 Da). Each light chain is bound to a heavy chain by a disulphide bond and by other non-covalent interactions such as salt linkages, hydrogen bonds and hydrophobic bonds to form a

heterodimer (H-L) shown in Figure 3-6. Such interactions connect the two identical heavy and light (H-L) chain combinations to each other thus forming the basic antibody structure. Amongst the antibodies of different specificity the first 110 amino acids of the amino terminal region of a light chain or a heavy chain show variability. These regions are called V regions:  $V_L$  in light chain and  $V_H$  in heavy chain (Kindt *et al.*, 2007).

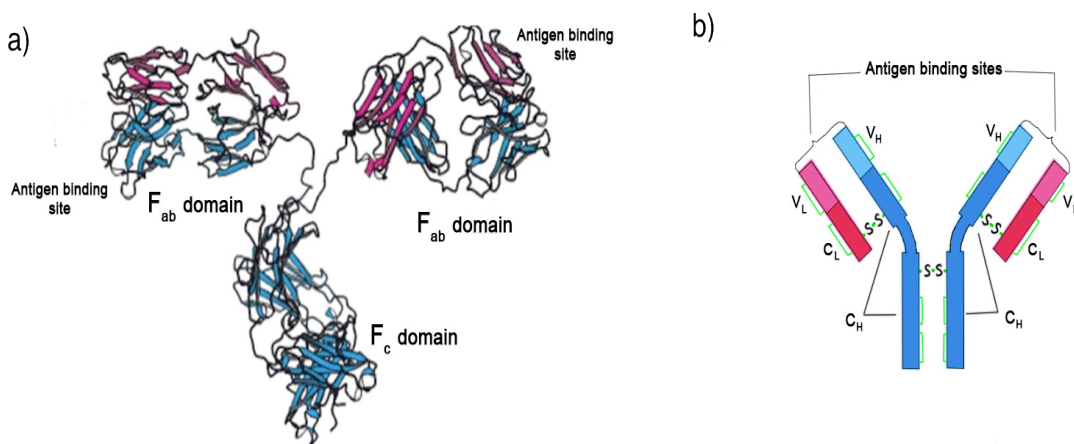


**Figure 3-6 Basic structure of an antibody (immunoglobulin).**

(a) IgG antibodies consist of four chains, two heavy chains (blue) and two light chains (red), linked by disulphide bonds. The heavy and light chains come together to form Fab domains, which have the antigen-binding sites at the ends. The two heavy chains form the Fc domain. The Fab domains are linked to the Fc domain by flexible linkers. (b) A schematic representation of an IgG molecule showing the antigen bonding sites, variable and constant region of heavy and light chains, and the disulphide bonds holding them together (Berg *et al.*, 2002).

The structure of each of the four heavy and light chain domains has the characteristic immunoglobulin fold consisting of two antiparallel sheets with an intermolecular disulphide bond. Most of the variation in the V region lies in the areas called complementarity-determining-regions (CDR's) and these CDRs (hypervariable loops) on both heavy and light chains form the antigen-binding site of the antibody molecule. The diversity in the variable region of the antibodies in living systems is generated through various factors such as the re-arrangement of the multiple gene segments in the germline DNA, somatic hypermutations, junctional flexibility. This unique property of antibodies is the key to their usefulness in immunosensors where a

device comprising an antigen or antibody species is coupled to a signal transducer, which detects the binding of the complementary species (Kindt *et al.*, 2007).

### 3.1.7. Phage Display Library

Phage display is a molecular technique where peptides or protein variants are displayed on the outer surface of bacteriophage (viruses infecting bacteria), encapsulating the genome of the displayed chimeric protein inside the phage particle.

#### 3.1.7.1. M13 phage genome

Filamentous bacteriophage M13 infects bacterial strains containing thread like appendages called F pilus. The bacteriophage particle is approximately 6.5 nm in diameter with a single stranded genome of about 6400 nucleotides. The phage genome is encapsulated in a flexible cylinder that is composed of major coat proteins pVIII encoded by gene VIII (Figure 3-7). At one end of the cylinder there are five molecules each of gene III and gene VI proteins. On the other end five molecules each of the small hydrophobic gene VII and gene IX proteins. This end contains packaging signal and is the first part of the phage to be assembled (Barbas *et al.*, 2001).

#### 3.1.7.2. Phage infection

The phage infection in a bacterial cell starts from the interaction of the F conjugative pilus of the bacteria with one of the domains of pIII protein of the bacteriophage (Figure 3-7). The pilus retracts and brings the pIII protein end into the periplasm of the bacterial cell. As the phage DNA is translocated into the cytoplasm the major and minor capsid proteins disassemble and join the population of newly synthesised phage proteins. The bacterial enzymes synthesise a complementary strand (-) against the viral single stranded DNA. The two strands form a covalently closed, supercoiled double stranded DNA called the parental replicative form (RF) DNA. The negative strand of the RF is the template for replication, which produce mRNAs that are then translated into phage proteins. The pII protein nicks the (+) strand resulting in a 3'hydroxyl that acts as a primer and a new viral strand is synthesized *via* rolling circle mechanism using bacterial enzymes. After one round the pII circularise the displaced

(+) strand which then forms a double stranded RF. The pV binds to the progeny (+) strands and prevents the RF formation. The pX also helps in proper replication of phage DNA. pII, pX, pV are present in the cytoplasm whereas the other phage proteins are incorporated into the bacterial membrane.

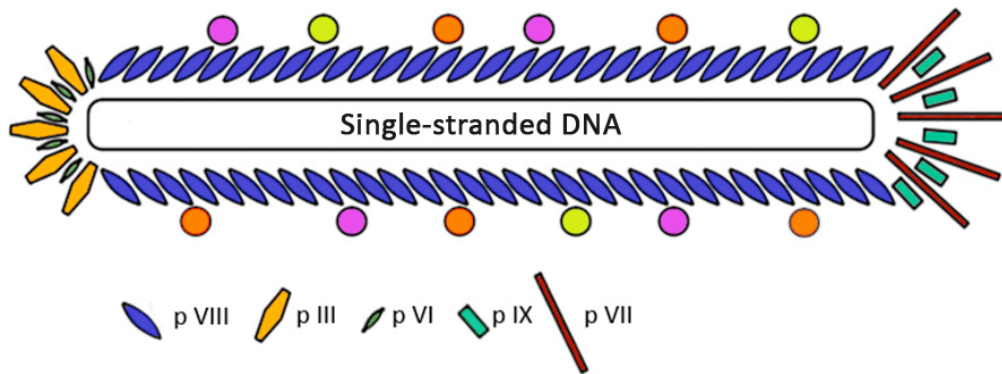


**Figure 3-7 Filamentous bacteriophage M13.**

In a M13 bacteriophage, the single stranded viral DNA coding for the proteins scFv and pIII is encapsulated by major coat protein pVIII. Typically five copies of pIII and one or zero copy of the scFv is displayed on the phage. The other proteins pVI, pIX and pVII are provided by the helper phage genome in the *E. coli*.

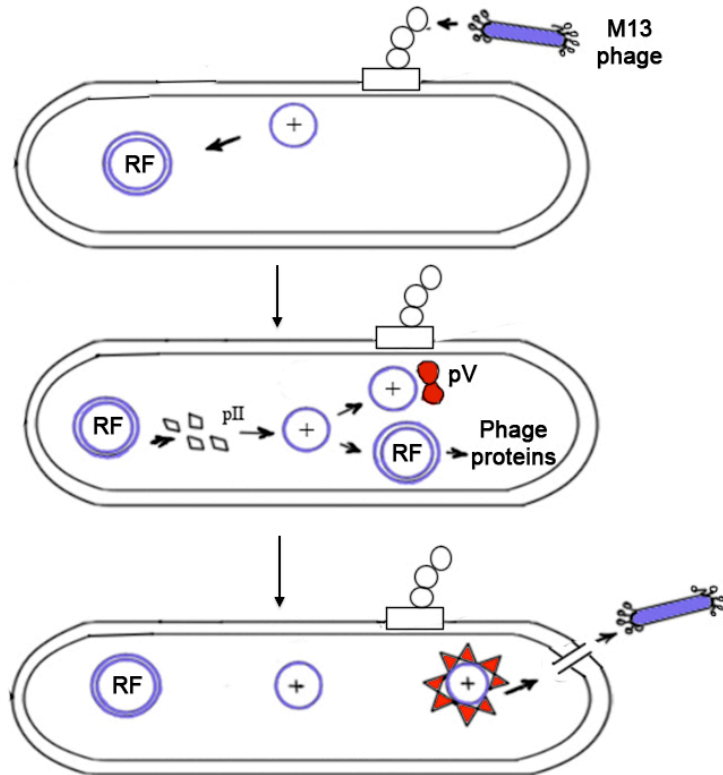


**Figure 3-8 Life cycle of bacteriophage.**

The life cycle of bacteriophage in bacteria involves infection, amplification of viral genome and assembly and release of new phage particles out of bacterial cell. The filamentous bacteriophage uses F pilus of the *E. coli* to insert its single stranded DNA. Single stranded DNA of the virus is changed into a double stranded molecule by the host machinery and is called replicative form (RF). Then the host machinery leads to production of viral proteins that are later assembled as new phage particles and released outside the bacterial cell. Adapted from (Drew, c2011).

### 3.1.7.3. Display of recombinant proteins on phage particles

In conventional phage display libraries, DNA fragments encoding peptides or proteins are incorporated into the phage genome so that the foreign peptides or proteins are displayed on the surface of the phage particles. Generally proteins are fused to pVIII and pIII coat proteins of filamentous phage. Insertion of the fusion sequence along the pVIII protein produces phage particles exposed along the surface of the phage but the inserts more than 6-8 residues are less efficiently packaged into the capsids. In case of pIII chimeric proteins larger inserts can be packaged well into the capsids. Although, a truncated form of pIII expressing the carboxy domain helps in incorporation of the fusion proteins into the phage coat proteins but the amino terminal domain of pIII prevents superinfection of a bacterial cell already infected once by a phage. To overcome these problems and enhance the phage display screening a phagemid vector is used.

#### *Phagemid*

A phagemid is a plasmid that bears a plasmid origin of replication, an antibiotic resistant marker for selection, origin of replication for viral and complementary strand synthesis. The phage particles are not released from the *E. coli* cells unless they are infected by helper phage. Helper phage provides structural proteins that are required for replication of the phagemid genome. To design phagemid vectors that express pIII fusion proteins, the amino terminal domain of pIII is deleted in order to allow infection by helper phage. Therefore only a part of pIII contains the displayed protein whereas the rest of the domain is expressed in the helper phage genome, which expresses the wild type pIII.

The phagemid DNA is packaged into the phage particles when the helper phage superinfects the bacterial cells. The helper phage bears a defective origin of replication so that packaging of the phagemid genome is favoured over the helper phage genome.

*pBSTG1*

pBSTG1 is a phagemid derived from pDHis II that was developed from pHEN1 (Hoogenboom *et al.*, 1991). It was used in the project to clone gene sequence for Adhiron 92 (see section 4.1) at *Nhe* I and *Not* I restriction sites (Figure 3-9). It consisted of a recombinant coding sequence flanked by *Nhe* I and *Not* I restriction sites. The fusion coding sequence in the phagemid vector consisted of DsbA secretion signal peptide, Adhiron, TAG codon and C-terminal half of gene III (*gIII*) of M13 bacteriophage. A signal sequence of DsbA (a periplasmic disulphide bond oxidoreductase) -DsbAss is fused to the protein coding sequence to allow efficient translocation to the periplasm. A histidine tag is introduced at the C-terminus of the Adhiron before the amber stop codon that helps in its purification using metal ion affinity column. A C-terminal fusion of a truncated *gIII* coding sequence is generated, allowing expression of a protein – pIII coat protein fusion. A small-unstructured colicin linker is inserted between the protein of interest and the pIII coat protein to present the protein of interest away from the surface of phage particles. The phagemid is referred to as pBSTG1-Adh. Only domain 3 of the pIII coat protein, which is required for insertion into the phage particle coat, is expressed. Therefore, one of the coat proteins on the surface of the phage particle must be from the wild-type pIII (from helper phage) in order for the phage to be able to re-infect *E. coli* and allow further rounds of screening. A small-unstructured colicin linker is inserted between the Adhiron and the pIII coat protein to present the Adhiron away from the surface of phage particles. A suppressible amber stop codon (TAG) is included between the protein of interest and pIII coat protein coding sequences, which is not recognised as a stop codon by suppressor strains of *E. coli* (*supE* strains) such as BL21 Star or ER2738. Suppressor strains have a mutation in the tRNA anti-codon loop which reads the TAG codon as glutamine instead of a stop codon thus generating the full-length fusion protein linked to the pIII coat protein. In non-suppressor strains (*e.g.* JM83), the amber stop codon is translated as a stop codon thus generating only soluble protein fragments, not linked to the pIII coat proteins.

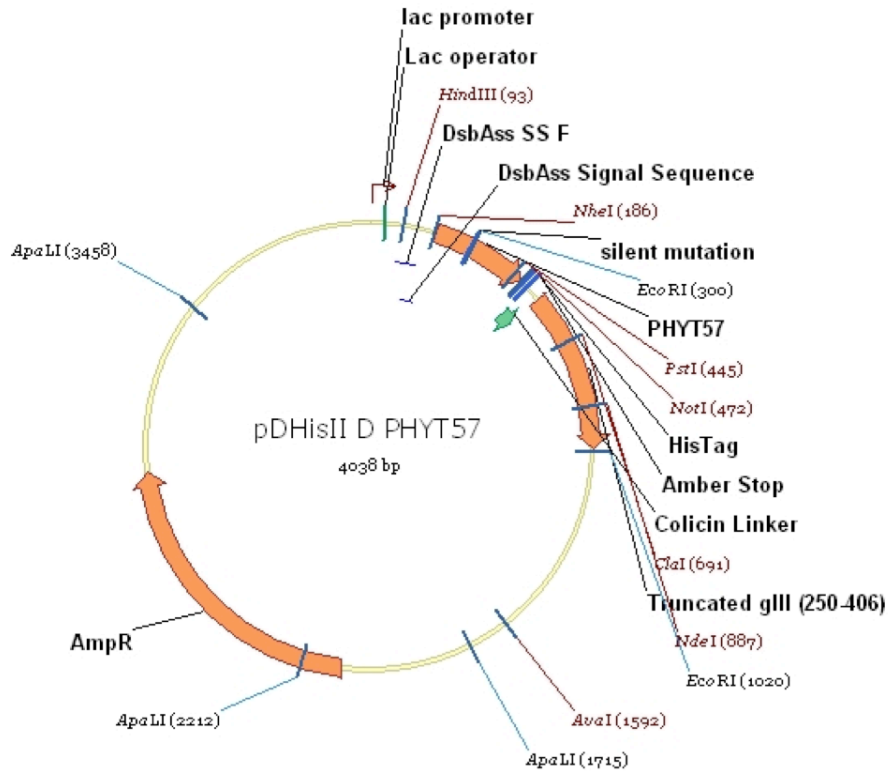


**Figure 3-9 Shows the vector map of pBSTG1 Adh phagemid.**

The binder sequence is PHYT57 (Phytocystatin 57) is flanked by *Nhe* I and *Not* I restriction sites followed by 6 histidine tags. Colicin linker coding sequence codes for a small linker between the binder and the coat protein to present the binder away from the surface of phage particles. *gIII* gene fused with the binder sequence expresses the truncated part of the pIII coat proteins and helps in incorporating the fusion proteins into phage coat proteins. DsbAss signal sequence targets translocation of the fusion protein to the periplasm. (Figure provided by Sarah Deacon, Astbury Centre for Structural Molecular Biology).

#### 3.1.7.4. Biopanning

Once the chimeric protein is presented on the surface of the bacteriophage, the phage particles are selected against the targets (antibodies, enzymes and other protein or non-protein molecules) using a selection process called panning (Figure 3-10). The library of the phage-displaying chimeric proteins is incubated on a receptor-coated surface. The surface is washed to remove non-specifically bound phages and the specifically bound phage particles are eluted out.

To enrich the pool of binding sequences bacterial cells are infected with the eluted phage followed by an infection with a helper phage. This cycle can be repeated 3-4 times with each cycle followed by an amplification step for more effective selection.

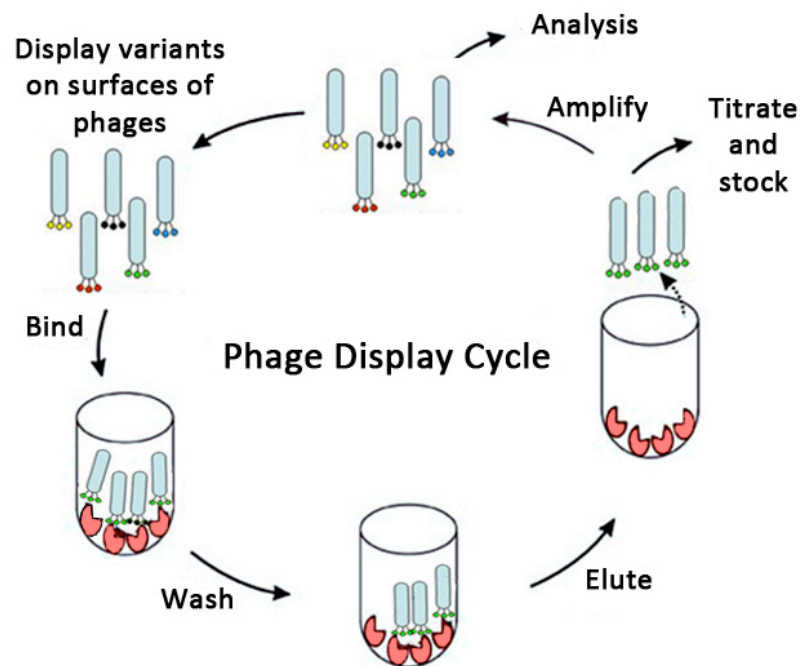


**Figure 3-10 Phage selection using Biopanning.**

The phage display libraries displaying peptide product on the bacteriophage are selected by an affinity based selection procedure called panning. It involves binding of the phage displaying chimeric protein by incubation on the receptor coated surface. The non-specifically bound phage particles are removed by washing and the specifically bound phage particles are eluted in end and the eluted pool is enriched by repetitive cycles of infection of selected phage particles in *E. coli*. Adapted from (Microbewiki, 2010).

## 3.2. Techniques

### 3.2.1. Electrophoretic techniques

Electrophoresis is defined as the migration of charged particles under the effect of electric field induced between the positive (anode) and the negative (cathode) electrode. Various biomolecules like proteins, oligonucleotides and nucleic acids exist as charged molecules at a particular pH in a solution. When an electric field is applied to move the molecules through the gel matrix, the cations (positively charged ions) move towards the cathode and the anions (negatively charged ions) move towards the anode (Wilson and Walker, 2000). A potential gradient,  $E$  is generated when a voltage difference is applied across the electrodes.  $E$  is equal to applied voltage ( $V$ ) divided by the distance between the electrodes ( $d$ ).

The velocity of the charged molecule is dependent on the force applied on the molecules bearing charge, ( $q$ ) Coulombs. The force applied is equal to  $E \times q$  Newtons. Taking into consideration the frictional force ( $f$  is the frictional force coefficient) on the molecule due to shape of the molecule, viscosity of the buffer, pore size of the medium, the velocity of the molecule is given by Equation (3.1)

$$v = E q / f \quad (3.1)$$

Ratio of the velocity of the ions to the electric field is termed as electrophoretic mobility ( $\mu$ ). The movement of the molecules when a potential difference is applied is dependent on their charge as well as the molecular weight.

A current is generated in the solution by the buffer ions as well as by the sample ions to a small proportion. Ohm's law expresses the relationship as between voltage, current and resistance as (Equation 3.2):

$$V/I = R \quad (3.2)$$

$V$  is the voltage applied between the electrodes (Volt),  $I$  is the current generated (Ampere) and  $R$  is the resistance (Ohm).

Ohm's law demonstrates that if the voltage is increased, it leads to increase in current and thus accelerates the electrophoretic separation. However, current

produces heat and excessive heat can lead to irregular movement of samples in the gel.

Electrophoresis is carried out on a porous support in which the buffer ions and the samples are able to migrate under the applied electric field. The two commonly used gel matrixes are:

### **Agarose gel**

Agarose is a natural linear polysaccharide made up of agarobiose, which comprises of repeating units of D-galactose and 3,6-anhydrogalactose. On dissolving the agarose powder in a boiling buffer solution a macroporous matrix is formed which has a pore size depending on the percentage of agarose used. It is used in a concentration range of 1-3% depending on the size molecules to be resolved. These gels are used both for proteins and nucleic acids. As the pore size is larger therefore, its mostly used for DNA fragments of 50-20,000 bp in size.

### **Polyacrylamide gel**

Polyacrylamide is formed by polymerization of acrylamide monomer cross-linked by N, N'-methyl-bis-acrylamide (BIS). The polymerization of the acrylamide molecules takes place as a free radical catalysis in presence of ammonium persulphate (APS) and base N, N, N', N'-tetramethylethylenediamine (TEMED). These gels can have varied pore size depending upon the percentage of both acrylamide and bis-acrylamide. Gels composed of higher percentage of acrylamide (12-20% w/v) retard the migration of large molecules more than the smaller ones whereas in gels composed of lower percentage of acrylamide (4-8% w/v) higher molecular weight molecules move faster than the smaller molecules. In SDS gel electrophoresis higher percentage of acrylamide (10 to 20 % w/v) is used for the separation of protein molecules.

#### **3.2.1.1. Agarose gel electrophoresis of DNA**

DNA molecules are mostly run on an agarose gel because of their large size as compared to proteins. The smaller the DNA molecule the faster it moves. For DNA size that ranges from 5-60 kb, 0.3% (w/v) agarose is used and for DNA size in the range of 0.1-3 kb, 2% (w/v) agarose concentration is used. The conformation of

DNA affects the mobility of the DNA molecule in the gel. During the plasmid DNA preparation there are different forms of DNA observed on the gel. The uncut plasmid migrates faster than the linearised plasmid. In the uncut DNA, the supercoiled form of the DNA moves faster than the relaxed DNA of the same mass because the supercoiled DNA is more compact.

The DNA in the gel is stained with a fluorescent dye called ethidium bromide that intercalates between the DNA base pairs. Under the ultra violet light (300nm wavelength), DNA bands appear orange red. Considering the harmful effects of ethidium bromide as a carcinogen, there are many alternatives to ethidium bromide like SYBR-based dyes used in nucleic acid detection that are significantly less mutagenic. It is essential to protect eyes from UV while visualising the DNA bands.

### **3.2.1.2. Electrophoresis of proteins**

Sodium dodecylsulphate (SDS) polyacrylamide gel electrophoresis (PAGE) is used for the separation of protein mixtures according to their size. SDS ( $\text{CH}_3\text{-CH}_{210}\text{-CH}_2\text{OSO}_3^-\text{Na}^+$ ) is an anionic detergent that binds to the proteins and creates a constant charge : mass ratio on the proteins. All proteins acquire a constant mass to negative charge ratio and thus, the separation of the proteins is based on their size. For denaturation, the protein samples are treated with  $\beta$ -mercaptoethanol and SDS that reduce the disulphide bridges present in the protein tertiary structure and disrupts all inter and intra molecular interactions in proteins. This yields polypeptide chains that are resolved on the gel on the basis of their molecular weight.

The SDS PAGE is prepared with a narrow lower percentage polyacrylamide stacking gel poured over a primary polyacrylamide resolving gel. Proteins are loaded into the wells and under the applied electric field, the negatively charged protein molecules move through the stacking gel towards the anode.

This is done to concentrate the proteins in the stacking gel forming a sharp band before they enter the main resolving gel. This is important so that all the proteins in the sample enter the separating gel at the same time thus improving the resolution of the protein separation. Owing to its small size bromophenol blue dye is used in the

protein samples to indicate the electrophoresis front. The gel is removed and stained in Commassie Brilliant Blue that forms a non-covalent complex with the proteins producing a blue colour, which is seen on the gel. The gel is then destained which removes the unbound background.

### **3.2.1.3. Western blotting**

Western blotting is a method to detect specific proteins that have been separated on a gel according to their size by gel electrophoresis. The gel containing the separated proteins is placed next to the membrane and the application of electrical current induces the proteins in the gel to move to the membrane. The detection of the specific proteins is done using antibodies against the target protein.

The method used in this thesis to transfer the proteins to the nitrocellulose membrane is called semi-dry blotting wherein a sandwich of paper / gel / membrane / paper wetted in transfer buffer is held between two horizontal plate electrodes (cathode and anode). The blotted nitrocellulose membrane is then incubated with BSA (bovine serum albumin) or non-fat dried milk to block the hydrophobic sites on the membrane. Then it is incubated in primary antibody directed against the protein of interest. To visualise the interaction of the primary antibody with the protein of interest, the membrane is incubated in an enzyme conjugated secondary antibody, that binds to the primary antibody. The blot is then incubated in enzyme-substrate solution wherein the enzyme converts the substrate into a coloured product that is observed as a band on the nitrocellulose. One of the most common enzymes used in conjugation with the secondary antibodies is horseradish peroxidase (HRP). HRP is a 44 kDa glycosylated hemoprotein that acts as an oxidoreductase that is used to reduce hydrogen peroxide. This property of HRP is used to generate fluorescent or luminescent signals. Horseradish peroxidase can also be used in enhanced chemiluminescence (ECL). In ECL the substrate is hydrogen peroxide and a chemiluminescent substrate called luminol. HRP oxidizes luminol to produce light, which can be detected by exposing a photographic film to the emitted light.

#### **3.2.1.4. Enzyme-Linked Immunosorbent Assay (ELISA)**

Enzyme-Linked Immunosorbent Assay (ELISA) is a solid phase technique designed to detect and quantify molecules like peptides, proteins, antibodies and hormones. The antigens are immobilized on the wells of a microtitre plate either directly to the surface or through capture antibodies. The primary antibodies are then applied that bind the antigens. If the primary antibody is conjugated with an enzyme, the detection of the antigens can be done directly. Depending upon the target molecule under investigation, the different types of ELISA shown in Figure 3-11 are as follows:

##### ***Direct ELISA***

Antigens are immobilized on the surface and detected using enzyme-conjugated antibodies. On addition of an enzyme substrate, a visible colour is obtained which can be quantified using a spectrophotometer. The colour intensity can be correlated to the amount of the analyte (antibody or antigen) present in the sample (Figure 3-11(a)).

##### ***Indirect ELISA***

Due to the constraint of the availability of enzyme-linked antibody specific against each target antigen, a single labelled antibody that can be used against different antibodies is used. This has led to the use of indirect ELISA where an unlabelled antibody against the antigen is used and is detected by using an enzyme labelled anti-immunoglobulin (Figure 3-11(b)).

##### ***Sandwich ELISA***

The antigen to be measured is bound to the surface through capture antibodies. The antigen is detected using an enzyme-conjugated antibody by forming a sandwich of the analyte between two primary antibodies (Figure 3-11(c)).

##### ***Competitive ELISA***

A mixture of unlabelled antibody and the sample containing antigen are incubated together and then added to an antigen-coated well. After washing the wells to remove excess antibodies, a secondary antibody conjugated with an enzyme is added which is detected using an enzyme substrate reaction. If the amount of antigen is

high in the sample the signal obtained is low as the amount of antibodies bound to the coated antigens is low and *vice versa* (Figure 3-11(d)).

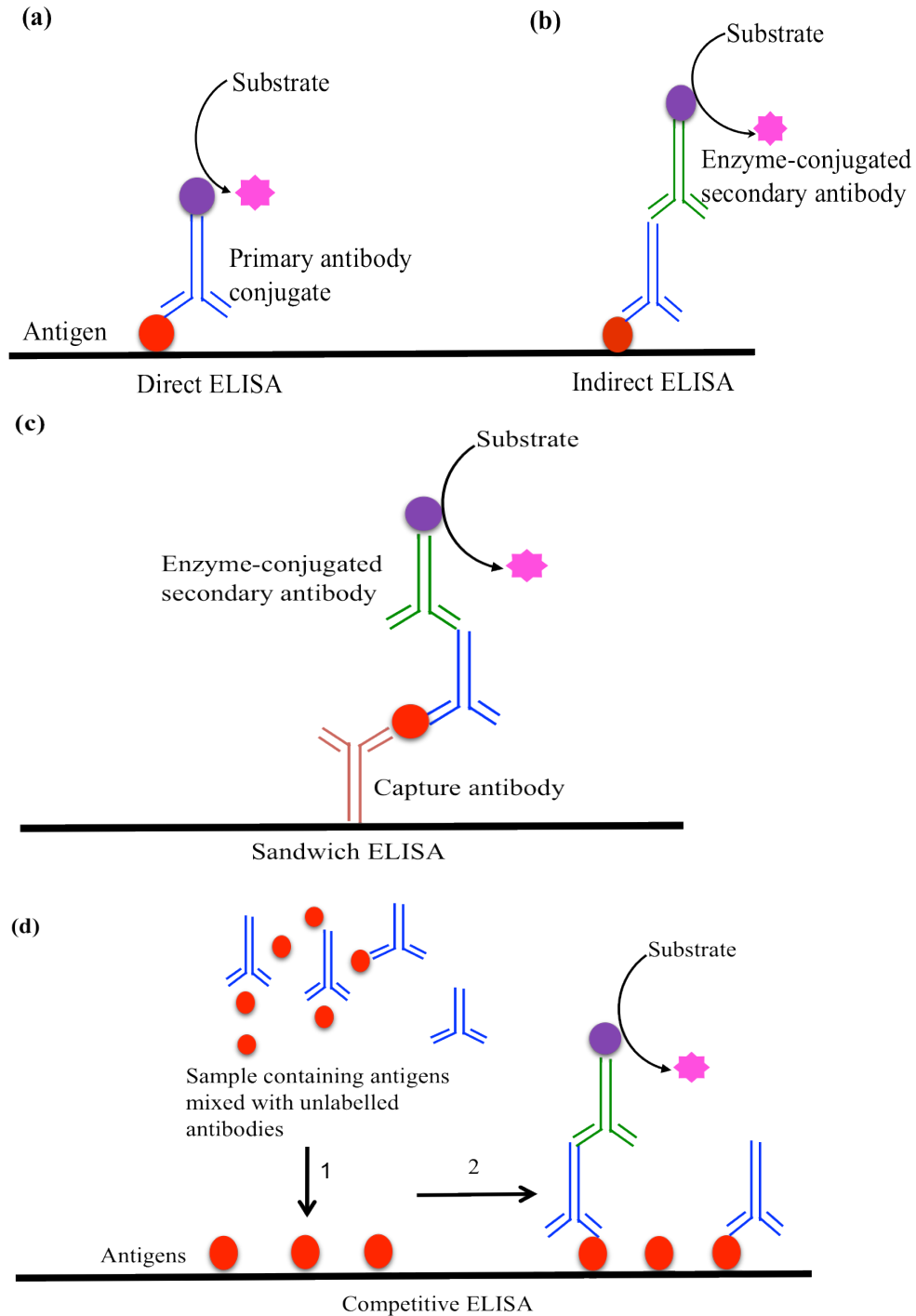


**Figure 3-11 Schematic representation of different types of ELISA.**

Adapted from (Abnova, c2014)

### 3.2.1.5. Protein purification using metal chelate chromatography

In this affinity chromatography an immobilised metal ion such as Cu, Zn, Hg, Cd or a transition metal like Co, Ni or Mn is used to purify proteins by reacting with indole groups in tryptophan, thiol groups in cysteine and imidazole groups in histidine tagged fusion proteins. The metals are generally bound to the matrix (agarose, sepharose) through iminodiacetate or tris (carboxymethyl) ethylenediamine ligands. The proteins with surface exposed amino acids form a coordinate bond that must be sufficiently stable to allow the protein to attach to the matrix and also can be retained when the non-specific contaminants are removed during elution. The strength of the binding of protein to the metal ions is dependent on various factors like pH of buffers, length of affinity tag. The release of proteins can be achieved by destabilizing the protein metal complex by changing the pH of the elution buffer or by using a complexing agent like imidazole. Histidine tagged proteins that contain a long stretch of histidine residues at the carboxyl or amino terminus of the protein binds to divalent or trivalent ions.

### 3.2.2. Spectrophotometry

Spectrophotometer is used to estimate the concentration of analyte in a sample based on the absorption or reflection of light by the sample. Spectrophotometry is based on the Beer-Lambert law, which states that the amount of light of a particular wavelength absorbed by a substance across a constant pathlength is directly proportional to both the concentration of absorber as well as the thickness of the layer as given in Equation (3.3).

$$A = \epsilon cl \quad (3.3)$$

Where  $\epsilon$  is the molar absorbance coefficient for the absorber at a particular wavelength ( $L \text{ mol}^{-1} \text{ cm}^{-1}$ );  $c$  is the concentration of absorbing solution ( $\text{mol L}^{-1}$ );  $l$  is the pathlength of the solution (cm).

Spectrophotometer consists of a light source capable of producing a whole range of continuous wavelengths. To allow only small range of wavelengths to be directed to the sample, filters and diffraction gratings are used to separate the light into its component wavelengths. After passing through the sample compartment, the

outcoming light is detected by the photodetector that converts the signal into absorbance, transmittance or the concentration values. The wavelength of light to be used depends on the sample to be detected. (The UV region lies between 200 to 400 nm and the visible region ranges from 400-700 nm)

In case of proteins with the aromatic amino acid residues namely tyrosine and tryptophan exhibits an absorption maxima at 280 nm (Pace *et al.*, 1995). Consequently proteins absorb UV-light in proportion to the aromatic amino acid content and the total concentration. The absorptivity coefficient of the proteins once established using their amino acid composition, the concentration of the proteins can be calculated.

The nucleic acids concentration can be measured at 260 nm mainly due to the electronic transitions by purines and pyrimidine components.

### **3.2.3. Circular Dichroism (CD)**

Circular dichroism is one of the methods to assess the structural properties of biomolecules. CD spectroscopy can analyse only optically active species. The optically active or chimeric molecules exist as mirror images.

CD is based on the concept of circular polarisation. When two linearly polarised light beams, oscillating perpendicular to each other and propagating with a phase difference of quarter wave superimpose on each other, the resultant wave is a helix and is called as a circularly polarize light (CPL). The helices are either right-handed or left handed CPL. Depending on the sample to be analysed different light sources are used in CD like far-UV to study secondary proteins, UV - analyse the tertiary structure of proteins and visible light- to monitor the interaction of proteins with metal ions.

In the CD spectrometer the sample is placed in a cuvette and a beam of light is passed through the sample. The light coming from the source is converted to CPL by an optical element termed as quarter-wave plate that keeps the two polarization states out of phase by a one quarter wave (Kelly *et al.*, 2005; Greenfield, 2007a; Van Holde *et al.*, 2006). Proteins have some important chromophores that include peptide bonds, disulphide bonds and aromatic amino acids. When a circularly polarised light

falls on a protein the secondary structural elements such as  $\alpha$ -helices,  $\beta$ -sheets,  $\beta$ -turns and random coil structures induce bands of distinct shape and magnitude (Figure 3-12). A helical structure shows an intense positive band at 190 nm and a negative band at 208 nm. The  $\beta$ -sheet protein has a negative band at 210-220 nm and a positive band between 195-200 nm.  $\beta$ -sheets may be parallel or anti parallel or mixed and therefore are more complex than the  $\alpha$ -helices. The spectrum showing a negative band around 200 nm may depict disorderliness / random coils in the protein.

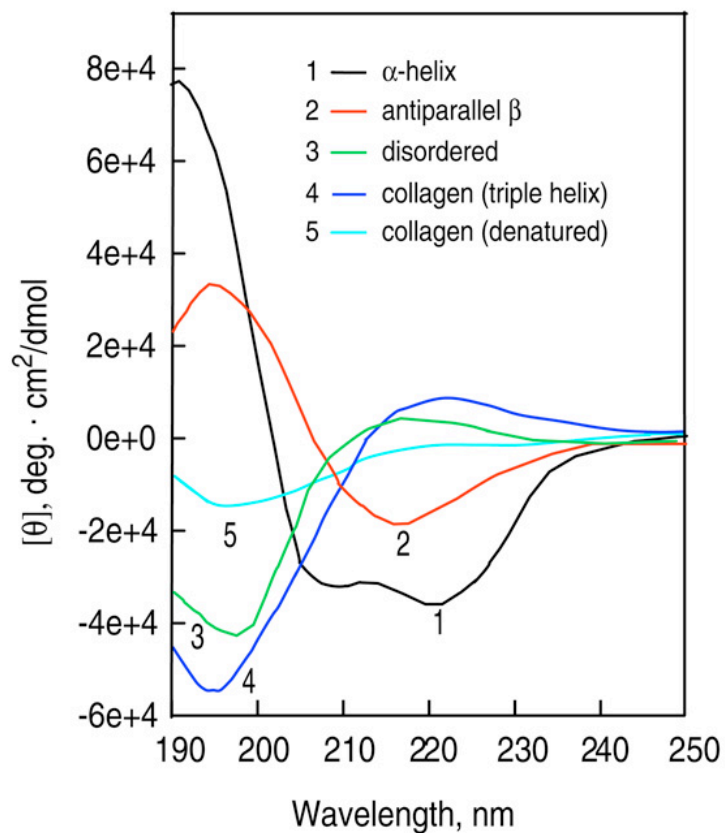


**Figure 3-12 Circular dichroism spectra.**

CD spectra of poly L-Lysine at pH 11.1 in the 1(black)  $\alpha$ -helical and red 2 (red) antiparallel  $\beta$ -sheet conformations and at pH 5.7 in the 3 (green) extended conformations and placental collagen in its 4 (blue) native triple-helical and 5 (cyan) denatured forms (Greenfield, 2007).

### 3.2.4. Differential scanning calorimetry (DSC)

DSC measures the change in the difference in heat flow rate to the sample and the reference material while the two specimens are subjected to identical temperature regimes in an environment heated or cooled at a controlled rate (Bhadeshia, 2002). Various DSC-based techniques have been developed to study the molecular transitions of biomolecules that includes unfolding processes in proteins, polynucleotides, and lipid assemblies. The heat capacity of a molecule changes as the thermal transitions take place with time and temperature.

By definition specific heat capacity is the amount of heat required to raise the temperature of a unit mass of a substance by 1 Kelvin. Molar heat capacity of a solution at constant pressure as a function of temperature is denoted as  $C_p$ .

In a basic DSC experiment, the sample cell contains a solution with the molecule of interest and a reference cell with only the solvent (Figure 3-13). Both the solutions in the cells are heated at constant rate. Difference in the heat energy uptake between the sample cell and the reference cell so as to maintain both the cells at the same temperature corresponds to the difference in heat capacities. This difference in heat capacity reveals the ability of the molecule to absorb heat and experience an increase in temperature. The output from any DSC experiment is a thermogram showing the excess heat capacity ( $C_p$ , sample minus reference) as a function of temperature (Cooper *et al.*, 2000).

In case of a protein molecule, as the temperature increases the protein changes its form from native to unfolded state that leads to change in the heat capacity of the protein.

Water (solvent) has a higher heat capacity than the protein because of its extensive hydrogen-bonding network. The non-polar groups of the protein molecule cannot make hydrogen bonds with the water molecules surrounding them. Therefore, the water molecules tend to maximize the hydrogen bonding within themselves leading to clathrate formation (Shinoda, 1977). Figure 3-13 shows three regions of thermogram of a simple globular protein: the pre-transition baseline, the endothermic unfolding transition and the post transition baseline.

As the temperature increases, the protein absorbs heat and the water molecules are exposed to the unfolding polypeptide chain and start reorganizing themselves as more non-polar side groups are exposed. The unfolding of the protein takes place over a temperature range characteristic for that protein. The pre-transition baseline shows a slightly positive slope as the heat capacity increases gradually with the temperature, giving rise to endothermic peak. The peak reaches to approximately the mid point temperature of process or the transition temperature ( $T_m$ ). At the transition point 50% of the protein is in the native state and the rest is denatured. A sharper peak in the thermogram indicates that the process is cooperative such that change in a single structural association disturbs all other points of association.

During the post transition process, the unfolding is complete and heat absorption decreases. A new baseline is established, that represents the  $C_p$  of the unfolded polypeptide and is usually found at a higher level than the pre transition baseline. The shift in the baseline is denoted as  $\Delta C_p$ . The partial heat capacity ( $C_p$ ) of the protein includes the heat capacity of the protein as well as the effect that protein has on the solvent (Freire, 1995). The heat capacity contributed by the protein is determined by subtracting a scan of a buffer blank from the protein sample before analyzing the data. (Arntfield and Murray, 1981).

The various factors responsible for the stability of the proteins involve hydrophobic interactions, hydrogen bonding, and conformational entropy (Pace *et al.*, 1996). The melting point or the transition point indicates the thermal stability of the protein. The higher the melting point, less susceptible the protein is to unfolding and denaturation at lower temperatures (Bruylants *et al.*, 2005). Reversibility of unfolding can be established by rescanning the sample under same conditions so as to obtain a second endothermic peak that superimposes the first peak. The determination of the reversibility of unfolding is important for extracting the complete thermodynamic properties of the protein (Chôma, 2006).

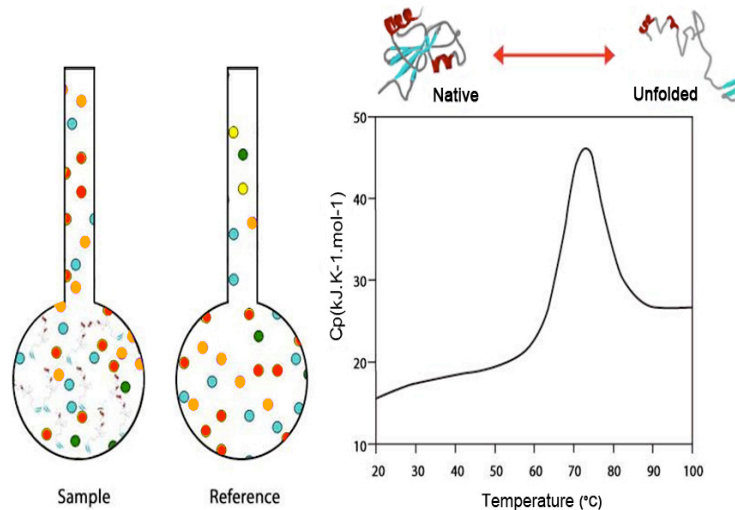


**Figure 3-13 Differential scanning calorimetry.**

Shows two cells heated at the same rate, the reference cell and the sample cell. On the right hand side is a thermogram that shows the change in partial heat capacity ( $C_p$ ) as the temperature increases. The  $C_p$  increases as the protein unfolds from its native state to an unfolded state. At the peak temperature  $T_M$ , half of the proteins are in native state and the rest are in denatured state. Adapted from (Frasca, c2014).

### 3.2.5. Surface plasmon resonance (SPR)

It is a technique to measure label-free biomolecular interactions in a real time environment while the ligands are immobilized on the surface and the analytes are passed over the surface. SPR based instruments use an optical method to measure the refractive index at an interface between two media of different refractive index. When a linearly polarised light comes from the higher refractive index (half circular prism), it bends towards the plane of interface (Figure 3-14). At a certain incident angle called the critical angle all the incident light is reflected within the circular prism. This phenomenon is called as the total internal reflection. Although the incident light is completely reflected but the electromagnetic field component is created in the lower refractive index media. This field is called as evanescent wave because there is an exponential decay of the wave amplitude with increasing distance from the interface. It has a depth of  $\sim 300$  nm from the sensor surface that is used for the measurements.

On the reflection side the prism is coated with a thin film of a noble metal. Gold is the most common metal used in most of the cases because it gives an SPR signal at convenient combinations of reflectance angle and wavelength. The intensity of

reflected light is reduced because of energy transfer to the gold electrons. When the energy of the incident light is just enough to excite the electrons on the gold surface, surface plasmon resonance is induced causing a dip in the intensity of reflected light. The angle at which the resonance occurs is called the resonance angle that depends on the refractive index of media on both sides of the thin gold film as well as the mass adsorbed onto the immediate vicinity of the film. The angle of resonance is sensitive to any change in the refractive index (RI) of the medium adjacent to the metal surface. For the detection of an interaction, one molecule (the ligand) is immobilised onto the sensor surface and an aqueous solution of the target molecule (analyte) is injected. When the binding takes place and the mass of analyte increases on the surface, there is a change in refractive index. This change of refractive index causes change in the angle of light at which the surface plasmon resonance occurs. Since it is not advantageous to directly deposit the biomolecules onto the surface, therefore surface functionalisation is done to create functionally active environment and to reduce non-specific binding.

This change in refractive index is measured in real time depicted by a sensorgrams and the result is depicted as response units (RU). The sensorgram provides important information about the rate of interaction including association and dissociation constants that provides information about the ligand-analyte binding kinetics.

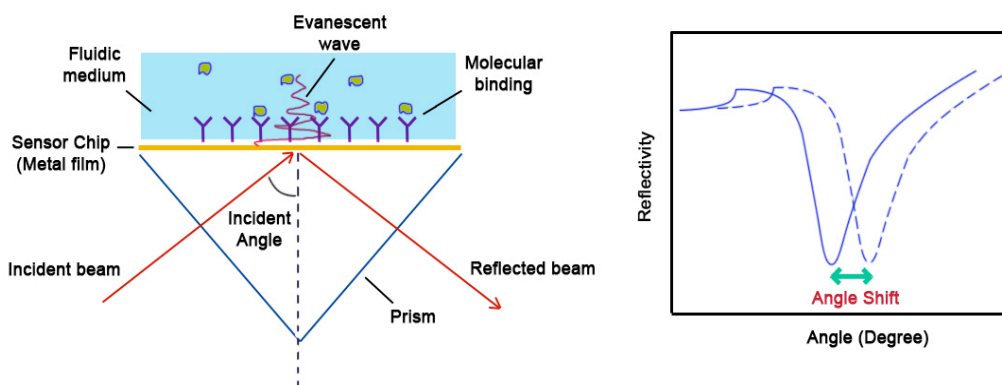


**Figure 3-14 Surface plasma resonance.**

The incident light falls on the hemi-cylindrical prism, it bends towards the plane of interface due to total internal reflection. Also there is an electromagnetic field component created in the lower refractive index that causes a dip in the intensity of reflected light. Adapted from (Biocompare, 2012)

### 3.2.6. Electrochemistry

Electrochemistry is the study of interplay between electricity and chemistry *i.e.* the relationship of chemical aspects to the electrical entities like current, potential or charge. Electrochemical processes take place at the electrode-electrolyte interface . The electrode surface forms a junction between the two phases formed by an ionic conductor and electronic conductor. This project involves the study of the processes between the two neighbouring phases that is influenced by the change in the properties of the interface. To understand the interfacial layer of the electrode and the electrolyte it is important to understand the concept of electrical double layer.

#### 3.2.6.1. Electrochemical double layer

Electrical double layer (EDL) is made up of electrical charge at the surface of the electrode itself and the charge of ions in the solution at small distance from the electrode surface. The charge on the electrode surface attract ions of opposite charge thus forming an ion atmosphere in the immediate vicinity of the electrode. This structure is called as electric double layer.

The electrical properties of the double layer can be related to a conventional plate condenser where the capacitance is given by Equation (3.4)

$$C = \epsilon \epsilon_0 A/d \quad (3.4)$$

Where C, capacitance between the parallel plates of the condenser (Farad /F);  $\epsilon$ , permittivity of the medium between the condenser plates (F/m);  $\epsilon_0$ , permittivity of the vacuum (F/m); A, electrode area ( $m^2$ ); d, distance between the charged plates (m).

The factors that affect the electrical double layer capacitance include the electrode material, area of the electrode, the electrolyte surrounding the electrode (Lu *et al.*, 2013).

### 3.2.6.2. Electrolytic cell

Electrolytic cell consists of a working electrode (WE) and a reference electrode (RE) surrounded by an electrolytic solution. One of the main electroanalytical instruments used to measure electrochemical reactions when a metal electrode is surrounded by an electrolyte is called a potentiostat. The potentiostat keeps the working electrode at a fixed potential with respect to the RE. The following section describes the different types of electrodes in an electrolytic cell.

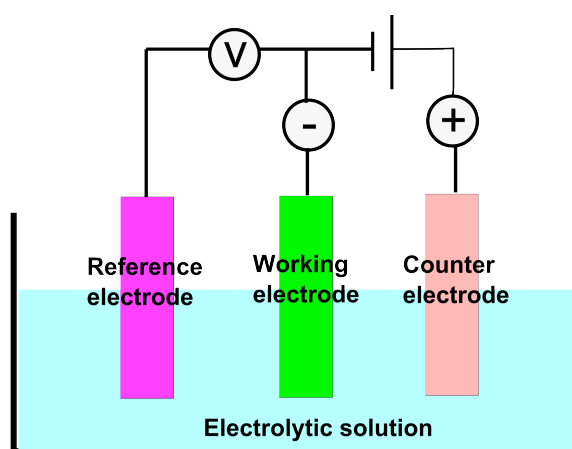


**Figure 3-15 Schematic of electrochemical cell.**

Shows the three electrode system of an electrolytic cell containing a reference, working and a counter electrode immersed in an electrolytic solution. The potential is applied on the working electrode with respect to the reference electrode and the current flow through the reference is controlled by allowing the current to flow through the counter electrode. Adapted from (Béron et al., 2010)

#### *Electrodes*

##### *Working electrode (WE)*

It is the electrode where the electrochemical reaction takes place and is generally made up of inert metals like gold, platinum etc.

##### *Reference electrode (RE)*

One of the most commonly used RE is a Ag/AgCl reference electrode. It consists of a glass tube containing a silver wire (Ag) coated with a layer of solid silver chloride (AgCl), immersed in a solution that is saturated with KCl and AgCl. The lower end

of the glass tube is sealed with a ceramic frit that allows the slow movement of ions from the inner chamber (filling solution) to the outer electrolyte. This steady movement of electrolytes through the porous ceramic frit can lead to development of a junction potential or can also cause contamination on the electrode surface. To overcome this problem a double junction reference electrode is constructed where inner element formed by the silver / silver chloride cell is inserted into an outer tube containing a different electrolyte which is then in contact with solution in the electrochemical cell through a second porous frit (Figure 3-16).

This double junction acts like a salt bridge and stabilises the potential between different solutions.

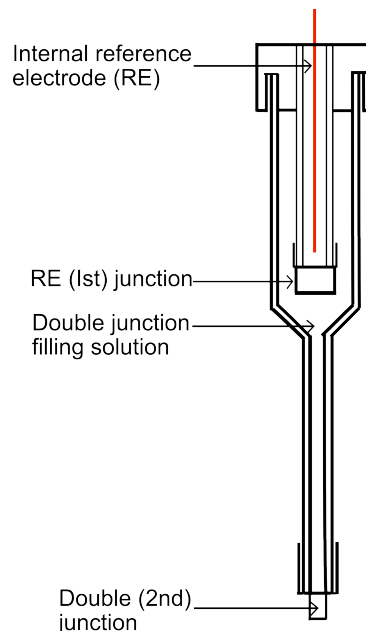


**Figure 3-16 Shows a double junction electrode with a built in reference electrode.**

Adapted from (Zoski, 2007)

### *Counter electrode (CE)*

During the electrochemical process in a two-electrode system, the current flows from the WE to the RE, which leads to charge accumulation on the RE, and thus the RE potential is not stable over time. Therefore, a three electrode system is used wherein a third electrode called as the counter electrode is connected to the WE. This

maintains the current flows between the RE and the CE. The counter electrode is generally made up of platinum wire due to its inertness and conducting property.

### 3.2.6.3. Cyclic voltametry (CV)

It is one of the commonly used methods to detect qualitative information about electrochemical reactions or interfacial properties of an electrode. CV uses the property of the surface to become positively or negatively charged by applying a voltage on it. By placing the electrode in a solution containing an electroactive component, the electrons are accepted or gained by the electroactive component from the surface. In CV a particular potential is swept between two potential values (V1 and V2). The surface is subjected to starting voltage of V1 with respect to the reference electrode and then surface voltage is changed to higher or lower voltage at a particular rate. Finally the voltage is changed back to the original value (V1) at the same rate. During this process the surface becomes negative or positive and the electroactive species gains or loses electrons to the surface. This leads to a measurable current. The CV voltametry is presented between current and potential, potential on X axis and current on the Y-axis.

If we consider an electrochemical reaction in an electrolytic solution containing a redox probe  $[\text{Fe}(\text{CN})_6]^{3-/4-}$ . In the forward scan  $\text{Fe}^{3+}$  gets reduced to  $\text{Fe}^{2+}$  and when the scan is reversed the product gets converted to  $\text{Fe}^{3+}$ . The flow of current is in the opposite sense to the forward sweep.

Figure 3-17 represents a typical voltamogram. In the voltamogram,  $E_{pa}$  represents the peak potential of the anodic sweep, and  $E_{pc}$  represents the peak potential for cathodic sweep. The difference between the anodic peak and the cathodic peak,  $\Delta E_{peak}$ , can be calculated. For a reversible redox couple  $\Delta E_{peak}$  is given by Equation (3.5)

$$n \Delta E_{peak} = 59 \text{ mV} \quad (3.5)$$

where n is the number of electrons involved in the redox reaction.

The ratio of the anodic peak current ( $i_{pa}$ ) to the cathodic peak current ( $i_{pc}$ ) is given by Equation (3.6).

$$i_{pa} / i_{pc} = 1 \quad (3.6)$$

The formal potential  $E_0$ , for a reversible redox couple is the average of the two peak potentials given by Equation (3.7).

$$E_0 = (E_{pa} + E_{pc}) / 2 \quad (3.7)$$

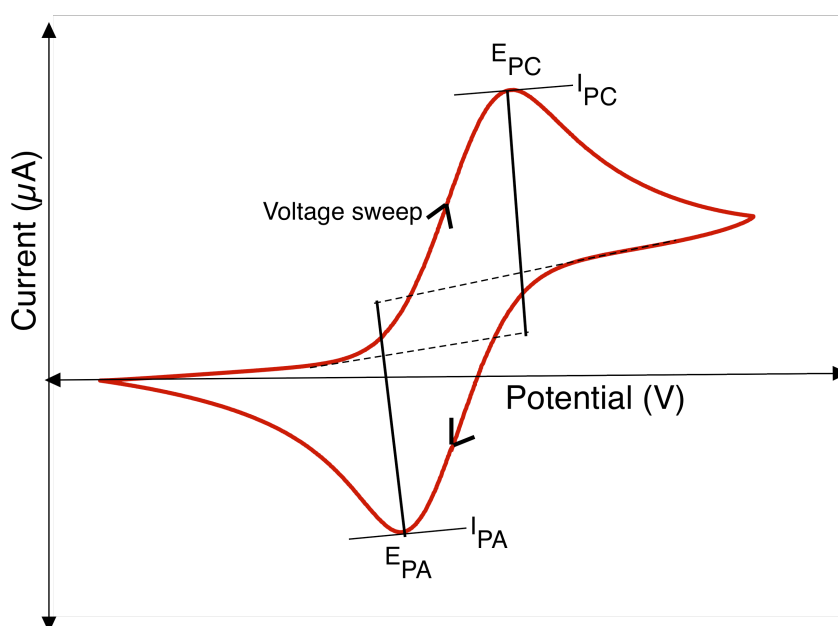


**Figure 3-17 Cyclic voltametry.**

Shows a voltamogram of a reversible redox couple for a single potential cycle.  $E_{PC}$  = Peak cathodic potential;  $I_{pc}$  = Peak cathodic current;  $E_{PA}$  = Peak anodic potential;  $I_{PA}$  = Peak anodic current.

Cyclic voltametry has been widely used to analyse the surface properties of an electrode as well as to know the oxidation / reduction state of a compound in an electrolyte.

### 3.2.6.4. EIS concept

Electrochemical impedance spectroscopy (EIS) is a technique for the study of conducting materials and interfaces. Unlike the most common electrochemical techniques that are based on the application of direct current or voltage, EIS is based on the superimposition of sine wave potential of small amplitude over polarization potential of constant value. Electrochemical impedance is measured using a small excitation signal expressed as function of time as given in Equation (3.8).

$$E(t) = E_0 \sin(\omega t) \quad (3.8)$$

$E(t)$  is the potential at time  $t$ ,  $E_0$  is the amplitude of the signal, and  $\omega$  is the radial frequency ( $\omega=2\pi f$ , frequency is expressed as  $f$ ). In a linear system, the response signal,  $I(t)$ , is shifted in phase ( $\phi$ ) and has a different amplitude,  $I_0$  as given in Equation (3.9).

$$I(t) = I_0 \sin(\omega t + \phi) \quad (3.9)$$

According to Ohm's law the resistance to the flow of current through an electrical resistor is the ratio of voltage and current as given in Equation (3.10).

$$R = V/I . \quad (3.10)$$

An expression analogous to Ohm's law allows us to calculate the impedance of the system as ratio of  $E(t)$  and  $I(t)$  as given in Equation (3.11).

$$\begin{aligned} Z &= E(t)/ I(t) \quad (3.11) \\ &= E_0 \sin(\omega t) / I_0 \sin (\omega t + \phi ) \\ &= Z_0 \sin(\omega t) / \sin (\omega t + \phi ) \end{aligned}$$

Using Euler's relation ( $e^{j\phi} = \cos(\delta) + j \sin(\delta)$ ), this can be written as

$$Z = Z_0 e^{j\phi} \quad (3.12)$$

The impedance is therefore expressed in terms of magnitude,  $Z_0$ , and a phase,  $\phi$  as given in Equation (3.12). It accounts for the combined opposition of all the

components within the electrochemical cell (resistors, capacitors) to the electron flow.

Impedance is expressed in the form of real and imaginary components. Ohmic resistance is the real component and the capacitive reactance is the imaginary one. When the imaginary impedance component ( $Z''$ ) is plotted against the real impedance ( $Z'$ ) at each excitation frequency, it is called as Nyquist plot (Figure 3-18(a)). Each point on the Nyquist plot is the impedance at one frequency. Impedance can be represented by vector arrow of length  $|Z|$  and the angle between the vector and x-axis is called the phase angle  $\phi$ . The lower frequency region is on the right hand side of the plot and the higher frequency region on the left hand side.

If both the logarithm of the absolute impedance,  $|Z|$  and the phase shift,  $\phi$ , of the impedance, are plotted against the logarithm of the excitation frequency, it is called as Bode plot (Figure 3-18(b)). The Nyquist plot does not show the frequency information unlike the Bode plot.

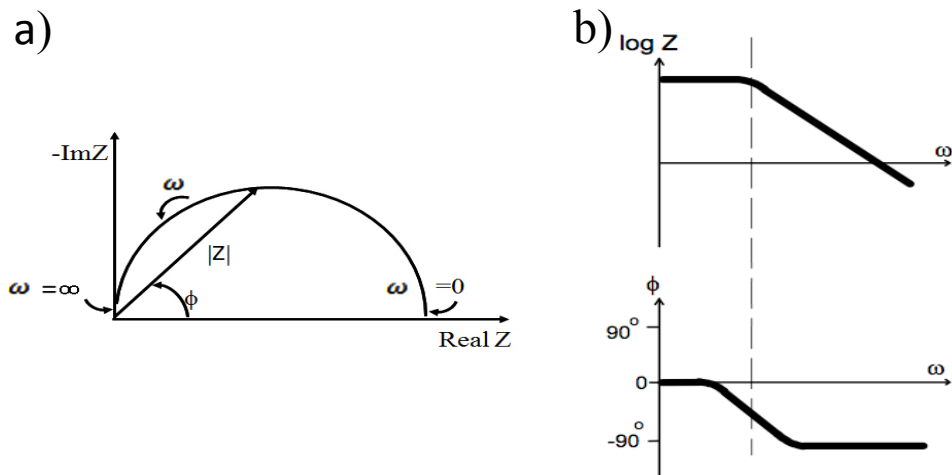


**Figure 3-18 The Nyquist plot and the Bode plot.**

(a) The Nyquist plot shows the real part of  $Z(\omega)$  is plotted on x axis (ReZ) and the imaginary part is plotted on the y axis ( $-ImZ$ ). (b) In the Bode plot impedance is plotted with log frequency on the x-axis and both the absolute values of the impedance ( $|Z|$ ) and the phase-shift ( $\phi$ ) on the Y-axis. Taken from (Gamry, c2014).

## Chapter 4. Development of a novel non-antibody based recognition molecule

### 4.1. Introduction

Over the past few years antibody-based biosensors called immunosensors have been used to detect various protein biomarkers (Conroy *et al.*, 2009). The main limitations in using antibodies as recognition molecules has been the complex and bulky nature of antibodies (see Chapter 2). Moreover antibodies require post translational modifications like formation of disulphide bonds and glycosylation, which restrains their production to eukaryotic expression systems.

An alternative to using antibodies is to utilise an entirely different class of small robust proteins as scaffolds, into which variable peptide sequences are inserted into their loops to generate artificial antibodies (Colas, 2008). Considerable efforts have been made to engineer many different protein scaffolds over the past years. These include, affibodies based on the Z-domain of Staphylococcal protein-A (Nord *et al.*, 1997; Wahlberg *et al.*, 2003), Kunitz domains (Nixon and Wood, 2006), designed ankyrin repeat proteins (DARPin) (Mosavi *et al.*, 2004), anticalins (Skerra, 2008) and repebodies (Lee *et al.*, 2012). The smaller size of these artificial antibodies reduces the steric hindrance when immobilised on the substrate and increases surface coverage during immobilisation (Huang *et al.*, 2005). These alternative scaffold proteins do not require post-translational modifications and therefore, are produced more economically and easily in yeast or bacteria (Colas *et al.*, 1996).

One of the approaches to produce a highly stable protein is to use a consensus design strategy wherein, a protein is designed based on the consensus from multiple sequence alignment of independent protein sequences all folding stably to the same structure (Main *et al.*, 2003). The underlying hypothesis of this approach is that as a result of selection during evolution of proteins, the residues that are important for their functioning and stability are the most conserved ones amongst the homologous proteins. Proteins generated through consensus design have shown higher stability

over their natural counterparts e.g. enzymes (Lehmann *et al.*, 2002) and antibodies (Knappik *et al.*, 2000). It has also shown that evolution selects for function and optimises stability only to the required environment but through consensus strategy the stability can be improved so that the protein can withstand different environmental conditions. Based on such a strategy, a new artificial binding protein scaffold called Adhiron has been engineered by McPherson group at the Centre for the Structural and Molecular Biology at the University of Leeds (Tiede *et al.*, 2014). It is based on a consensus sequence of plant-derived phytocystatins. Phytocystatin proteins (~100 amino acids) naturally inhibit cysteine proteinases (Kondo *et al.*, 1991). This designed consensus protein is an ideal scaffold, due to its small monomeric nature, high solubility, stability and no requirement for post-translational modification. Due to its potential to present constrained peptide sequences for molecular recognition it was investigated as an option for a non-antibody protein scaffold. The consensus sequence was shortened to give rise to two versions namely Adhiron 92 that consists full-length adhiron scaffold and Adhiron 81 with N-terminal truncated amino acids. Codon optimisation was done on Adhiron 92 sequences so that it is well expressed in *E. coli*. Figure 4-1 shows the amino acid sequence of the codon-optimised Adhiron 92 scaffold with secondary structure elements that include four  $\beta$ -sheets and one  $\alpha$ -helix.

The crystal structure of Adhiron scaffold (92 residues) has been revealed. Adhiron consists of a four-strand anti-parallel  $\beta$ -sheet core and a central helix, which is a characteristic of proteins belonging to cystatin family (Figure 4-1). It has a compact structure and the unstructured loops are limited, which signifies a stable protein. Residues 1-10 and 90-92 were not clearly visible in the crystal structure and were assumed to be disordered. Loop 1 was positioned between the first and the second  $\beta$ -strand. The loop 2 was present between the third and the fourth  $\beta$ -strand.

The Adhiron scaffold showed a melting temperature of 101 °C that makes it a highly thermally stable scaffold. The high thermal stability and compact structure of Adhiron scaffold supported the fact that consensus sequence based protein modelling results in designing highly stable proteins.

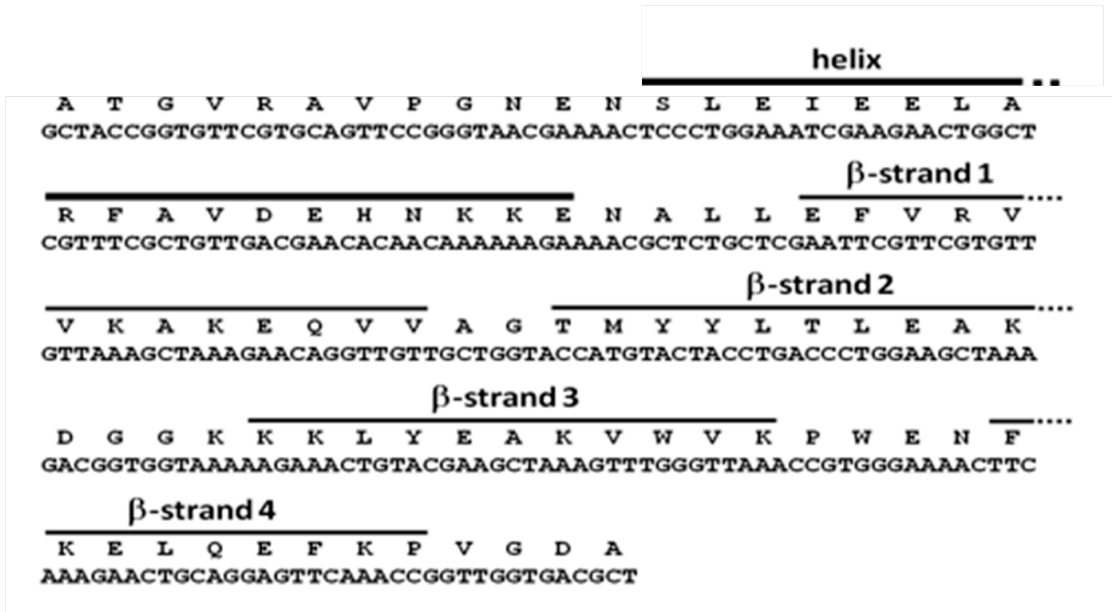


**Figure 4-1 Amino acid sequence of Adhiron92 scaffold with secondary structure elements.**

The figure depicts the amino acid sequence of of codon-optimised Adhiron92 scaffold showing the position of secondary structures ( $\alpha$ -helix and  $\beta$ -sheets) (Tiede *et al.*, 2014).

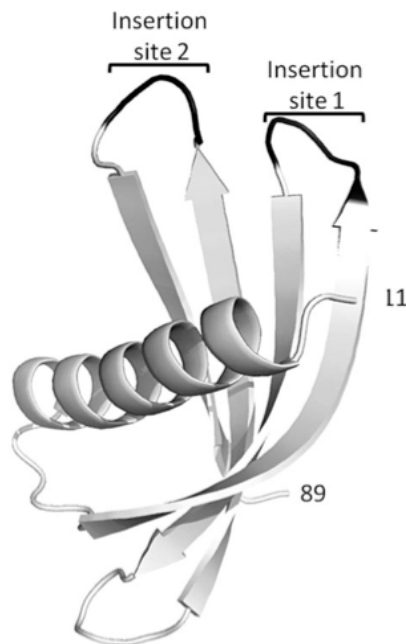


**Figure 4-2 X-ray crystal structure of Adhiron 92 scaffold.**

Adhiron92 scaffold has a single alpha helix and the four anti-parallel beta strands are shown in white with the insertion sites for library production shown in black. Residues 1-10 and 90-92 are not visible in the structure (Tiede *et al.*, 2014).

This chapter discusses briefly the creation of Adhiron based library followed by cloning of the library into pBSTG1 phagemid (see section 3.1.7.2.). Adhiron based phagemid library was used to select binders against anti-myc tag antibodies using phage display library by the BSTG group.

It then discusses the selection of Adhiron myc binders, their cloning and expression in vector pET-11(a). Initially, a random binder-Adhiron GST B4 was selected against a different protein (glutathione S-transferase) and was used to optimise the cloning of Adhiron sequence into pET-11(a), its expression and purification. The optimised conditions were then used for the cloning, expression and purification of ten Adhiron myc binders.

The optimisation of the expression and purification was done to establish the best conditions for high yield of Adhiron myc binders and for maintenance of their stability and purity for the subsequent analysis.

## 4.2. Materials and methods

The materials and methods used in cloning, expression, purification and characterisation of the Adhiron myc binders are described here in detail.

### 4.2.1. Materials

#### 4.2.1.1. Bacterial strain

Different strains of bacterium *Escherichia coli* were used at various steps of the protocol depending upon the requirement.

##### *XL10 Gold (Stratagene)*

XL10-Gold cells are tetracycline and chloramphenicol resistant. The cells are deficient of restriction systems [ $\Delta(\text{mcrA})183 \Delta(\text{mcrCB-hsdS SMR-mrr})173$ ]. Inactivation of endonuclease I gene and deficiency of *recA* improves the quality of miniprep DNA and ensures insert stability. The transformation efficiency of ligated and large super-coiled DNA is improved by the Hte phenotype. The *lacIqZAM15* gene on the F' episome allows blue-white screening for recombinant plasmids. This plasmid is also ideal for constructing complex plasmid libraries as it decreases size bias and therefore, produces larger libraries. XL10-Gold ultracompetent cells were purchased from.

##### *BL21 Star (DE3) (Stratagene)*

OmpT, an outer membrane protease present on the chromosomal DNA of *E. coli* is absent in this bacterial strain, therefore reducing the degradation of heterologous proteins. DE3 lysogen present in the strain carries the T7 RNA polymerase gene under the *lacUV5* promoter. T7 RNA polymerase over-expresses itself in the presence of IPTG (Isopropyl  $\beta$ -D-thiogalactoside) due to de-repression of the *lacUV5* promoter. The mutated *rne* gene that encodes a truncated RNase E enzyme lacks the ability to degrade mRNA, thus increasing the mRNA stability. This leads to higher basal expression of heterologous genes. This strain is *E. coli* B/r strain that does not contain lon protease.

#### 4.2.1.2. Vectors

##### *Phagemid vector pBSTG1*

pBSTG1 phagemid containing different Adhiron myc binder sequences was obtained from BSTG group (see section 3.1.7.2). It consisted of a recombinant coding sequence flanked by *Nhe* I and *Not* I restriction sites. It contains an ampicillin (*amp*) resistant gene for selection.

##### *Cloning and expression vector pET-11(a)*

The pET-11a vector carries a T7 promoter and a T7 termination site. It comprises of a multiple cloning site, *Lac* I repressor coding sequence, pBR322 origin of replication and an ampicillin resistant gene (*amp*). It is 5677 bp in size (Figure 4-3).

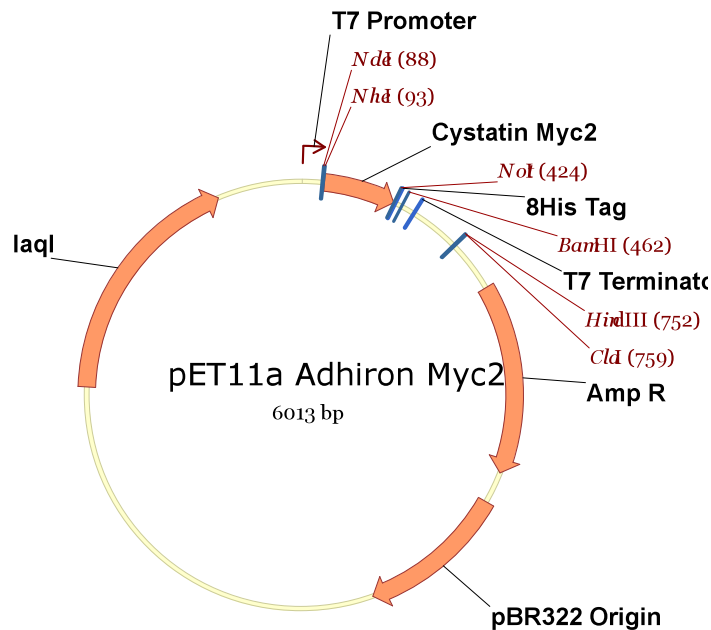


**Figure 4-3 Schematic representation of pET-11(a) adhiron myc binder 2 plasmid.**

(Figure provided by Sarah Deacon, Astbury Centre for Structural Molecular Biology).

#### 4.2.1.3. Growth media for *E. coli*

##### *Luria-Burtani broth (LB)*

The composition of the Luria-Burtani broth (Appendix-Table 1).

##### *LB agar*

LB media was prepared as mentioned in Appendix-Table 1 and dispensed into bottles. Then 15 g/L of agar bacteriological (agar no.1) was added to the bottles to get a final concentration of 1.5% (w/v). The agar media was autoclaved immediately at 121°C, 15 psi for 20 min and stored at room temperature.

##### *Autoinduction media*

###### *ZY Component*

Yeast extract 5 g/L and bactotryptose (tryptone) 10 g/L were dissolved in deionised water.

###### *1 M MgSO<sub>4</sub>*

24.65 g of MgSO<sub>4</sub>.7H<sub>2</sub>O was dissolved in 100 mL deionised water. The solution was filter sterilised through a 0.22 µm filter.

###### *40 % (w/v) glucose*

40 g of glucose was dissolved in 100 mL deionised water. Solution was filter sterilised through a 0.22 µm filter.

###### *20 X NPSC*

See Appendix-Table 2.

###### *Trace elements*

See Appendix-Table 3.

###### *ZYP-0.8G Media*

See Appendix-Table 4 .

###### *Pre-formulated autoinduction media*

Pre-formulated autoinduction media from ForMedium™ were used that included: LB-Luria Burtani, 2YT-Yeast tryptone, TB-Terrific Broth, SB-Super Broth. The AIM

or auto induction media as produced and supplied by ForMedium™ are based on the work of F. William Studier (Studier, 2005).

#### **4.2.1.4. Bacterial antibiotic selection**

See Appendix-Table 5.

#### **4.2.1.5. Bacterial Growth conditions**

##### ***LB growth conditions***

The LB agar media plates streaked with the *E. coli* bacterial culture were incubated in a stationary incubator at 37 °C. Starter cultures were set-up by inoculating single colonies from LB-agar plates into 5-10 mL LB media containing the appropriate antibiotic and incubated in an orbital incubator at 37 °C, 200 rpm. Larger scale cultures were set-up by a 1/500 - 1/1000 dilution of starter culture into the required volume of media using a flask to media ratio of 5:1.

For plasmid extraction, cultures were grown to saturation overnight. Unless otherwise stated all *E. coli* cultures were grown at 37 °C.

##### ***Autoinduction growth conditions***

The plasmids were transformed into selected *E. coli* strain for expression and the transformed culture was streaked on an LB plate. The next day a single colony was picked from LB-agar plate and grown in 2 mL of ZYP-0.8G containing appropriate antibiotics in a 24 deep-well plate. The plate was incubated at 37 °C at 1300 rpm for 6 hr in a plate incubator. 20 µl of the starter culture was used to inoculate 2 ml of pre-formulated autoinduction media –LB, 2YT, TB, SB (ForMedium, UK) in a 24 deep well plate and grown at 25 °C at 1300 rpm in a plate shaker (Incubator 1000, Heidolph UK). At different time intervals -16, 24, 40, 48, 60, 72 hr 200 µl of samples were collected from each culture. Cells were harvested and pellets were frozen at -20 °C.

For scaling up the culture, 400 mL of selected autoinduction media contained in 2 L baffled flask was inoculated with 200 µL of the 2 mL starter culture. Flasks were grown at 25 °C at 250 rpm for the appropriate incubation time.

The cells are harvested by centrifugation at 3000 gm (Rotana 460R, Hettich lab technology) for 30 min and frozen at -20 °C.

## **4.2.2. Techniques**

### **4.2.2.1. Plasmid isolation**

The Wizard Plus SV Minipreps DNA Purification System (Promega) was used for plasmid isolation as per the manufacturer's instructions.

### **4.2.2.2. Agarose gel electrophoresis**

0.5 to 1 % (w/v) agarose was dissolved in 1 X TAE buffer (Appendix-Table 6). The solution was boiled in a microwave oven, poured onto a casting tray. SYBR Safe DNA gel stain (Invitrogen) (1:10,000) was mixed in the gel before it solidified. A comb was placed across the end of the gel to form wells. The gel was allowed to cool down at room temperature until it solidified. The tray was put in 1 X TAE buffer-filled electrophoretic chamber, containing positive electrode at one end and a negative electrode at the other end. The comb was removed and allowed the buffer to cover the gel up to 1mm.

Gel-loading buffer (Appendix-Table 7) was added to the samples (1/10) and loaded into the wells, along with a prestained DNA marker (MassRuler DNA Ladder Mix, Fermentas). A DC power source was connected to the electrophoretic apparatus and 100 V fixed voltage was applied. The power was disconnected when the trail of bromophenol was seen at the bottom of the gel. The agarose gel apparatus used was RunOne electrophoretic cell (EmbiTec).

### **4.2.2.3. Restriction digestion**

Restriction enzymes - *Nde* I, *Nhe* I-HF, *Not* I-HF, *Bam* HI-HF and *Dpn* I (NEB) were used as per the manufacturer's instructions (Appendix-Table 8). High fidelity (HF) enzymes were used to avoid star activity. Star activity is caused when the restriction enzymes cleave sequences similar but not identical to the defined restriction site.

#### 4.2.2.4. Gel extraction of DNA fragments

The samples were run on 1 % (w/v) agarose gel and the desired fragments were extracted from the gel by using the gel extraction kit (The Wizard SV Gel and PCR Clean-Up System, Promega). It is a silica-membrane based method, which can bind to 40 µg of DNA. After binding to the membrane the DNA was eluted in deionized water. The protocol was followed as per the manufacturer's instructions.

#### 4.2.2.5. Polymerase chain reaction

KOD Hot Polymerase (Novagen) (Mizuguchi *et al.*, 1999), is a premixed complex of KOD DNA Polymerase and two monoclonal antibodies that inhibit DNA polymerase and 3'-5' exonuclease activities at ambient temperatures. This inhibition reduces non-specific amplification as the mispriming events occurring during initial temperature increase. The composition of KOD Hot Polymerase mix for PCR reaction is given in Appendix-Table 9.

#### Phusion DNA polymerase master mix (NEB)

It consists of a novel *Pyrococcus*-like enzyme fused with processivity enhancing domain to increase fidelity and speed. It generates blunt ended products. The composition of Phusion DNA polymerase mix is given in Appendix-Table 10. After amplification, reaction mixture was incubated in 1 µl of *Dpn* I enzyme at 37 °C for 1 hr.

Amplification was carried out using MJResearch Thermal Cycler, using the cycling conditions mentioned in Appendix-Table 11. A 5 µL aliquot of the PCR product was analysed on an agarose gel to confirm the yield and size.

#### 4.2.2.6. DNA ligation

For the successful ligation of DNA molecules ligation reaction is set up in such a way that many recombinant molecules are formed and less of vector / vector and insert / insert products are formed. The total concentration of DNA molecules and the molar ratio of insert to vector molecules is considered. For cohesive ends:

3:1 insert:vector ratio, 9-90 fmol (Femtomoles) of insert, 3-30 fmol of vector and 10-100 ng of total DNA were used.

#### *Calculations*

Considering ligation of Adhiron GST B4 into pET-11(a) vector.

Size of plasmid pET-11(a) = 5639 bp (base pairs)

Molecular mass of ds(double stranded) DNA fragment = Number of bp x 660Da

Molecular mass of ds plasmid = 5639 x 660 =  $3.7 \times 10^6$  Da

1 mole =  $3.7 \times 10^6$  g

1 fmol = 3.7 ng

15 fmol = 55.5 ng

Size of Adhiron GST B4 insert = 374 bp

Molecular mass of ds insert = 374 x 660 Da

1 mole = 374 x 660 g

1 fmol = 0.24 ng

45 fmol = 10.8 ng

Total DNA = 66.4 ng

Ligation was set up using the composition in Appendix-Table 12, using T7 DNA ligase and ligase buffer (NEB). The reaction mixture was kept at room temperature for 2 hr.

Note: Restriction enzymes that were used to cut the DNA fragments were heat inactivated before setting up ligation reactions. The heat deactivation conditions for restriction enzymes are given in Appendix-Table 13.

#### **4.2.2.7. Zero Blunt PCR cloning**

Zero Blunt PCR cloning kit (Invitrogen) was used to clone blunt-end PCR products. It consists of a cloning vector pCR blunt along with ExpressLink™ T4 DNA Ligase for ligation purpose. It is designed to clone blunt PCR fragments with a low background

of non-recombinants. pCR-Blunt vector contains a lethal *E. coli ccdB* gene fused to the C-terminus of *lacZ $\alpha$* . On ligation of the blunt fragment into the vector, the *lacZ $\alpha$ -ccdB* gene expression is disrupted and therefore, only the positive recombinants are able to grow and the non-recombinant cells die. The plasmid has Kanamycin and zeocin resistant genes for selection. It has M13 forward and reverse priming sites for sequencing. The Zero blunt PCR cloning mixture is given in Appendix-Table 14. The reaction mixture was incubated for 5 min at room temperature and transformed into XL10 Gold cells.

#### **4.2.2.8. Transformation**

Cells were taken out from the -80 °C freezer and allowed to thaw on ice. 1  $\mu$ l of plasmids obtained after a miniprep or 5  $\mu$ l ligation mixture obtained after ligation reaction of two DNA fragments were mixed with 50  $\mu$ l XL10 Gold cells / BL21 Star (DE3) cells and incubated on ice for 15 min. Then the mixture was heat shocked at 42 °C for 45 sec followed by incubation on ice for 2 min (Hanahan, 1983). 250  $\mu$ l of LB was added to the cells and incubated in a shaker incubator at 37 °C for 1hr. 100  $\mu$ l of the culture was streaked on agar plates.

#### **4.2.2.9. Colony PCR using GoTaq polymerase**

Single colonies were picked from plates using an inoculation needle and swirled in 100  $\mu$ L of deionised water. The needle was then put in 4 mL LB containing carbenicillin at 37 °C on a shaker incubator at 250 rpm to perform minipreps. The 100  $\mu$ L solution was boiled at 100 °C to lyse the cells and 2  $\mu$ L of the solution was added to 18  $\mu$ l of GoTaq Green mastermix (Promega) in PCR tubes.

#### ***GoTaq Green master Mix***

The composition of the master mix used in the PCR is given in Appendix-Table 15.

Green GoTaq Flexi Buffer increases the density of the sample and contains two dyes (a blue dye and a yellow dye) that separate during electrophoresis, allowing reactions to be loaded directly onto an agarose gel without the addition of loading dye.

Positive control: pBSTG1 vector containing GST B4 insert.

Negative control: Uncut pET-11(a) vector and a reaction mixture of the GoTaq polymerase without the DNA templates.

Thermocycling conditions used are given in Appendix-Table 16.

#### **4.2.2.10. Protein extraction and purification**

##### ***Cell lysis***

###### *Using lysis buffer*

Cell lysis was performed using a cell lysis buffer (Appendix-Table 17). In expression trials 1 ml sample was collected from 400 mL cell culture, the sample was centrifuged at 16000 g using GenFuge 24D from (Progen). The pellet was resuspended in 200  $\mu$ l of lysis buffer and incubated at room temperature with agitation on a plate mixer at 1000 rpm for 35 min.

###### *Using sonication*

The cell pellet obtained after centrifugation of 400 mL culture at 3000 g for 30 min (4 °C). The pellet was resuspended in 50 mL binding buffer and pipetted until the pellet was completely dissolved. The resuspended pellet was sonicated using Branson sonicator. It was done using 50 % duty cycle for 30 seconds on and 30 sec off for 5 cycles. The tube containing the suspended cells was kept on ice throughout the sonication to prevent overheating.

To separate the solubilised fraction from the cell debris, the sample was centrifuged at 16000 g (Beckman, Avanti) for 20 min.

##### ***Purification***

Purification was done using 1 mL Hitrap column (GE healthcare). The column was first washed with deionised water. 100 mM NiSO<sub>4</sub> was prepared by dissolving 2.628 g in 100 ml of deionised water. 0.5 ml of 0.1 M NiSO<sub>4</sub> solution was loaded on the column. Then the column was washed with deionised water and preequilibrated with 10 CV (column volume) of binding buffer (Appendix-Table 18). Using a syringe, the cleared supernatant obtained after the cell lysis of the bacterial cell-pellet was applied

on to the column. The first flow through was collected for analysis. Then the column was washed with 10 CV of binding buffer followed by 10 CV of wash buffer (Appendix-Table 19). The fractions were collected from binding buffer and wash buffer for further analysis. 10 CV of elution buffer (Appendix-Table 20) was run through the column and 1 mL fractions were collected in a 96 well plate. 10  $\mu$ L of the collected samples were run on 15 % (w/v) SDS PAGE. The elution fractions containing protein (observed on the gel) were pooled together. The column was stripped using 5 CV of stripping buffer (Appendix-Table 21), washed with deionised water and then column was stored in 20 % (v/v) ethanol at 4 °C.

#### **4.2.2.11. Dialysis**

The proteins eluted in elution buffer were dialysed using Biodesign dialysis tubing (3.5 kD MWCO) purchased from Thermo Fisher Scientific.

The tubing was cut according to the volume of the solution and one end was folded and pinched in a clamp. The solution was pipetted into the tubing through its open end. The end was tied off using another clamp. The tubing was placed in 1 L of 1 X PBS / phosphate buffer saline (Appendix-Table 22). A stir bar was added in the beaker and it was put on a stir plate overnight in the cold room. The dialysis buffer was changed twice the following day.

#### **4.2.2.12. Sodium dodecyl sulphate polyacrylamide gel electrophoresis (SDS-PAGE)**

1/3 volume of sample denaturing mix (Appendix-Table 23) was added to each sample (purified and dialysed proteins) and boiled for 5 min. The samples were left to cool on a bench before loading them on to the gel. The samples were analysed on a 15 % (w/v) SDS PAGE (Appendix-Table 24 and 25) (Laemmli, 1970). Protean III gel (Bio-Rad) apparatus was used to set up the gel electrophoresis. 1 X running buffer (Appendix-Table 26) was poured into the buffer chamber. A constant voltage of 150 V was applied across the gel with initial current ~60 mA and the electrophoresis was run for 45-60 min. The gel was removed from the apparatus and stained with Coomassie brilliant blue (Appendix-Table 27) for 30 min to 1 hr. Then it was

destained in destaining solution (Appendix-Table 28) for 6-7 hr and the destaining solution was changed thrice in between.

All solutions were stored at room temperature.

#### **4.2.2.13. Dot blots**

The samples were lysed using lysis buffer. Lysed cells were dissolved in dot blot solubilisation buffer (Appendix-Table 29). 12.5  $\mu$ l of lysed cells were mixed and vortexed thoroughly with 37.5  $\mu$ l of solubilisation buffer so that the final concentration is 37.5 mM TRIS, 225 mM NaCl and 6 M GuHCl. The samples are then incubated at room temperature at for 1 hr to achieve complete solubilisation.

A piece of thick blotting paper and a piece of nitrocellulose membrane were cut to the required size for the number of samples. Nitrocellulose membrane was placed on top of blotting paper and clamped into place using dot blot apparatus. 3  $\mu$ l of solubilised samples were pipetted on to the membrane aiming to blot onto centre of each well.

His-tagged TEV concentrations made in the dot blot solubilisation buffer were used as control. The samples were allowed to dry once all were loaded onto the membrane. The membrane was blocked for 1 hr at room temperature in 3 % (w/v) BSA and 1 X TBST buffer.

#### **4.2.2.14. Western blots**

A strip of nitrocellulose and 6 pieces of thick blotting paper were cut of the same size as the gel. The nitrocellulose and the gel were soaked in transfer buffer (Appendix-Table 30) for 10 min. 3 pieces of soaked blotting paper were placed in the middle of the lower electrode-anode and the pre-soaked nitrocellulose was placed on top. The gel was placed over the stack of the blotting paper and nitrocellulose, which was further layered by 3 pieces of blotting paper. The upper electrode-cathode was placed onto the stack. The proteins were blotted from the gel to the nitrocellulose membrane by applying a constant current 0.8 mA per  $\text{cm}^2$  for 1 hr. The blot was further analysed by immuno detection of proteins.

#### **4.2.2.15. Immuno detection of proteins**

The membrane was blocked in 3 % (w/v) BSA in 1 X TBST buffer for 1 hr at room temperature. It was then washed in 1 X TBST buffer for 10 min. The buffer was decanted and the step was repeated twice. Immunodetection of the proteins was done using anti-histidine horseradish peroxidase (HRP) conjugated antibody purchased from R&D Systems. 1/5000 dilution of the antibodies was prepared in TBST containing 3 % (w/v) BSA. The membrane was incubated in the antibody solution for 1 hr at room temperature or 4 °C overnight.

The chemiluminescent detection was done using SuperSignal West Pico chemiluminescent substrate (Thermo Scientific).

1 mL of reagent A was mixed with 1 mL of reagent B and pipetted onto the membrane, covering the area of detection for 2 min and visualised under Syn gene bioimaging system (Scientific lab supplies).

#### **4.2.2.16. Characterisation**

##### ***Circular Dichroism Spectroscopy***

CD measurements of the purified binders were carried out on an Applied Photophysics Chirascan CD spectropolarimeter. 1 mg/mL of each protein was prepared in 1 X PBS for analysis. The spectra were collected from 190 to 260 nm and repeated with two scans. The data were analysed using Dichroweb analysis server (Whitmore and Wallace, 2004) based on CDSSTR algorithm calculated using SP175 reference data set (Sreerama and Woody, 2000; Lees *et al.*, 2006).

##### ***Differential Scanning Calorimetry***

DSC measurements were carried out on VP-DSC (Microcal). The Adhiron scaffold and Adhiron myc binders were prepared at a concentration of 0.5 mg/mL in 1 X PBS at pH 7.4. Protein samples and buffer were degassed twice under vacuum for 10 min. The scanning was performed between 11 °C and 130 °C at a scan rate of 90 °C/hr with a 15 min prescan equilibration. Repeated heating and cooling cycles were performed on the proteins.

### **4.3. Results**

The consensus strategy based design of Adhiron scaffold showed high thermal stability (101 °C) and well-defined secondary structures with two variable loops (Figure 4-1 and 4-2). The application of this scaffold as an artificial antibody was still to be determined. To check the functioning of the adhiron scaffold when different randomised inserts are present in the two loops and the N-terminus of the scaffold, a library based on Adhiron with randomised inserts in the three variable regions was obtained from Sloning technologies.

#### **4.3.1. Generation of Adhiron based library by BSTG**

The Adhiron scaffold with randomised insertions in the three variable regions were cloned into pBSTG1 phagemids by the BSTG, University of Leeds, UK.

These phagemids were transformed into the *E. coli* ER2738 cells and the phage particles were produced using M13KO7 helper phage for superinfection. The library size was approximately  $1 \times 10^{10}$ , with a complexity up to 86 % after phage production, indicating a very high quality of the library.

##### **4.3.1.1. Phage display**

A phage display was performed by using polyclonal anti-myc tag antibodies, to prove the versatility and stability of the Adhiron scaffold when peptide inserts were present in different loops to target c-myc epitope (EQKLISEEDL). This epitope was chosen to compare the sequences of the binding scaffolds with the c-myc epitope.

Anti-myc tag antibodies were biotinylated to allow immobilisation *via* streptavidin. The phage particles eluted were incubated with ER2738 cells and then the cells were infected with M13K07 helper phage. After three rounds of panning, 48 Adhiron myc binder clones were picked up randomly and then a phage ELISA was performed.

#### 4.3.1.2. Phage ELISA

The phage ELISA was performed to investigate binding of the 48 Adhiron myc binder clones to anti-myc tag antibodies.

Streptavidin coated plates were labelled with biotinylated anti-myc tag antibodies. The phage-containing medium was added to the wells. The binding was confirmed by using HRP-conjugated anti-phage antibody. The binding was visualised using 3,3',5,5'-Tetramethylbenzidine (TMB) liquid substrate. Figure 4-4 shows the 96 well ELISA plate, wherein the binding of all clones was checked against anti-myc tag antibodies (well A1 to H6). The binding of the clones was also checked against the blocking agent (casein) from well A7 to H12. Binder in A1 has a control in A7 and likewise for the other binders. Binders in C5 and H6 showed signal in their corresponding control wells thus they were not specific for the anti-myc tag antibodies.

Out of the 48 clones, 20 were randomly selected and sequenced (Figure 4-5). Their sequencing results confirmed the similarity of sequences in different loops of the Adhiron myc binders with the myc epitope sequence (EQKLISEEDL).

The similarity of the sequences in different loops with the myc epitope proved the functionality of the scaffold to present the binding regions in different loops. Depending on the intensity of colour obtained in the phage ELISA, the 20 binders were named from clone 1 to clone 20 and were investigated further as the candidate binders to be used for the biological layer of the biosensor.

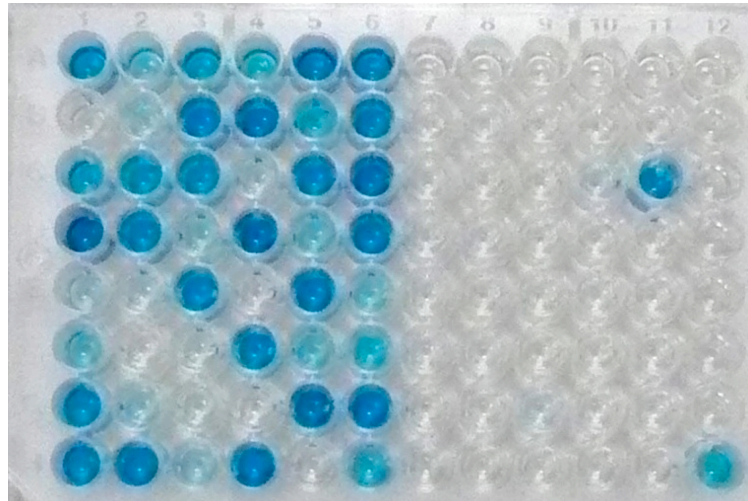


**Figure 4-4 ELISA to show binding of Adhiron myc binders.**

Shows the 96 well plate ELISA done on 48 Adhiron myc binder clones randomly chosen after three rounds of panning of phage display library. A1 to H6 were immobilised with the 48 clones and A7 to H12 corresponding to the control against the blocking against where A1 has a control well A7 and similarly each clone has its corresponding control well. The binders in well C11 and H12 shows non-specific binding. (Provided by Christian Tiede, Bioscreening Technology Group, Biomedical and Health Research Centre, University of Leeds).

	1	10	20	30	40	50	60	70	80	90	100
11_05_17-clone1	(1)	SASASMISEED	VRAVPGNENSLEIEELARFAVDEHNKKNALLEFVRVWKAKEQ	VPDS	PEGN	IMYYLPLEAKDGGKKKLYEAKVWVK	DHGSTIRDD	NEFK			
11_05_17-clone6	(1)	SASASMISEED	VRAVPGNENSLEIEELARFAVDEHNKKNALLEFVRVWKAKEQ	VPDS	PEGN	IMYYLPLEAKDGGKKKLYEAKVWVK	DHGSTIRDD	NEFK			
11_05_17-clone2	(1)	SASASLVSEED	VRAVPGNENSLEIEELARFAVDEHNKKNALLEFVRVWKAKEQ	WIKVNPHEG	IMYYLPLEAKDGGKKKLYEAKVWVK	EFDKHERIAN	NEFK				
1_05_17-clone11	(1)	SASASLVSEED	VRAVPGNENSLEIEELARFAVDEHNKKNALLEFVRVWKAKEQ	ETVDHTSTQ	IMYYLPLEAKDGGKKKLYEAKVWVK	FMSYHG-WP	NEFK				
11_05_17-clone3	(1)	SASASLKREED	VRAVPGNENSLEIEELARFAVDEHNKKNALLEFVRVWKAKEQ	IMFP	WGLD	IMYYLPLEAKDGGKKKLYEAKVWVK	NDPTPGDFM	NEFK			
1_05_17-clone16	(1)	SASASLVSEDD	VRAVPGNENSLEIEELARFAVDEHNKKNALLEFVRVWKAKEQ	SHSESMIMG	IMYYLPLEAKDGGKKKLYEAKVWVK	QEMRQWLAE	NEFK				
1_05_18-clone18	(1)	SASASHVEPHN	VRAVPGNENSLEIEELARFAVDEHNKKNALLEFVRVWKAKEQ	HTLLSEEDY	IMYYLPLEAKDGGKKKLYEAKVWVK	YFMWKHDIN	NEFK				
1_05_17-clone12	(1)	SASASTQYEGS	VRAVPGNENSLEIEELARFAVDEHNKKNALLEFVRVWKAKEQ	LAENWYGER	IMYYLPLEAKDGGKKKLYEAKVWVK	AGIVSEEDM	NEFK				
1_05_17-clone10	(1)	SASASQTHSDG	VRAVPGNENSLEIEELARFAVDEHNKKNALLEFVRVWKAKEQ	QYINVELHW	IMYYLPLEAKDGGKKKLYEAKVWVK	AGQKLAEE	NEFK				
1_05_17-clone13	(1)	SASASLNKQW	VRAVPGNENSLEIEELARFAVDEHNKKNALLEFVRVWKAKEQ	DHCY	ISEG	IMYYLPLEAKDGGKKKLYEAKVWVK	PTFRMEEMQ	NEFK			
1_05_17-clone14	(1)	SASASPKFHHT	VRAVPGNENSLEIEELARFAVDEHNKKNALLEFVRVWKAKEQ	DWQQ	ITEP	IMYYLPLEAKDGGKKKLYEAKVWVK	READVTPFMT	NEFK			
1_05_17-clone15	(1)	SASASGDHLAH	VRAVPGNENSLEIEELARFAVDEHNKKNALLEFVRVWKAKEQ	MSQT	IDEP	IMYYLPLEAKDGGKKKLYEAKVWVK	YQLEGPQTYN	NEFK			
11_05_17-clone5	(1)	SASASPKWMLP	VRAVPGNENSLEIEELARFAVDEHNKKNALLEFVRVWKAKEQ	QAEHGL	ISTG	IMYYLPLEAKDGGKKKLYEAKVWVK	GREHFWKID	NEFK			
11_05_17-clone9	(1)	SASASLLTENE	VRAVPGNENSLEIEELARFAVDEHNKKNALLEFVRVWKAKEQ	SWCH	ISEG	IMYYLPLEAKDGGKKKLYEAKVWVK	HYQPF-RAN	NEFK			
11_05_17-clone8	(1)	SASASDFHVST	VRAVPGNENSLEIEELARFAVDEHNKKNALLEFVRVWKAKEQ	ATQQ	LAED	IMYYLPLEAKDGGKKKLYEAKVWVK	WVMIAADDP	NEFK			
11_05_17-clone4	(1)	SASASSHENHC	VRAVPGNENSLEIEELARFAVDEHNKKNALLEFVRVWKAKEQ	TBOQ	LIGE	IMYYLPLEAKDGGKKKLYEAKVWVK	LDVQTFPR	NEFK			
11_05_17-clone7	(1)	SASASLVDHHH	VRAVPGNENSLEIEELARFAVDEHNKKNALLEFVRVWKAKEQ	YOAPE	PQLY	IMYYLPLEAKDGGKKKLYEAKVWVK	PIQHLISET	NEFK			
1_05_17-clone20	(1)	SASASHKIVIM	VRAVPGNENSLEIEELARFAVDEHNKKNALLEFVRVWKAKEQ	QYINK	HNEG	IMYYLPLEAKDGGKKKLYEAKVWVK	HQQLLSEF	NEFK			
1_05_17-clone17	(1)	SASASDMAHLP	VRAVPGNENSLEIEELARFAVDEHNKKNALLEFVRVWKAKEQ	RMYHG	PHEA	IMYYLPLEAKDGGKKKLYEAKVWVK	QMOTLLSET	NEFK			
1_05_17-clone19	(1)	SASASQDLVDE	VRAVPGNENSLEIEELARFAVDEHNKKNALLEFVRVWKAKEQ	HVSNEMVIM	IMYYLPLEAKDGGKKKLYEAKVWVK	RDDNLLRHT	NEFK				

**Figure 4-5 The sequences of the 20 Adhiron myc binders.**

The Adhiron myc binders were numbered from position of clone 1 to clone 20 in decreasing order of their intensities obtained in the phage ELISA. (Provided by Christian Tiede, Bioscreening Technology Group, Biomedical and Health Research Centre, University of Leeds).

### 4.3.2. Selection of Adhiron myc binders

Ten out of the twenty binders were chosen for this project. The selection was based on the position of sequences resembling the myc epitope presented in different loops of the scaffold. The following Adhiron myc binders were chosen:

Adhiron myc binders 1, 2, 4, 5, 7, 11, 13, 17, 18 and 20. Figure 4-6 shows the sequence alignment of the chosen Adhiron myc binders. The sequence alignment was done using Clustal W. The Adhiron myc selected show binding to anti-myc tag antibodies and similarity in the sequences corresponding to the myc epitope EQKLISEEDL.

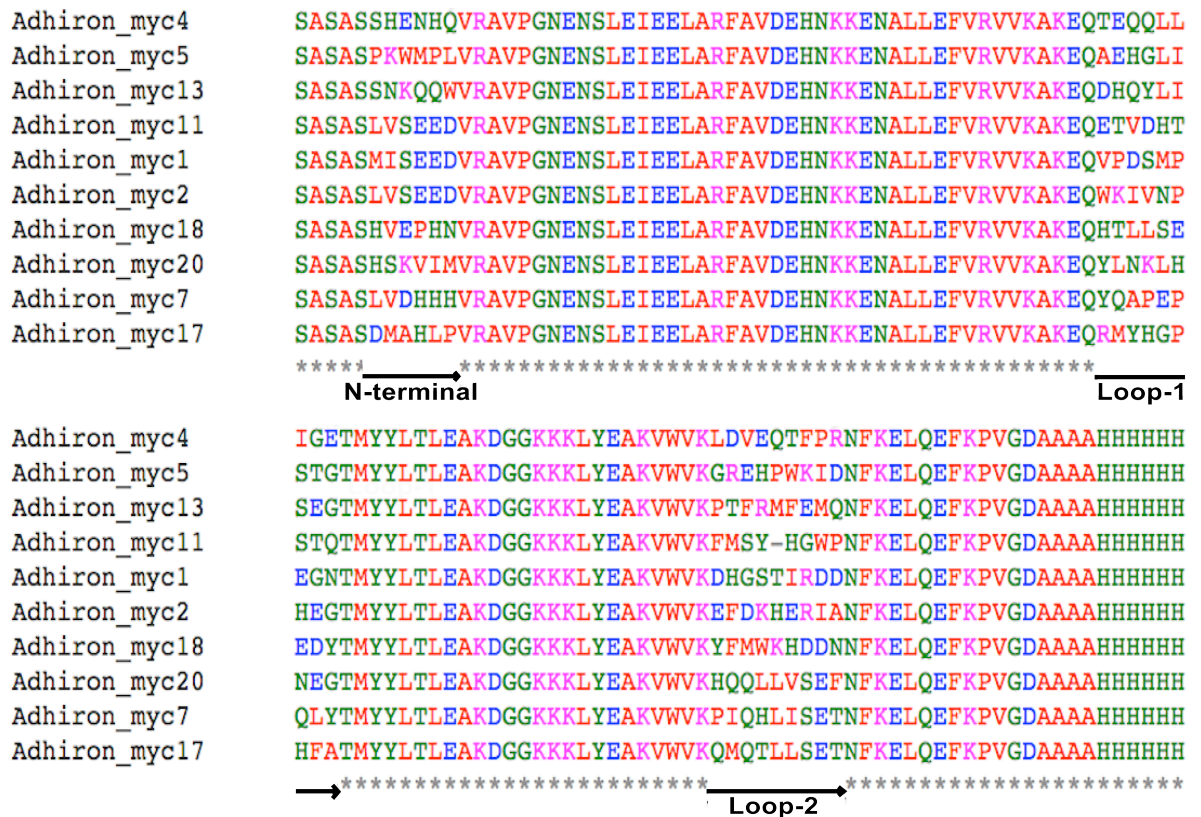


**Figure 4-6 The sequence alignment of the ten selected Adhiron myc binders.**

The sequence alignment of Adhiron myc binders shows the following- Single letters: aminoacids, star (\*): conserved sequence, the N-terminal, loop 1 and 2 represent the three variable regions where the random amino acids sequences have been inserted. (Key: Colour Red: small hydrophobic, aromatic and not Y. Blue: acidic. Magenta: basic, Green: hydroxyl, amine, amide, basic aminoacids.)

### 4.3.3. Cloning

The phage coat proteins fused with Adhiron myc binders could obscure the study of interaction of Adhiron myc binders with the anti-myc tag antibodies. Thus, the Adhiron sequence was cloned into

pET-11(a), to increase its expression and to remove the phage coat particles fused with the protein. The expression and purification of the Adhiron based sequences had not been optimised previously and therefore, at the start of the project it optimisation was performed using a random binder-Adhiron GST B4, selected against a different protein (glutathione S-transferase). The optimised conditions were then used for the cloning, expression and purification of the Adhiron myc binders.

#### 4.3.3.1. Checking plasmids on agarose gel

Different pBSTG1 phagemids containing the ten Adhiron myc binders and Adhiron GST B4 binder were transformed into XL10 Gold cells. pET-11(a) expression vector was also transformed into XL10 Gold cells. Colonies were obtained on LB plate from each transformation. Single colony was picked from each plate and used for plasmid miniprep. The minipreps were run on 1 % (w/v) agarose gel Figure 4-7. The two bands obtained on loading the minipreps of pBSTG1 constructs and GST B4 were most likely corresponding to open-circular (nicked) and supercoiled DNA. The open-circular (nicked) form of the plasmid migrates slowly than the supercoiled DNA. The DNA from pET-11(a) transformed cells showed a single band corresponding to the intact plasmid DNA in the cells.

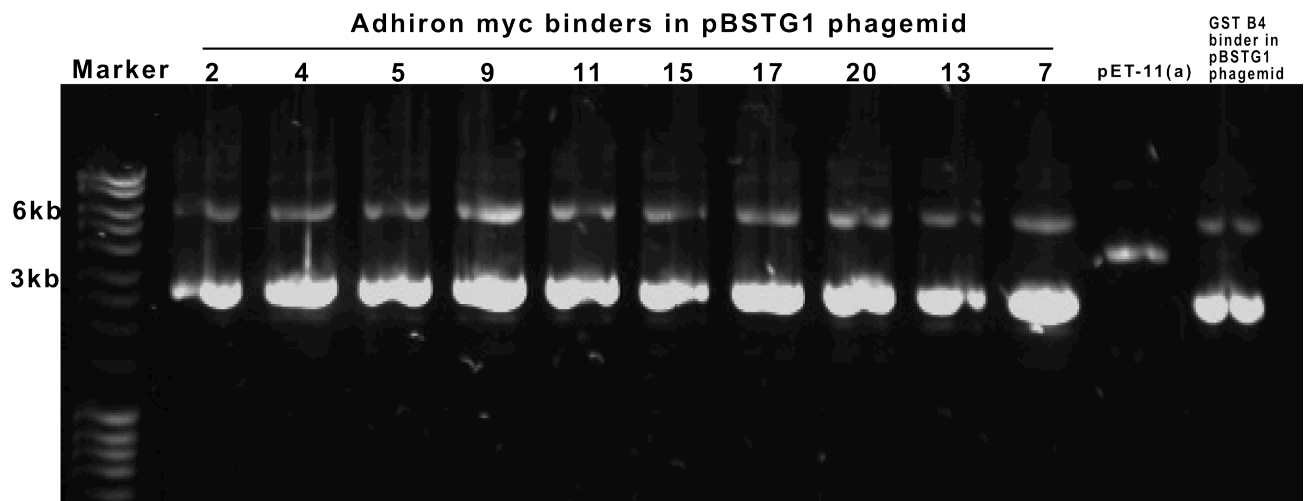


**Figure 4-7 Gel electrophoresis of Adhiron binders from plasmid.**

Showing agarose gel electrophoretic analysis on 1% (w/v) agarose gel of pBSTG1 construct containing Adhiron myc binder sequences, Adhiron GST B4 binder and pET-11(a) vector. Marker lane consists of a MassRuler DNA ladder mix.

#### **4.3.3.2. Incorporating *Nde* I and *Bam* HI restriction sites into Adhiron GST B4 sequence.**

To incorporate the *Not* I and *Nhe* I restriction sites into the Adhiron myc binders, the same restriction sites needed to be incorporated into the pET-11(a) vector. This was done using the Adhiron GST B4 binder sequence by inserting the Adhiron GST B4 sequence was cloned into pET-11(a) vector using the following strategy.

pET-11(a) vector contained *Nde* I and *Bam* HI restriction sites. The *Nde* I and *Bam* HI restriction sites were incorporated into the Adhiron GST B4 binder sequence so that it could be incorporated into pET-11(a). PCR amplification of the Adhiron GST B4 binder was done using primers that were designed to incorporate *Nde* I and *Bam* HI restriction sites along with an octa-histidine tag flanking the Adhiron GST B4 binder sequence. Octa-histidine tag was incorporated for the purification of the binders in the subsequent experiments. Figure 4-8 shows the schematic of the steps involved in creating *Not* I and *Nhe* I restriction sites in pET-11(a) vector.

The primers used were forward primer containing *Nde* I restriction site and a reverse primer containing 8-histidine tags and *Bam* HI restriction site. The PCR was done using KOD Hot Start DNA Polymerase to produce blunt ended DNA fragments.

#### **4.3.3.3. Ligation of PCR products into pCR-Blunt vector**

The PCR products were then ligated into pCR-Blunt vector. pCR-Blunt vector is designed to clone blunt ended PCR fragments with a low background of non-recombinants.

The blunt ended PCR products were loaded on 1% (w/v) agarose gel and then gel extracted using the Wizard SV Gel and PCR Clean-Up System. The gel-extracted fragments were ligated into the linearised pCR-Blunt vector that included kanamycin resistant gene and lethal *ccdB* gene based selection to avoid the survival of non-recombinant cells. The ligation reaction was transformed into XL10 cells and grown on kanamycin containing LB plates. No colonies were obtained on the LB.

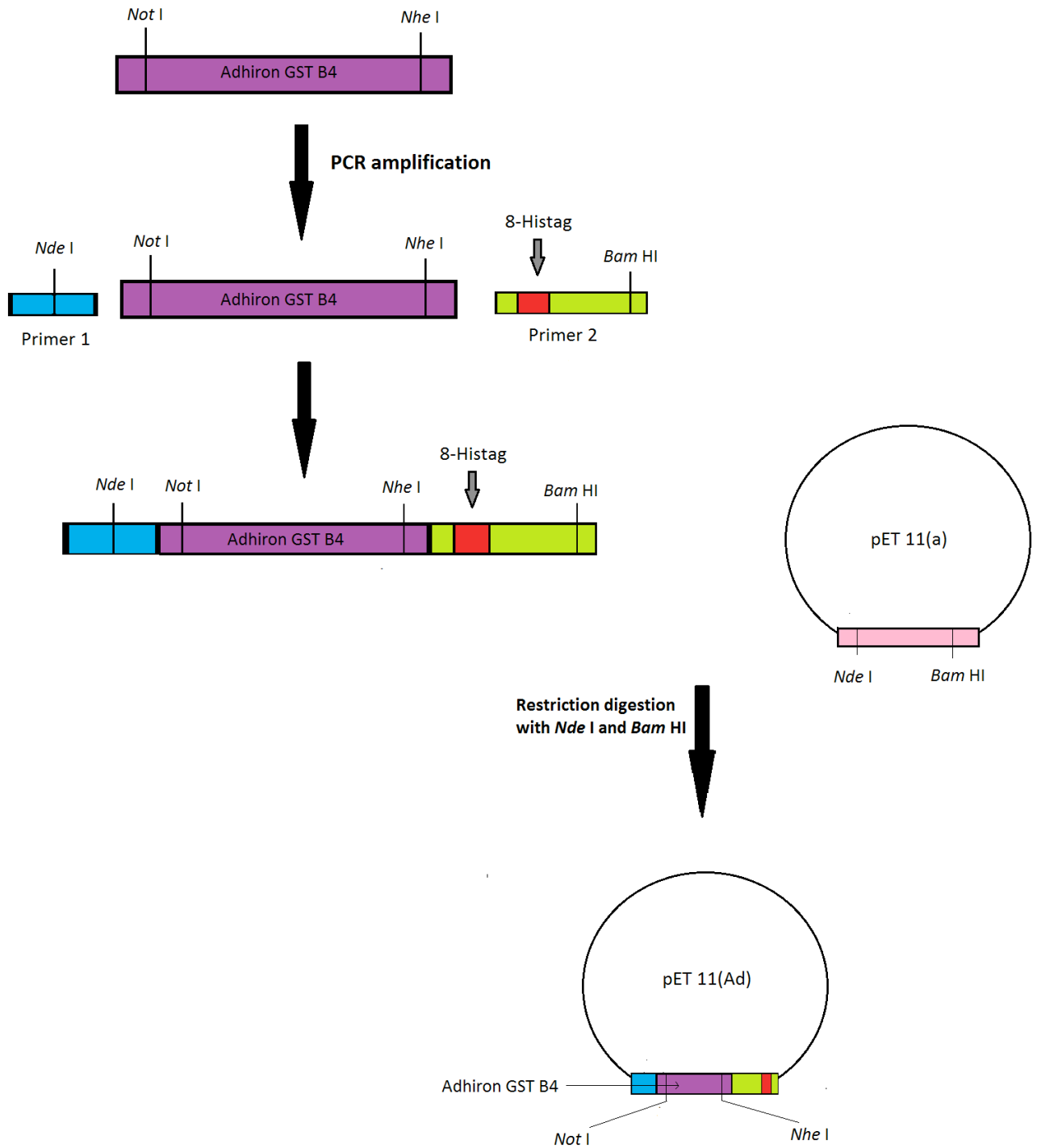


**Figure 4-8 A schematic of incorporating *Not*I and *Nhe*I restriction sites into pET-11(a) vector.**

The Adhiron GST B4 sequence containing *Not*I and *Nhe*I was inserted into pET-11(a) vector after amplifying Adhiron GST B4 sequence using PCR amplification. Primer 1 corresponds to forward primer and primer 2 corresponds to the reverse primer used in PCR amplification.

plate inoculated with ligation mixture containing only pCR-Blunt vector and no insert whereas colonies were obtained on the experimental LB plate (pCR-Blunt vector + insert). Three single colonies were picked and grown overnight for plasmid miniprep. The plasmids obtained from the cultures of three selected colonies, were sent for sequencing.

The sequencing result for one of the colonies was correct. The result confirmed the correct insertion of Adhiron GST B4 sequence flanked by *Nde* I, *Bam* HI and 8 his-tag incorporated into pCR-Blunt with no addition or deletion of amino acids.

#### **4.3.3.4. Ligation of Adhiron GST B4 sequence into pET-11(a)**

The minipreps of the pCR blunt adhiron GST B4 and the pET-11(a) vectors were then double digested using *Nde* I and *Bam* HI restriction sites. The digested fragments were run on a 1% (w/v) agarose gel. The inserts as well as the linearised pET-11(a) vector were gel extracted and ligated. The ligated mixture was transformed into XL10 Gold cells, grown and plated on carbenicillin containing LB plates. Colonies were obtained on the plates containing ligation mixture (pET-11(a) + insert) whereas no colonies were obtained on the control plates (pET-11(a) and no insert). In order to select the colonies for sequencing of the inserts initially a direct screening of the colonies was done using colony PCR.

#### **4.3.3.5. Colony PCR**

To confirm the presence of Adhiron containing fragment in the pET-11(a) vector, five single colonies were picked from the plate for analysis. To screen the inserts directly from the bacterial cell colonies, the cells were subjected to colony PCR. The PCR on the cells was done using GoTaq Hot start Polymerase and the PCR products were directly loaded on 1% (w/v) agarose gel. The controls used in colony PCR were as follows:

For positive control – XL10 Gold cells with pBSTG1 plasmid incorporated with Adhiron GST B4 binder.

For negative control - XL10 Gold cells with pET-11(a) vector without an insert and a PCR reaction mixture with no template DNA.

Figure 4-9 shows the products of the colony PCR done on five selected colonies along with the negative and positive controls. The bands were observed migrating in between 300 and 400 bp size corresponding to the expected length of the insert fragments. The primers corresponded to the

Adhiron sequences and therefore, the PCR amplification was observed in case of pET-11(a) vector containing Adhiron sequence as well as in case of the positive control pBSTG1 vector, incorporated with Adhiron GST B4 sequence. Cells with pET-11(a) vector without an insert and a reaction mixture with no template DNA, used as negative controls showed no band on the gel.

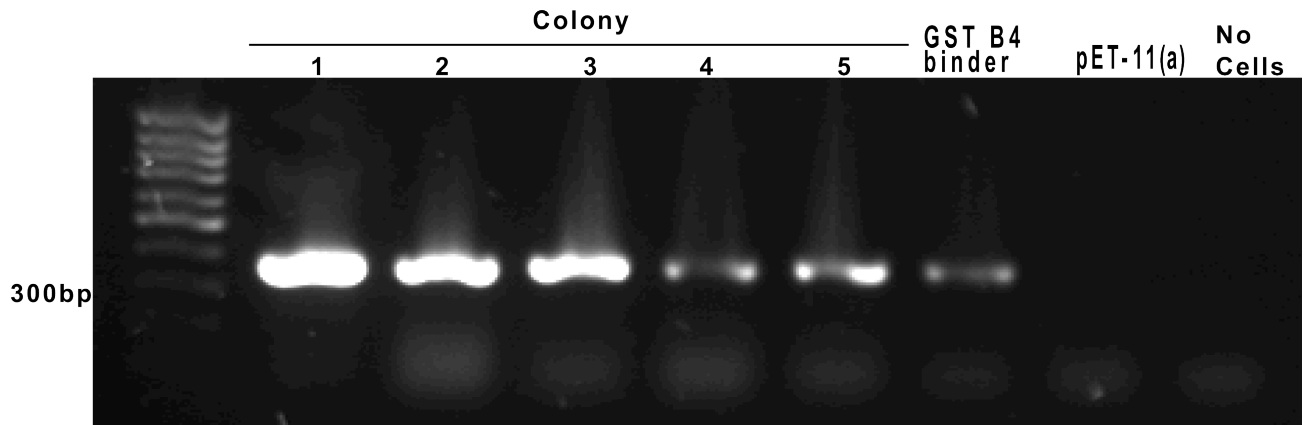


**Figure 4-9 Colony PCR.**

Colony PCR products from the 5 selected Adhiron clones run on a 1 % (w/v) agarose gel. Bands corresponding to bp were observed in each lane corresponding to the expected size of the Adhiron fragments. GST B4 binder containing pDHis vector was used as a positive control where a band is observed near 300 bp. Negative controls including pET-11(a) without the Adhiron fragment and PCR reaction mixture containing no cells were used.

The five colonies showing bands on the 1% (w/v) agarose gel in Figure 4-9 were further grown and the plasmids were extracted using miniprep kit. The DNA obtained was sent for sequencing.

The sequences obtained from the five colonies confirmed the correct Adhiron GST B4 sequence flanked by *Not* I and *Nhe* I restriction sites followed by an octa-histidine-tag incorporated in the pET-11(a) vector. No mutations were identified in the sequences. This vector was named as pET-11(Ad) expression vector (Figure 4-10).

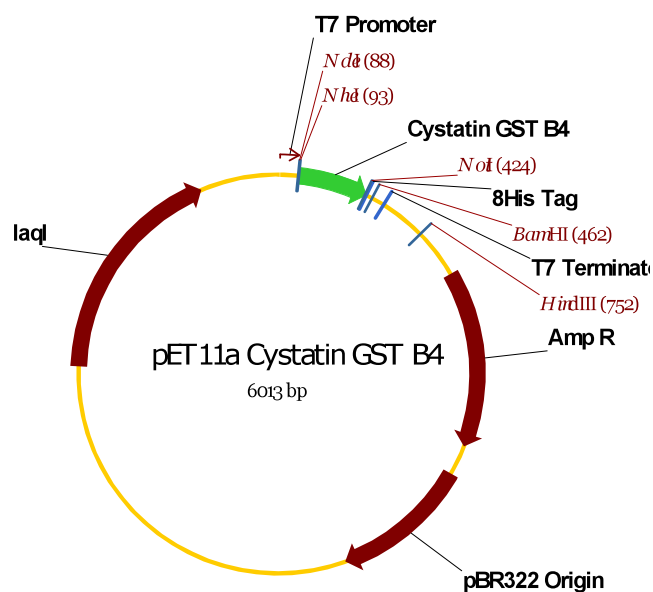


**Figure 4-10 Vector pET-11(Ad).**

The vector map of pET-11(Ad) expression vector after the incorporation of *Not* 1, Adhiron GST B4 named as cystatin GST B4 in the figure, *Nhe* I restriction site and octa-histidine tag. It has a T7 promoter and terminator gene. Ampicillin resistant gene for selection and pBR322 origin of replication. (Figure provided by Sarah Deacon, Astbury Centre for Structural Molecular Biology).

#### 4.3.3.6. Cloning Adhiron myc binders into pET-11(Ad) expression system

The Adhiron myc binder fragments present in pBSTG1 vector were amplified using PCR (Phusion DNA polymerase).

The PCR products obtained were digested with *Dpn* I to get rid of the methylated template plasmid DNA and to retain the PCR amplified products. The products were purified using gel extraction purification. The purified fragments were digested using *Nhe* I and *Not* I restriction enzymes. Figure 4-11 shows the bands obtained after running the double digested fragments on 1 % (w/v) agarose gel. The PCR products obtained corresponded to the theoretical size of Adhiron myc binder inserts (374 bp).

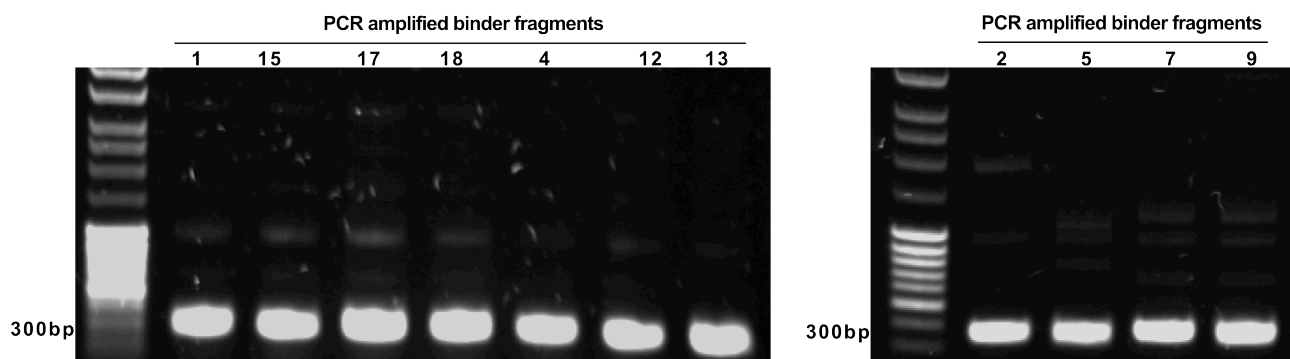


**Figure 4-11 Gel electrophoresis for Adhiron myc binder inserts.**

The 1 % (w/v) agarose gel showing the bands at migrating between 300-400 bp. The myc Adhiron binder fragments were amplified using PCR amplification. 10 kb DNA marker was used.

pET-11(Ad) was digested with *Not* I and *Nhe* I restriction enzymes. The digested mixture was run on 1 % (w/v) agarose gel and the linearised pET-11(Ad) fragment was gel extracted. The gel-extracted pET-11(Ad) fragment was ligated with previously obtained Adhiron myc binder inserts. Figure 4-12 shows the schematic of the incorporation of Adhiron myc binder into pET-11(Ad) expression vector.

The ligation mixture of each binder was transformed into XL10 Gold cells and colonies were obtained for all the transformations except the negative control transformation that contained pET-11(Ad) fragment and no insert. Plasmid DNA was extracted from positive colonies from each transformation by miniprep kit. The plasmid DNA obtained corresponding to each Adhiron myc binder was sent for sequencing. The sequencing results confirmed successful cloning of the anti-myc tag antibody binders into the pET-11(Ad). These plasmids were used for expression and purification of the respective binders.

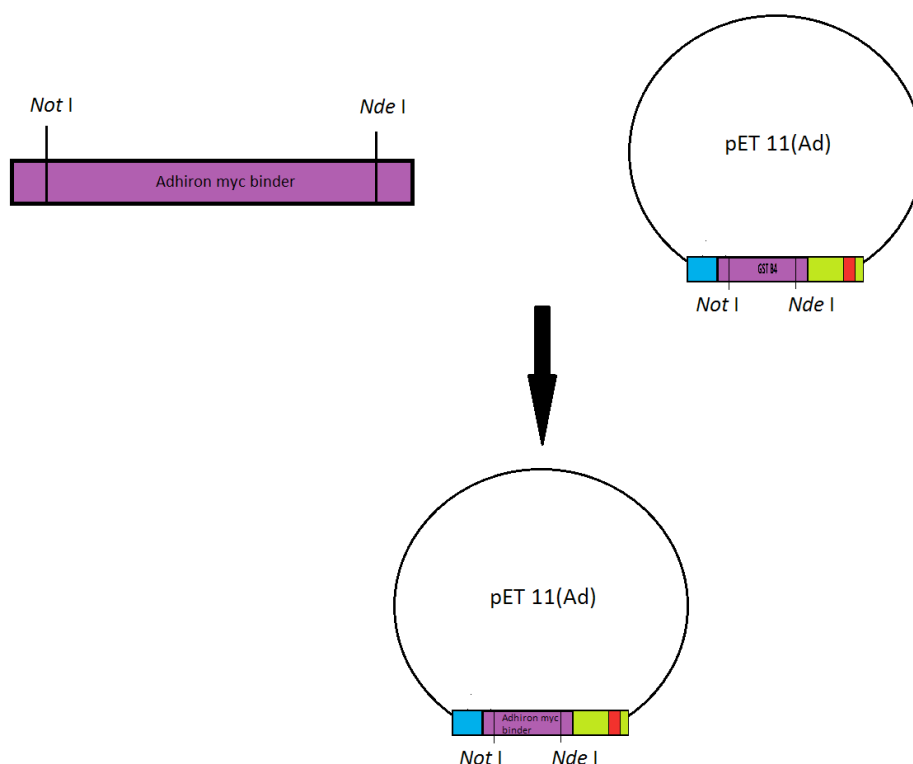


**Figure 4-12 Shows the schematic of incorporating Adhiron myc binders into the pET-11(Ad) vector.**

The PCR amplified Adhiron myc binder sequences and pET-11(Ad) was digested with *Not I* and *Nhe I* restriction sites and were ligated using T7 ligase enzyme.

#### 4.3.4. Optimisation of expression of Adhiron based binders

Out of all the Adhiron based binders cloned, Adhiron GST B4 binder was used to optimise the expression and purification protocol to be used for remaining Adhiron based myc binders. Adhiron GST B4 binder cloned into pET-11(Ad) vector was transformed in a number of different *E. Coli* strains. Optimum production conditions were determined by culturing transformed *E. coli* strains in a wide range of auto induction media for varying intervals.

##### 4.3.4.1. Dot blot

pET-11(Ad) vector containing Adhiron GST B4 binder was transformed into four different expression hosts - BL21 Star (DE3), C41 (DE3), C43 (DE3) and BL21 Gold (DE3) cells, each grown in a starter culture and then sub-cultured in different ForMedium™ autoinduction media (LB, TB, SB and 2YT). 200 µl of sample was collected from each subculture at six different time points 16, 24, 40, 48, 60, 72 hr post inoculation and analysed on a dot blot (see section 4.2.4.5).

Figure 4-13 shows the chemiluminescent detection of 200  $\mu$ l of sample collected from each sub-culture at different time points of 16, 24, 40, 48, 64, 72 hr into a 96 well plate. BL21 Star cells showed maximum chemiluminescence. Based on it, six combinations of growth media and time points were chosen for further analysis - BL21 Star cells incubated in 2YT for 24, 40 and 48 hr; BL21 Star cells incubated in TB for 40, 48, and 72 hr.

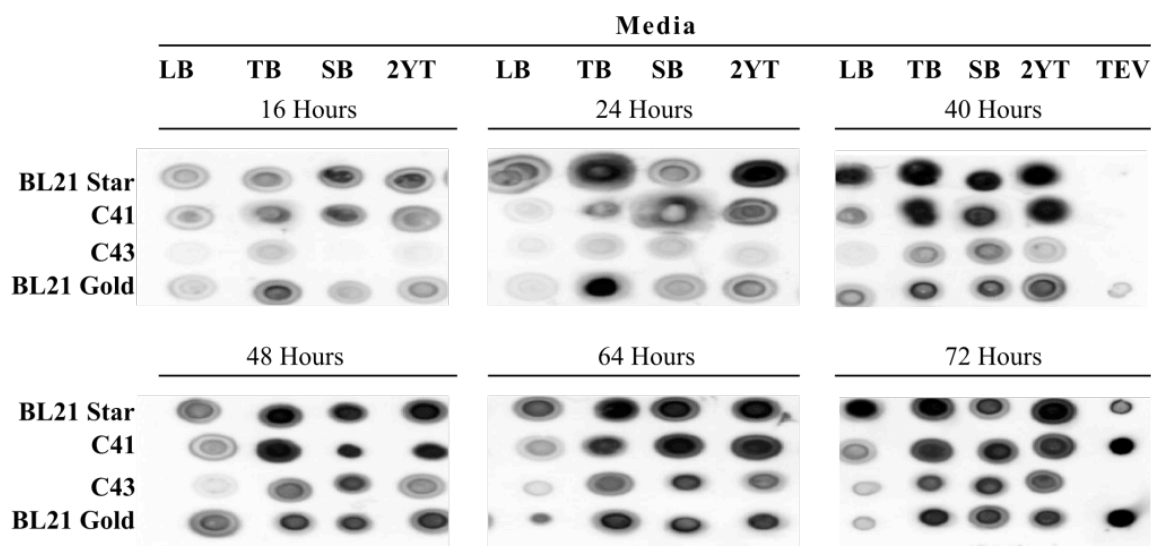


**Figure 4-13 Dot blot for optimising expression of Adhiron binders.**

Chemiluminescence detection of dot blot on GST B4 protein samples collected from cell cultures of BL21 Star (DE3), C41 (DE3), C43 (DE3), BL21 Gold (DE3) harvested at different time intervals of 16, 24, 40, 48, 64, 72 hr. The various media used were LB, TB, SB, 2YT. In the final column different concentrations of his-tagged TEV protein provide a positive control.

#### 4.3.4.2. Western blots

The expressed Adhiron GST B4 binder was used for determining solubility of the proteins. A western blot was done on the samples collected from the cell cultures selected in the dot blot analysis. The cells were harvested from the following combinations - BL21 Star cells grown in 2YT for 24, 40, 48 hr and in TB for 40, 48, 72 hr.

The total cell lysate as well as the supernatant of the cell lysates was analysed by western blot using anti-histidine tag antibodies (see section 4.2.4.6). Figure 4-14 shows the western blot done on the (a) supernatant and (b) total cell lysate of the samples obtained from the selected combinations.

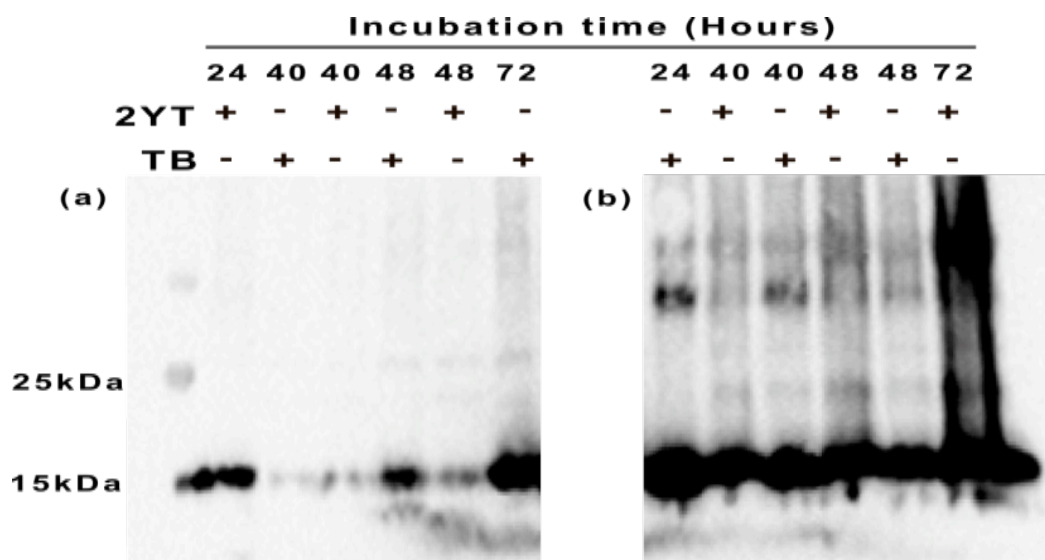


**Figure 4-14 Western blotting to detect expression of Adhiron GST B4.**

Western blot showing the chemiluminescent detection using anti his-tag antibodies done on the a) soluble fraction and (b) total cell lysate obtained from the harvested cultures expressing Adhiron GST B4 in ForMedium™ 2YT and TB and harvested at different incubation times (24 hr, 40 hr, 48 hr and 72 hr). Bands are observed migrating in the range of 12-15 kDa.

The western blot confirmed expression of the octa-histidine tagged GST B4 binder. Protein bands were observed migrating in the range of 11-13 kDa when compared to the protein markers. The bands corresponded to the molecular weight of the Adhiron GST B4 binder. Protein was found in the soluble fraction for all of the samples, however, the band intensity was higher when expressed in 2YT for 24 hr, TB for 48 hr and TB for 72 hr. TB 72 hr was not used further to grow Adhiron based binders because of time constraints. Therefore, combinations 24 hr 2YT and 48 hr TB were further selected for expression of the Adhiron GST B4 binder in BL21 Star cells.

#### **4.3.4.3. Expression and purification of Adhiron GST B4 binder in 2YT and TB ForMedium™ autoinduction media**

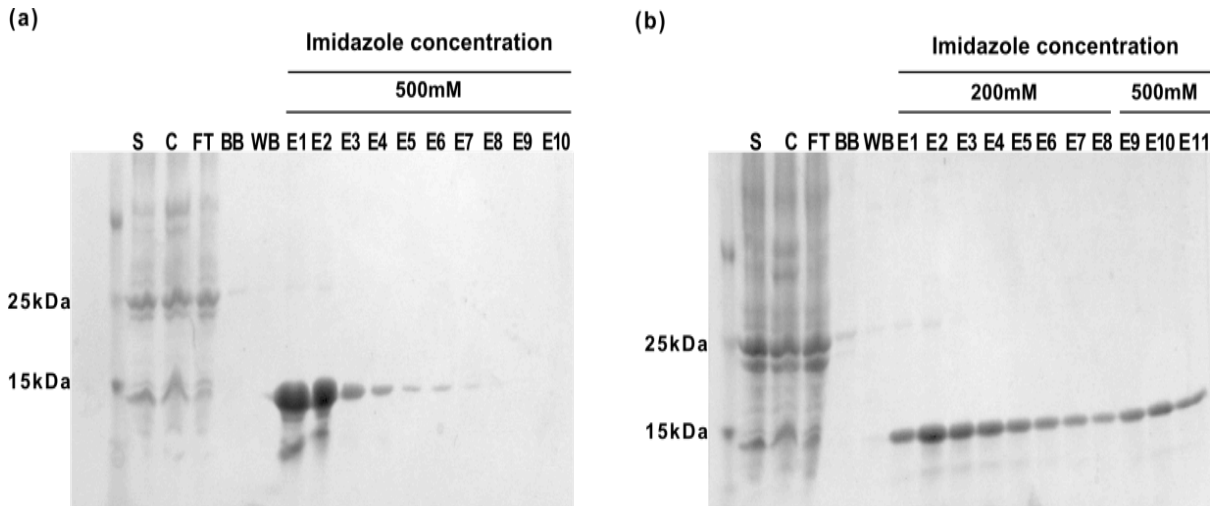
To further optimise the growth conditions of Adhiron GST B4 binder, pET-11(Ad) containing Adhiron GST B4 binder was transformed into BL21 Star DE3 cells. A single colony was picked and incubated in the starter culture. 400 mL of 2YT and TB ForMedium™ autoinduction media each were inoculated with the starter culture. The cells were harvested, lysed and the solubilised fraction was used for affinity column purification of Adhiron GST B4 binder (see section 4.2.4.2). At each step of the purification 1 ml samples were collected. 10 µl of the each sample was used to run on a 15 % (w/v) SDS PAGE in order to check the amount of Adhiron GST B4 binder in the collected samples as well to assure its purity.

Figure 4-15 shows the 15 % (w/v) SDS PAGE analysis of the protein samples obtained from a culture of BL21 Star DE3 cells grown in 2YT and TB ForMedium autoinduction media for 24 and 48 hr respectively.

In both the gel profiles in Figure 4-15 (a, b) the bands migrating between 10 and 15 kDa protein markers correspond to the expected size of Adhiron GST B4 binder *i.e.* 14.4 kDa. The band corresponding to the Adhiron GST B4 binder present in the cell lysate confirmed the expression of the binder whereas its presence in the soluble fraction (S) obtained after the crude cell lysate was centrifuged showed that the proteins were most likely correctly folded. The fraction of the flow through obtained after the supernatant was allowed to run through the affinity column showed that most of the endogenous proteins were eluted out and also some of the unbound Adhiron GST B4 binder has also eluted in the flow through.

The fractions obtained after washing the column with binding buffer (BB) and wash buffer (WB) showed no bands on the gel suggesting that either the Adhiron GST B4 binders were specifically bound to the Ni<sup>+</sup>-chelated column or were eluted in the previous steps as non-specifically bound proteins. The bands corresponding to the Adhiron GST B4 binders were observed in the elution fractions.

In case of expression of Adhiron GST B4 binder in BL21 Star DE3 cells, grown in 2YT ForMedium™ for 24 hr (Figure 4-15(a)) fractions of proteins (E1 to E10) were eluted in elution buffer containing 500 mM imidazole (see section 3.2.1.5). Imidazole was used to elute his-tagged Adhiron GST B4 binder bound to the columns as it displaces the his-tag, bound to the Ni<sup>+</sup>-chelated column *via* a co-ordination complex. Intensity of the bands corresponding to the Adhiron GST B4 binder was observed to decrease in the subsequent elutions and the first three fractions had the maximum amount of eluted protein. Due to the high concentration of imidazole, it was difficult to measure the true concentration of the proteins. Imidazole interferes with determination of protein concentration as its UV absorption spectra coincides with that of the proteins *i.e.* 280 nm. Moreover to avoid the effect of imidazole on the Adhiron GST B4 binder lower concentration of imidazole was used. In case of Adhiron GST B4 binder expressed in TB ForMedium™ for 48 hr (Figure 4-15(b)), fractions E1 to E8 were eluted in 200 mM imidazole and then fractions from E9 to E11 were eluted using 500 mM imidazole solution so as to check if the proteins were still bound to the column.



**Figure 4-15 Purification of Adhiron GST B4 grown in different autoinduction media.**

Showing a 15 % (w/v) SDS PAGE profile of the fractions collected during the purification of Adhiron GST B4 expressed in BL21 Star DE3 cells grown in (a) 2YT ForMedium™ for 24 hr and (b) TB ForMedium™ for 48 hr. Elution fractions were collected in 500 mM and 200 mM imidazole containing elution buffer. 10  $\mu$ L of each fraction was loaded in the wells. 10  $\mu$ L of total cell lysate and soluble fraction was loaded per lane. A total of 20  $\mu$ L out of each 100  $\mu$ L elution was loaded onto the gel. The gel was run at 200 V for 1 hr. M= Marker lane, S= Soluble fraction, T= Total cell lysate, BB= fractions collected from binding buffer wash, WB= Fractions collected from wash buffer.

#### 4.3.4.4. Dialysis

Dialysis of proteins was important to exchange the buffer to 1X PBS as well as get rid of imidazole and other contaminants, that can affect the Adhiron binders and their interaction with the myc antibodies in the subsequent experiments. All the eluted fractions were pooled together and dialysed in 10 mM PBS, pH 7.2 (see section 4.2.4.3). Adhiron GST B4 binder samples from both the undialysed pooled fractions and dialysed pooled fractions were run on a 15 % (w/v) SDS PAGE. 10  $\mu$ L of the pooled elutions of GST B4 Adhiron grown in 2YT and TB ForMedium™ (24 hr) eluted in 500 mM imidazole was run on 15 % (w/v) SDS PAGE before and after dialysis (Figure 4-16). The gel profile of the elution showed that the Adhiron GST B4 binder was intact after dialysis in 10 mM PBS (pH 7.2) and no degraded was observed after the dialysis.

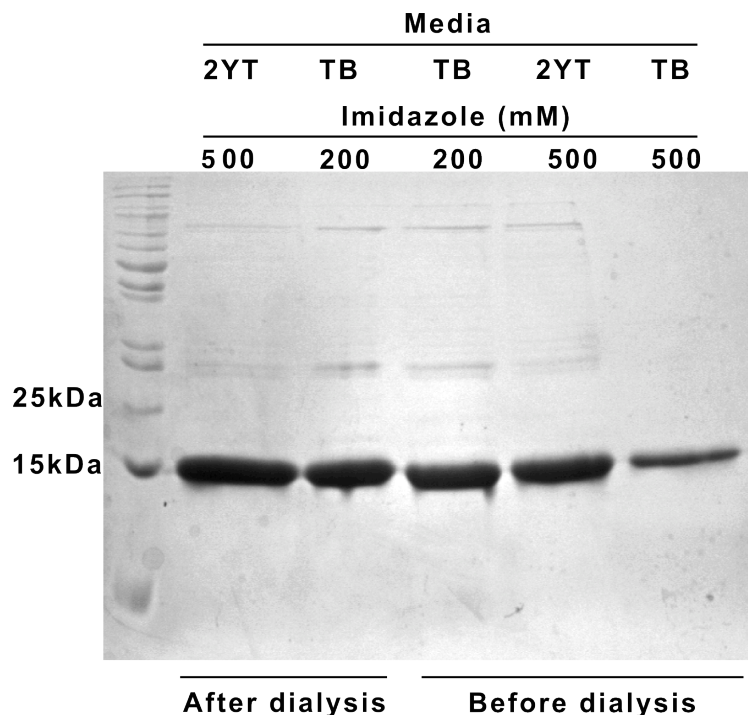


**Figure 4-16 SDS PAGE of Adhiron GST B4 after dialysis in 10 mM PBS (pH 7.2).**

SDS PAGE (15% (w/v)) showing pooled elution fractions from the purification of GST B4 Adhiron grown in 2YT ForMedium™ (24 hr) and TB ForMedium™ (48 hr) after and before dialysis in 10 mM PBS. GST B4 binder was eluted in elution buffer containing 200 mM and 500 mM imidazole concentration. 20  $\mu$ L of sample was loaded in each well.

The yield of Adhiron GST B4 binder when expressed in BL21 Star (DE3) in TB ForMedium™ for 48 hr was 6.5 mg/L whereas when expressed for 24 hr in 2YT ForMedium™ was 3.5 mg/L. Thus, the expression of Adhiron GST B4 in BL21 Star (DE3) (TB ForMedium™) for 48 hr followed by purification using 200 mM imidazole solution was chosen as the best condition for the expression and purification of Adhiron myc binders.

#### 4.3.5. Expression of Adhiron myc binders

pET-11(Ad) vector carrying Adhiron fragment with the myc binder sequences - were transformed in BL21 Star (DE3) cells. Single colonies corresponding to each binder were picked and a starter culture was inoculated followed by sub-culturing into 400 mL of TB ForMedium™.

To confirm the expression of the Adhiron myc binders before harvesting cells from 400 mL cultures, 1 mL sample was harvested, lysed and the binder expression was analysed using 15 % (w/v) SDS PAGE and western blot (see section 3.2.1.3).

#### 4.3.5.1. Adhiron myc binders 1, 2, 4 and 18

Adhiron myc binders 1, 2, 4 and 18 were grown in two batches. Figure 4-17 shows analysis of 1 ml sample from both the batches on 15 % (w/v) SDS PAGE (see section 4.2.4.4). Bands were migrating in the range of 11-12 kDa molecular weight. The theoretical molecular weights of the Adhiron myc binders were in the range of 13-14 kDa (Appendix-Table 31). The difference could be due to the folding properties of the binders.

On the 15 % (w/v) SDS PAGE, Adhiron myc binder 1 (M.W. 13.8 kDa) and Adhiron myc binder 2 (M.W. 14.08 kDa) showed higher molecular weights as compared to Adhiron myc binder 4 (M.W. 14.05 kDa) and Adhiron myc binder 18 (M.W. 14.2 kDa). This could again be attributed to the fact that the binders showed different extent of denaturation depending on their stability. The variation in denaturation affects the mobility of the proteins on SDA PAGE. So most likely Adhiron myc binder 1 and 2 can be more unfolded as compared to the other binders thus migrating at a higher molecular weight.

A second band was observed in each lane running in the range of molecular weight 22-24 kD, which corresponded to the molecular weight of dimer.

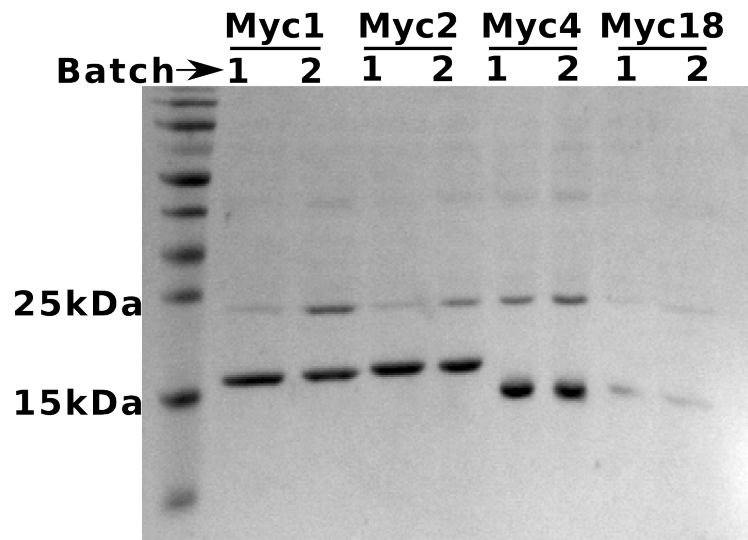


**Figure 4-17 SDS PAGE of Adhiron myc binder 1,2,4 and 18.**

Shows the 15 % (w/v) SDS PAGE profile of soluble fractions obtained from 1 ml sample of cell cultures growing Adhiron myc binders 1, 2, 4, 18 in two different batches each. 10  $\mu$ L of the soluble fraction was loaded onto the wells and the SDS PAGE was run at 220 V for 1 hr.

To check the expression of the Adhiron his-tag myc binders a western blot was done using anti-his tag antibodies on the total cell lysates (C) as well as the soluble fraction (S) of the 1 ml samples.

Figure 4-18 shows the chemiluminescent detection of bands in the cell lysate and soluble fractions of different cultures migrating in the range of 10-15 kDa molecular weight, which corresponds to the molecular weights of Adhiron his-tag myc binders. The bands obtained on the gel corresponding to the cell lysate depicts the expression of the Adhiron his-tag myc binders and the ones corresponding to the soluble fraction indicated that the Adhiron his-tag myc binders were more likely in correctly folded state. The intensity of the bands was brighter in the cell lysate as compared to the soluble fraction.

The faint bands observed in the range of 22-24 kDa molecular weight confirmed the formation of intra-molecular dimers within Adhiron his-tag myc binders. The bands corresponding to Adhiron his-tag myc binder 1 and 2 from both the batches corresponded to higher molecular weights as compared to the other binders.

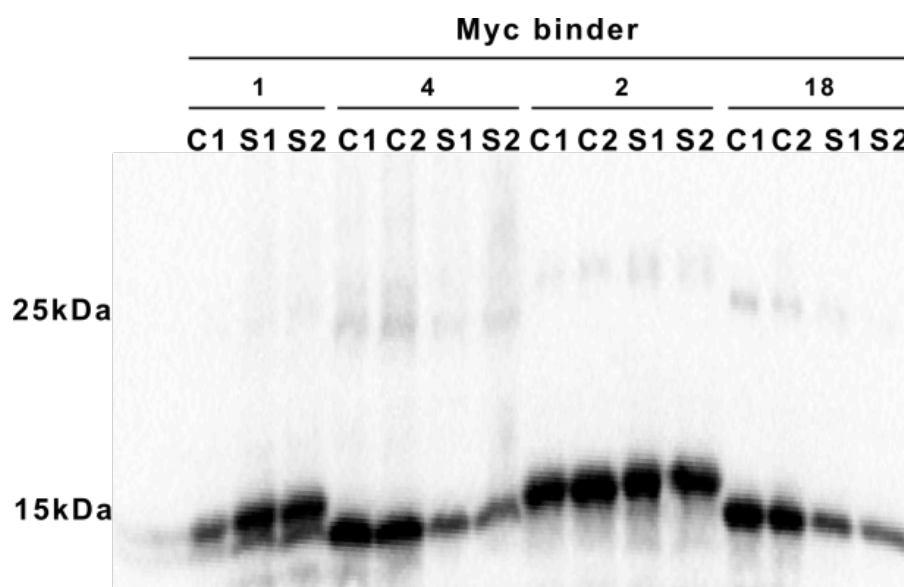


**Figure 4-18 Western blot of total cell lysates and soluble fractions of Adhiron myc binder 1, 4, 2 and 18.**

Shows the western blot done on the total cell lysates and the soluble fractions obtained from 1ml sample of two different batches of cell cultures growing Adhiron his-tag myc binders 1, 4, 2 and 18. Total cell lysate obtained from batch 1 and 2 designated as C1 and C2 respectively. Soluble fraction obtained from batch 1 and 2 designated as S1 and S2 respectively.

#### 4.3.5.2. Adhiron myc binders 5, 7, 13 and 17

1 mL samples collected from two different batches of cell cultures growing Adhiron binders 5, 7, 13 and 17 were subjected to 15 % (w/v) SDS PAGE (see section 4.2.4.4). Figure 4-19 shows the gel profile of the cell lysate and supernatant of 1 ml samples. Bands migrating between 10-15 kDa

corresponded to the expected molecular weights of Adhiron binders 5, 7, 13 and 17 (Appendix-Table 31). The intensity of bands corresponding to Adhiron myc binders 5, 7, 13 and 17 observed in Figure 4-19 is lower as compared to that observed in case of Adhiron myc binders 1, 2, 4,18 shown in Figure 4-17. This could be due to difference in handling of cultures or attributed to different levels of protein expression. Bands were also observed in the range of 22-25 kDa molecular weight indicating dimerisation of the binders taking place.

Western blotting done on the cell lysates and soluble fractions of 1 ml samples using anti his-tag antibodies is shown in Figure 4-20. It confirmed the expression of Adhiron his-tag myc binders 5, 7, 13 and 17.

The 15 % (w/v) SDS PAGE (see section 4.2.4.4) and western blot done (see section 4.2.4.6) on the samples established the expression of the Adhiron myc binders, which were then purified from the cell cultures of larger volume (400 mL).

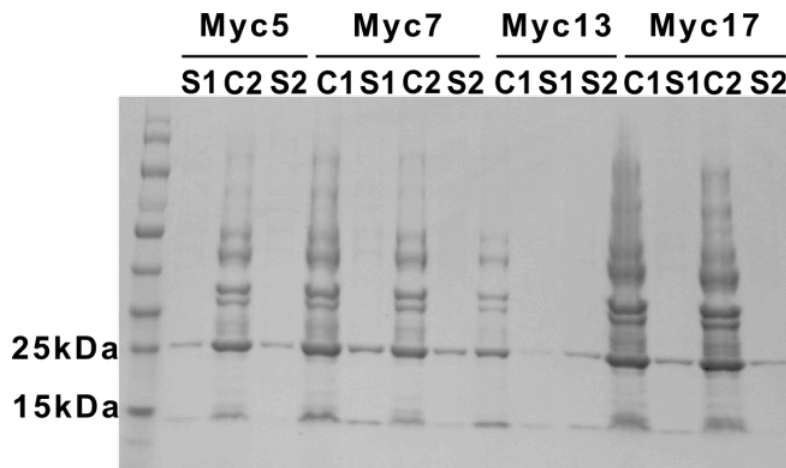


**Figure 4-19 SDS PAGE of total soluble fraction and cell lysate of Adhiron myc binder 5, 7, 13 and 17.**

Shows the 15 % (w/v) SDS PAGE done on the total cell lysate (C) and the soluble fraction (S) obtained from 1 ml sample of two different batches of cell cultures growing Adhiron myc binders 5, 7, 13 and 17. Total cell lysate from batch 1 and 2 designated as C1 and C2 respectively. Supernatant from batch 1 and 2 designated as S1 and S2 respectively. 10  $\mu$ L of the sample was loaded onto the wells and the SDS PAGE was run at 220 V for 1 hr.

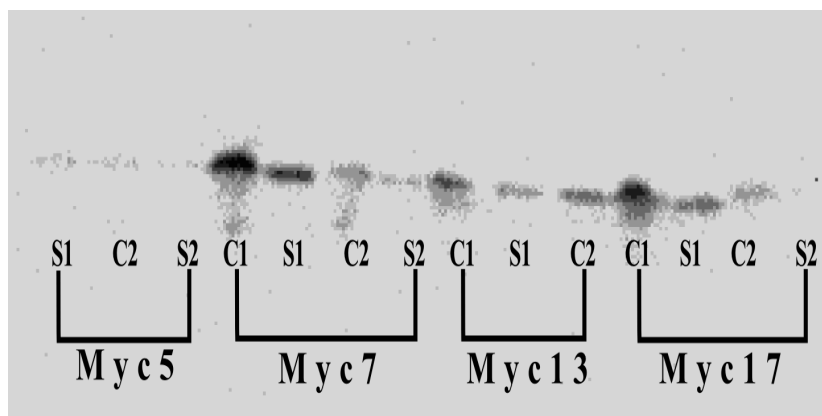


**Figure 4-20 Western blot of soluble fractions and the cell lysates of Adhiron myc binder 5, 7, 13 and 17.**

Shows the western blot done on the total cell lysates and the soluble fractions of cell lysates obtained from 1ml samples of two different batches of cell cultures growing Adhiron myc binders 5, 7, 13 and 17. Total cell lysate from batch 1 and 2 designated as C1 and C2 respectively. Supernatant from batch 1 and 2 designated as S1 and S2 respectively.

#### 4.3.6. Purification of Adhiron myc binders

Purification of the Adhiron myc binders was done using Ni<sup>+</sup> chelated Hi-trap affinity columns. The 400 mL culture of BL21 Star (DE3) cells transformed with pET-11(Ad) vector containing Adhiron myc binder was harvested and cells were lysed using sonication. The cell lysate was centrifuged and the soluble fraction of the crude extract was allowed to flow through the column. The flow through fractions were collected (FT) followed by collecting fractions after adding different buffers –binding buffer (BB), wash buffer (WB) and finally the elution buffer (E) for eluting the Adhiron myc binders. 10 µL of the samples collected were run on a 15 % (w/v) SDS PAGE.

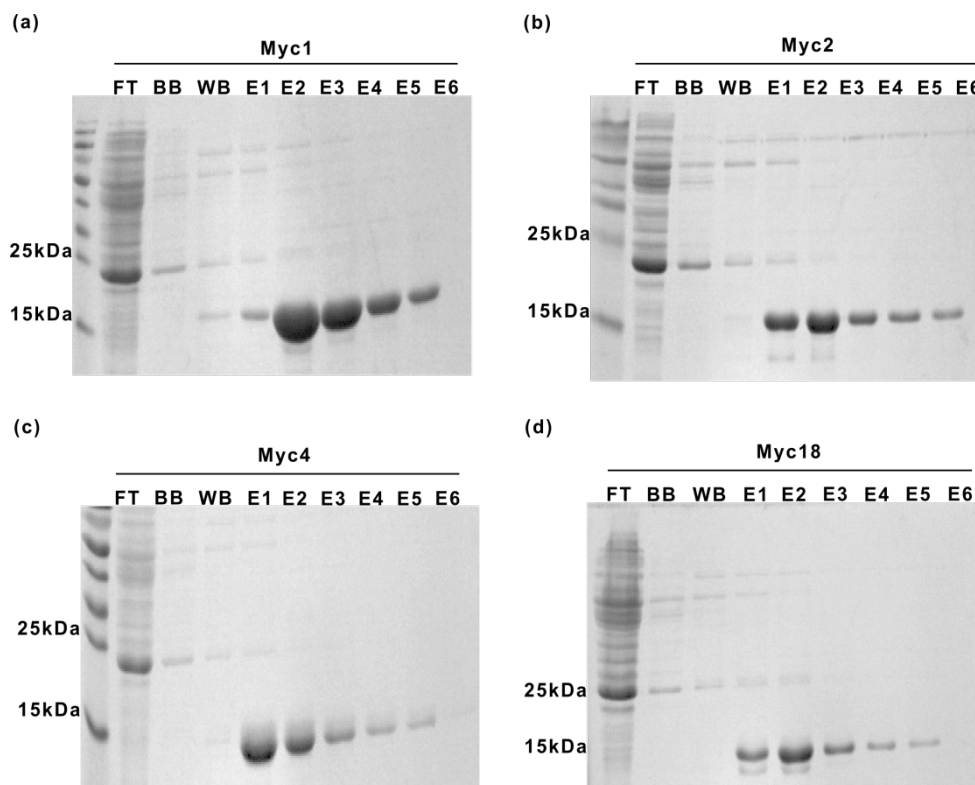
##### 4.3.6.1. Adhiron myc binders 1, 2, 4,18

Figure 4-21 shows the 15 % (w/v) SDS PAGE profiles of fractions collected during purification of Adhiron myc binders 1, 4, 2 and 18. Most of the endogenous proteins corresponding to different molecular weights were eluted in the flow through (FT). Bands of non-specifically bound endogenous proteins were observed in the fractions collected from the binding buffer and wash buffer flows.

In the elution fractions (E1-E6) bands migrating in the range of 12-15 kDa molecular weight were observed that corresponded to the molecular weights of the Adhiron myc binders. In case of first two elution fractions (E1 and E2) of Adhiron myc binders 1, 2 and 18, some discrete bands are observed in the range of 12-10 kDa other than the main band corresponding to Adhiron myc binders. These

could be due to degradation of the binders taking place or due to different folding of the binders that gives rise to different migration properties.

Some bands observed in the elution lanes (E) showed host protein contaminants that could be minimised by using Tween 20 in the wash buffer. Tween 20 was used during the purification of the other binders to get rid of the non-specifically bound endogenous proteins.



**Figure 4-21 Purification of Adhiron myc binder 1, 2, 4 and 18.**

Shows 15 % (w/v) SDS PAGE profile of fractions collected during the purification of Adhiron myc binders 1, 4, 2 and 18. The bands obtained are in the molecular weight range of 12-15 kDa. 10  $\mu$ L of the soluble fraction was loaded onto the wells and the SDS PAGE was run at 220 V for 1 hr.

M= Marker lane, FT= Flow through fraction on  $\text{Ni}^{+}$  chelated column, BB= Fractions collected after binding buffer was applied to the column, WB= Fractions collected after wash buffer was applied to the column. E= Elution fractions collected by applying elution buffer containing 200mM imidazole.

#### 4.3.6.2. Adhiron myc binders 5, 7, 13 and 17

An extra step of washing with wash buffer containing tween was included in purification of Adhiron myc binders 5, 7, 13 and 17. Figure 4-22 (a, b) shows gel profile of fractions collected during the purification of Adhiron myc binder 5. The flow through (FT) fraction did not contain the Adhiron myc binder 5. The binding buffer (BB) and wash buffer (WB) fractions showed the removal of non-

specifically bound proteins. Running wash buffer containing tween (TW) was followed by running wash buffer (W) without tween to get rid of tween in the column. Fainter bands of endogenous proteins were observed in the later wash buffer fractions (W1, W2). The elution fractions E1 to E9 depicted in Figure 4-22(a, b), eluted in elution buffer with 200 mM imidazole showed a gradient of decreasing band intensity corresponding to Adhiron myc binder 5. Bands corresponding to 22-25 kDa marker proteins were observed that were more likely due to dimerisation of the binders (see section 4.2.2.14). A light band observed for elution fraction E10 collected after running elution buffer containing 500 mM imidazole showed that most of the specifically bound Adhiron myc binder 5 proteins were eluted in the previous elutions.

Figure 4-22(b, c and d) shows the 15 % (w/v) SDS PAGE profile of fractions collected during the purification Adhiron myc binder 7. Band corresponding to Adhiron myc binder 7 was observed in the elution fractions. In Figure 4-22(c) the gel profile of fractions corresponding to binding buffer (BB), wash buffer containing tween (TW) followed by washes with wash buffer (W) showed very light bands of host protein contaminants. Elutions fractions (E1-E7) showed bands migrating at the Adhiron myc binder 7 molecular weight. In Figure 4-22(d) shows the gel profile of elution E8 containing band corresponding to Adhiron myc binder 7 along with some contaminant proteins and a higher elution of specifically bound Adhiron myc binder 7 in 500mM imidazole containing elution buffer (E9) than observed in E8.

Figure 4-22(d, e) shows 15 % (w/v) SDS PAGE gel profile of fractions collected during the purification of Adhiron myc binder 13. Endogenous proteins were collected in the flow through fractions as observed in the gel profile. The elution fractions (E4-E9) of binder 13 show a more dimerised form of the binder as compared to all other binders.

Figure 4-22(e, f) shows fractions collected during purification of Adhiron myc binder 17. Bands corresponding to molecular weight 12-15 kDa were observed in the gel profile of elution fractions corresponding to the Adhiron myc binder 17.

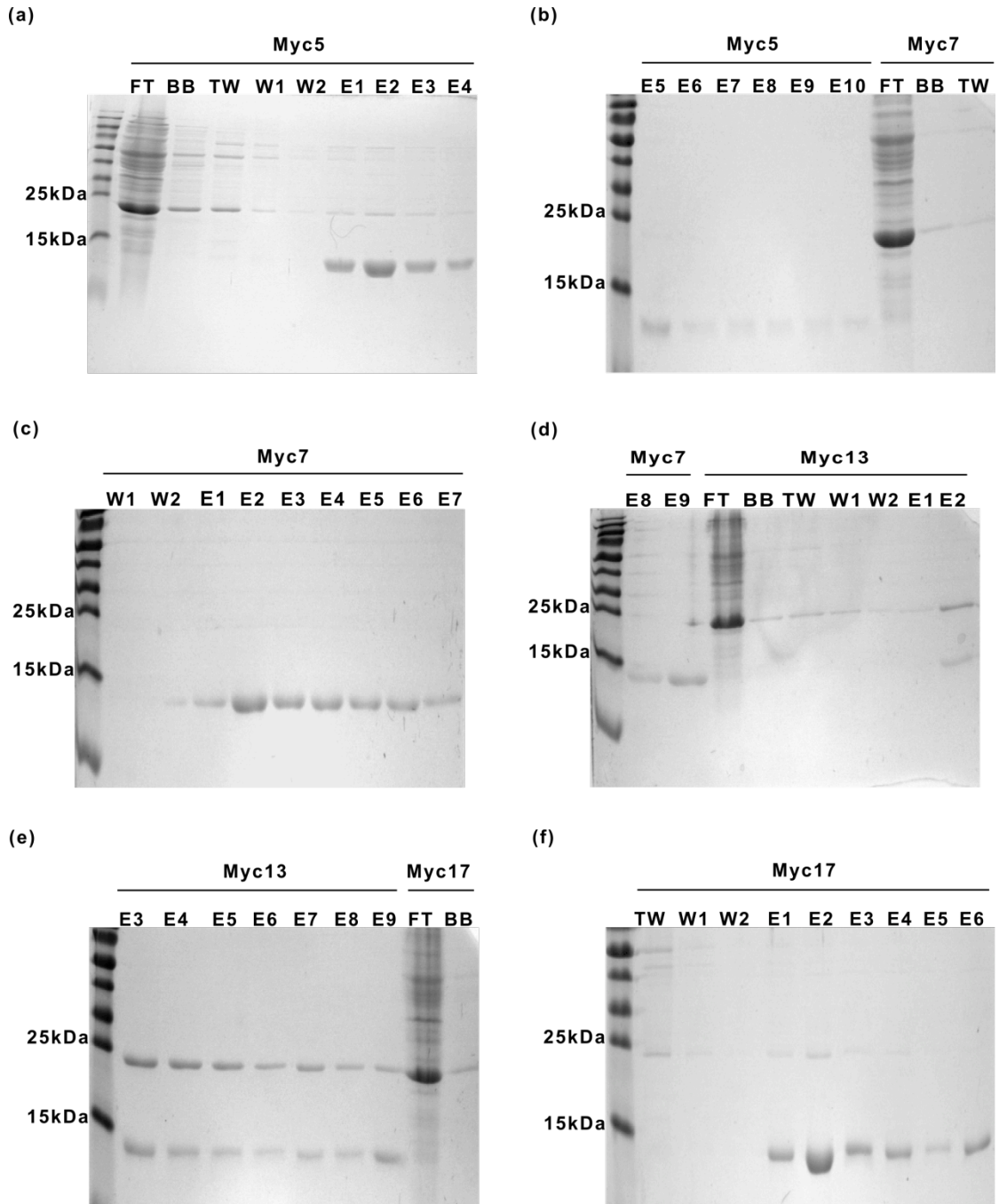


**Figure 4-22 Purification of Adhiron myc binder 5, 7, 13 and 17.**

Shows 15 % (w/v) SDS PAGE done on fractions collected during the purification of binder 5, 7, 13 and 17 using a Hitrap protein purification column.

M= Marker lane, S= Supernatant of cell lysate, FT= Flow through, BB= Fractions collected with binding buffer, TW = Wash with tween, W= Fractions with wash buffer and E= Elution fractions.

#### 4.3.6.3. Adhiron myc binders 11 and 20

Figure 4-23 shows the 15 % (w/v) SDS PAGE profile of the fractions obtained during the purification of the Adhiron myc binder 11 and 20. Most of the unwanted proteins present in the

supernatant of the cell lysate were extracted in the flow through (FT) fractions. In case of Adhiron myc binder 11 the band corresponding to the binder protein (12-15 kDa) showed less intensity in the elution fractions. This could be because of low expression level of the binder in the bacterial strain or degradation of the proteins due to sequence specific proteolysis. The Adhiron myc 20 binder bands migrating at the molecular weight to 12-15 kDa showed a gradient in band intensity from E1 to E7 corresponding to elutions done in 200 mM imidazole. Higher intensity bands are obtained from E8 - E10 corresponding to elutions done in 500 mM imidazole.

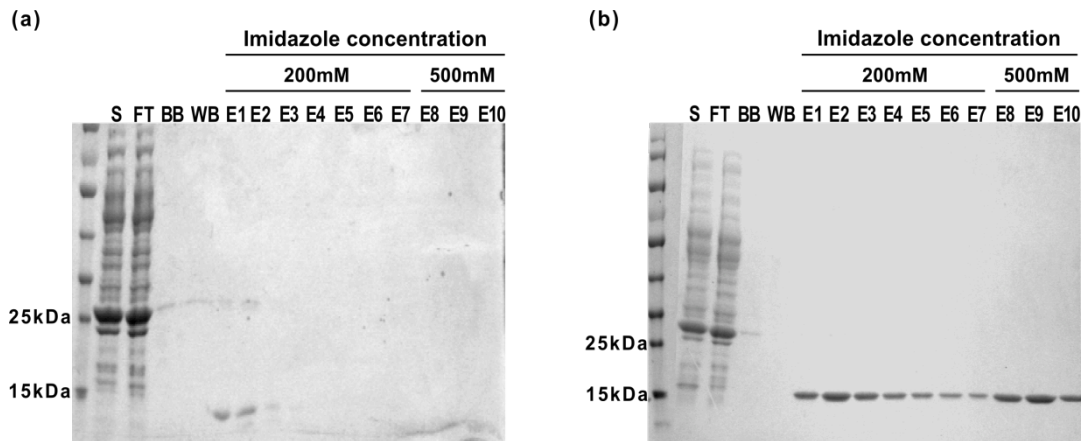


**Figure 4-23 Purification of Adhiron myc binder 11 and 20.**

SDS-PAGE (15% (w/v)) showing fractions collected during the purification of Adhiron myc (a) binder 11 and (b) binder 20, using a Hitrap protein purification column. The elution fractions from E1-E7 in case of both the binders were collected using elution buffer containing 200mM imidazole and fractions E8-E10 were collected using elution buffer containing 500 mM imidazole concentration.

M= Marker lane, S= Soluble fraction, FT= Flow through, BB= Fractions collected with binding buffer, WB= Fractions collected with wash buffer and E = Fractions collected with elution buffer.

#### 4.3.7. Dialysis of purified Adhiron myc binders

All the elutions of respective binders were pooled together and then dialysed in 10 mM PBS (pH 7.2). Adhiron myc 13 showed formation of precipitate during dialysis. The dialysed binders were then analysed on 15 % (w/v) SDS PAGE shown in Figure 4-24. Adhiron scaffold showed a lower molecular weight (Figure 4-24(a)) as compared to the Adhiron based binders. This corresponds to the shorter length of loops in Adhiron scaffold. Adhiron myc binder 1 and 2 showed higher molecular weight than the rest of the binders (Figure 4-24(b)).

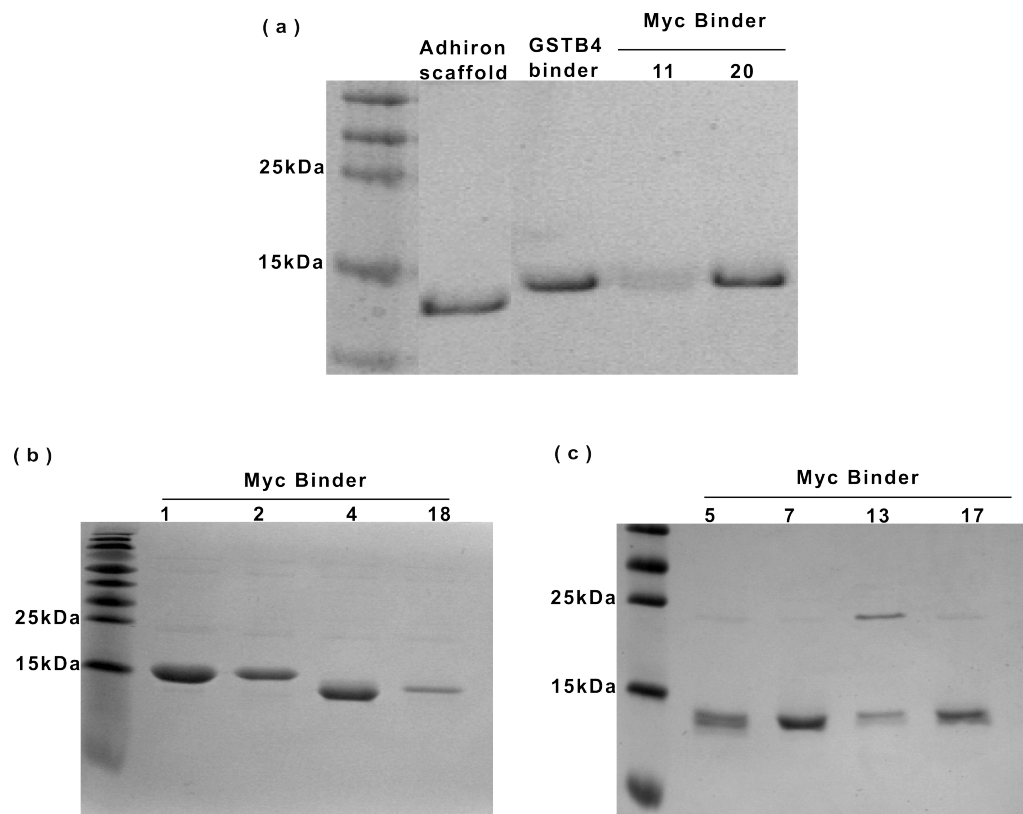


**Figure 4-24 SDS PAGE of Adhiron scaffold, Adhiron GST B4 binder and ten Adhiron myc binders.**

Shows the 15 % (w/v) SDS PAGE profile of proteins after dialysis in 1 X PBS (a) Adhiron scaffold, Adhiron GST B4 binder, Adhiron myc binder 11 and 20, (b) Adhiron myc binders 1, 2, 4, 18 and (c) Adhiron myc binders - 5, 7, 13 and 17. 10  $\mu$ g of protein was loaded in each lane.

### 4.3.8. Characterisation

#### 4.3.8.1. Circular Dichroism (CD)

The secondary structure of the proteins was analysed using CD. In Figure 4-25, the CD spectrum of Adhiron scaffold and Adhiron myc binders show well-defined anti parallel  $\beta$ -pleated sheets corresponding to positive peak at 195 nm and a broad negative peak above 210 nm (see section 3.2.3). The higher percentage of  $\beta$ -sheets had masked the  $\alpha$ -helical structure. Myc 18 showed a prominent  $\alpha$ -helical structure depicted by negative bands at 208 nm and 218 nm (see section 3.2.3). The variation in the measured ellipticity was different for different binders perhaps due to the difference in folding of various sequences of the loop regions in the Adhiron scaffold and Adhiron myc binders.

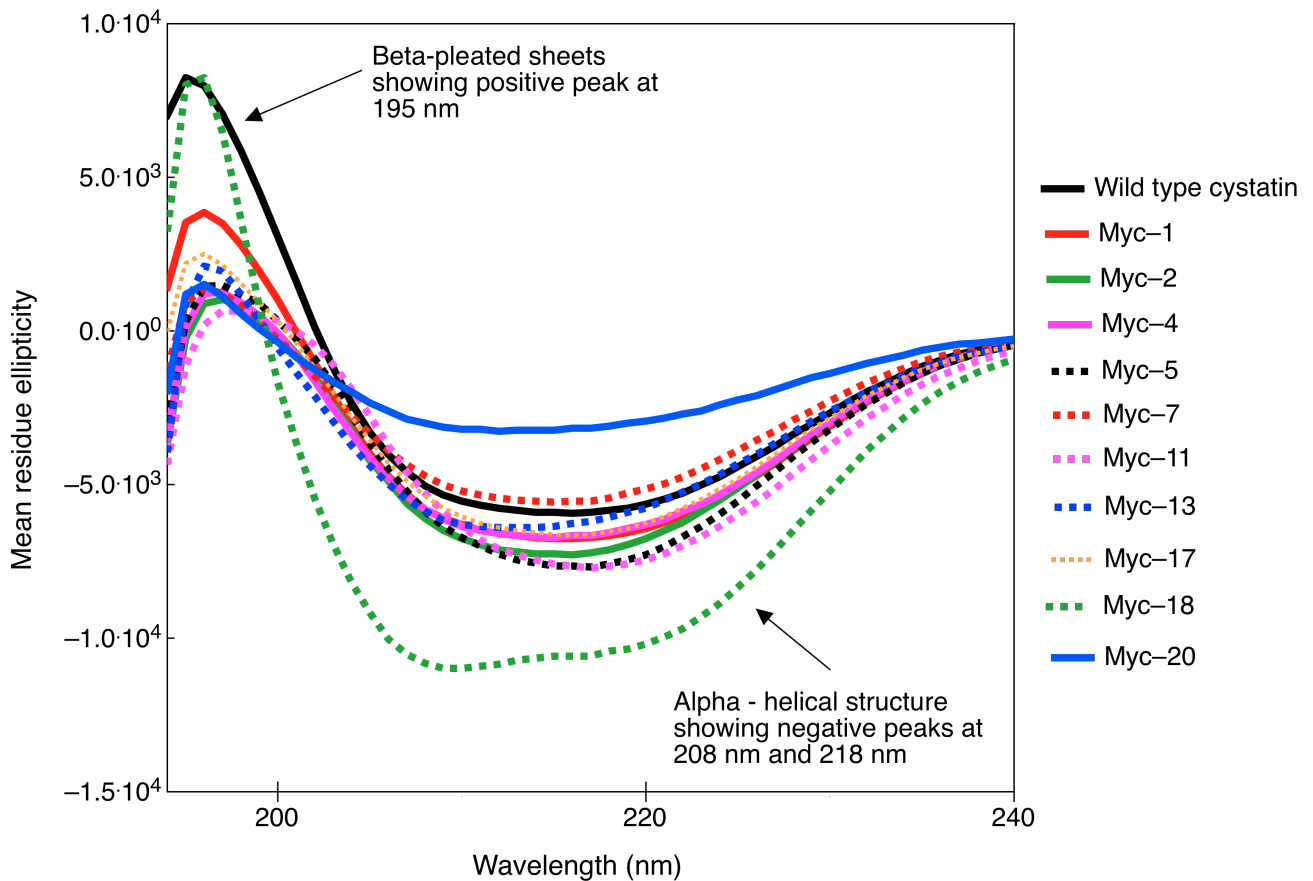


**Figure 4-25 Circular dichroism of Adhiron myc binders.**

Secondary structure of wild type phytocystatin based Adhiron scaffold and the binder variants shown by CD. At 195 nm a positive peak is observed and above 210 nm a broad negative peak is observed in all the binders. The spectra were recorded in the far-UV (190-260 nm) range at a protein concentration of 0.5 mg/ml. The analysis was done using the Dichroweb reference set CDSSTR.

#### 4.3.8.2. Differential Scanning Calorimetry (DSC)

Thermal stability of the protein was analysed using DSC. Figure 4-26 shows the profiles of heat capacity (CP) vs. temperature of proteins subjected to temperature scans, between 11 °C to 90 °C/130 °C at the rate of 90 °C/hr. The normal functioning of the instrument was assured by checking the unfolding of lysozyme protein (Figure 4-26(a)) under the same heating and cooling conditions which showed a  $T_m$  of 72 °C for protein lysozyme (Chôma, 2006).

Amongst all the ten binders, Adhiron myc binder 2 was chosen for forming the biological recognition layer of the EIS based biosensor (see Chapter 5). Due to interest in the best binding candidate (Adhiron myc binder 2), the transition temperature of Adhiron myc binder 2 was studied. The transition temperature of Adhiron myc binder 2 was analysed by using temperature ranging from 11 °C to 90 °C. Figure 4-26(b) establishes that the Adhiron myc binder 2 shows reversibility of unfolding reaction. The repeated scanning of the Adhiron myc binder 2 under identical conditions gave endotherms having the same transition temperature of 85 °C. The sharpness of the peaks indicates that the process is cooperative in nature.

The initial temperature scan on Adhiron scaffold was done from 11 °C to 90 °C and no peak was observed. This experiment was repeated twice (data not shown). Later, the maximum temperature was increased to 130 °C and the Adhiron scaffold showed a melting temperature of 101 °C (Figure 4-26(a)).<sup>1</sup> As compared to the Adhiron myc binder 2, the melting temperature for Adhiron scaffold increased to 101 °C shown in Figure 4-26(c). The lower melting point of Adhiron myc binder 2 can be attributed to the structural instability brought by the inserts in the loops. The non-reversibility of unfolding reaction (scan 2) in case of Adhiron scaffold (Figure 4-26(c)) could be because of the high maximum temperature of scanning that prevents proper refolding of the polypeptide chain. The high transition temperature of the Adhiron scaffold corresponds to the high thermostability of the scaffold. This was most likely due to the consensus-based design of the Adhiron scaffold that gives it high thermostability. The disulphide bridges do not contributing to the stability as neither the scaffold nor the loops in the binders contain any cysteine residues. It can also be due to more salt bridges and hydrogen bonding (Jaenicke, 2000) for which the crystal structure of the Adhiron scaffold needs to be analysed.

---

<sup>1</sup> Acknowledgement: As there was not enough Adhiron scaffold protein left of the original purification for this DSC experiment, this experiment was performed by William Morton and Sarah Deacon on the Adhiron scaffold protein purified by William Morton using the vector and protocols used in the rest of this study.

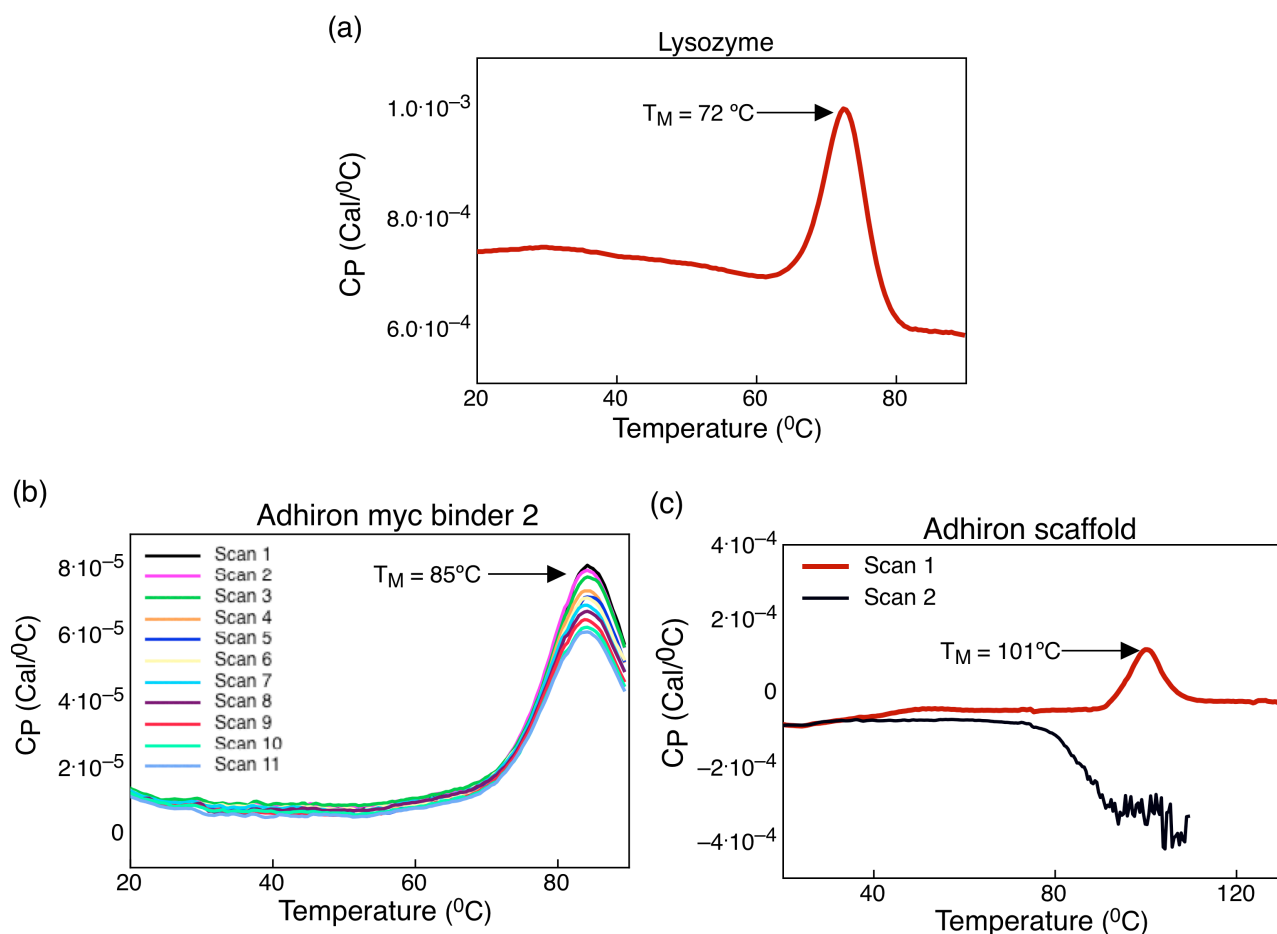


**Figure 4-26 Differential scanning calorimetry of lysozyme, Adhiron myc binder 2 and Adhiron scaffold.**

DSC profiles of heat capacity vs. temperature performed on 0.5 mg/mL protein samples prepared in 1 X PBS buffer at pH7.4. The temperature scanning was done between 11 °C and 130 °C at the rate of 90 °C/hr. (a) lysozyme as control, (b) Adhiron myc binder 2 and (c) Adhiron scaffold.

The characterisation results depicted high thermal stability and intact secondary structure of the Adhiron myc binders. The binders were further characterised in order to choose the best binder against monoclonal anti-myc tag antibodies and develop an EIS based biosensor.

#### 4.4. Discussion

This chapter describes the cloning and purification of binders based on a novel protein scaffold called Adhiron developed by McPherson group at the Centre for the Structural and Molecular Biology, University of Leeds. Adhiron is based on a consensus sequence of plant-derived phytocystatin. It consists of four-strand anti-parallel  $\beta$ -sheet core and a central helix. It showed a

high melting temperature of 101 °C which could be attributed to the consensus protein design of the Adhiron scaffold.

To prove the versatility of the Adhiron scaffold, a library based on randomised aminoacid sequences commercially obtained from Sloning Biotechnology was created. The BSTG at the Centre for the Structural and Molecular Biology, University of Leeds cloned these randomised oligonucleotides into a phagemid named as pBSTG1 and selected binders against monoclonal anti-myc tag antibodies using phage display library. The ten Adhiron myc binders were selected for this project from the phage display library. These binders were successfully cloned into the pET expression vector. As the expression of the Adhiron scaffold was not performed previously in the pET expression vector therefore optimisation of the conditions for expression and purification was done. All the Adhiron myc binders were expressed in soluble form with a yield in the range of 4-8 mg. The Adhiron myc binder 13 was forming aggregates. The observed precipitation of Adhiron myc binder 13 could be due to difference in the folding of the loops. It will be useful to change the buffer conditions or use a stabilising agent in the dialysis buffer like glycerol that can prevent precipitation of the binder. Although on 15 % (w/v) SDS PAGE, most of the Adhiron myc binders showed less endogenous contaminants in the elution fractions but there was a band observed in the range of 24-25 kDa that could be because of the formation of dimers. In order to get binders of high purity, a size exclusion chromatography can be performed to get rid of the dimers. Formation of dimers can interfere with the use of Adhiron binders in different biological assays.

The secondary structure of the binders was maintained as was seen in the circular dichroism, although the fractions of  $\alpha$ -helices and  $\beta$ -sheets varied amongst the binders. The thermal stability of the Adhiron scaffold and Adhiron myc binder 2 was high. Moreover, Adhiron myc binder 2 showed reversibility in folding. Over the past few years various scaffolds have been introduced. The recent consensus based artificial antibody called reprobodies exhibited a melting temperature of 85 °C but the thermal stability of the phycocystatin based Adhiron scaffold and its variant Adhiron binder 2 was unusually high. The factors that provide a high melting temperature to the scaffold will be an interesting field to explore. The thermostability of a protein influences its overall stability and therefore the Adhiron based binders will be quite promising when used in different environmental conditions. Although the thermal stability of the scaffold has been established, the determination of the resistance of the binder stability to different pHs will prove to be very significant.

Full characterisation of all the Adhiron myc binders was not possible because the main objective of the work was to get a well-characterised binder with maximum binding affinity and use that for further electrochemical experiments to fabricate a biosensor.

## **Chapter 5. Fabrication of an impedimetric biosensor based of a non-antibody recognition protein –Adhiron myc binder 2**

### **5.1. Introduction**

The previous chapter discussed a non-antibody based capture molecule based on a scaffold called Adhiron, which was used to present different peptides in its three variable regions consisting of an N-terminal region and two variable loops (loop1 and loop2). The scaffolds presenting different peptides were then selected against anti-myc tag antibody using a phage display library. The chapter discussed the selection of ten Adhiron myc binders, their cloning into the pET expression system, expression, purification, as well as the detailed characterisation of the binders.

This chapter discusses the work carried out to create an EIS based biosensor, built on the best Adhiron myc binder against monoclonal anti-myc tag antibodies. To determine the best Adhiron myc binder against monoclonal anti myc tag antibodies, ELISA was performed on all the ten binders. To detect the binding of the Adhiron myc binders to monoclonal anti-myc tag antibodies an indirect ELISA was performed using an enzyme conjugated secondary antibody against the monoclonal anti-myc tag antibodies.

The affinity of the best Adhiron myc binder against monoclonal anti-myc tag antibodies was established using SPR. SPR is used to detect biomolecular interaction in real time in a label-free environment (see section 3.2.5). SPR was used to determine the affinity of binding and analyse the kinetics involved, including the dissociation and association of the binding of monoclonal anti-myc tag antibodies to the surface immobilised Adhiron myc binder.

The selected Adhiron myc binder as the biological recognition layer was then used to fabricate a label-free EIS based biosensor for the detection of monoclonal anti-myc tag antibodies.

#### **5.1.1. Electrochemical impedance spectroscopy**

EIS measures the electrochemical impedance of an interface in AC steady state with constant DC bias. A small sinusoidal voltage is applied at a particular frequency and the resulting current is measured. The process is repeated at different frequencies. We are particularly interested in non-faradaic biosensing, which allows a more precise study of the interfacial layer. In case of electrochemical biosensors the interface is composed of the electrochemical double layer, which forms above the surface of a metal electrode submerged in an electrolyte (see Chapter 2). In non-

faradaic measurements the biosensing depends on the changes in the local environment of the electrode surface arising due to change in capacitive or resistive behaviour of the surface.

#### 5.1.1.1. EIS based biosensor

EIS based biosensors have been promising for the development of label-free biosensors. They are generally categorised as faradaic and non-faradaic biosensors (see section 2.2.2). Since the non-faradaic EIS based biosensors do not require an additional redox agent to improve their sensitivity they can be used in label-free point of care diagnostics. For the fabrication of EIS based biosensor, it is important to develop a sensitive detection platform, formed by a substrate on to which biological recognition molecules are immobilised.

In terms of electrochemistry the interface between the electrode and the electrolyte can be compared to a parallel plate capacitor, potentially with significant leakage. The capacitance depends on the change in the dielectric properties or the thickness of the dielectric layer according to Equation (5.1).

$$C = \epsilon \epsilon_0 A / d \quad (5.1)$$

Where C, capacitance between the parallel plates of the condenser (Farad /F);  $\epsilon$ , permittivity of the medium between the condenser plates (F/m);  $\epsilon_0$ , permittivity of the vacuum (F/m); A, electrode area ( $m^2$ ); d, distance between the charged plates (m).

The sensitivity to detect the binding of analytes is dependent on the capacitance of the sensor, which is inversely proportional to the thickness of the dielectric layer as given in the relationship Equation 5.1 (Gebbert *et al.*, 1992; Berggren *et al.*, 2001). If  $C_i$  is the initial capacitance of the sensor formed by the insulating layer and the recognition molecules and  $C_a$  is the capacitance of the analyte binding to the surface, then the total capacitance measured, is given by Equation (5.2).

$$1 / C_i + 1 / C_a = 1 / C_t \quad (5.2)$$

For the sensor to be highly sensitive the initial capacitance formed by the insulating layer and the biological recognition molecules should be very large as compared to the capacitance due to the analyte binding so that any change in the capacitance due to the binding of the analyte can be detected.

Directly immobilised biological recognition molecules do not act as ideal dielectric layers and therefore non-conducting polymer –polyethylene glycol was used to lower the the ionic movement through the layer (Berney *et al.*, 1997). Although this was not a success because the biological recognition molecules could not detect the analytes. This could be because of charged protein recognition molecules that interact with ions in the solution or due to denaturation of proteins on surface (Bergveld, 1991; Schasfoort *et al.*, 1990; Berney *et al.*, 1997). In order to improve the

sensitivity of the sensors the biological recognition molecules have been grafted on to insulating layers formed on the electrode / substrate.

Initially one of the most widely used techniques to graft insulating layers on to the gold substrate was Langmuir Blodgett technique (LBL) (Bergveld, 1991). Langmuir Blodgett films are formed by transferring a layer of amphiphilic molecules from air-water interface to air-solid interface (Zasadzinski *et al.*, 1994). In contrast to the arduous formation of LB films, fabrication of self assembled monolayers (SAM) was introduced by Nuzzo and Allara, involving the direct absorption of alkanethiolates ( $X-C_n-SH$ ) onto the gold substrate (Nuzzo and Allara, 1983).

Alkanethiolates form organic assemblies on the gold surface *via* formation of gold-thiol (Au-S) bonds. The tail part of an alkanethiol contains an exposed functional group ( $X$  *i.e.*  $-COOH$ ,  $-NH_2$ ,  $-CN$ ,  $-OH$  etc) that can be used to bind biomolecules (Ostuni *et al.*, 1999). The tethering of biomolecules to the SAMs also helps in maintaining their conformational flexibility (Bigdeli *et al.*, 2008). Formation of SAMs with different lengths of alkyl chain and terminal functional groups has been well studied and characterised (Dubois and Nuzzo, 1992; Whitesides *et al.*, 2005; Laibinis *et al.*, 1991). The order of the monolayers formed on the gold substrate is dependent on the length of the alkyl chain wherein SAMs formed from longer alkyl chain ( $n > 10$ ) are more densely packed as compared to those formed from shorter alkyl chains (Bain *et al.*, 1989). Alkanethiolates ( $n > 11$ ) form trans-extended monolayers at an angle of  $30^\circ$  (tilt) with respect to the gold substrate (Dubois and Nuzzo, 1992; Whitesides *et al.*, 2005). The densely packed SAMs form a highly insulating layer on the gold surface that impedes the penetration of electrons and water or ionic molecules at the interfacial surface (Boubour and Lennox, 2000a; Porter *et al.*, 1987).

An important consideration during the immobilisation of biological molecules has been the surface fouling or non-specific binding of protein molecules to the surface. In order to form anti-fouling surfaces, SAMs presenting poly (ethylene glycol) or PEG groups have been used that resist the binding of proteins to the surface (Ostuni *et al.*, 2001; Mrksich and Whitesides, 1997). The protein resistance of PEG is associated with the hydrophilic nature of the PEG which prevents the non-specific protein absorption to the surface (Wang *et al.*, 1997). Owing to the protein resistance property, PEG – SAM have been extensively used for modifying biosensing surfaces.

PEG-SAM used in the following experiments, consists of a functional  $-COOH$  group exposed on the PEG molecule for the covalent immobilisation of biological recognition molecules. These bulky functional groups cause steric hindrance and therefore destabilise the SAM layer of the sensor-giving rise to defects (Harder *et al.*, 1998; Mendoza *et al.*, 2007; Schreiber, 2000). The defects can be formed mainly due to the presence of a bulky  $-COOH$  groups attached to the PEG molecules that destabilise the SAM (Love *et al.*, 2005). Defects in a monolayer can also arise due to formation of less compact SAMs leading to pinholes. "Pinholes are the result of imperfect absorption of the alkanethiols to the gold surface during the self assembly step or subsequent loss of thiol during

rinsing, storage, or use” (Finklea *et al.*, 1993). The time dependent formation of pinholes / defects is discussed in section 5.4.3.1.

These pinholes / defects increase the permeability of ions (non-faradaic) or electrons (faradaic) to and from the surface and thus an ideal capacitive / insulating surface is not formed. The movement of ions through the SAM is called as the non-faradaic charge transport which can be detected using EIS (Zaccari *et al.*, 2014).

EIS is based on the superimposition of sine wave potential of small amplitude over polarisation potential of constant value. The relation between voltage and current can be represented by the complex electrical impedance  $Z$  of the surface (see section 3.2.6.4) (Evans *et al.*, 2008). The complex impedance is measured as the ratio of electrochemical voltage applied ( $E_t$ ) to the current response ( $I_t$ ).

$$\begin{aligned} Z &= E_t / I_t \\ &= E_0 \sin(\omega t) / I_0 \sin(\omega t + \phi) \\ &= Z_0 \sin(\omega t) / \sin(\omega t + \phi) \end{aligned}$$

Where  $E_0$  is the amplitude of the signal,  $I_0$  is the amplitude of current and  $\phi$  is the phase shift of response signal ( $I_t$ ) from the input signal ( $E_t$ ) (see section 3.2.6.4).

The changes taking place on the surface can be depicted by a Bode plot that represents logarithm of the absolute impedance,  $|Z|$  and the phase,  $\phi$ , plotted against the logarithm of the excitation frequency. In case of pure capacitive impedance the current and voltage are out of phase by  $90^\circ$ , which is observed as the phase of the impedance ( $-90^\circ$ ) in the lower frequency range. The change in the phase (phase shift) from an ideal capacitive phase ( $>-90^\circ$ ) can be attributed to the non-faradaic movement of ions or water molecules through the defects (Ihalainen *et al.*, 2014; Boubour and Lennox, 2000a; Zaccari *et al.*, 2014). Based on such changes in interfacial ionic movement, an EIS based biosensor fabricated for detecting the binding of monoclonal anti-myc tag antibodies to Adhiron myc binder.

This chapter discusses the development of EIS based Adhiron myc binder biosensor which also includes selection of the best Adhiron myc binder against monoclonal anti-myc tag antibodies from the ten binders discussed in the previous chapter.

## 5.2. Materials

Reagents and chemicals were purchased from Sigma-Aldrich unless mentioned. TMB (3, 3', 5, 5'-Tetramethylbenzidine) / substrate solution (SeramunBlau fast purchased from Seramun Diagnostica GmbH). Carboxymethylated dextran chips (CM5) were purchased from GE Healthcare Life Sciences. Chemicals used in SPR were supplied by GE health care - NHS, EDC, and ethanolamine. Monoclonal anti-myc tag antibodies, anti-B2M antibodies were purchased from Abcam. Alkanethiol-PEG (SH-(CH<sub>2</sub>)<sub>11</sub>-(EG)<sub>3</sub>-OCH<sub>2</sub>-COOH) was purchased from Prochimia, Poland. Ag/AgCl saturated KCl reference electrode, Potassium ferrocyanide K<sub>4</sub>[Fe(CN)<sub>6</sub>]<sup>3-/4-</sup> were purchased from WVR.

## 5.3. Methods

### 5.3.1. Surface Plasmon Resonance

A BIAcore 3000 instrument from GE LifeSciences was used to carry out affinity assays. The Biocore 3000 has a microfluidic chamber with open channels. On pressing the sensor chip against the open channels of the chamber, four flow cells are formed where continuous flow of liquid is maintained and the buffers or samples can be switched during the analysis without disturbing the sample boundaries.

A CM5 chip was used for all SPR studies, and the immobilisation of the binders on the CM5 chip was done using amine coupling chemistry. The dextran surface was activated using a mixture of equal volumes of 10 mM NHS (N-hydroxysuccinimide) and 400 mM EDC (N-ethyl-N'-(dimethylaminopropyl)-carbodiimide). 10 µg/mL Adhiron scaffold, Adhiron myc binder 2 and Adhiron myc binder 4 was immobilised in 10 mM acetate buffer pH 5.5 (pH chosen based on the scouting experiments) on channel 2, 3 and 4 respectively. No binder was immobilised on channel 1. Only buffer was allowed to flow on channel 1. The flow rate was maintained at 5 µL/min. Excess reactive groups on the surface were deactivated by using 35 µL of 1M ethanolamine (pH 8.5). A concentration series of monoclonal anti-myc tag antibodies prepared in 1 X PBS, pH 7.4 was injected over the four channels at a constant flow rate of 20 µL/min. The surface was regenerated using 1 X PBS containing 1M NaCl.

The binding curves were fitted using the proFit software, Quansoft Switzerland.

### 5.3.2. ELISA

10 µg/ml of Adhiron myc binder, Adhiron scaffold and Adhiron GST B4 binder were incubated in a 96 well plate (Nunc MaxiSorp). Solutions were prepared in 10 mM PBS buffer, pH 7.2. Each one of them was incubated in three wells in a column. The plate was incubated overnight at 4 °C. The samples were decanted and 250 µl of 2 X casein blocking buffer was added in each well and incubated for 2 hr at room temperature. The wells were washed 3 times with 10 mM PBST (0.1% (w/v) Tween-20 in 10 mM PBS, pH 7.2).

The first row corresponding to each binder was incubated in 1 µg/ml of monoclonal anti-myc tag antibodies. The second row corresponding to each binder was incubated in 1 µg/ml BSA (bovine serum albumin) and third row corresponding to each binder was incubated in 1 µg/ml anti-B2M antibodies. The antibodies and BSA were prepared in 10 mM PBS (pH 7.2). The plate was incubated for 1 hr at room temperature. An anti-mouse-antibody conjugated with horseradish peroxidase (1:4000) was added as manufacturer's protocol (Promega) in all the wells and incubated for 1 hr at room temperature. After washing ten times with 1 X PBST, 1 ml of TMB substrate solution was added and the intensity of emission was measured after 5 min at 650 nm using a Multiskan ascent plate reader (Thermo Fisher Scientific).

### 5.3.3. Electrochemical impedance spectroscopy

#### 5.3.3.1. Electrochemical cell set up

EIS measurements were done using VSP-3 electrochemical workstation (BioLogic science instruments) consisting of a conventional three-electrode system that included a working electrode, Ag/AgCl saturated KCl reference electrode and platinum wire as a counter electrode. The measurements were taken in the frequency range of 100 kHz to 50 mHz at 80 mV DC potential vs. reference (Ag/AgCl). The gold electrodes were fabricated by Evatec (Switzerland) by evaporating 20 nm Ti followed by 80nm gold onto Si/SiO<sub>2</sub> wafers using EBM (Electron beam evaporation) using gold of 99.999% purity.

#### 5.3.3.2. Cleaning the gold electrode

The gold electrode was sonicated in acetone for 5 min twice in fresh acetone solutions. Then the surface was rinsed in ethanol. After cleaning, the surfaces were used within 15 min.

#### 5.3.3.3. SAM formation

The cleaned gold surface was incubated for 24 hr or 48 hr in a solution of 1 mM alkanethiol-PEG solution prepared in 200-proof ethanol containing 0.05% (v/v) acetic acid. The surface was then dried in nitrogen and mounted on to the cell.

#### 5.3.3.4. CV Measurements

The mounted gold surface was firstly rinsed with 10 mM PBS (pH 7.2) 2-3 times and then incubated in 800  $\mu$ L volume of 10mM PBS for 15 min. The CV measurements were done in 10 mM PBS (pH 7.2) buffer containing 1 mM  $[\text{Fe}(\text{CN})_6]^{3-/4-}$  probe at a scan rate of 62 mV/sec.

#### 5.3.3.5. Immobilisation of binders

The carboxyl groups of the alkanethiol-PEG monolayer were activated by incubating the surface in EDC (400 mM)–NHS (100 mM) for 10 min. EDC-NHS solution was prepared in 100 mM MES buffer, pH5.5. The surface was incubated in 10  $\mu$ g/mL Adhiron myc binder 2 (prepared in 100 mM acetate buffer pH 5.5) for 1 hr. Then blocking of the remaining active sites was accomplished by incubating the surface in 1M ethanolamine (pH 8.5) for 30 min. The surface was then washed with 10 mM PBS (pH 7.2).

#### 5.3.3.6. EIS measurements

The EIS measurements were taken in 10 mM PBS (pH 7.2) in the frequency range of 100 kHz to 50 mHz at 0 mV or 80 mV DC potential vs. reference (Ag/AgCl).

## 5.4. Results

In order to build the biological recognition layer for the detection of monoclonal anti-myc tag antibodies the best binder amongst all the ten Adhiron myc binders expressed and purified in the previous chapter was selected. The selection was based on ELISA and SPR results.

The well-characterised binder was then used for fabrication of EIS based biosensor that included surface modification, immobilisation of the selected binder and the use of different strategies to detect the monoclonal anti-myc tag antibodies.

### 5.4.1. ELISA

The ten binders selected from the phage ELISA were Adhiron myc 1, 2, 4, 5, 7, 11, 13, 17, 18 and 20. The optimisation of the expression and purification conditions was done on Adhiron GST B4 binder, which has been used as a control in ELISA. To check the interaction of Adhiron myc binders to the monoclonal anti myc-tag antibodies ELISA was performed in a 96 well plate.

The binding of different Adhiron myc binders, Adhiron scaffold and Adhiron GST B4 binder to monoclonal anti myc tag antibodies was detected by using anti-mouse-antibody conjugated with horseradish peroxidase. In order to check the non-specific binding of the secondary antibody *i.e.* anti-mouse-antibody conjugated with horseradish peroxidase to the adhiron binders, control wells immobilised with the binders (Adhiron myc binders, Adhiron scaffold and Adhiron GST B4 binder) were incubated in 1  $\mu\text{g}/\text{mL}$  BSA. The wells were then subjected to anti-mouse antibody conjugated with horseradish peroxidase without the intermittent step of incubation in anti-myc tag antibodies. In order to check the non-specific binding of antibodies to Adhiron myc binders, the wells immobilised with the respective binders were also incubated in monoclonal anti-B2M antibodies.

The presence of the anti-myc tag antibodies on the surface was detected by the intensity of blue colour produced on addition of TMB substrate. The intensity of the colour depicted the strength of binding which was measured using an ELISA plate reader. Figure 5-1 shows the intensity plot of Adhiron myc binders, Adhiron scaffold and Adhiron GST B4 binder against monoclonal anti-myc tag antibodies after dividing their response from the BSA control wells that corresponded to the non-specific binding of anti-mouse-antibody conjugated with horseradish peroxidase.

Adhiron myc binder 13 demonstrated the maximum response against monoclonal anti-myc tag antibodies followed by Adhiron myc binder 2, binder 11 and binder 7. Adhiron myc binder 2 was chosen as the best candidate for further experiments, because Adhiron binder 13 was prone to aggregation as discussed in section 4.3.6. Amongst the Adhiron myc binders, Adhiron myc binder 4 and 18 showed least response to monoclonal anti-myc tag antibodies. The response of the

immobilised binders to monoclonal anti-B2M antibodies was negligible thus further establishing the specificity of the binding of Adhiron myc binders to monoclonal anti-myc tag antibodies.

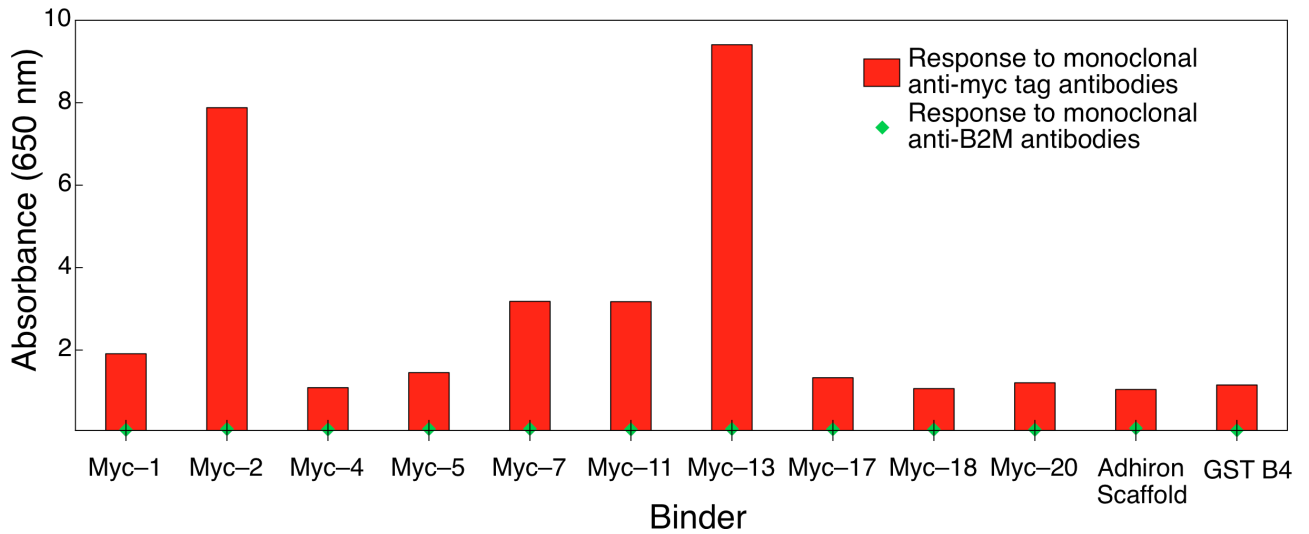


**Figure 5-1. ELISA on Adhiron myc binders, Adhiron scaffold and GST B4 binder.**

The ELISA results shown in the figure give the absorbance measured by the ELISA plate reader at 650 nm. The binding of monoclonal anti-Myc tag antibodies to the Adhiron myc binders was detected using anti-his tag antibodies conjugated with HRP (horseradish peroxidase). The chart has been developed after dividing the BSA-control absorbance from the absorbance obtained from each ligand on the surface. The green dots represent the intensity of absorbance obtained by incubating the binders with monoclonal anti-B2M antibodies.

Adhiron scaffold and the Adhiron GST B4 binder showed minimal binding to the monoclonal anti-myc tag antibodies establishing that the interaction shown by the Adhiron myc binders towards monoclonal anti-myc tag antibodies was a result of the sequences inserted in the variable regions of the adhiron scaffold. This further proved that the Adhiron myc binder 2 was not binding non-specifically to monoclonal anti myc-tag antibodies.

The variability in the binding of monoclonal anti-myc tag antibodies to the Adhiron myc binders was attributed to the different sequences inserted into the Adhiron loops corresponding to each Adhiron myc binder. Figure 5-2 shows the sequence alignment of the loops of the ten selected Adhiron myc binder showing similarity with the myc epitope sequence EQKLISEEDL that is recognised by the anti myc tag antibodies. Adhiron myc binder 2, 1, 18 and 7 show maximum similarity with the myc epitope. The sequence similarity of Adhiron myc binder 2, 1 and 7 corresponds to the binding signal obtained in ELISA but Adhiron myc binder 18 does not show binding in ELISA. Adhiron myc binder 13 shows the highest binding in ELISA but has less similarity with the epitope. This could be attributed to the fact that the binding of monoclonal anti-myc tag antibodies is not only dependent on the myc epitope, but also on the neighbouring sequences or the folding of the loops. There could also be cross talk between the different loops or

the Adhiron scaffold while the monoclonal myc-tag antibody binds to the Adhiron myc binders. Based on the ELISA result SPR was done on Adhiron myc binder to obtain its affinity to monoclonal anti myc-tag antibody.

```

Mycepitope          --EQKLISEEDL 10
Adhironmyc_1       -----MISEED-- 6
Adhironmyc_2       -----LVSEED-- 6
Adhironmyc_11      -----LVSEED-- 6
Adhironmyc_18      ---HTLLSEEDY 9
Adhironmyc_7       -PIQHLISET-- 9
Adhironmyc_17      -QMQTLLSET-- 9
Adhironmyc_4       TEQQLLIGE--- 9
Adhironmyc_20      -HQQLLVSEF-- 9
Adhironmyc_13      -DHQYLISEG-- 9
Adhironmyc_5       -AEHGLISTG-- 9
                    : : :

```

**Figure 5-2 Sequence alignment of Adhiron myc binders with myc epitope.**

The sequence alignment of the three variable regions of the ten selected Adhiron myc binders showing similarity with myc epitope EQKLISEEDL. The end row represents the number of amino acids. Key: Single letters present aminoacids, “.” semi-conservative substitution, “:” conservative substitution, Colour Red: small hydrophobic, aromatic and not Y. Blue: acidic. Magenta: basic, Green: hydroxyl, amine, amide, and basic aminoacids.

#### 5.4.2. Surface plasmon resonance

To characterise the interaction of Adhiron myc binder 2 with monoclonal anti myc tag antibodies, SPR was used. The SPR sensor chip has a layer of carboxymethylated dextran (a flexible unbranched carbohydrate polymer) (CM) on top of the gold layer carboxyl groups. The carboxyl groups allow the attachment of the ligands to the surface by covalent bonding. It also creates a hydrophilic environment for the interaction. Each CM5 chip consists of four flow cells to allow running of parallel experiments. These channels were named as channel 1, 2, 3 and 4.

The injection of different buffers or binding of molecules on the surface results in the change of refractive index on the sensor surface, which is then detected, with the change in resonance angle (see section 3.2.5). For the immobilisation of the ligands to the surface, NHS-EDC chemistry was used. Figure 5-3 shows the activation of the carboxylic groups on the SAM surface by using the EDC-NHS coupling. The carboxyl groups are activated to NHS which are subsequently displaced by an amine containing ligand molecule. The immobilisation of the ligand molecule takes place through the formation of peptide bond between the carboxylic group of the SAM and the amine group of the ligand.

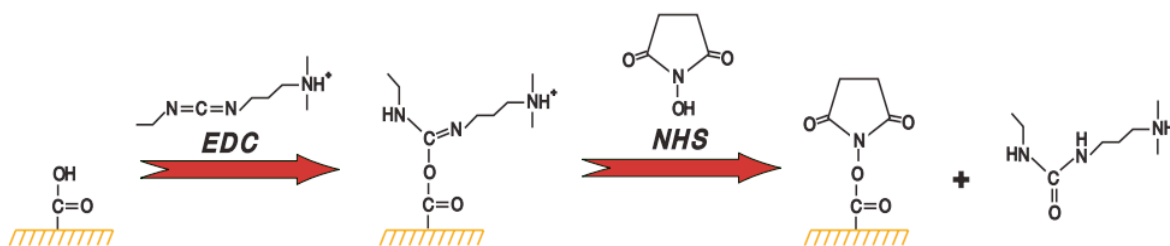


**Figure 5-3 Activation of carboxylic group using EDC-NHS chemistry.**

Schematic of activation of carboxymethyl dextran of the CM5 chip using EDC and NHS coupling. The biological recognition layer binds to the activated carboxylic group and forms an amide bond with the dextran surface. Taken from (GE healthcare, 2011)

Channel 1 of the SPR instrument was used to check the change in the SPR angle due to the refractive index of the buffer. The channel 2 was functionalised with Adhiron scaffold so as to check binding of the monoclonal anti-myc tag antibodies to the wild type Adhiron scaffold. Adhiron myc binder 2 was immobilised on Channel 3 and Adhiron myc binder 4 was immobilised on channel 4. Adhiron myc binder 4 was used as a negative control as it showed minimal binding to monoclonal anti-myc tag antibodies in ELISA.

Figure 5-5 shows the response obtained after injecting 250 nM monoclonal anti-myc tag antibodies. Monoclonal anti-myc tag antibodies lower than 250 nM of concentration could not be detected using SPR (data not shown). Figure 5-5(a) shows the binding curve obtained for Adhiron myc binder 2 after subtracting the response due to the change in refractive index of 10 mM PBS, pH 7.2 (channel 1). Based on the association and dissociation curve, the dissociation constant ( $K_D$ ) of Adhiron myc binder 2 was calculated using Profit. The  $K_D$  was  $140 \pm 10$  nM. The rate of dissociation of the monoclonal anti-myc tag antibodies,  $k_{off}$  was calculated as  $0.01 \text{ s}^{-1}$  which was much higher than the rate of association *i.e.*  $k_{on}$  *i.e.*  $72 \times 10^{-6} \text{ nM}^{-1} \text{ sec}^{-1}$ .

Figure 5-4 (b) shows the sensogram of Adhiron scaffold after subtracting the response due to the change in refractive index of buffer (channel 1). There was no response observed against monoclonal anti-myc tag antibodies, which corresponded to the ELISA result where Adhiron scaffold did not show response (Figure 5-1).

The sensogram shown in Figure 5-4 (c) showed the response of Adhiron myc binder 4 after subtracting the response due to change in refractive index of buffer (channel 1). Adhiron myc binder 4 did not show any binding against monoclonal anti-myc tag antibodies, which corresponded to the ELISA result wherein Adhiron myc binder 4 was showing minimal response against monoclonal anti-myc tag antibodies (Figure 5-1).

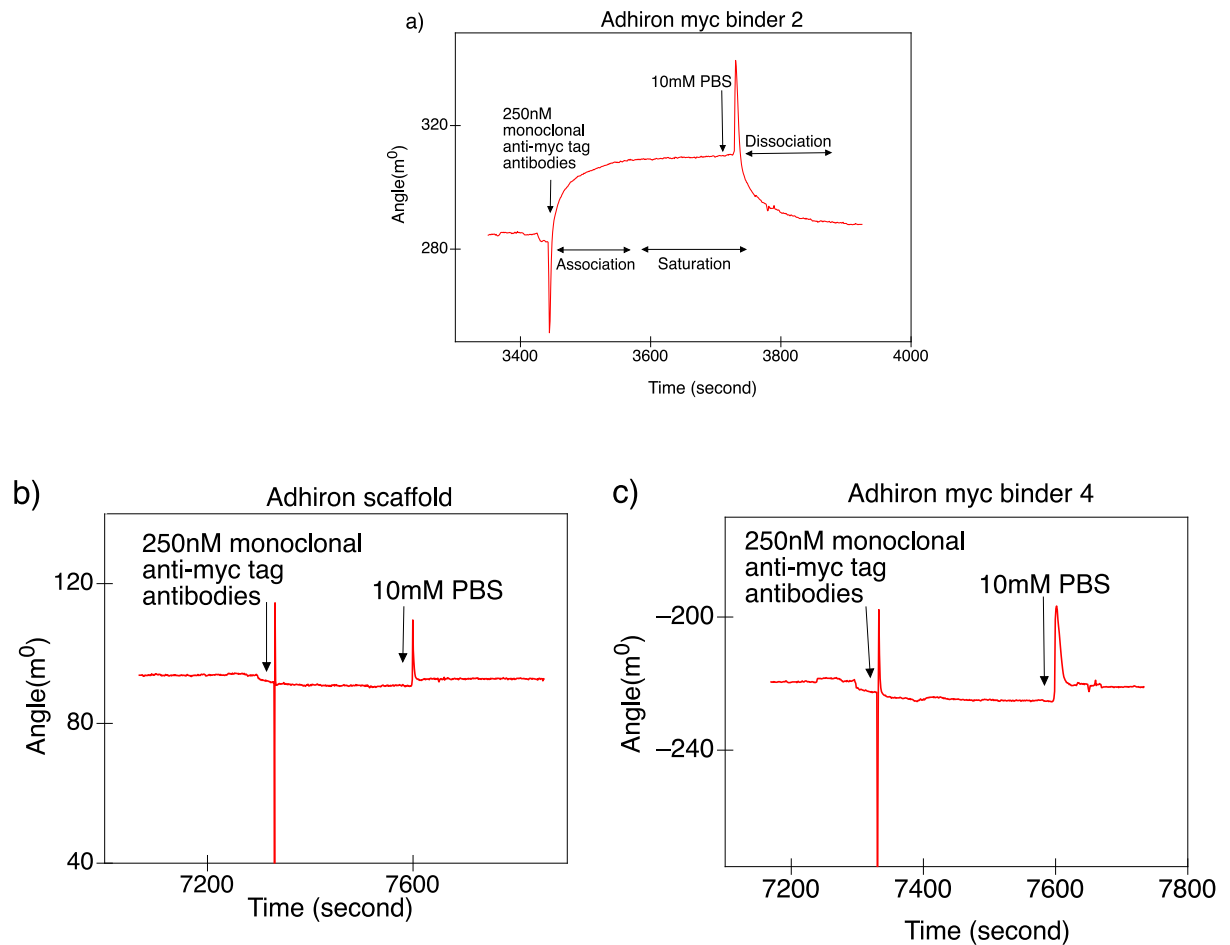


**Figure 5-4 Surface Plasmon resonance sensograms of Adhiron myc binder 2, Adhiron scaffold and Adhiron myc binder 4.**

Sensograms obtained after 250 nM monoclonal anti-myc tag antibodies were allowed to flow across the sensor chip immobilised with (a) Adhiron myc binder 2, (b) Adhiron scaffold and (c) Adhiron myc binder 4. The sensograms were obtained after subtracting the response from channel 1 (not shown) that was used to detect the change in refractive index due to 10 mM PBS (pH 7.2) injection.

### 5.4.3. Electrochemical impedance spectroscopy

Based upon the results obtained from the ELISA and SPR experiments, Adhiron myc binder 2 was selected as the biological layer to fabricate the label-free EIS based biosensor.

For the fabrication of a non-faradaic impedimetric biosensor a clean gold surface was incubated in 1mM alkanethiol-PEG (SH-(CH<sub>2</sub>)<sub>11</sub>-(EG)<sub>3</sub>-OCH<sub>2</sub>-COOH) (see section 5.1.1.1). Gold has been used as the substrate in biosensing because of its inertness to form stable oxide surfaces and resistance to various atmospheric contaminants (Bain *et al.*, 1989). Through the thiol group, the SAM forms self-assembled monolayer on the gold surface *via* Au-S (gold-sulphide) bond and through the carboxy head group it facilitates the attachment of the amine containing groups of the ligand.

#### 5.4.3.1. Establishing the formation and properties of the PEG-SAM

The formation of a SAM on a gold surface was characterised by investigating the impedance of the SAM. The insulating property of the SAM was investigated by studying the movement of electrons as well as ions to and from the gold electrode in the following sections.

##### *Electron transfer through the PEG-SAM*

To check the quality of SAM on the gold surface and the electronic transfer through the SAM cyclic voltametry (CV) was performed on the surface. CV was done on a clean gold electrode incubated in 1mM SH-(CH<sub>2</sub>)<sub>11</sub>-EG<sub>3</sub>-OCH<sub>2</sub>-COOH for 24 hr. The CV was performed using 1 mM potassium ferro/ferri cyanide [Fe(CN)<sub>6</sub>]<sup>3-/4-</sup> dissolved in 10 mM PBS (pH 7.2) buffer solution.

Figure 5-5 shows the comparison of cyclic voltametry of the bare gold (a) and the gold surface incubated in SAM for 24 hr measured in equal concentration of [Fe(CN)<sub>6</sub>]<sup>3-/4-</sup> complex. The CV of bare gold (black curve) resembles the current-voltage curve of a gold surface when exposed to buffer containing ferro / ferri cyanide redox couple (Rickert *et al.*, 1996). The cathodic peak (E<sub>PC</sub>) was observed at 0.23 V and the anodic peak (E<sub>PA</sub>) was observed at 0.14 V (see section 3.2.6.3). The formal potential (E<sub>PC</sub>+ E<sub>PA</sub>)/2 was 0.16 V. The CV plot of the SAM modified electrode (red curve) showed the behaviour of a well-defined highly ordered monolayer. The current was decreased in case of SAM immobilised surface showing that the electron transfer property of the surface was almost completely blocked by the SAM.

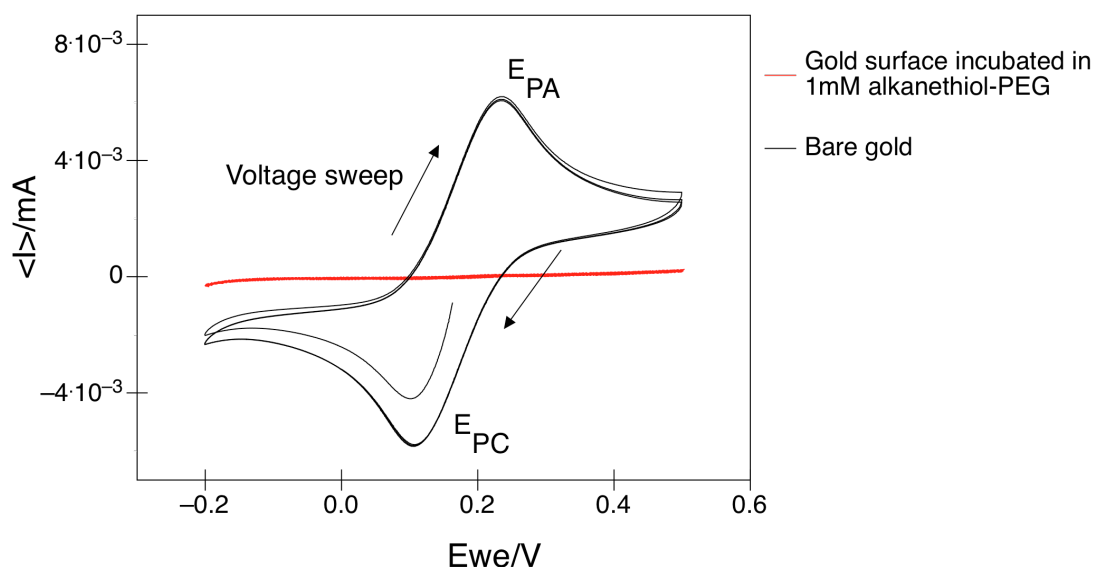


**Figure 5-5. Cyclic voltammetry on bare gold and gold grafted with self assembled monolayer.**

Shows the cyclic voltamogram of a bare gold electrode (black) and a gold electrode incubated in 0.1 mM thiol solution (red curve) both measured in 10 mM  $K_3Fe(CN)_6$  in 10 mM PBS, pH 7.2. The cathodic peak ( $E_{PC}$ ) was observed at 0.23 V and the anodic peak ( $E_{PA}$ ) was observed at 0.14 V.

### ***Ionic transfer through the PEG- SAM***

Cyclic voltametry depicted the decrease of movement of electrons through the formation of PEG-SAM on the gold electrode. Furthermore, the effect of PEG-SAM formation on the movement of ions through the surface was investigated. This was done by measuring the absolute impedance ( $|Z|$ ) as well as phase angle ( $\phi$ ) of the interfacial surface.

The absolute impedance ( $|Z|$ ) as well as the phase angle ( $\phi$ ) were measured in the frequency range of 100 kHz to 50 mHz at 0 mV DC potential applied at the working electrode vs. reference (Ag/AgCl) in 10mM PBS without the redox active species. To assess the behaviour of SAM formed on the gold electrode the Bode plots showing the absolute impedance ( $|Z|$ ), as well as the phase angle ( $\phi$ ) vs. frequency were studied.

The Bode plots of four different surfaces were compared- a bare gold surface, three gold electrodes incubated in 1 mM thiol solution ( $SH-(CH_2)_{11}-EG_3-OCH_2-COOH$ ) for 24, 48 and 64 hr respectively. Incubation for different time periods was done to optimise the incubation time for the formation of SAM with least defects or pinholes.

Figure 5-6 (a) shows the absolute impedance  $\log |Z|$  vs.  $\log$  frequency plot of a bare gold surface and surfaces incubated in 1 mM thiol solution for 24, 48 and 64 hr. The

measurements were taken in the frequency range of 100 kHz to 50 mHz, the response was noted at 0.1 Hz (Figure 5-6(b)) because at this frequency the phase showed least change due to change in bulk solution and it was more responsive towards the changes in the interfacial layer.

The absolute impedance of the gold electrodes was observed to increase when incubated in thiol solution compared to bare gold surface. The formation of SAM on the gold electrode impedes the movement of ions or water molecules thus showing a three time increase in the absolute impedance (Boubour and Lennox, 2000a). Figure 5-6(b) shows that the absolute impedance was more when the surface was incubated for 48 hr than for 24 hr. This was attributed to the fact that the prolonged incubation reduces pinholes and defects in the SAM (Agonafer *et al.*, 2012). The impedance shown by surfaces incubated in 48 hr or more was varying with different surfaces but always higher than 24 hr incubation (data not shown). This showed that the gold surface incubated for 48 hr or more in thiol solution produced more compact SAM film thus impeding the change in dielectric properties of the SAM. The effect of incubation is more pronounced when the phase shift was compared in the following section.

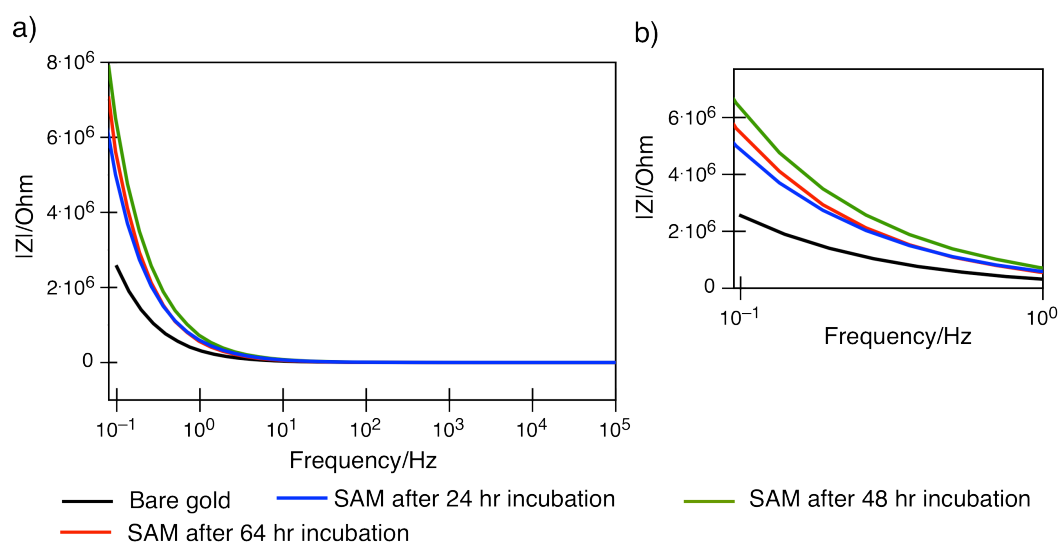


**Figure 5-6. Absolute impedance vs. frequency of various surfaces.**

Shows the plot of absolute impedance  $|Z|$  vs. frequency measurement of bare gold surface, a gold surface incubated in thiol solution for 24, 48 and 64 hr (a) frequency range 100 kHz to 50 mHz (b) lower frequency range 0.1 Hz to 1 Hz.

Figure 5-7 shows the change in phase vs. frequency plots of bare gold, gold surface incubated in thiol solution for 24, 48 and 64 hr depicting the phase vs. frequency plot in the frequency range of (a) 100 kHz to 50 mHz and (b) 0.1 Hz to 0.3 Hz. In Figure 5-7 (a) the phase shown by the bare gold is different along the whole

frequency range from the SAM immobilised surfaces. On comparing the phase in between the SAM immobilised surfaces, the change was minimal in the higher frequency range (0.5 Hz to 100 kHz). This could be attributed to the fact that the solution resistance remains the same in case of all the SAM immobilised surfaces.

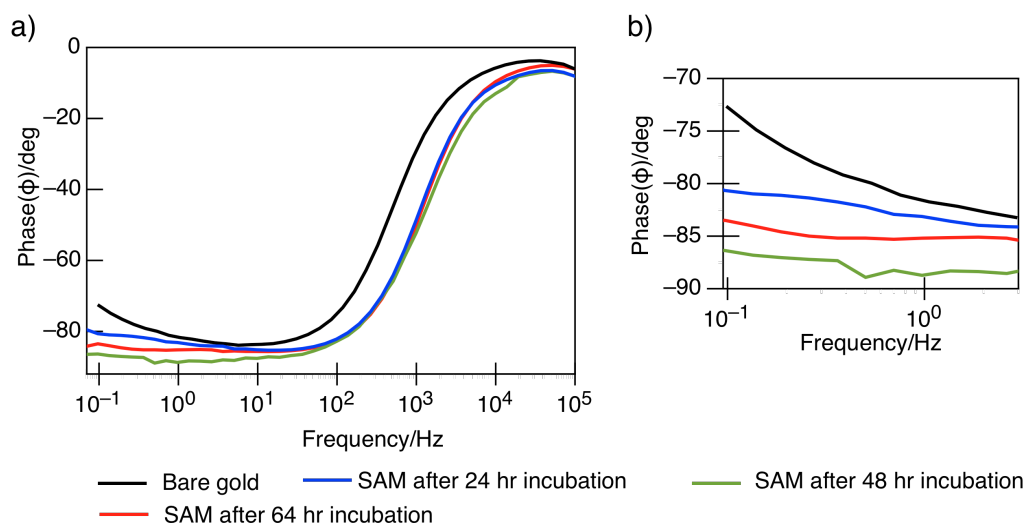


**Figure 5-7. Phase vs. frequency of different surfaces.**

Shows the Bode plot of phase vs. frequency measurement of bare gold surface, a gold surface incubated in thiol solution for 24, 48 and 64 hr (a) frequency range 100 kHz to 50 mHz, (b) lower frequency range 0.1 to 0.3 Hz.

In Figure 5-7(b) the phase obtained at 0.1 Hz for the bare gold, gold surface incubated in thiol solution for 24, 48 and 64 hr was  $-72.9^{\circ} \pm 0.3$ ,  $-79.1^{\circ} \pm 0.9$ ,  $-84.9^{\circ} \pm 0.5$  and  $-82.6^{\circ} \pm 0.6$  respectively. The phase change from bare gold to the SAM coated surfaces is attributed to the formation of an insulating layer of SAM that changes its interfacial ionic permeability, observed in the lower frequency range. The phase for an ideal electrochemical double layer capacitor is  $\leq -88^{\circ}$  (Boubour and Lennox, 2000a). The deviation in phase from an ideal electrochemical double layer observed in case of bare gold can be attributed to the roughness / contamination of the gold electrode. On incubating the surface in thiol solution for 24 hr the phase observed ( $-79.1^{\circ} \pm 0.9$ ) was lower than that of bare gold. This could be because of the formation of SAM on to the gold surface that covers the electrode surface and decreases surface contamination. The phase angle observed for the gold surface incubated in thiol solution for 48 hr ( $-84.9^{\circ} \pm 0.5$ ) was four degrees lower as compared to that of gold incubated in thiol solution for 24 hr. This showed that incubation of SAM for more than 24 hr allowed more surface coverage by SAM thus reducing the pinholes / defects and thus reducing the movement of ions through the SAM (see section 5.1.1.1).

The time dependent formation of pinholes / defects in SAMs immobilised on gold electrodes has been well studied (Ulman, 1996; Agonafer *et al.*, 2012; Whitesides *et al.*, 2005). The SAM formation is described in two major steps. The initial quick step (5-6 min) of chemisorption of SAMs from the solution onto the substrate (bonding between head group and gold surface), followed by the slow process of reordering of alkane chains that are held by van der Waals forces. The longer incubation period of gold substrate helps in annealing the pinholes / defects thus decreasing the permeation of ions through the SAM (Agonafer *et al.*, 2012; Boubour and Lennox, 2000a).

The phase obtained for SAM incubated in thiol solution for 64 hr was  $-82.6^{\circ} \pm 0.6$ . The increase in phase observed when SAM was incubated for more than 48 hr could be due to change in the the rearrangement of PEG molecules over time.

As the 48 hr incubation time formed more compact SAM on the gold surfaces and 64 hr incubation time, sometimes showed worst phase than 48 hr, therefore in the future experiments the cleaned gold surfaces were incubated for 48 hr in 1 mM SH-(CH<sub>2</sub>)<sub>11</sub>-EG<sub>3</sub>-OCH<sub>2</sub>-COOH.

Although both absolute impedance  $|Z|$  and phase  $\phi$  of impedance ( $Z$ ) were used to assess the formation of SAM, it has been observed that measuring the change in phase is more reliable than measuring the change in absolute impedance as the phase does not change with the electrode area (Boubour and Lennox, 2000a; Evans *et al.*, 2008). Therefore, in the following experimental sections, change in phase ( $\phi$ ) has been used to measure changes at the interface of SAM and buffer.

### ***Stability of SAM over time***

The decreased current in the CV (Figure 5-5) and a phase angle of  $-84.9^{\circ} \pm 0.5$  (Figure 5-7) signified that the insulating layer impeded electron transfer and any change in dielectric properties of the surface respectively. In order to immobilise the Adhiron myc binder 2 onto the surface and later detect the binding of monoclonal anti-myc tag antibodies to the binder, it was important to establish a stable insulating monolayer.

To check the change in the surface behaviour with time, the stability of SAM was checked in 5 subsequent measurements by changing the 10 mM PBS buffer (pH 7.2) after every 15 min. The phase ( $\phi$ ) of impedance ( $Z$ ) was measured in the frequency range of 100 kHz to 50 mHz at 0 mV DC potential applied at the working electrode vs. reference (Ag /AgCl).

The contribution of non-faradaic charge transport was higher in the lower frequency range therefore, the change in interfacial layer with time was detected by the change in phase in the lower frequency range (0.1 Hz). Figure 5-8 shows the change in phase of SAM in the lower frequency range (0.09-0.36 Hz). At 0.1 Hz, the phase was drifting by approximately  $2^\circ$  in five subsequent readings. Thus there was a change involved at the surface of the monolayer with time, imparting instability to the surface.

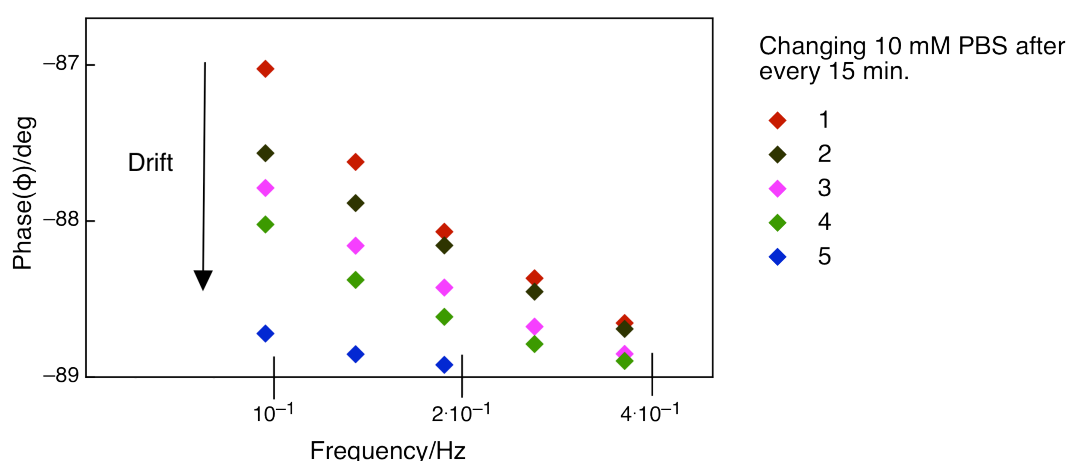


**Figure 5-8. Phase vs. Frequency of surface in 10 mM PBS (pH 7.2).**

Shows the phase in the lower frequency range of 0.09-0.36 Hz for 5 subsequent readings taken after incubation of the SAM immobilised surface in 10 mM PBS (pH 7.2) for 15 min.

This change was most likely due to the reorganization of monolayer surface with time. The effect of different functional groups present at the terminal ends (-OH, -COOH) of SAMs, has been well studied. It has been observed that the hydrophilic end groups attributed to orientational changes of the hydrocarbon chain. The COOH group-terminated SAMs showed higher degree of disorder (Dannenberger *et al.*, 1997; Himmel *et al.*, 1997). The reorganization was attributed to the fact that the monolayers have high surface free energies that they tend to reduce by burying their polar functional groups in the monolayer surface (Evans *et al.*, 1991). Although the reason for instability could not be understood completely but it could also arise due to the effect of solvent that destroys the ordered structure of PEG-SAM by penetrating into the PEG part or underlying alkane chain (Zolk *et al.*, 2000; Vanderah *et al.*, 2003).

In order to detect the binding of biological molecules in the interfacial layer formed by the insulating layer of SAM and the physisorbed ionic layer of the buffer, the stability of SAM was important, and this will be addressed in the following section.

### ***Stabilisation of SAM by potential tuning***

The instability of SAM with time was attributed to the time dependent reorganization of the polar functional groups into the carbon chain. This issue of instability was reduced by introducing the potential induced stabilisation of the surface by ramping of surface to a higher DC potential of 200 mV (Bioelectronics group, University of Leeds).

Clean gold surfaces were incubated in 1mM thiol solution for 48 hr as above. The surfaces were then subjected to a ramping DC potential from 0 V to 0.2 V *vs.* reference (Ag/AgCl) over 15 cycles. After 15 cycles of ramping, the phase measurements were taken on incubating the surface in 10 mM PBS (pH 7.2) for 15 min and changing the buffer each time. Figure 5-10(a) showed that the change in phase over 4 subsequent cycles was in the acceptable range of 0.1° to 0.4° unlike observed in case when no ramping was done (Figure 5-9 (b)). The surface becomes stable and the drift in baseline was not observed after third reading.

Most likely the ramping step reorients the flexible carboxylic group terminated PEG of the SAM and aligns all in such a way that a compact high SAM is formed. The time dependent reorientation made faster by subjecting the SAM to a higher potential, could also be due to interaction of Au-S bond. At more positive potential, the gold substrate is positively charged as compared to the electronegative sulphur head groups. This can increase the dipole–dipole interactions and arranges the SAM more compactly (Sahalov *et al.*, 2007). The stability observed makes the surface suitable to be used as a sensor surface.

The stable SAM formed after subjecting it to 15 cycles of 200 mV DC voltage was then used after immobilisation of the biological recognition layer *i.e.* Adhiron myc binder 2.

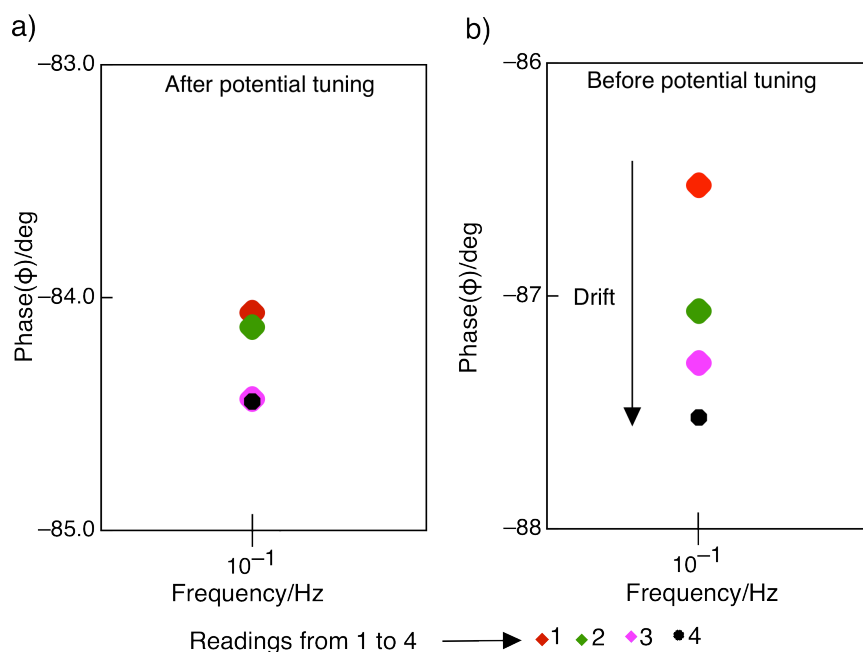


**Figure 5-9. Comparison of surface stability in buffer before and after 200 mV potential tuning.**

Shows the phase at 0.1 Hz for five subsequent readings taken after incubation of the SAM immobilised surface in 10 mM PBS (pH 7.2) for 15 min (a) after potential tuning at 200 mV (b) before potential tuning at 200 mV.

#### 5.4.3.2. Immobilisation of Adhiron myc binder 2

After immobilisation of carboxylic group containing PEG-SAM on the gold surface, the surface was incubated in 10 µg/mL Adhiron myc binder 2 using amine coupling chemistry (see section 6.3.3). The surface was then subjected to a DC potential of 0 mV vs. reference (Ag/AgCl) in the frequency range of 100 kHz to 50 mHz.

Figure 5-10 shows Bode plot depicting phase response of the surface before and after immobilisation of Adhiron myc binder 2. The phase ( $\phi$ ) of impedance ( $Z$ ) shown by surface at 0.1 Hz, before immobilisation of the binder was  $-85^\circ$ . SAM with a phase of  $-85^\circ$  (non-ideal capacitive layer) depicted that the SAM formed allowed the movement of ions (through defects) unlike in case of perfectly insulating layer. This could be attributed to the amorphous nature of PEG on the SAM (Love *et al.*, 2005) (see section 5.1.1.1). The phase at 0.1 Hz after immobilisation of Adhiron myc binder 2 was  $-88^\circ$ . The change in phase showed a reduction in the non-faradaic movement of ions near the interfacial layer. This change could be attributed to the formation of a more compact layer by the immobilisation of Adhiron myc binder 2 (diameter of 3 nm) blocking the pinholes or due to the interaction of COOH-terminated PEG molecules with the Adhiron myc binder 2 changing the electronic environment of the interfacial surface (Mendoza *et al.*, 2007; Schreiber, 2000).

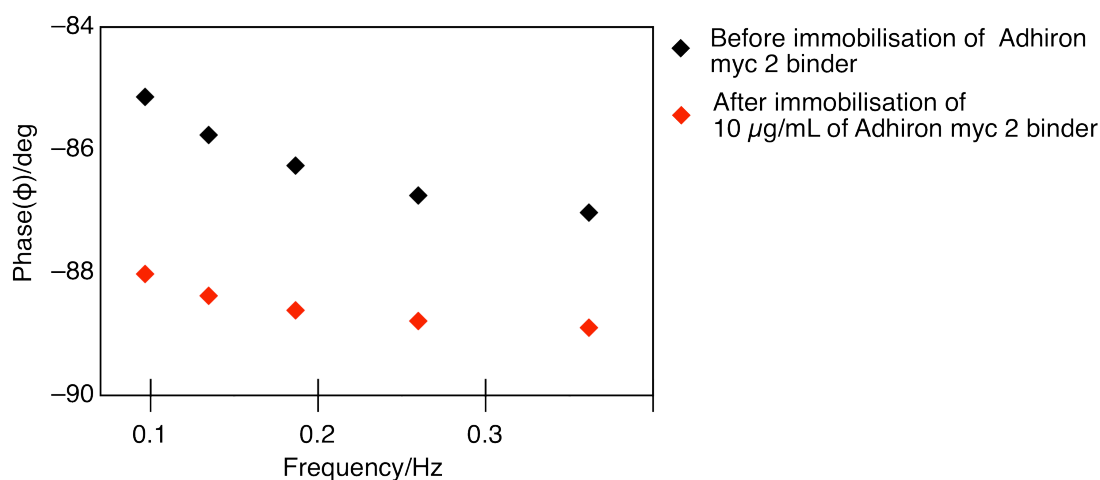


**Figure 5-10. Phase vs. Frequency before and after immobilisation of 10 µg/ml of Adhiron myc binder 2.**

Shows the Bode plot depicting the phase of a SAM immobilised gold surface before the immobilisation of Adhiron myc binder 2 and after the immobilisation of 10 µg/mL Adhiron myc binder 2. The surface was subjected to a DC potential of 0 mV and the frequency range shown is from 0.1 Hz – 0.36 Hz.

#### 5.4.3.3. Demonstration of biosensing using Adhiron based biological recognition molecule

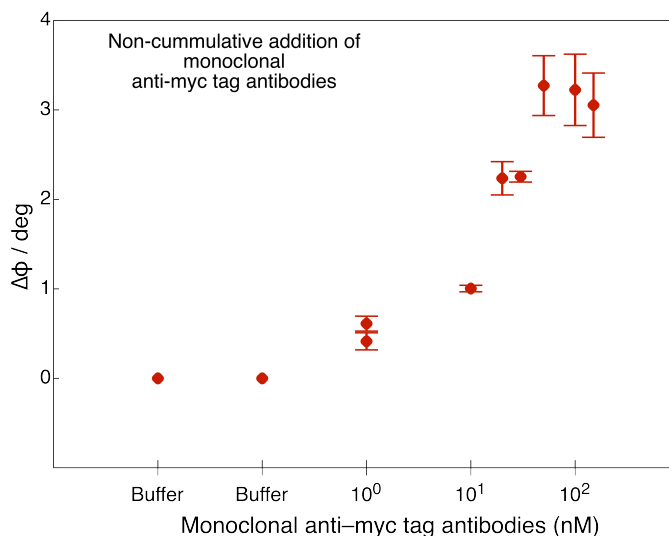
After the immobilisation of Adhiron myc binder 2, the surface was subjected to 200 mV DC voltage *vs.* reference (Ag/AgCl) for stabilisation. This was done to obtain a stable phase after immobilisation of the Adhiron myc binder 2.

Figure 5-11 shows the change in phase ( $\Delta\phi$ ) of the sensor at 0.1 Hz after incubating the surface in different concentrations of monoclonal anti-myc tag antibodies. Change in phase, ( $\Delta\phi$ ) corresponds to the change in phase angle (degree) with respect to the initial phase angle, measured in 10 mM PBS (pH 7.2) before adding the monoclonal anti-myc tag antibodies. The surface was subjected to 80 mV DC potential *vs.* reference (Ag/AgCl) for the measurements. 80 mV DC potential was chosen because of the higher sensitivity observed at a higher potentials  $> 0$  mV DC bias (see Chapter 6).

To check the stability of the surface before adding the monoclonal anti-myc tag antibodies, the phase of the surface was measured in 10 mM PBS (pH 7.2) twice after incubation for 15 min each. No change in phase was observed in 10 mM PBS (pH 7.2) incubations establishing stability of the sensor surface.

On addition of 1 nM of monoclonal anti-myc tag antibodies to the surface and incubating for 15 min, the sensor showed a response of 0.4° phase shift. So as to

check the response of the sensor when incubated in the same concentration, the sensor was incubated again in 1 nM of monoclonal anti-myc tag antibodies and the phase shift increased by 0.2°. The phase shift observed increased when the surface was incubated in higher concentrations of monoclonal anti-myc tag antibodies (10-50 nM). A saturation phase was observed after 50 nM concentration of monoclonal anti-myc tag antibodies *i.e.* from 50-150 nM. The surface was rinsed with 10 mM PBS (pH 7.2) after each incubation.



**Figure 5-11. response of the sensor surface towards different concentration of monoclonal anti myc tag antibodies.**

Shows change in phase ( $\Delta\phi$ ) vs. different concentrations of monoclonal anti-myc tag antibodies. The measurements were taken after incubating the surface immobilised with Adhiron myc binder 2 in different concentrations of monoclonal anti-myc tag antibodies for 15 min. The surface was incubated in 1 nM monoclonal anti-myc tag antibodies twice.

The phase shift observed when monoclonal anti-myc tag antibodies were added to the surface could be because of the change in the the dielectric properties of the interfacial surface or the charge distribution that arrises due to the binding of a charged bulky monoclonal anti myc tag antibodies. The binding of the antibodies can cause rearrangement of the PEG layer. These rearrangement in the PEG can then destabilise the underneath alkyl monolayers (Schreiber, 2000). This in turn can increase the non-faradaic ionic movement which is observed as the increase in phase shift (Zaccari *et al.*, 2014).

This shows that the sensing platform formed by the SAM and the biological recognition molecules / Adhiron myc binder 2 was sensitive enough to detect the

binding of monoclonal anti-myc tag antibodies. It also showed that the sensing platform was more sensitive than SPR, which was detecting the concentration of monoclonal anti-myc tag antibodies two orders of magnitude higher (see section 3.2.5).

As an alternative approach to rinsing the surface in between subsequent incubations, a different strategy of adding monoclonal anti-myc tag antibodies was used which is discussed in the following section.

#### **5.4.3.4. Using cumulative addition of anti-myc tag antibodies**

The surface immobilised with SAM was incubated in 10  $\mu\text{g/mL}$  of Adhiron myc binder 2 and 200 mV DC voltage induced stabilisation of surface was done after the SAM formation. The stabilisation of the surface was also done after the immobilisation of 10  $\mu\text{g/mL}$  of Adhiron myc binder 2 on the surface. The measurements were taken at 80 mV DC potential applied to the surface *vs.* reference (Ag/AgCl).

Figure 5-13 shows the change in phase ( $\Delta\phi$ ) *vs.* increasing concentration of anti myc-tag antibodies. Two initial readings were taken in 10 mM PBS (pH 7.2). The buffer was changed twice and the readings were taken after 15 min incubation each. To avoid the regeneration and washing steps in between, new concentrations were added so as to prevent the surface from drifting from its initial baseline, a cumulative addition of concentrations (0.1 nM to 200 nM) of monoclonal anti-myc tag antibodies was done. The response of the sensor was linear from 0.1 nM to 100 nM and then the sensor showed saturation at 200 nM. The change in phase ( $\Delta\phi$ ) on addition of 0.1 nM anti-myc tag antibodies was 0.3°. Although the linear response was observed but the change in overall phase observed was lower than the change in phase observed in Figure 5-12. This was most likely due to fewer Adhiron myc binder 2 left unoccupied on the surface with subsequent injections, as there was no removal of the solution and no rinsing in between the addition of new concentrations. The cumulative way of addition of antibodies most likely leads to the setting up of a new baseline for the next concentration to be added.

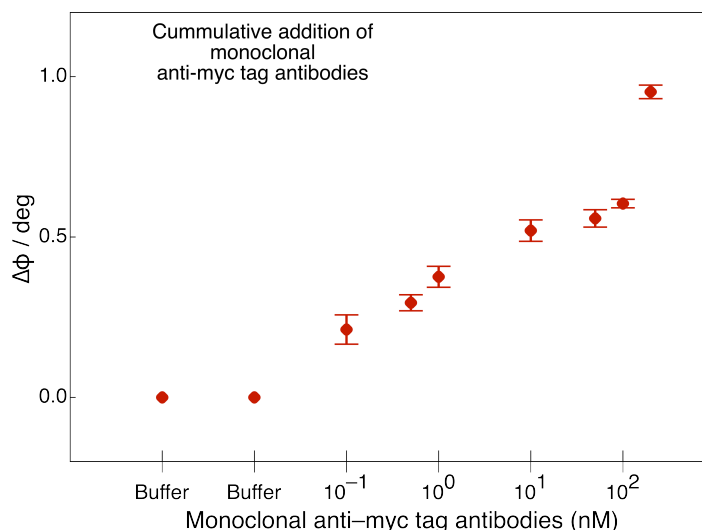


**Figure 5-12. Cumulative addition of different concentrations of monoclonal anti-myc tag antibodies.**

Shows the phase response ( $\Delta\phi$ ) of a sensor surface, immobilised with Adhiron myc binder 2, when incubated in different concentrations of monoclonal anti-myc tag antibodies for 15 min. The concentrations were added in a cumulative way without rinsing the surface in between or changing the buffer.

The following section gives a brief overview of the EIS based Adhiron myc binder 2 depicted by a schematic diagram (Figure 5-13).

Figure 5-13 shows a schematic of the EIS based Adhiron myc binder 2 biosensor used to detect monoclonal anti-myc tag antibodies. After the formation of -COOH-PEG-SAM on the surface, the initial phase observed was  $> -90^\circ$ , which is attributed to the presence of defects or pinholes in the monolayer depicted in the Figure 5-12 (see section 5.1.1.1). On immobilisation of Adhiron myc binder-2 on to the surface, the phase decreases as compared to the initial phase. One of the potential explanations, can be in terms of a compact layer of Adhiron myc binder 2 formed that decreases the penetration of ions. Although a direct cause of this change is still under investigation, there are various possible factors involved in changing the electrical environment of the interfacial surface upon the binding of monoclonal anti-myc tag antibodies, such as, the flexible -PEG molecules, conformational changes in the biological recognition layer (Adhiron myc binder 2) or the change in ionic environment at the interface due to the charged antibodies bound to the surface (see section 5.4.3.3).

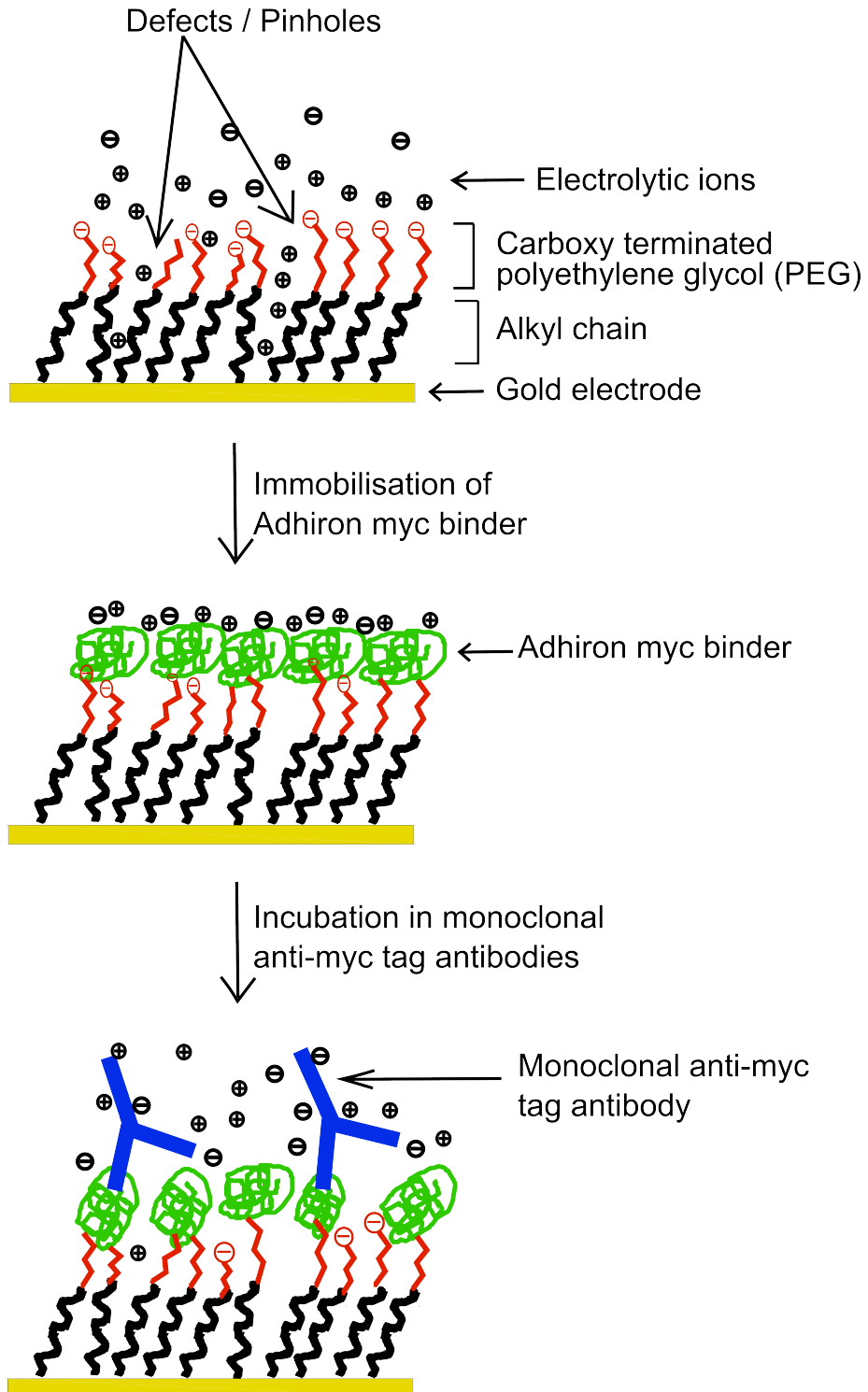


**Figure 5-13. The working of Adhiron myc binder 2 based impedimetric biosensor.**

Shows the schematic of the working of Adhiron myc binder 2 based EIS biosensor. (a) The immobilisation of carboxylic acid terminated alkylthiol self-assembled monolayer on to the gold surface *via* thiol bonding (Au-S). (b) The Adhiron myc binder 2 was immobilised on the SAM surface through amine coupling to form a sensitive sensing platform. (c) Binding and detection of monoclonal anti-myc tag antibodies.

#### 5.4.4. Discussion

The present work demonstrated the working of a label-free impedimetric biosensor using Adhiron myc binder 2 as the biological recognition molecule to detect monoclonal anti-myc tag antibodies.

In ELISA Adhiron myc binder 13 showed the maximum response followed by Adhiron myc binder 2, 11 and 7. On relating the binding with the similarity of the sequences present in the three variable regions of the binders with the myc epitope EQKLISEEDL, Adhiron myc binder 13 showed sequence similarity to myc epitope in its second loop. Although it showed the maximum signal in ELISA, it was discarded during the experiments because it was aggregating. Adhiron myc binder 2 and myc 11 presented similarity in sequences with the myc epitope EQKLISEEDL in the first variable region of the Adhiron scaffold (Figure 5-3). Although Adhiron myc binder 18 was also showing similarity with the myc epitope but the loop presenting the similar sequences was the second variable region. The difference in binding could be because of the presentation of the binding epitope in different variable regions that affects the binding of the antibodies to the Adhiron myc binders.

In the process of biosensor fabrication, the sensing platform constituted of the Adhiron myc binder 2 immobilised on the SAM layer (SH-(CH<sub>2</sub>)<sub>11</sub>-(EG)<sub>3</sub>-OCH<sub>2</sub>-COOH) formed on a gold electrode. The sensing platform allowed the non-faradaic movement of ions, which was used to detect the binding of monoclonal anti-myc tag antibodies to the Adhiron myc binder 2 molecules. The lowest concentration of monoclonal anti-myc tag antibodies detected was 0.1 nM and the detection was done over 3 orders of magnitude. The detection of the monoclonal anti-myc tag antibodies was done over a range of concentrations (0.1-200 nM), which shows that the system could be used for many different concentrations without the need for a regeneration step.

One of the limitations of the sensor was the variation of the response with respect to detection limit and dynamic range on different sensor surfaces, which could be attributed to the fact that the immobilisation of the ligand on the surface was a multistep process, that could lead to variability in the number of ligands bound to the SAM molecules and thus change the impedance between sensors. Moreover the immobilisation of Adhiron myc binder 2 on to the SAM through amine coupling can conceal the anti-myc tag binding site. This can be a reason for the difference in sensor response. The limitations in the system are also coherent with those observed in the work done by other researchers in similar field (Bart *et al.*, 2005). These limitations need to be addressed and worked upon so as to get more reproducible and similar responses from different sensor surfaces.

## Chapter 6. Voltage induced modulation of the sensitivity of the impedimetric biosensor

### 6.1. Introduction

After the fabrication of an impedimetric biosensor with the Adhiron myc binder 2 forming the biological recognition layer for detection of monoclonal anti-myc tag antibodies, the next aim of the project was to improve the sensitivity of the label free biosensor.

Sensitivity of a biosensor is an important aspect in case of detection of biomarkers in clinical samples. Blood serum contains different concentrations of biomarkers depending upon the physiological condition of a person. The detection of the biomarkers by a biosensor can vary depending upon the concentration of the biomarkers in the sample or the affinity of the biological recognition molecules towards the biomarkers. To improve the sensitivity of the biosensors various strategies have been employed to enhance the detection signal. Electroactive probe molecules (methyl blue) – modified reporter probe complementary to the capture probes have been used to detect the target molecules (Yang and Zhang, 2010). This is a limitation in case of label-free impedimetric biosensors in which label-free strategies have to be explored for increasing the sensitivity. Using a higher affinity probe molecule or biological recognition molecule can also enhance the sensitivity of the biosensor *e.g.* smaller antibody fragments for detection of *E. coli* cells proved to increase the sensitivity of the sensor (based on quartz crystal microbalance) over the use of whole antibodies (Sharma and Mutharasan, 2013). Another approach to detect biomarkers at extremely low concentrations has been to use the desirable properties of nano particles that include high surface area to volume ratio and electrical conductivity (Li and Cui, 2013). Cai *et al.* fabricated a molecular imprinting based recognition molecule (molecularly imprinted polymer-MIP) to detect template proteins. A non-conducting polymer was coated over an array of carbon nanotubes which increased the sensitivity of the sensing platform and the binding of the template proteins was detected (subpicogram per litre) using change EIS (Cai *et al.*, 2010).

The label-free detection of monoclonal anti-myc tag antibodies on the EIS-based Adhiron biosensor was mainly dependent on the non-faradaic changes at the interfacial plane. These changes in the non-faradaic movement of ions through the PEG-SAM was facilitated by the presence of pinholes / defects in the SAM. In such

a case the sensitivity of the SAM can be varied by tuning the number of pinholes / defects present in the SAM that largely depends on the packaging of SAM. The order or packaging of SAM can be changed using mixed SAMs (Chapman *et al.*, 2000; Zaccari *et al.*, 2014). The number of pinholes / defects and therefore the non-faradaic movement of ions can be tuned by varying the concentration ratios of the mixed SAMs (Zaccari *et al.*, 2014).

One of the inspiring approaches that nature has provided is based on bilayer membranes. The SAMs can be compared to bilayer membranes that have been widely studied to understand the mechanism of transport of molecules into the cells. The permeability of these biological membranes increases by using strong electrical pulses (voltage pulse). The phenomenon is widely used to transport molecules in and out of cells (Weaver and Chizmadzhev, 1996). An interesting work was published in the year 2000 (Boubour and Lennox, 2000b) wherein impedance spectroscopy was used to study the effect of applying different voltages (DC biases) on SAMs formed from n-alkanethiols. The work showed that SAMs behaved like insulators until a critical potential ( $V_c$ ) was applied and at potentials more cathodic than the  $V_c$ , the SAMs show a significant change in the phase angle in the low frequency region. These changes suggested that the defects formed in the SAMs allowed ion and water penetration. The change in phase was also shown partly reversible showing that the changes induced due to DC potential were not permanent.

The working of the Adhiron myc binder 2 biosensor is based on the dielectric properties of the interfacial layer formed by the SAM and the Adhiron myc binder 2. When the Adhiron myc binder 2 binds to monoclonal anti-myc antibody, there is a change at the interface of the sensor surface that can be detected as the change in phase. In an ideal situation, if the SAM layer and the biological recognition molecules are compactly bound such that no holes or defects are present, it will impede the passage of ions through the SAM. Thus, there will be no detection of any change encountered by the interfacial layer. In such a situation if defects are induced in the SAM so that the movement of ions is allowed, the detection will be possible. Bart *et al* observed a higher sensor response at 0.2 V than 0 V *vs.* a saturated calomel reference electrode during the detection of interferon-Y (IFN-Y) (Bart *et al.*, 2005).

Based on such lines one of the promising approaches to improve the sensitivity of the EIS based Adhiron myc binder 2 biosensor was to induce defects in the SAM in using a higher DC bias. Figure 6-1 shows a schematic depicting the change in the movement of ions through the interfacial layer on applying a positive DC potential to the working electrode against the reference electrode (Ag/AgCl). The surface at

0 V DC bias consists of some defects, which corresponds to its non-ideal insulating behaviour (phase  $> -90^\circ$ ). On applying a higher DC bias there are various effects that can increase the permeability of the ions. Firstly, on applying higher potential the number of ions moving towards the surface increases thus increasing the non-faradaic current. Secondly, since the PEG molecules on the surface are charged therefore the effect of voltage can cause conformational changes in the PEG molecules. Such changes can either induce new defects in the SAM or can enhance the movement of ions to the unreachable defects of the SAM by opening paths for the ions to move to and from the electrode. The reversibility in the rearrangement of SAM was depicted by the restoration of the original phase of the SAM at 0 V DC bias and back to the same higher bias. This shows that the change in the rearrangement is not permanent as long as the voltage does not cause the desorption of the alkyl thiols from the surface.

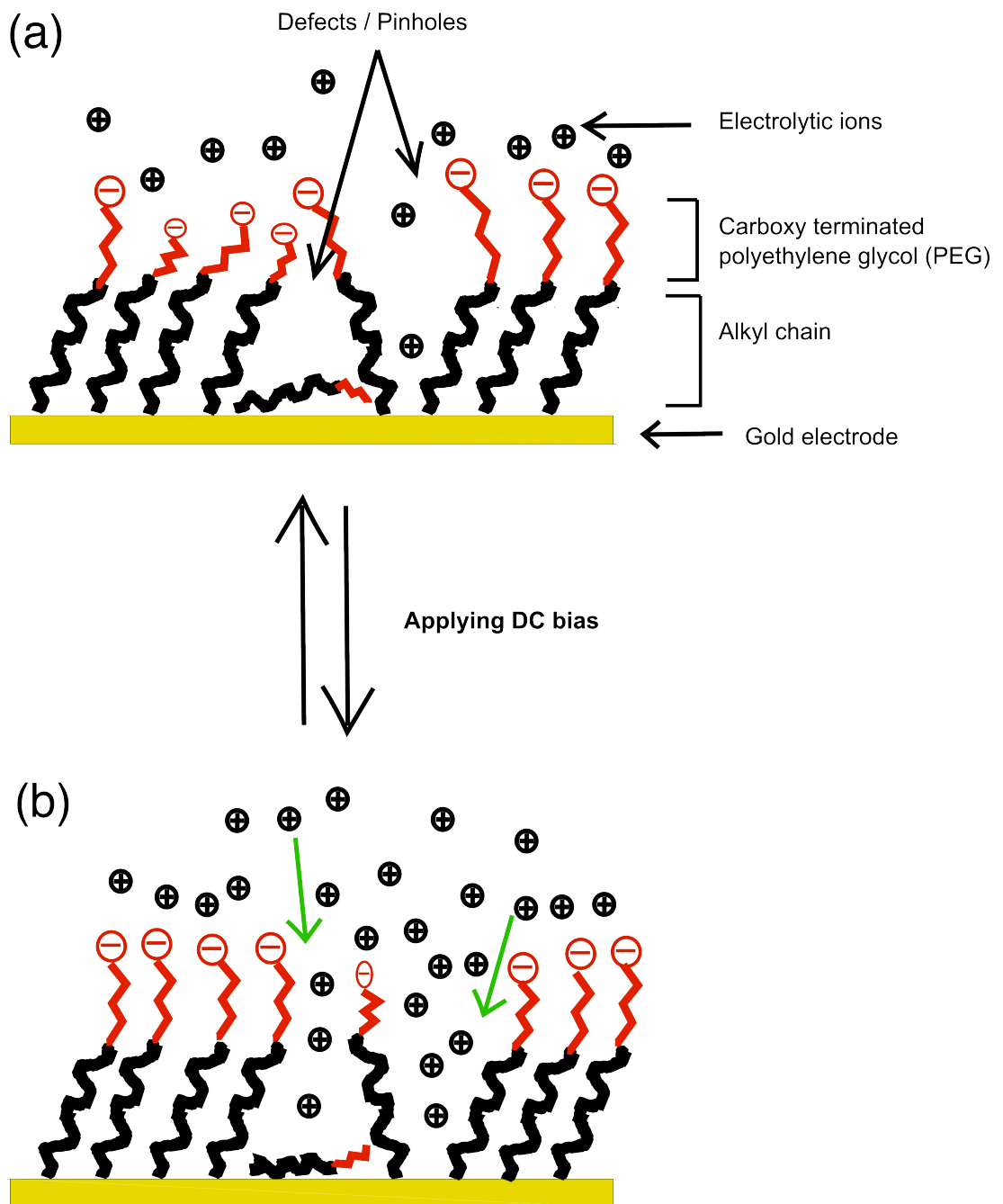


**Figure 6-1. Schematic representation of potential induced defects in SAM.**

Schematic showing the change in interfacial surface from (a) to (b) when a higher DC bias is applied to the surface with respect to the reference electrode. It shows the defects induced in the PEG-SAM surface (b) at a higher DC bias that increases permeation of ions into the SAM. It also depicts the reversibility of the SAM when the DC bias is restored to the original potential.

In light of inducing defects by applying higher DC voltages and thus changing the sensitivity of the biosensor, the project aimed to develop a model system in order to investigate any change in the sensitivity by changing the DC bias.

The initial experiments to investigate the modulation of the biosensor sensitivity using DC biases were done using Adhiron myc binder 2. The concept was then carried forward to change the sensitivity of a biosensor based on Adhiron IL8 binder to detect IL8 protein. IL8 protein is a biomarker in various clinical disorders e.g urinary bladder cancer, pulmonary diseases (Shahzad *et al.*). IL8 is a cytokine produced in blood cells and tissues and is associated with different inflammatory diseases (Baggiolini and Clark-Lewis, 1992). Recently, a biosensor for the detection of IL8 protein was developed by the Bioelectronics Laboratory at the University of Leeds, and this biosensor assay was then employed for the DC bias studies for tuning the sensitivity of a biosensor. This biosensor was chosen for further investigation as it showed very low detection limit (<100 fg/ml), large dynamic range, and furthermore, is clinically more relevant than the Adhiron myc binder 2.

This chapter discusses about the behaviour of SAM at different DC biases and the improvement of sensitivity of EIS based biosensor.

## 6.2. Materials

Reagents and chemicals were purchased from Sigma-Aldrich unless mentioned. Alkanethiol with terminal ethylene glycol functionalised with carboxylic group (SH-C<sub>11</sub>-(EG)<sub>3</sub>-OCH<sub>2</sub>-COOH) was purchased from Prochimia, Poland. IL8 protein and monoclonal anti-myc tag antibodies were purchased from Abcam. Ag/AgCl saturated KCl reference electrode.

## 6.3. Methods

The cleaning of gold surface was done using method described in section 5.3.3. The cleaned gold surface was incubated in 1 mM alkanethiol-PEG (SH-(CH<sub>2</sub>)<sub>11</sub>-(EG)<sub>3</sub>-OCH<sub>2</sub>-COOH) solution for 48 hr. The surface was then subjected to 15 cycles of 0.2 V DC potential *vs.* reference (Ag/AgCl). The immobilisation of 10 µg/mL Adhiron myc binder 2 and Adhiron IL8 protein was done using the EDC-NHS coupling chemistry (section 5.3.3.). This was followed by subjecting the surface to 15 cycles of 0.2 V DC potential *vs.* reference (Ag/AgCl).

The surface was then incubated in different concentrations of monoclonal anti –myc tag antibodies and IL8 protein. The EIS measurements were taken in 10 mM PBS,

pH 7.2 (for Adhiron myc binder 2 sensor) and in 10 mM PB, pH 7.2 (for Adhiron IL8 binder sensor) in the frequency range of 100 kHz to 50 mHz at different DC biases *vs.* reference (Ag/AgCl).

## 6.4. Results

To investigate the change in sensitivity of a sensor with the change in DC bias various experiments were done initially to ascertain the behaviour of the SAM immobilised gold electrode on applying different DC voltages.

### 6.4.1. Applying different voltages to the SAM

To investigate into the effect of different DC biases on SAM (with respect to reference Ag/AgCl), the surface was subjected to different potentials with respect to the reference (Ag/AgCl). So as to set the potential range where the surface behaves reversible, an arbitrary range of 0 to 0.35 V DC potentials was chosen. After 0.1 V the voltage was applied in 0.05 V steps.

#### 6.4.1.1. Phase change *vs.* frequency

Figure 6-2 shows the phase *vs.* frequency (100 kHz to 50 mHz) profile obtained after the surface was subjected to 0, 0.1, 0.15, 0.2, 0.25, 0.3 and 0.35 V *vs.* reference (Ag/AgCl). There was negligible change observed in the frequency range of 100 kHz to 10 Hz. This is attributed to the fact that the solution resistance dominates in the higher frequency range and therefore no shift was observed in the range of 100 kHz to 10 Hz.

Figure 6-2(b) shows the change in the phase in the frequency range 10 Hz to 50 mHz. The phase at 0.1 Hz was increasing with the increase in DC bias. Although the phase shift is observed at 10 Hz as well but the shift at 0.1 Hz was more prominent and therefore 0.1 Hz was chosen as the frequency to measure the phase. The phase at 0.1 Hz was less negative ( $> -90^\circ$ ) with the increase in DC bias. The change was attributed to the defects created in the SAM that increased the movement of ions (Boubour and Lennox, 2000b).

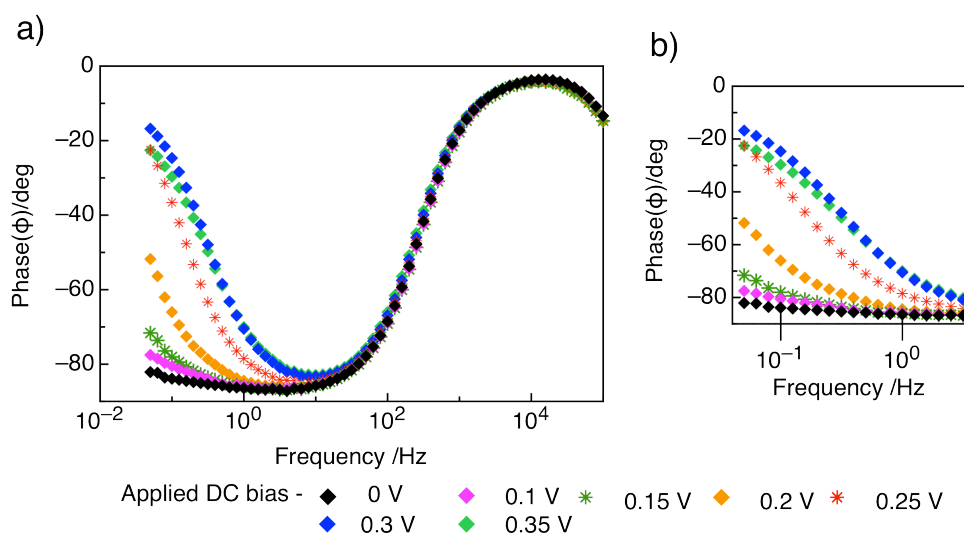


**Figure 6-2. Phase vs. Frequency at different DC biases applied to the SAM immobilised gold surface.**

Shows the Bode plot depicting phase vs. frequency. The surface was subjected to different DC biases (0, 0.1, 0.15, 0.2, 0.25, 0.3 and 0.35 V) against the working electrode with respect to reference (Ag/AgCl). (a) shows the plot in the frequency range of 100 kHz to 50 mHz and (b) shows the response in the frequency range of 0.05 Hz to 0.3 Hz.

#### 6.4.1.2. Absolute impedance vs. frequency

Figure 6-3 shows the change in absolute impedance  $|Z|$  vs. frequency (0.1-0.5 Hz) on applying different DC bias 0, 0.1, 0.15, 0.2, 0.25, 0.3 and 0.35 V. The absolute impedance of the surface decreases with the increase in voltage, which proved that the surface showed less resistant to the movement of ions at higher voltages due to interfacial changes allowing non-faradaic movement of ions. The absolute impedance at different DC biases coincide in the higher frequency range (data not shown).

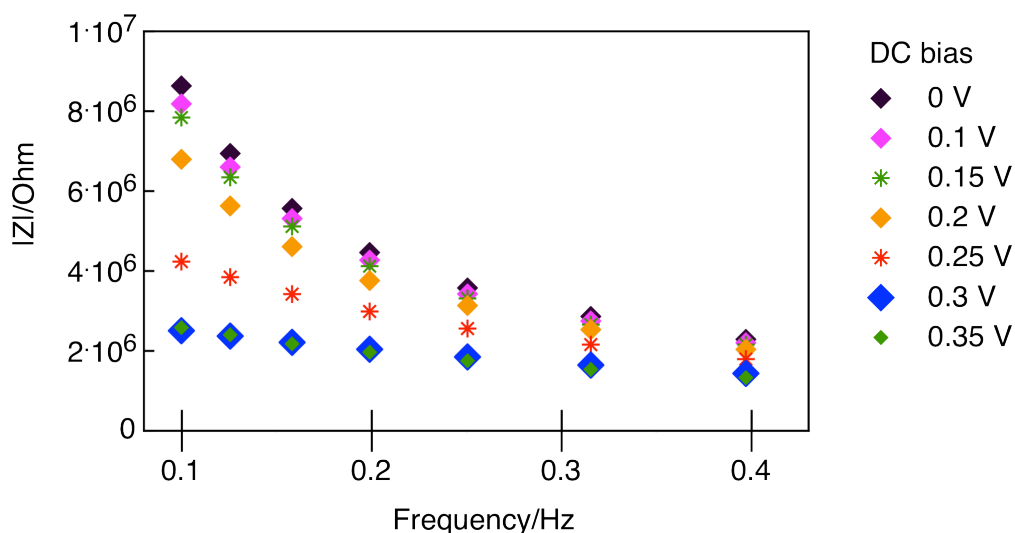


**Figure 6-3. Absolute impedance change with respect to frequency at different DC biases.**

Shows the absolute impedance *vs.* frequency (0.1 to 0.3 Hz). The surface was subjected to different DC biases (0, 0.1, 0.15, 0.2, 0.25, 0.3 and 0.35 V) against the working electrode with respect to reference (Ag/AgCl).

#### 6.4.1.3. Reversibility of phase at DC bias

In order to investigate whether the DC voltages caused any permanent perturbation to the SAM and on basis of that select an appropriate voltage range to work with, the SAM immobilised surface was subjected to various voltages.

The reversibility in the potential induced defects in the SAM was checked on the basis of restoration of the original phase of the SAM at 0 V after applying higher DC biases. The reversibility of the defects was also checked by checking the restoration of phase at a particular DC bias when different DC voltages were applied in between.

Clean gold surface with immobilised SAM was incubated in 10 mM PBS (pH 7.2) and the measurements were taken at different DC potentials (0-0.4 V) *vs.* reference (Ag/AgCl) in the frequency range of 100 kHz to 50 mHz. The phase corresponding to 0 V DC bias was taken as a reference phase for comparing the surface reversibility at different DC biases. The reversibility at each potential was checked by returning back to the 0 V DC bias. The phase at the same DC bias was also checked twice by applying different voltages in between. This was done to check if different voltages were causing any permanent change in the interfacial layer of the sensor. The DC biases applied to check the reversibility were as follows:

### 0 V and 0.1 V

Figure 6-4 shows that the phase measured over the whole range of frequencies at 0 V potential did not change after applying 0.1 V of DC bias. The phase measured at 0 V before and after applying 0.1 V DC bias were overlapping. The phase measured at 0.1 V also overlapped after the potential was set back to 0 V. Figure 3(b) elaborates the phase measured in the lower frequency range (0.1 to 0.36 Hz).

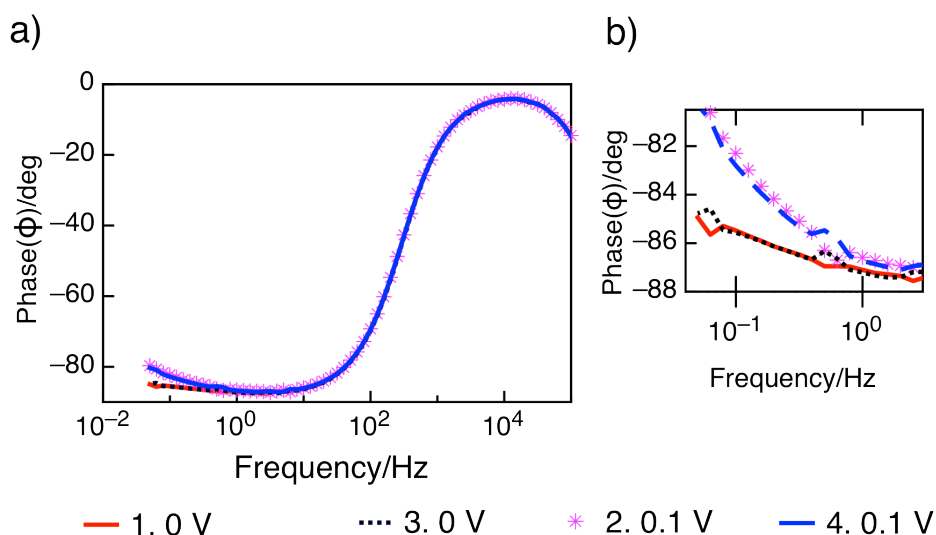


**Figure 6-4 Reversibility in defects caused by potential change, checked at 0 V and 0.1 V applied to the surface against reference (Ag/AgCl).**

Shows the phase vs. frequency in the range of a) 100 kHz to 50 mHz and b) 0.1 Hz to 0.3 Hz. The reversibility of the defects induced in the SAM were analysed by checking the restoration of the phase of the surface subjected to different DC biases 0 and 0.1 V vs. the reference (Ag/AgCl).

### 0 V, 0.15 V, and 0.2 V

Figure 6-5 shows the phase measured over the whole range of frequencies (100 kHz to 50 mHz) at DC potentials corresponding to 0, 0.15, and 0.2 V. After subjecting the surface to 0.15 V as well as 0.2 V, it did not show change in phase with respect to 0 V. The phase at 0.2 V overlapped with the previous phase measured at the same potential in the lower frequency range (0.1 to 0.36 Hz) (Figure 6-5). This showed the maintenance of reversibility in the rearrangement of SAM at 0.15 V and 0.2 V DC potentials.

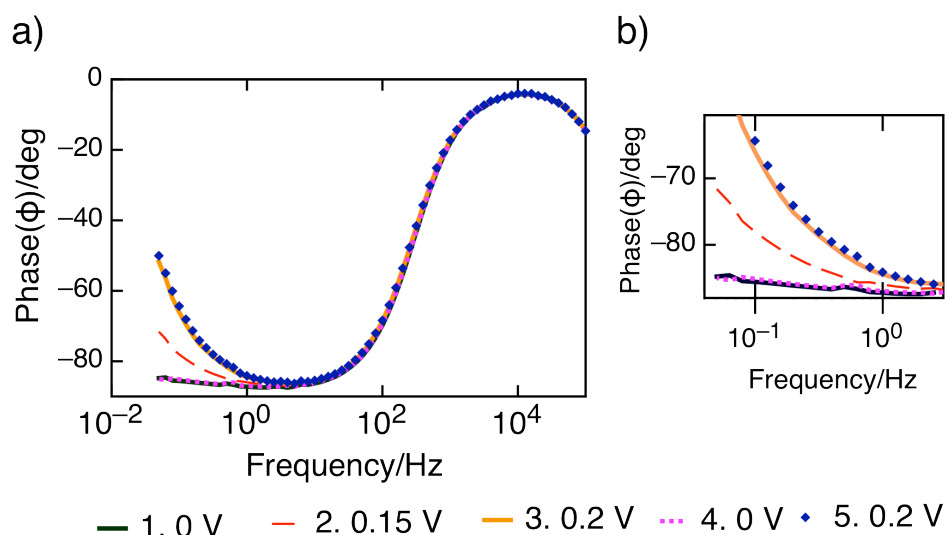


**Figure 6-5 Reversibility in defects caused by potential change, checked at five different voltages applied to the surface against reference (Ag/AgCl).**

Shows the phase vs. frequency in the range of a) 100 kHz to 50 mHz and b) 0.1 Hz to 0.3 Hz. The reversibility of the defects induced in the SAM were analysed by checking the restoration of the phase of the surface subjected to different DC biases 0 V, 0.15 V and 0.2 V vs. the reference (Ag/AgCl).

#### ***0 V, 0.25 V, 0.3 V and 0.4 V***

Figure 6-6 shows the phase measured over the whole range of frequencies (100 kHz to 50 mHz) when the surface was subjected to 0, 0.25, 0.3 and 0.4 V DC bias. After subjecting the surface to 0.25, 0.3 and 0.4 V, the phase did not change at 0V with respect to the previous phases measured before applying higher voltages. Figure 6-6(b) shows the phase response measured in the lower frequency range (0.1 to 0.36 Hz). In the lower frequency range the phase at 0 and 0.4 V overlapped with the previous phase measured at the same potentials respectively. This showed the reversibility in the phase response of the SAM-immobilised surface subjected to 0.25, 0.3 and 0.4 V DC potentials.

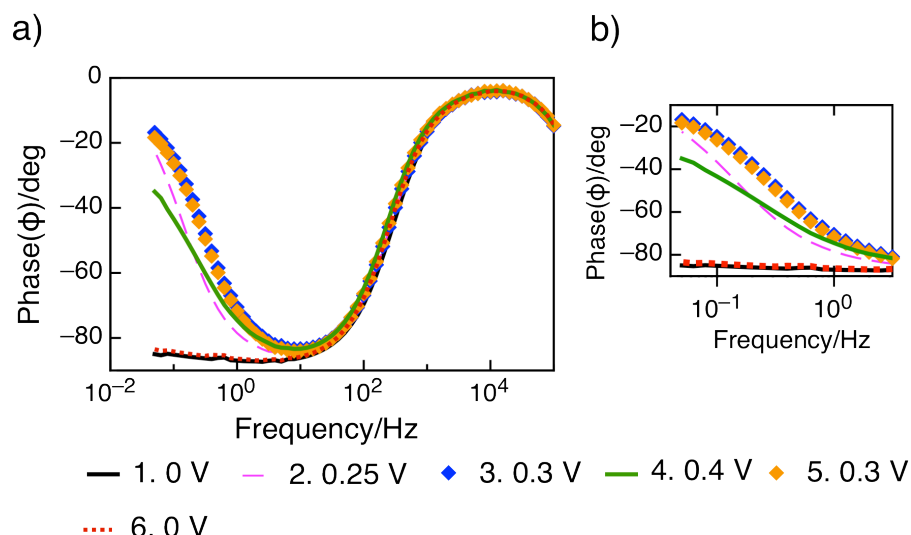


**Figure 6-6 Reversibility in defects caused by potential change, checked at six different voltages applied to the surface against reference (Ag/AgCl).**

Shows the phase vs. frequency in the range of a) 100 kHz to 50 mHz and b) 0.1 Hz to 0.3 Hz. The reversibility of the defects induced in the SAM were analysed by checking the restoration of the phase of the surface subjected to different DC biases 0, 0.25, 0.3 and 0.4 V vs. the reference (Ag/AgCl).

The coinciding of the phase readings corresponding to different frequencies when measured at the same DC bias and no change in the phase observed at 0V confirmed that the DC bias was not causing any permanent change to the interfacial layer of the sensor and the defects formed were replaceable. This could be attributed to the rearrangement of the  $-\text{COOH-PEG-SAM}$  surface.

In order to investigate into the change of sensitivity of the surface, a model system based on Adhiron myc binder 2 for the detection of anti myc tag antibodies was used.

#### 6.4.1.4. Using different potentials to detect monoclonal anti-myc tag antibodies

The concept of potential induced defects was used in the Adhiron myc binder 2 based biosensor in order to check the change in sensitivity of the biosensor detecting monoclonal anti-myc tag antibodies.

##### *Immobilisation of Adhiron myc binder 2*

In order to compare the phase at different DC potentials after the immobilisation of Adhiron myc binder 2 the surface was subjected to different DC biases.

The surface was immobilised with 10  $\mu\text{g/mL}$  of Adhiron myc binder 2 using NHS-EDC coupling. The measurements were taken in the frequency range of

100 kHz to 50 mHz at the following DC potentials *vs.* reference (Ag/AgCl) - 0, 0.05, 0.08, 0.1, 0.15, 0.18 and 0.2 V. Figure 6-7 shows the phase *vs.* frequency plot in the lower frequency range (0.1 to 0.3 Hz). There was an increase in phase (-88.5° to -68.2°) shown in Figure 6-7(b). The increase in phase was attributed to the increase in the movement of ions into the SAM surface.

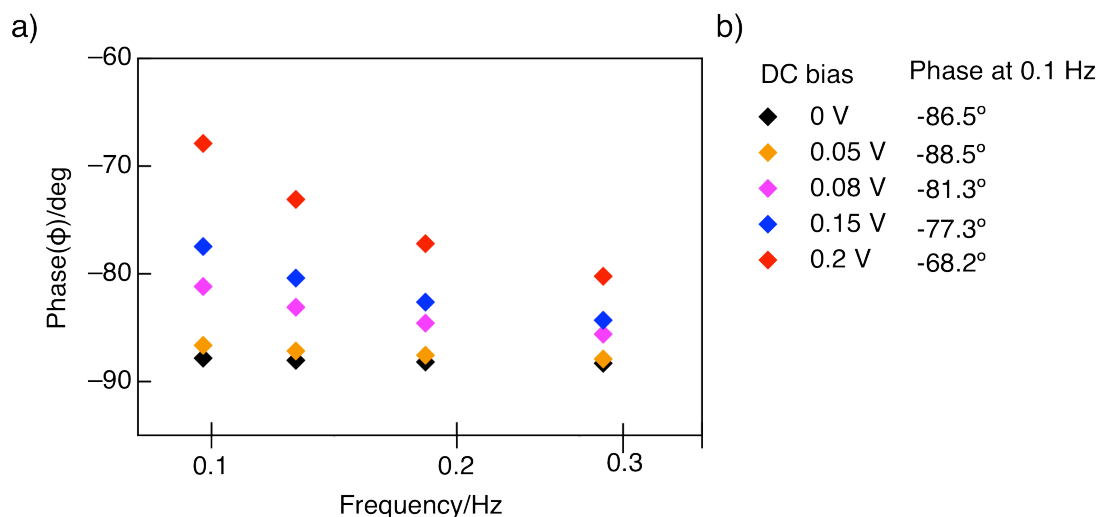


**Figure 6-7 Phase vs. Frequency measured at different potentials after incubating the SAM surface with Adhiron myc binder 2.**

Shows the phase *vs.* frequency at different potentials of the SAM surface incubated in 10 µg/mL Adhiron myc binder 2. (a) shows the phase *vs.* frequency plot in the frequency range of 0.1 - 0.3 Hz and (b) shows the phase at 0.1 Hz at different voltages ranging from -88.5 to -68.2°.

### ***Adding monoclonal anti-myc tag antibodies***

In order to compare the phase shift in between DC biases different concentrations of monoclonal anti-myc tag antibodies were added to the surface immobilised with Adhiron myc binder 2.

The sensor was incubated in different concentrations of monoclonal anti-myc tag antibodies ranging from 30 nM to 60 nM for 15 min. The surface was subjected to four different DC biases against reference Ag/AgCl. Although the complete frequency scan of the response was taken in the range of 100 KHz to 50 mHz but the binding curve was plotted corresponding to the measurements taken at 0.1 Hz frequency.

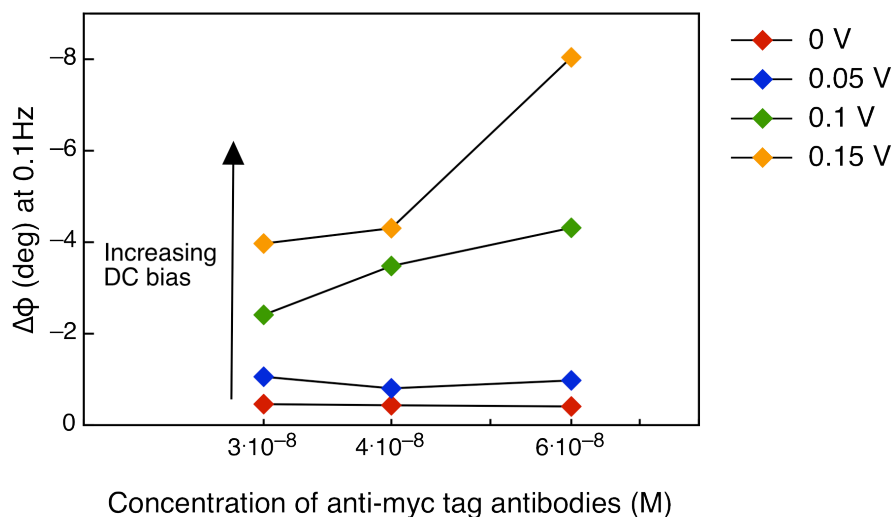


**Figure 6-8 Change in phase ( $\Delta\phi$ ) measured at 0.1 Hz after incubating the sensor surface in different concentrations of monoclonal anti myc tag anti bodies at different voltages applied to the surface.**

Shows the change in phase ( $\Delta\phi$ ) at 0.1 Hz at DC potentials 0, 0.05, 0.1 and 0.15 V vs. the reference (Ag/AgCl). The measurements were taken after incubation of the surface immobilised with 10  $\mu\text{g/mL}$  Adhiron myc binder 2 in different concentrations of monoclonal anti-myc tag antibodies ranging from 30 to 60 nM.

A comparison of the change in phase ( $\Delta\phi$ ) at 0.1 Hz with respect to the initial phase measured in 10 mM PBS (pH 7.2) to the phase obtained after binding different concentrations of monoclonal anti-myc tag antibodies (30 nM to 60 nM) at various DC biases is shown in Figure 6-8. The phase shift at each concentration of anti-myc tag antibodies was measured with respect to the initial phase reading of the surface immobilised with Adhiron myc binder 2 in 10 mM PBS (pH 7.2).

At each concentration, the change in phase ( $\Delta\phi$ ) was increasing in the increasing order of the applied DC bias. At 0 and 0.05 V the sensor showed minimal response to all the three concentrations. The response increased at 0.1 V DC bias and was maximum at 0.15 V for all three concentrations of the monoclonal anti-myc tag antibodies. An increase in response on applying a higher DC bias could be related to the increase in the number of defects that increase the permeability of the surface to ions / water molecules thus showing higher phase shifts.

#### 6.4.1.5. Checking the reversibility of phase Adhiron myc binder 2 sensor

In order to be sure that the response was due to the interaction of monoclonal anti-myc tag antibodies with Adhiron myc binder 2, buffer injections were done in between the injections of monoclonal anti-myc tag antibodies. Figure 6-9 shows the change in phase ( $\Delta\phi$ ) at 0.1 Hz, when buffer injection was done after 100 nM and

after 300 nM concentration of monoclonal anti-myc tag antibodies. The complete solution was taken out and the sensor was incubated in fresh 10 mM PBS (pH 7.2) for 15 min. It was observed that with the buffer injections the phase was shifting back towards the original baseline. This was attributed to the fact that the dissociation constant of the interaction of Adhiron myc 2 binder and monoclonal anti myc-tag antibodies was quite high ( $140 \pm 10$  nM) as observed in the SPR data (see section 5.4.2) therefore on incubation of the surface in buffer, the equilibrium shifts and the phase observed corresponds to the initial phase when no antibodies were added. A constant shift in baseline was observed in this case. This was because in this experiment the sensor surface was washed after taking each measurement, which could change the arrangement of the PEG-SAM. In the following experiments the analytes were added in a cumulative way avoiding the rinsing steps in between.

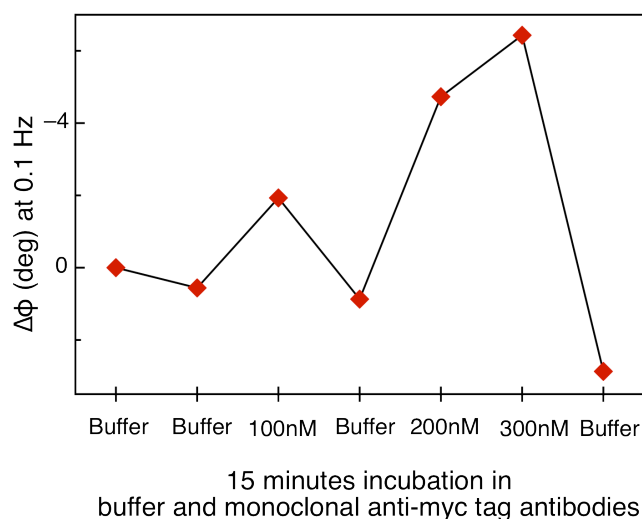


**Figure 6-9 Regeneration of sensor surface on incubating in 10 mM PBS, pH 7.2.**

Shows the change in phase ( $\Delta\phi$ ) at 0.1 Hz at 0.1 V DC bias applied to the surface against the reference (Ag/AgCl). The phase obtained when the surface is incubated in 100 nM and 300 nM restores back to the phase obtained when incubated in 10 mM PBS (pH 7.2).

#### 6.4.1.6. Voltage induced sensitivity using Adhiron IL8 binder

After observing an increase in the response of the Adhiron myc binder 2 biosensor for detecting monoclonal anti-myc tag antibodies, the voltage induced sensitivity was further applied to an Adhiron IL8 binder based impedimetric biosensor. The biosensor was developed to detect interleukin 8 protein (IL8). The sensitivity improvement of this biosensor for the detection of IL8 protein was more relevant clinically as it is an important biomarker for different diseases (see section 6.1).

The following section discusses the effect of higher DC bias on the sensitivity of an Adhiron IL8 biosensor.

***Immobilisation of IL8 binder on the sensor surface.***

Adhiron IL8 binder was immobilised on the SAM derivatised surface using NHS-EDC chemistry. The measurements were taken at 0V DC bias applied to the surface against the reference (Ag/AgCl).

Figure 6-10 shows the change in phase before and after the incubation of 10  $\mu\text{g/mL}$  Adhiron IL8 binder on the surface in the frequency range of 100 kHz to 50 mHz. A phase change from  $-80.5^\circ$  before immobilisation to  $-83.4^\circ$  after 10  $\mu\text{g/mL}$  Adhiron IL8 binder immobilisation was observed at 0.1 Hz (shown with an arrow) (Figure 6-10(b)). The change in phase showing a less non-faradaic movement of ions in the lower frequency range shows the formation of a more packed SAM that does not allow ions to permeate through it.

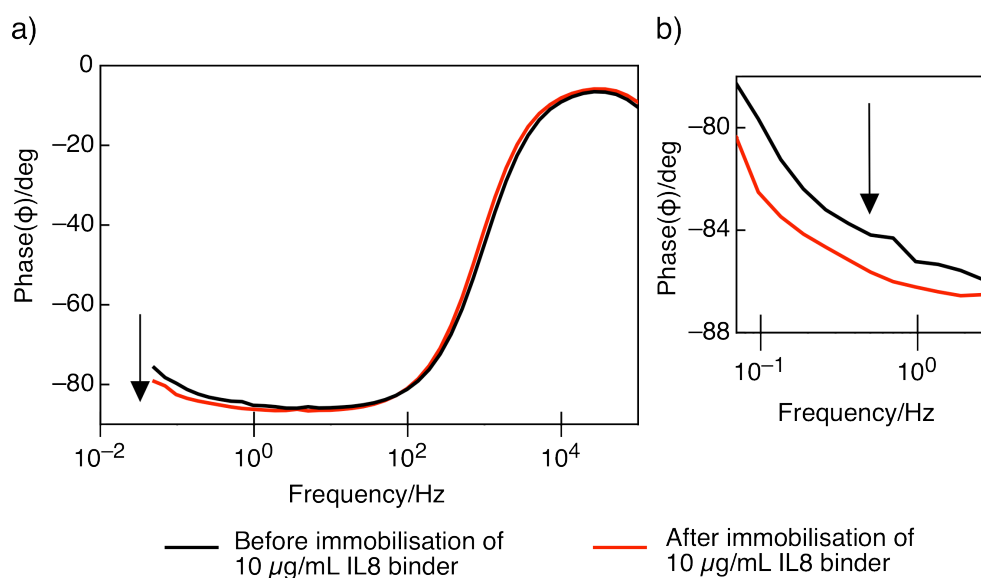


**Figure 6-10 Change in phase vs. Frequency before and after incubation of 10  $\mu\text{g/ml}$  of Adhiron IL8 binder.**

Shows the Bode plot depicting change in phase vs. frequency range (a) 100 kHz to 50 mHz and (b) 0.1 to 0.3 Hz before and after the incubation of gold surface in 10  $\mu\text{g/mL}$  Adhiron IL8 binder. The phase changes from  $-80.5^\circ$  to  $-83.4^\circ$  at 0.1 Hz (shown by an arrow).

### ***Checking surface stability after immobilisation of Adhiron IL8 binder***

After the immobilisation of Adhiron IL8 binder on the SAM containing gold surface, stability of the sensor surface was checked in 10 mM phosphate buffer, pH 7.2, before adding different concentrations of IL8 protein.

The surface was incubated in 10 mM PB (pH 7.2) without adding the IL8 protein. The measurements were taken after every 15 min for 5 subsequent buffer incubations at 0, 0.04, 0.08 and 0.12 V DC bias against the reference (Ag/AgCl).

Figure 6-11 shows the phase of the surface plotted against 0.1 Hz frequency at 0, 0.04, 0.08 and 0.12 V DC bias. The change in phase observed increased with the increase in the DC bias that was corresponding to the increase in defects with the increase in DC bias.

At 0 V the overall phase change observed in the five subsequent buffer incubations was  $\pm 0.3^\circ$ . Similarly for 0.04, 0.08 and 0.12 V the observed phase change was  $\pm 0.3^\circ$ ,  $\pm 0.4^\circ$  and  $\pm 0.5^\circ$  respectively as shown in Figure 6-11 (b). This range of change in phase observed was kept as the baseline drift corresponding to each DC voltage for the IL8 biosensor.

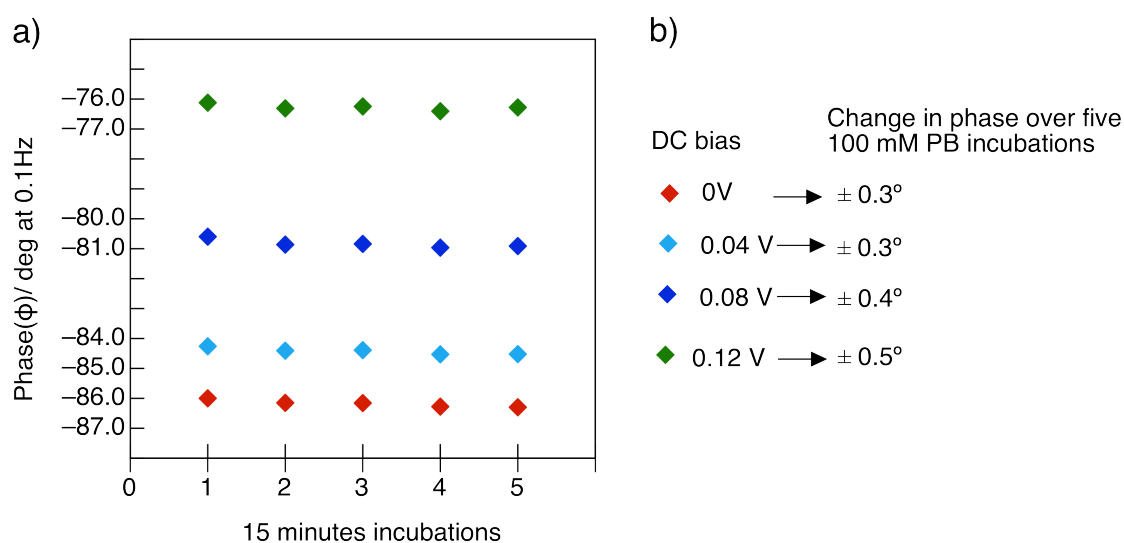


**Figure 6-11 Stability check of the SAM immobilised surface at different potentials.**

Shows phase of a surface after immobilisation of 10  $\mu\text{g/mL}$  Adhiron IL8 binder in five subsequent incubations in 10 mM PB (pH 7.2). The Adhiron IL8 binder was immobilised on a gold electrode modified with SAM. (a) The measurements were taken at 0.1 Hz at 0, 0.04, 0.08 and 0.12 V DC bias applied to the surface vs. reference (Ag/AgCl). (b) The overall phase change observed in the five subsequent buffer incubations for the Adhiron IL8 sensor.

### ***Adding different concentrations of IL8 protein***

The gold surface containing SAM immobilised with Adhiron IL8 binder showed drift in the baseline over five subsequent buffer incubations corresponding to each voltage (0, 0.04, 0.08 and 0.12 V). The phase change observed over five subsequent buffer incubations was considered as the baseline drift. The above mentioned voltages were then used to check the change in sensitivity of the sensor against different concentrations of IL8 protein, keeping in consideration the baseline drift.

For checking the phase response (0.1 Hz) to different concentrations of IL8 protein at different DC potentials *i.e.* 0, 0.04 and 0.08 V *vs.* reference (AgCl) three different surfaces immobilised with Adhiron IL8 binder were used respectively. Before injecting the IL8 protein concentration on to the surface immobilised with 10 µg/mL Adhiron IL8 binder, a baseline was established by incubating the surface in 10 mM PB (pH 7.2) for 15 min. Then the different concentrations of IL8 protein ranging from 0.1 pM to 10<sup>6</sup> pM were added in a cumulative way (see section 5.4.3.4).

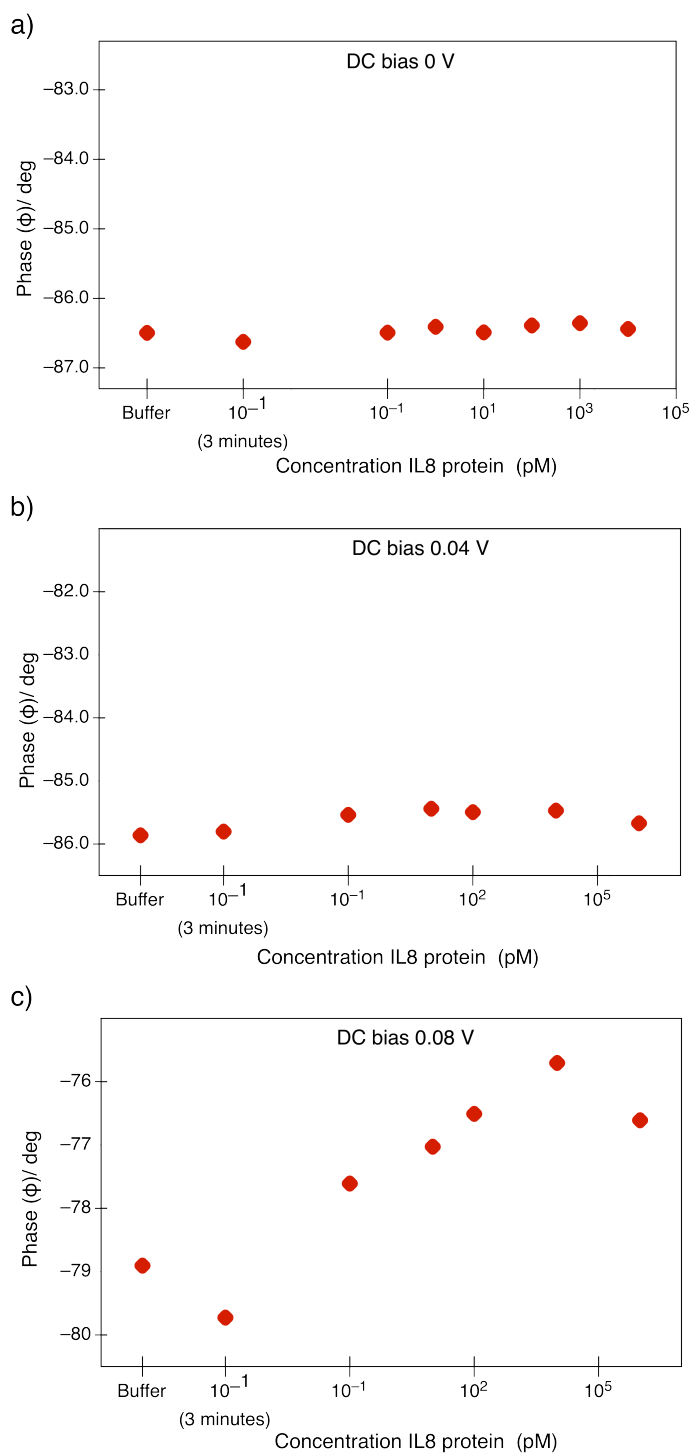
After injecting the first concentration of IL8 protein (0.1 pM), a measurement was done at 3 min and then 15 min of incubation. The measurement of phase after 3 min of injecting the first concentration of IL8 protein was done to take into consideration the change in the baseline (phase shift) due to addition of IL8 protein that changes the interfacial environment and causes a transition in baseline.

Figure 6-12 shows the phase *vs.* frequency profiles of Adhiron IL8 immobilised surfaces subjected to three different voltages 0 V(a), 0.04 V(b) and 0.08 V(c). A decrease in phase was observed after 3 min incubation in 0.1pM IL8 protein concentration for each DC bias. The initial decrease in phase could be due to the change in the dielectric properties of the interfacial surface that causes conformational changes in the SAM impeding the movement of ions. This effect is more prominently observed in the sensor surface subjected to 0.08 V DC bias.

The measurement of phase at 0.1 Hz after 15 min of incubation of the first concentration of IL8 protein did not show any change in case of 0 V and showed a phase shift of less than 0.1° in case of 0.04 V DC bias. A less than 0.1° shift could not be considered a response to the IL8 protein concentration because the baseline shift in buffer for 0.04 V DC bias was  $\leq \pm 0.3^\circ$  (Figure 6-11). In case of sensor subjected to 0.08 V DC bias, the phase shift was 2° that was attributed to the increased sensitivity of the surface due to higher DC potential applied to the surface.

The change in the phase from 3 min incubation to 15 min incubation was an interesting feature. It was more likely due to the flexible –COOH-PEG that causes some rearrangement in the SAM initially and then reaches a stable arrangement.

The response was linear for IL8 protein concentrations from 0.1 pM to  $10^4$  pM (10 nM). On incubating the surface in  $10^6$  pM (1  $\mu$ M) concentration of IL8 protein, the phase decreases. This phenomenon was observed in IL8 based sensors after a saturation was reached (data not shown). This could be attributed to the increase in the number of IL8 protein molecules bound to the sensor surface that change interfacial properties and impede the movement of ions / water molecules.



**Figure 6-12 Response of the Adhiron IL8 biosensors to different concentrations of the IL8 protein at different potentials.**

Shows the phase response of different SAM derivatised gold surfaces immobilised with  $10 \mu\text{g/mL}$  Adhiron IL8 binder against different concentrations of IL8 protein. The measurements were done after incubating the surfaces in  $10 \text{ mM PB}$  ( $\text{pH } 7.2$ ) for  $15 \text{ min}$ , concentration of  $0.1 \text{ pM}$  IL8 protein for  $3 \text{ min}$  and then  $15 \text{ min}$  for each concentration of IL8 protein ( $0.1 \text{ pM}$  to  $10^6 \text{ pM}$ ). The DC bias applied against reference  $\text{Ag/AgCl}$  was (a)  $0 \text{ V}$ , (b)  $0.04 \text{ V}$  and (c)  $0.08 \text{ V}$ .

#### 6.4.1.7. Limitations of the current set-up

The main limitation of the Adhiron based IL8 biosensor based experiments was the non-reproducibility of the results on different sensors corresponding to the same voltage. The phase shift observed on addition of first concentration of IL8 protein was different on different sensors when subjected to the same DC potential. Figure 6-13 shows the variation in response to monoclonal anti-myc tag antibodies between two different sensor surfaces immobilised with 10  $\mu\text{g/mL}$  Adhiron IL8 binder. The change in phase ( $\Delta\phi$ ) at 0.1 Hz, observed in case of sensor 1 after incubating the surface in 0.1 pM IL8 protein concentration was 1° whereas for sensor 2 was 2°. This inter-sensor variation could arise due to various reasons such as the difference in the number of IL8 binders immobilised on to the surface, the conformation of binders once immobilised on the surface, the handling of the sensor during the various steps involved from the cleaning of gold surface till the addition of IL8 protein.

In order to avoid intersensor variations, same sensor was used to detect the binding of IL8 protein under different DC biases.

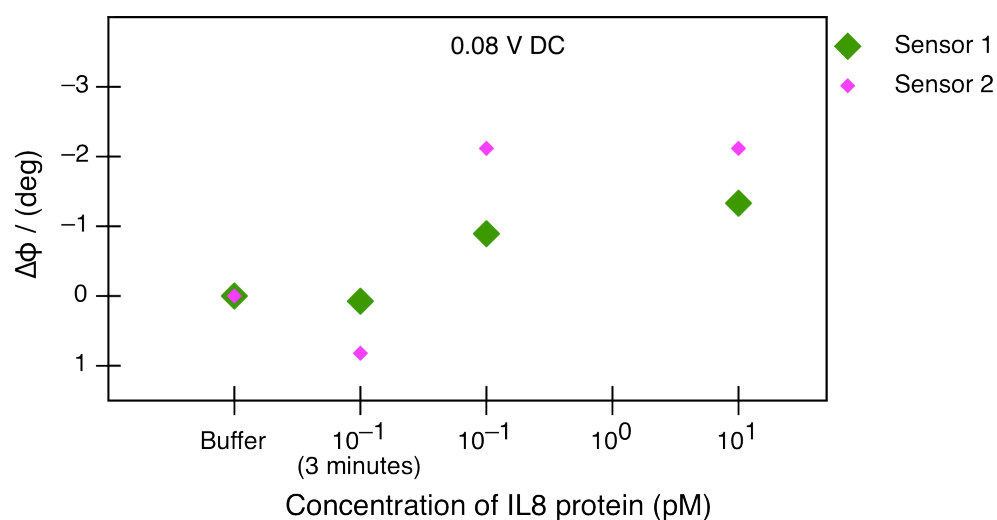


**Figure 6-13 Inter-sensor variation in response of the Adhiron IL8 biosensor to the IL8 protein.**

Shows the change in phase ( $\Delta\phi$ ) response of two different SAM derivatised gold surfaces, immobilised with 10  $\mu\text{g/mL}$  Adhiron IL8 binder, on adding different concentrations of IL8 protein. The measurements were taken after incubating the surfaces in 10 mM PB (pH 7.2) for 15 min, 0.1 pM concentration of IL8 protein for 3 min, 15 min followed by incubation in 10 pM concentration of IL8 protein for 15 min.

#### **6.4.1.8. Checking change in sensitivity with different potentials on the same sensor.**

A SAM derivatised surface was used to immobilise 10  $\mu\text{g/mL}$  Adhiron myc binders using EDC-NHS chemistry. The stability of the surface was checked in 10 mM PB (pH 7.2) by measuring the phase (at 0.1 Hz) of the surface subjected to increasing order of DC bias *i.e.* 0, 0.04 and 0.08 V. The surface was then incubated in different concentrations of IL8 protein.

Figure 6-14 shows that that the response at 0 mV and 0.04 mV was negligible. Whereas the phase shift at 0.08V and 0.12V (Appendix-Figure 1) was higher as compared to 0 and 0.04V but range of phase shift observed was similar to phase shifts obtained when buffer injections were done on the surface immobilised with Adhiron IL8 binder 5 (Figure 6-11). The phase shift observed in case of surface subjected to 0.08V DC bias was around  $-0.3^\circ$  and in case of 0.12V was  $-0.35^\circ$ . Taking the response in buffer injections into consideration, it can be said that there was no response detected by the sensor when incubated in IL8 protein. As the Adhiron IL8 binder was showing interaction with the IL8 protein on SPR ( $30\text{m}^\circ$  shift) (data not shown) and when different surfaces were used for single DC biases applied (Figure 6-12, 6-13), there can be a possibility that the surface immobilised with Adhiron IL8 binder was affected by the range of different DC biases applied to the same surface affecting the conformation of the Adhiron IL8 binder or the IL8 proteins.

The effect of applying subsequent higher DC potential to the sensor immobilised with Adhiron IL8 binder needs to be further investigated.

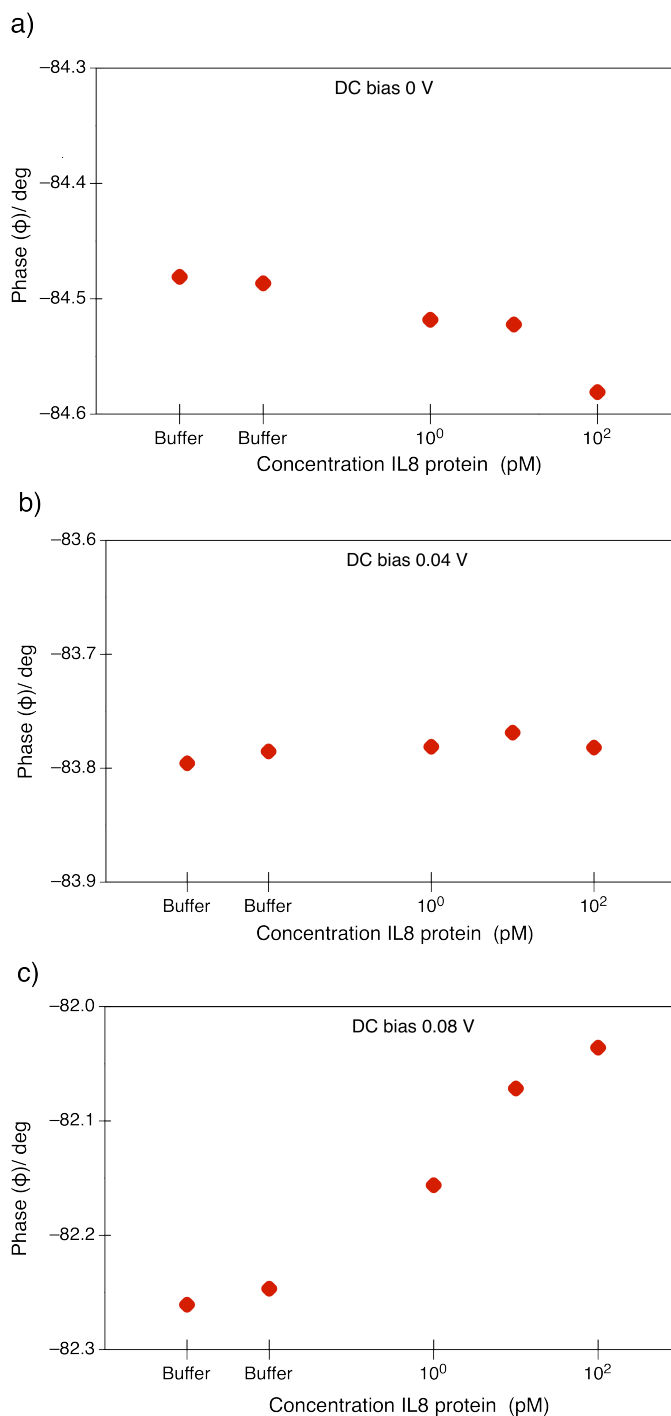


**Figure 6-14 Response of IL8 biosensor to IL8 protein on a surface subjected to different potentials.**

Figure shows the phase response of a SAM derivatised gold surface immobilised with 10  $\mu\text{g}/\text{mL}$  Adhiron IL8 binder at different concentrations of IL8 protein. The measurements were taken by subjecting the surface to different DC biases against reference electrode Ag / AgCl at 0.1 Hz. The DC biases applied were (a) 0 V, (b) 0.04 V and (c) 0.08 V.

## Conclusion

This chapter aimed at increasing the sensitivity of the label-free impedimetric biosensor by tuning the DC potential applied to the surface. Initially the effect of DC bias on the surface of SAM was studied by applying different DC biases (0-0.4 V) to the surface vs. reference Ag/AgCl. It was demonstrated that the voltage was able to induce defects in the SAM surface and the defects were increasing as the applied DC voltage increased. This was monitored with the change in phase in the lower frequency range (0.1-0.3 Hz) that corresponded to the change in the dielectric properties of the interfacial layer whereas no significant change was observed in the higher frequency range (100 kHz - 50 mHz), indicating that the solution resistance was not affected by the applied DC bias.

It was more likely that a higher DC bias changed the conformation of the flexible -COOH-PEG chain, grafted on to the hydrophobic alkyl chain and induced defects in the SAM that facilitated the penetration of water and ion molecules through the SAM. It has been observed that the change in the insulating properties of a SAM depends on its length as well as the terminal functional group (-X) attached to the SAM. More hydrophilic terminal group (-COOH) instead of hydrophobic group (-CH<sub>3</sub>) leads to increased permeability of ions through the SAMs (Boubour and Lennox, 2000b).

The reversibility of the defects on the surface was observed for a range of DC potentials (0-0.4 V), which indicated that the restoration of the surface was possible after subjecting the surface to different voltages. Also the defects could be induced without causing any permanent change to the surface. The reversibility of the effect needs to be studied with respect to time so as to know the time frame in which the sensor can be more effective.

Initially to investigate the change in sensitivity of the sensor by increasing the DC potential induced defects, Adhiron myc binder 2 based sensor was used. It was observed that the sensitivity of the surface immobilised with Adhiron myc binder 2 to detect the monoclonal anti-myc tag antibodies was increasing as the potential was increased in a defined range of DC potentials (0 V to 0.15 V). In case of Adhiron IL8 based biosensor, although the increase in sensitivity observed with the increase in DC potential was promising but it also showed inter sensor variations between different sensor surfaces subjected to same DC bias. This could be attributed to various factors involved like the variability of the immobilisation of SAM on the gold surface, immobilisation of the Adhiron based binders on the surface, changes taking place on the surface with time as there were various steps involved in between (Bart *et al.*, 2005). The inter sensor variations involving various factors was

an important limitation in the study of DC bias induced sensitivity and needed further investigation.

Using the same sensor surface (subjected to different DC biases) for checking the change in sensitivity of the Adhiron IL8 binder based sensor, was not successful. The DC potentials applied to the surface could be affecting the conformation of the biological recognition layer. Although the stability of the SAM subjected to subsequent DC potentials was established but the effect of different DC potentials on the biological layer formed by Adhiron IL8 binder has not been studied in details. The conformational stability of Adhiron IL8 binder on applying different potentials needs to be investigated in more details.

## Chapter 7. Conclusions

Biosensors have been an important tool of diagnostics. The performance of a biosensor is strongly dependent on the biological layer that interacts with the analyte or the biomarkers and the transducer surface that converts the detection of binding into an electronic signal. Despite this the majority of the work aimed at improving the detection sensitivity, speed and reduction of signal / noise ratio has been done on the electrical part of the biosensors. But the role of the biological recognition molecules is equally important, as they are the ones that bind the analyte molecules. The affinity of the biological molecules to the analytes, specificity in binding, the stability of the biological recognition molecules affect the over all performance of the biosensor. Thus, the aim of this project was to study alternative biomolecular recognition molecules other than the commonly used antibodies, and to investigate the performance of label-free biosensors based on such anti-body mimetics.

To achieve this aim amongst the various biological recognition molecules available like antibodies, nucleic acid aptamers, molecular imprinted polymers etc, a class of biological recognition molecules was selected called peptide aptamers. Peptide aptamers are defined as ‘combinatorial protein molecule consisting of a variable peptidic sequence inserted within a constant scaffold protein’ (Baines, 2006). Peptide aptamers unlike their naturally occurring antibodies counterparts are smaller and structurally less complex, devoid of disulphide bonds and post-translational modifications. Such properties exhibited by peptide aptamers make them suitable for the *in vitro* production.

A novel peptide scaffold based on phytocystatin protein, was developed by the McPherson group at the Astbury Centre for Structural Molecular Biology at the University of Leeds. This newly developed peptide scaffold is called Adhiron. Adhiron were designed according to a consensus protein design strategy, which involves designing the protein on the basis of sequence alignment of a number of other proteins that fold into the same structure. This strategy has been successful in developing proteins with more stability as compared to the other counterparts. Adhiron consists of a four-strand anti-parallel  $\beta$ -sheet core and a central helix. It has two loops, one positioned between the first and the second b-strand, and the second between third and fourth b-strand.

An Adhiron-based set of binders against the myc epitope (EQKLISEEDL) was selected using a phage display library by the Bioscreening Technology Group (BSTG), University of Leeds. Ten Adhiron-based myc binders against the anti-myc tag antibodies were initially selected for this project to develop the biological

recognition layer of an impedimetric biosensor. All the binders were successfully cloned into pET 11(a) expression vector. Expression and purification of Adhiron-based binders was optimised and the binders were expressed at high yields. The yield of each purified myc binders in soluble form ranged from 4-8 mg and the molecular weight of the binders ranged from 11-14 kDa. The different molecular weight of binders was attributed to difference in the amino acid sequences in the variable regions of the Adhiron scaffold. Additional bands were observed at a higher molecular weight (24-25 kDa) that corresponded to dimerised Adhiron myc binders. The formation of dimers can hamper the use of Adhiron myc binders in detection assays. To eliminate dimerised Adhiron myc binders contamination, the expressed binders were purified using standard techniques. The purified and characterised Adhiron myc binders were soluble proteins with well defined structural properties ( $\alpha$ -helical and  $\beta$ -sheet structures) and high thermal stability. The melting temperature of the Adhiron scaffold and Adhiron binder 2 were 101 °C and 85 °C, respectively. The high thermal stability of Adhiron scaffold can be attributed to the consensus protein design of the scaffold. On the basis of ELISA, done against the monoclonal anti-myc tag antibodies, Adhiron myc binder 2 was selected to form the biological recognition layer for the detection of monoclonal anti-myc tag antibodies on an impedimetric biosensor. The empty Adhiron scaffold did not show any binding to monoclonal anti-myc tag antibodies. The difference in binding efficiency of the Adhiron myc binders was attributed to the variability in amino acid sequences in the three variable loops. Adhiron myc binder 2 contained the sequences similar to myc epitope at the N-terminus of the scaffold. This provides more flexibility to Adhiron myc binder 2 to bind the monoclonal anti myc tag antibodies. Although the N-terminus of Adhiron myc binder 1 as well as 11 were also showing similarity to myc epitope sequences they did not show binding to monoclonal anti-myc tag antibodies. This reflects the possibility of involvement of other loops and the Adhiron scaffold in the binding. SPR results showed that the  $K_D$  value of Adhiron myc binder 2 was  $140 \pm 10$  nM with a high dissociation rate.

The Adhiron myc binder 2 was then used for forming the biological layer of label-free impedimetric biosensor. A self assembled monolayer (SH-(CH<sub>2</sub>)<sub>11</sub>-(EG)<sub>3</sub>-OCH<sub>2</sub>-COOH) was formed on a gold surface. It was observed that the formation of SAM decreased the electron transfer and formed a highly insulating SAM layer. The impedimetric measurements were based on the phase change observed for the electrochemical impedance at 0.1 Hz when a DC bias was applied to the working electrode surface.

The PEG-SAM formed on the gold surface showed instability when incubated in 10 mM PBS (pH 7.2). This could be attributed to the reorganisation of the polyethylene chain as it is conformationally more flexible than the hydrocarbon

chain on which it is grafted. A methodology to stabilise the sensor before use was developed by the Bioelectronics Group at the university of Leeds. The methodology used potential tuning of the surface by applying a 0.2 V DC bias to the working electrode against the reference electrode Ag/AgCl over 15 cycles and demonstrated to lead to highly stable sensor surface.

The Adhiron myc binder 2 was grafted onto the SAM *via* amine coupling. The interface formed by Adhiron myc binder 2 on the SAM was a highly insulating layer that was important in formation of a sensitive impedimetric biosensor. The lowest concentration of monoclonal anti-myc tag antibodies detected after immobilisation of Adhiron myc binder 2 on the surface was 0.1 nM and the detection was done over 3 orders of magnitude. Different concentrations of the monoclonal anti-myc tag antibodies, over a range of 0.1-200 nM, were successfully detected. The fabricated Adhiron myc binder 2 based impedimetric sensor showed high sensitivity to the monoclonal anti myc tag antibodies. Due to high  $K_D$  of binding of Adhiron myc binder 2 to monoclonal anti-myc tag antibodies, the detection of binding was observed at a high concentration of 200 nM whereas with the highly sensitive impedimetric biosensor, concentration of monoclonal anti-myc tag antibodies as low as 0.1 nM was detected.

A cumulative method of adding different concentrations of monoclonal anti-myc tag antibodies to the sensor surface was used to avoid any disturbance on the interfacial surface caused due to rinsing of the surface in between the measurements. The response was lower as compared to the previous methodology. This could be because the number of binding sites were decreasing with each new concentration of monoclonal anti-myc tag antibodies being added.

One of the limitations of the sensor surface was the inter-sensor variation observed during the measurement of response on different sensors. The behaviour of inter-sensor variation was observed by other groups as well (Berggren, 1998). The variations in response on different sensors could be due to difference in SAM formation, density of adhiron myc binders on the surface, handling errors etc. The unpredictable orientation of Adhiron myc binder 2 on the surface (*via* amine coupling) could lead to unavailability of the monoclonal antibody binding site.

The change in sensitivity on applying different DC biases to the surface against the reference electrode was investigated. Finite DC biases could be used to induce defects in the SAM. These defects were reversible and were attributed to the conformational changes in the flexible acidic chain attached to the hydrophobic alkyl chain of SAM. The effect of applying different DC biases on the sensitivity of the biosensor was investigated using the Adhiron myc binder 2 as the biological recognition molecule to detect the monoclonal anti-myc tag antibodies. The

sensitivity of the Adhiron myc binder biosensor increased as increasing DC biases were applied to the surface.

The change in sensitivity was further investigated in a clinically relevant biosensor based on Adhiron IL8 binder for detection of IL8 protein, used as a biomarker for diagnosis of various clinical conditions. Initially, IL8 sensors showed increased sensitivity on sensor surfaces subjected to higher DC bias. But significant inter-sensor variations were observed between independently prepared sensor surfaces subjected to the same DC bias. This requires to investigate more into the variations observed at the surface which might be due to effect of different DC biases on the conformational of the biological recognition layer.

## References

- Abnova. c2014. *Types of ELISA methods*. [Online]. [Accessed 22 September 2013]. Available from:  
<http://www.abnova.com/support/resources.asp?switchfunctionid={70196CA1-59B1-40D0-8394-19F533EB108F}>
- Agonafer, D.D., Chainani, E., Oruc, M.E., Lee, K.S. and Shannon, M.A. 2012. Study of insulating properties of alkanethiol self-assembled monolayers formed under prolonged incubation using electrochemical impedance spectroscopy. *Journal of Nanotechnology in Engineering and Medicine*. **3**(3), pp.031006(1-6).
- Anderson, L. and Seilhamer, J. 1997. A comparison of selected mRNA and protein abundances in human liver. *Electrophoresis*. **18**(3-4), pp.533-7.
- Andersson, M., Rönmark, J., Areström, I. and Nygren, P. Å. 2003. Inclusion of a non-immunoglobulin binding protein in two-site ELISA for quantification of human serum proteins without interference by heterophilic serum antibodies. *Journal of Immunological Methods*. **283**(1-2), pp.225-234.
- Anker, J. N., Hall, W. P., Lyandres, O., Shah, N. C., Zhao, J. and Van Duyne, R. P. 2008. Biosensing with plasmonic nanosensors. *Nature Materials*. **7**(6), pp.442-53.
- Arntfield, S. D. and Murray, E. D. 1981. The influence of processing parameters on food protein functionality I. Differential scanning calorimetry as an indicator of protein denaturation. *Canadian Institute of Food Science and Technology Journal*. **14**(4), pp.289-294.
- Arntz, Y., Seelig, J. D., Lang, H. P., Zhang, J., Hunziker, P., Ramseyer, J. P., Meyer, E., Hegner, M. and Gerber, C. 2003. Label-free protein assay based on a nanomechanical cantilever array. *Nanotechnology*. **14**(1), pp.86-90.
- Arshady, R. and Mosbach, K. 1981. Synthesis of substrate-selective polymers by host-guest polymerization. *Die Makromolekulare Chemie*. **182**(2), pp.687-692.
- Baggiolini, M. and Clark-Lewis, I. 1992. Interleukin-8, a chemotactic and inflammatory cytokine. *Federation of European Biochemical Societies Letters*. **307**(1), pp.97-101.
- Bain, C. D., Troughton, E. B., Tao, Y. T., Evall, J., Whitesides, G. M. and Nuzzo, R. G. 1989. Formation of monolayer films by the spontaneous assembly of organic thiols from solution onto gold. *Journal of the American Chemical Society*. **111**(1), pp.321-335.
- Barbas, C. F., Burton, D. R., Scott, J. K. and Silverman, G. J. 2001. *Phage display: a laboratory manual*. New York: Cold Spring Harbor Laboratory Press.

- Bart, M., Stigter, E. C., Stapert, H. R., de Jong, G. J. and van Bennekom, W. P. 2005. On the response of a label-free interferon-gamma immunosensor utilizing electrochemical impedance spectroscopy. *Biosensors & Bioelectronics*. **21**(1), pp.49-59.
- Bartlett, J. M. and Stirling, D. 2003. A short history of the polymerase chain reaction. *Methods in Molecular Biology*. **226**, pp.3-6.
- Berg, J. M., Tymoczko, J. L. and Stryer, L. 2002. *Biochemistry*. 5th ed. New York: W. H. Freeman.
- Berger, D. 1999. A brief history of medical diagnosis and the birth of the clinical laboratory. Part 1-Ancient times through the 19th century. *MLO Med Lab Obs*. **31**(7), pp.28-30.
- Berggren, C., Bjarnason, B. and Johansson, G. 2001. Capacitive Biosensors. *Electroanalysis*. **13**(3), pp.173-180.
- Berggren, C. and Johansson, G. 1997. Capacitance measurements of antibody-antigen interactions in a flow system. *Analytical Chemistry*. **69**(18), pp.3651-3657.
- Bergveld, P. 1991. A critical evaluation of direct electrical protein detection methods. *Biosensors and Bioelectronics*. **6**(1), pp.55-72.
- Berney, H., Alderman, J., Lane, W. and Collins, J. K. 1997. A differential capacitive biosensor using polyethylene glycol to overlay the biolayer. *Sensors and Actuators B: Chemical*. **44**(1), pp.578-584.
- Béron, F., Carignan, L., P., Ménard, D. and Yelon, A. 2010. *Extracting individual properties from global behaviour: first-order reversal curve method applied to magnetic nanowire arrays*. [Online]. [Accessed 7 November 2013]. Available from: <http://www.intechopen.com/books/electrodeposited-nanowires-and-their-applications/>
- Bhadeshia, H. 2002. Differential scanning calorimetry. *Materials Science & Metallurgy University of Cambridge*. [Online]. [Accessed 2013]. Available from: [http://www.uzaktanegitimplatformu.com/UEP/uep\\_ylisans/ey2/ey2\\_download/DSC%20Thermal2.pdf](http://www.uzaktanegitimplatformu.com/UEP/uep_ylisans/ey2/ey2_download/DSC%20Thermal2.pdf)
- Bigdeli, S., Talasaz, A. H., Stahl, P., Persson, H. H., Ronaghi, M., Davis, R. W. and Nemat-Gorgani, M. 2008. Conformational flexibility of a model protein upon immobilization on self-assembled monolayers. *Biotechnology & Bioengineering*. **100**(1), pp.19-27.
- Binz, H. K., Amstutz, P., Kohl, A., Stumpp, M. T., Briand, C., Forrer, P., Grutter, M. G. and Pluckthun, A. 2004. High-affinity binders selected from designed ankyrin repeat protein libraries. *Nature Biotechnology*. **22**(5), pp.575-82.
- Binz, H. K., Amstutz, P. and Pluckthun, A. 2005. Engineering novel binding proteins from nonimmunoglobulin domains. *Nature Biotechnology*. **23**(10), pp.1257-68.

- Biocompare. 2012. *SPR Sensitivity and Detection Limit*. [Online]. [Accessed August 2013]. Available from: <http://www.biocompare.com/Application-Notes/118383-SPR-Sensitivity-and-Detection-Limit/>
- Boubour, E. and Lennox, R. B. 2000a. Insulating properties of self-assembled monolayers monitored by impedance spectroscopy. *Langmuir*. **16**(9), pp.4222-4228.
- Boubour, E. and Lennox, R. B. 2000b. Potential-induced defects in n-alkanethiol self-assembled monolayers monitored by impedance spectroscopy. *The Journal of Physical Chemistry B*. **104**(38), pp.9004-9010.
- Bradbury, A., Velappan, N., Verzillo, V., Ovecká, M., Chasteen, L., Sblattero, D., Marzari, R., Lou, J., Siegel, R. and Pavlik, P. 2003. Antibodies in proteomics I: generating antibodies. *Trends in Biotechnology*. **21**(6), pp.275-81.
- Brennan, C., Christianson, K., Surowy, T. and Mandeckí, W. 1994. Modulation of enzyme activity by antibody binding to an alkaline phosphatase-epitope hybrid protein. *Protein Engineering Design and Selection*. **7**(4), pp.509-14.
- Brown, T. 2001. *Gene cloning and DNA analysis: an introduction*. 4th ed. New Jersey: John Wiley & Sons.
- Bruylants, G., Wouters, J. and Michaux, C. 2005. Differential scanning calorimetry in life science: thermodynamics, stability, molecular recognition and application in drug design. *Current Medicinal Chemistry*. **12**(17), pp.2011-2020.
- Brzin, J., Kopitar, M., Turk, V. and Machleidt, W. 1983. Protein inhibitors of cysteine proteinases. I. Isolation and characterization of stefin, a cytosolic protein inhibitor of cysteine proteinases from human polymorphonuclear granulocytes. *Hoppe-Seyler's Zeitschrift für physiologische Chemie*. **364**(2), pp.1475-1480.
- Cai, D., Ren, L., Zhao, H., Xu, C., Zhang, L., Yu, Y., Wang, H., Lan, Y., Roberts, M. F., Chuang, J. H., Naughton, M. J., Ren, Z. and Chiles, T. C. 2010. A molecular-imprint nanosensor for ultrasensitive detection of proteins. *Nature Nanotechnology*. **5**(8), pp.597-601.
- Cai, H., Lee, T. M. H. and Hsing, I. M. 2006. Label-free protein recognition using an aptamer-based impedance measurement assay. *Sensors and Actuators B: Chemical*. **114**(1), pp.433-437.
- Calabrò, P., Golia, E. and Yeh, E. T. 2009. CRP and the risk of atherosclerotic events. *Seminars in Immunopathology*. **31**(1), pp.79-94.
- Canfield, R. E., O'Connor, J. F., Birken, S., Krichevsky, A. and Wilcox, A. J. 1987. Development of an assay for a biomarker of pregnancy and early fetal loss. *Environmental Health Perspective*. **74**, pp.57-66.
- Carnes, E. and Wilkins, E. 2005. The development of a new, rapid, amperometric immunosensor for the detection of low concentrations of bacteria part I:

- design of the detection system and applications. *American Journal of Applied Sciences*. **2**(3), pp.597-606.
- Cass, A. E. G., Davis, G., Francis, G. D., Hill, H. A. O., Aston, W. J., Higgins, I. J., Plotkin, E. V., Scott, L. D. L. and Turner, A. P. F. 1984. Ferrocene-mediated enzyme electrode for amperometric determination of glucose. *Analytical Chemistry*. **56**(4), pp.667-671.
- Castro, C. and Gourley, M. 2010. Diagnostic testing and interpretation of tests for autoimmunity. *Journal of Allergy and Clinical Immunology*. **125**(2 Suppl 2), pp.S238-47.
- Cete, S., Yasar, A. and Arslan, F. 2006. An amperometric biosensor for uric acid determination prepared from uricase immobilized in polypyrrole film. *Artificial cells, blood substitutes, and immobilization biotechnology*. **34**(3), pp.367-80.
- Chakraborty, R., Lidsky, A. S., Daiger, S. P., Guttler, F., Sullivan, S., Dilella, A. G. and Woo, S. L. 1987. Polymorphic DNA haplotypes at the human phenylalanine hydroxylase locus and their relationship with phenylketonuria. *Human Genetics*. **76**(1), pp.40-6.
- Chaniotakis, N. A. 2004. Enzyme stabilization strategies based on electrolytes and polyelectrolytes for biosensor applications. *Analytical and Bioanalytical Chemistry*. **378**(1), pp.89-95.
- Chapman, R. G., Ostuni, E., Yan, L. and Whitesides, G. M. 2000. Preparation of mixed self-assembled monolayers (SAMs) that resist adsorption of proteins using the reaction of amines with a SAM that presents interchain carboxylic anhydride groups. *Langmuir*. **16**(17), pp.6927-6936.
- Chaste, J., Eichler, A., Moser, J., Ceballos, G., Rurali, R. and Bachtold, A. 2012. A nanomechanical mass sensor with yoctogram resolution. *Nature Nanotechnology*. **7**(5), pp.301-304.
- Chia-en, A. C., Chen, W. and Gilson, M. K. 2007. Ligand configurational entropy and protein binding. *Proceedings of the National Academy of Sciences*. **104**(5), pp.1534-1539.
- Chôma, C. T. 2006. *Characterizing Protein Stability by DSC*. [Online]. [Accessed 15 October 2013]. Available from: <http://lnbio.cnpem.br/spectroscopyandcalorimetry/files/2012/08/DSCnote3.pdf>
- Chou, P. C., Rick, J. and Chou, T. C. 2005. C-reactive protein thin-film molecularly imprinted polymers formed using a micro-contact approach. *Analytica Chimica Acta*. **542**(1), pp.20-25.
- Chu, T. C., Twu, K. Y., Ellington, A. D. and Levy, M. 2006. Aptamer mediated siRNA delivery. *Nucleic Acids Research*. **34**(10), pp.e73.

- Clark, L. C. and Lyons, C. 1962. Electrode systems for continuous monitoring in cardiovascular surgery. *Annals of the New York Academy of sciences*. **102**(1), pp.29-45.
- Colas, P. 2008. The eleven-year switch of peptide aptamers. *Journal of Biology*. **7**(1), pp.2.1-2.5
- Colas, P., Cohen, B., Jessen, T., Grishina, I., McCoy, J. and Brent, R. 1996. Genetic selection of peptide aptamers that recognize and inhibit cyclin-dependent kinase 2. *Nature*. **380**(6574), pp.548-50.
- Conroy, P. J., Hearty, S., Leonard, P. and O'Kennedy, R. J. 2009. Antibody production, design and use for biosensor-based applications. *Seminars in Cell & Developmental Biology*. **20**(1), pp.10-26.
- Cooper, A., Nutley, M. A. and Wadood, A. 2000. Differential scanning microcalorimetry. *Protein-ligand interactions: hydrodynamics and calorimetry*. pp.287-318.
- Cox, W. G. and Singer, V. L. 2004. Fluorescent DNA hybridization probe preparation using amine modification and reactive dye coupling. *Biotechniques*. **36**(1), pp.114-22.
- Cull, M. G., Miller, J. F. and Schatz, P. J. 1992. Screening for receptor ligands using large libraries of peptides linked to the C terminus of the lac repressor. *Proceedings of the National Academy of Sciences, U S A*. **89**(5), pp.1865-9.
- Dannenberger, O., Weiss, K., Himmel, H. J., Jäger, B., Buck, M. and Wöll, C. 1997. An orientation analysis of differently endgroup-functionalised alkanethiols adsorbed on Au substrates. *Thin Solid Films*. **307**(1), pp.183-191.
- Datar, R., Kim, S., Jeon, S., Hesketh, P., Manalis, S., Boisen, A. and Thundat, T. 2009. Cantilever sensors: nanomechanical tools for diagnostics. *MRS Bulletin*. **34**(06), pp.449-454.
- Deka, J., Kuhlmann, J. and Muller, O. 1998. A domain within the tumor suppressor protein APC shows very similar biochemical properties as the microtubule-associated protein tau. *European Journal of Biochemistry*. **253**(3), pp.591-7.
- Dennis, M. S. and Lazarus, R. A. 1994a. Kunitz domain inhibitors of tissue factor-factor VIIa. I. Potent inhibitors selected from libraries by phage display. *Journal of Biological Chemistry*. **269**(35), pp.22129-36.
- Dennis, M. S. and Lazarus, R. A. 1994b. Kunitz domain inhibitors of tissue factor-factor VIIa. II. Potent and specific inhibitors by competitive phage selection. *Journal of Biological Chemistry*. **269**(35), pp.22137-22144.
- Dijkema, M., Kamp, B., Hoogvliet, J. C. and van Bennekom, W. P. 2001. Development of an electrochemical immunosensor for direct detection of interferon-gamma at the attomolar level. *Analytical Chemistry*. **73**(5), pp.901-907.

- Doi, N. and Yanagawa, H. 1999. Design of generic biosensors based on green fluorescent proteins with allosteric sites by directed evolution. *Federation of European Biochemical Societies Letters*. **453**(3), pp.305-307.
- Drew, E. c2011-2014. *Module 1.1: Start-up Genome Engineering*. [Online]. [Accessed 12 September 2013]. Available from: [http://ocw.mit.edu/courses/biological-engineering/20-109-laboratory-fundamentals-in-biological-engineering-fall-2007/labs/mod1\\_1/](http://ocw.mit.edu/courses/biological-engineering/20-109-laboratory-fundamentals-in-biological-engineering-fall-2007/labs/mod1_1/)
- Dubois, L. H. and Nuzzo, R. G. 1992. Synthesis, structure, and properties of model organic surfaces. *Annual Review of Physical Chemistry*. **43**(1), pp.437-463.
- Ellington, A. D. and Szostak, J. W. 1990. *In vitro* selection of RNA molecules that bind specific ligands. *Nature*. **346**(6287), pp.818-22.
- Evan, G. I., Lewis, G. K., Ramsay, G. and Bishop, J. M. 1985. Isolation of monoclonal antibodies specific for human c-myc proto-oncogene product. *Molecular & Cellular Biology*. **5**(12), pp.3610-6.
- Evans, D., Johnson, S., Laurenson, S., Davies, A. G., Ko Ferrigno, P. and Walti, C. 2008. Electrical protein detection in cell lysates using high-density peptide-aptamer microarrays. *Journal of Biology*. **7**(1), pp.3.1-3.11.
- Evans, S. D., Sharma, R. and Ulman, A. 1991. Contact angle stability: Reorganization of monolayer surfaces? *Langmuir*. **7**(1), pp.156-161.
- Feilmeier, B. J., Iseminger, G., Schroeder, D., Webber, H. and Phillips, G. J. 2000. Green fluorescent protein functions as a reporter for protein localization in *Escherichia coli*. *Journal of bacteriology*. **182**(14), pp.4068-4076.
- Ferlay, J., Steliarova-Foucher, E., Lortet-Tieulent, J., Rosso, S., Coebergh, J. W., Comber, H., Forman, D. and Bray, F. 2013. Cancer incidence and mortality patterns in Europe: estimates for 40 countries in 2012. *European Journal of Cancer*. **49**(6), pp.1374-403.
- Finklea, H. O., Snider, D. A., Fedyk, J., Sabatani, E., Gafni, Y. and Rubinstein, I. 1993. Characterization of octadecanethiol-coated gold electrodes as microarray electrodes by cyclic voltammetry and ac impedance spectroscopy. *Langmuir*. **9**(12), pp.3660-3667.
- FitzGerald, K. 2000. *In vitro* display technologies - new tools for drug discovery. *Drug Discovery Today*. **5**(6), pp.253-258.
- Frasca, V. c2014. *Differential scanning calorimetry*. [Online]. [Accessed 5 October 2013]. Available from: <http://www.huck.psu.edu/facilities/calorimetry-up/guides/dsc>
- Freitag, J. ed. 2012. *The diabetes epidemic and its impact on Europe*. [Online]. [Accessed 2013]. Available from: <http://www.oecd.org/els/health-systems/50080632.pdf> from Diabetesforum
- Fu, X., Gao, X., He, S., Huang, D., Zhang, P., Wang, X., Zhang, S., Dang, R., Yin, S. and Du, E. 2013. Design and selection of a camelid single-chain antibody

yeast two-hybrid library produced *de novo* for the cap protein of porcine circovirus type 2 (PCV2). *PLoS One*. **8**(3), pp.e56222.

- Fukuda, I., Kojoh, K., Tabata, N., Doi, N., Takashima, H., Miyamoto-Sato, E. and Yanagawa, H. 2006. *In vitro* evolution of single-chain antibodies using mRNA display. *Nucleic Acids Research*. **34**(19), pp.e127.
- Gamry. c2014. *Basics of Electrochemical Impedance Spectroscopy*. [Online]. [Accessed 2011]. Available from: <http://www.gamry.com/application-notes/basics-of-electrochemical-impedance-spectroscopy>
- Gebbert, A., Alvarez-Icaza, M., Stoecklein, W. and Schmid, R. D. 1992. Real-time monitoring of immunochemical interactions with a tantalum capacitance flow-through cell. *Analytical Chemistry*. **64**(9), pp.997-1003.
- Gilbert, J. C., DeFeo-Fraulini, T., Hutabarat, R. M., Horvath, C. J., Merlino, P. G., Marsh, H. N., Healy, J. M., Boufakhreddine, S., Holohan, T. V. and Schaub, R. G. 2007. First-in-human evaluation of anti von Willebrand factor therapeutic aptamer ARC1779 in healthy volunteers. *Circulation*. **116**(23), pp.2678-86.
- GE Healthcare 2011. *Biacore Sensor Surface Handbook*. [Online]. AB ed. [Accessed July 2013]. Available from: <https://www.biacore.com/lifesciences/products/Consumables/guide>
- Greenbaum, D., Colangelo, C., Williams, K. and Gerstein, M. 2003. Comparing protein abundance and mRNA expression levels on a genomic scale. *Genome Biology*. **4**(9), pp.e117.
- Greenfield, N. 2007. Using circular dichroism spectra to estimate protein secondary structure. *Nature Protocols*. **1**(6), pp.2876-2890.
- Gronewold, T. M. 2007. Surface acoustic wave sensors in the bioanalytical field: recent trends and challenges. *Analytica Chimica Acta*. **603**(2), pp.119-28.
- Gygi, S. P., Rochon, Y., Franza, B. R. and Aebersold, R. 1999. Correlation between protein and mRNA abundance in yeast. *Molecular Cell Biology*. **19**(3), pp.1720-30.
- Hanahan, D. 1983. Studies on transformation of *Escherichia coli* with plasmids. *Journal of Molecular Biology*. **166**(4), pp.557-580.
- Harada, K. and Frankel, A. D. 1995. Identification of two novel arginine binding DNAs. *EMBO J*. **14**(23), pp.5798-811.
- Harder, P., Grunze, M., Dahint, R., Whitesides, G. M. and Laibinis, P. E. 1998. Molecular conformation in oligo(ethylene glycol)-terminated self-assembled monolayers on gold and silver surfaces determines their ability to resist protein adsorption. *The Journal of Physical Chemistry B*. **102**(2), pp.426-436.
- Himmel, H. J., Weiss, K., Jäger, B., Dannenberger, O., Grunze, M. and Wöll, C. 1997. Ultrahigh vacuum study on the reactivity of organic surfaces

- terminated by OH and COOH groups prepared by self-assembly of functionalized alkanethiols on Au substrates. *Langmuir*. **13**(19), pp.4943-4947.
- Holst, G. and Grunwald, B. 2001. Luminescence lifetime imaging with transparent oxygen optodes. *Sensors and Actuators B: Chemical*. **74**(1), pp.78-90.
- Hoogenboom, H. R. and Chames, P. 2000. Natural and designer binding sites made by phage display technology. *Immunology Today*. **21**(8), pp.371-378.
- Hoogenboom, H. R., Griffiths, A. D., Johnson, K. S., Chiswell, D. J., Hudson, P. and Winter, G. 1991. Multi-subunit proteins on the surface of filamentous phage: methodologies for displaying antibody (Fab) heavy and light chains. *Nucleic Acids Research*. **19**(15), pp.4133-7.
- Huang, L., Reekmans, G., Saerens, D., Friedt, J. M., Frederix, F., Francis, L., Muyldermans, S., Campitelli, A. and Hoof, C. V. 2005. Prostate-specific antigen immunosensing based on mixed self-assembled monolayers, camel antibodies and colloidal gold enhanced sandwich assays. *Biosensors and Bioelectronics*. **21**(3), pp.483-490.
- Hulka, B. S. and Wilcosky, T. 1988. Biological markers in epidemiologic research. *Archives of Environmental Health*. **43**(2), pp.83-9.
- Hulko, M., Hospach, I., Krasteva, N. and Nelles, G. 2011. Cytochrome C biosensor—A model for gas sensing. *Sensors*. **11**(6), pp.5968-5980.
- Ihalainen, P., Pettersson, F., Pesonen, M., Viitala, T., Määttä, A., Österbacka, R. and Peltonen, J. 2014. An impedimetric study of DNA hybridization on paper-supported inkjet-printed gold electrodes. *Nanotechnology*. **25**(9), pp.094009.
- Iorio, M. V., Ferracin, M., Liu, C. G., Veronese, A., Spizzo, R., Sabbioni, S., Magri, E., Pedriali, M., Fabbri, M., Campiglio, M., Menard, S., Palazzo, J. P., Rosenberg, A., Musiani, P., Volinia, S., Nenci, I., Calin, G. A., Querzoli, P., Negrini, M. and Croce, C. M. 2005. MicroRNA gene expression deregulation in human breast cancer. *Cancer Research*. **65**(16), pp.7065-70.
- Jaenicke, R. 2000. Stability and stabilization of globular proteins in solution. *Journal of Biotechnology*. **79**(3), pp.193-203.
- James, E. A., Schmeltzer, K. and Ligler, F. S. 1996. Detection of endotoxin using an evanescent wave fiber-optic biosensor. *Applied Biochemistry & Biotechnology*. **60**(3), pp.189-202.
- Jayasena, S. D. 1999. Aptamers: an emerging class of molecules that rival antibodies in diagnostics. *Clinical Chemistry*. **45**(9), pp.1628-50.
- Jermutus, L., Honegger, A., Schwesinger, F., Hanes, J. and Pluckthun, A. 2001. Tailoring *in vitro* evolution for protein affinity or stability. *Proceedings of the National Academy of Sciences, USA*. **98**(1), pp.75-80.

- Johnson, A., Song, Q., Ko Ferrigno, P., Bueno, P. R. and Davis, J. J. 2012. Sensitive affimer and antibody based impedimetric label-free assays for C-reactive protein. *Analytical Chemistry*. **84**(15), pp.6553-6560.
- Kara, P., Meric, B. and Ozsoz, M. 2008. Application of impedimetric and voltammetric genosensor for detection of a biological warfare: anthrax. *Electroanalysis*. **20**(24), pp.2629-2634.
- Kelly, S. M., Jess, T. J. and Price, N. C. 2005. How to study proteins by circular dichroism. *Biochimica et Biophysica Acta (BBA) - Proteins and Proteomics*. **1751**(2), pp.119-139.
- Kimhi, O. and Bianco-Peled, H. 2007. Study of the interactions between protein-imprinted hydrogels and their templates. *Langmuir*. **23**(11), pp.6329-6335.
- Kindt, T. J., Goldsby, R. A., Osborne, B. A. and Kuby, J. 2007. *Kuby immunology*. 6 ed. London: Macmillan.
- Knappik, A., Ge, L., Honegger, A., Pack, P., Fischer, M., Wellnhöfer, G., Hoess, A., Wolle, J., Plückthun, A. and Virnekas, B. 2000. Fully synthetic human combinatorial antibody libraries (HuCAL) based on modular consensus frameworks and CDRs randomized with trinucleotides. *Journal of Molecular Biology*. **296**(1), pp.57-86.
- Kohl, A., Binz, H. K., Forrer, P., Stumpp, M. T., Plückthun, A. and Grütter, M. G. 2003. Designed to be stable: Crystal structure of a consensus ankyrin repeat protein. *Proceedings of the National Academy of Sciences*. **100**(4), pp.1700-1705.
- Köhler, G. and Milstein, C. 1975. Continuous cultures of fused cells secreting antibody of predefined specificity. *Nature*. **256**(5517), pp.495-7.
- Koide, A., Bailey, C. W., Huang, X. and Koide, S. 1998. The fibronectin type III domain as a scaffold for novel binding proteins. *Journal of Molecular Biology*. **284**(4), pp.1141-1151.
- Koivunen, E., Wang, B. and Ruoslahti, E. 1995. Phage libraries displaying cyclic peptides with different ring sizes: ligand specificities of the RGD-directed integrins. *Nature Biotechnology*. **13**(3), pp.265-70.
- Kondo, H., Abe, K., Emori, Y. and Arai, S. 1991. Gene organization of oryzacystatin-II, a new cystatin superfamily member of plant origin, is closely related to that of oryzacystatin-I but different from those of animal cystatins. *Federation of European Biochemical Societies Letters*. **278**(1), pp.87-90.
- Ladner, R. C., Guterman, S. K., Roberts, B. L., Markland, W., Ley, A. C. and Kent, R. B. 1993. *Directed evolution of novel binding proteins*. United States Patent: 5,223,409.
- Laemmli, U.K. 1970. Cleavage of Structural Proteins during the Assembly of the Head of Bacteriophage T4. *Nature*. **227**(5259), pp.680-685.

- Lai, R. Y., Plaxco, K. W. and Heeger, A. J. 2006. Aptamer-based electrochemical detection of picomolar platelet-derived growth factor directly in blood serum. *Analytical Chemistry*. **79**(1), pp.229-233.
- Laibinis, P. E., Whitesides, G. M., Allara, D. L., Tao, Y. T., Parikh, A. N. and Nuzzo, R. G. 1991. Comparison of the structures and wetting properties of self-assembled monolayers of n-alkanethiols on the coinage metal surfaces, copper, silver, and gold. *Journal of the American Chemical Society*. **113**(19), pp.7152-7167.
- Lee, S. C., Park, K., Han, J., Lee, J. J., Kim, H. J., Hong, S., Heu, W., Kim, Y. J., Ha, J. S., Lee, S. G., Cheong, H. K., Jeon, Y. H., Kim, D. and Kim, H. S. 2012. Design of a binding scaffold based on variable lymphocyte receptors of jawless vertebrates by module engineering. *Proceedings of the National Academy of Sciences, USA*. **109**(9), pp.3299-304.
- Lees, J. G., Miles, A. J., Wien, F. and Wallace, B. A. 2006. A reference database for circular dichroism spectroscopy covering fold and secondary structure space. *Bioinformatics*. **22**(16), pp.1955-1962.
- Legendre, D., Vucic, B., Hougardy, V., Girboux, A. L., Henrioul, C., Van Haute, J., Soumillion, P. and Fastrez, J. 2002. TEM-1 beta-lactamase as a scaffold for protein recognition and assay. *Protein Science*. **11**(6), pp.1506-18.
- Lehmann, M., Loch, C., Middendorf, A., Studer, D., Lassen, S. F., Pasamontes, L., van Loon, A. P. and Wyss, M. 2002. The consensus concept for thermostability engineering of proteins: further proof of concept. *Protein Engineering Design and Selection*. **15**(5), pp.403-11.
- Li, F. and Cui, H. 2013. A label-free electrochemiluminescence aptasensor for thrombin based on novel assembly strategy of oligonucleotide and luminol functionalized gold nanoparticles. *Biosensors & Bioelectronics*. **39**(1), pp.261-7.
- Love, J. C., Estroff, L. A., Kriebel, J. K., Nuzzo, R. G. and Whitesides, G. M. 2005. Self-assembled monolayers of thiolates on metals as a form of nanotechnology. *Chemical Reviews*. **105**(4), pp.1103-1170.
- Lowry, J. P. and O'Neill, R. D. 1992. Strategies for reducing ascorbate interference at glucose oxidase modified conducting organic salt electrodes. *Journal of Electroanalytical Chemistry*. **334**(1), pp.183-194.
- Lu, M., Beguin, F. and Frackowiak, E. 2013. *Supercapacitors: Materials, Systems and Applications*. [Online]. John Wiley & Sons. [Accessed 2013]. Available from: <http://books.google.co.uk/>
- Lu, Z., Murray, K. S., Van Cleave, V., LaVallie, E. R., Stahl, M. L. and McCoy, J. M. 1995. Expression of thioredoxin random peptide libraries on the Escherichia coli cell surface as functional fusions to flagellin: a system designed for exploring protein-protein interactions. *Nature Biotechnology*. **13**(4), pp.366-72.

- Lupold, S. E., Hicke, B. J., Lin, Y. and Coffey, D. S. 2002. Identification and characterization of nuclease-stabilized RNA molecules that bind human prostate cancer cells via the prostate-specific membrane antigen. *Cancer Research*. **62**(14), pp.4029-33.
- Main, E. R., Jackson, S. E. and Regan, L. 2003. The folding and design of repeat proteins: reaching a consensus. *Current Opinion in Structural Biology*. **13**(4), pp.482-9.
- Malhotra, R., Patel, V., Vaque, J. P., Gutkind, J. S. and Rusling, J. F. 2010. Ultrasensitive electrochemical immunosensor for oral cancer biomarker IL-6 using carbon nanotube forest electrodes and multilabel amplification. *Analytical Chemistry*. **82**(8), pp.3118-23.
- Malon, A., Vigassy, T., Bakker, E. and Pretsch, E. 2006. Potentiometry at trace levels in confined samples: ion-selective electrodes with subfemtomole detection limits. *Journal of the American Chemical Society*. **128**(25), pp.8154-8155.
- Mann, A. P., Somasunderam, A., Nieves-Alicea, R., Li, X., Hu, A., Sood, A. K., Ferrari, M., Gorenstein, D. G. and Tanaka, T. 2010. Identification of thioaptamer ligand against E-selectin: potential application for inflamed vasculature targeting. *PLoS One*. **5**(9).
- Markland, W., Ley, A. C., Lee, S. W. and Ladner, R. C. 1996. Iterative optimization of high-affinity proteases inhibitors using phage display. 1. Plasmin. *Biochemistry*. **35**(24), pp.8045-57.
- Marquette, C. A., Lawrence, M. F. and Blum, L. J. 2006. DNA covalent immobilization onto screen-printed electrode networks for direct label-free hybridization detection of p53 sequences. *Analytical Chemistry*. **78**(3), pp.959-964.
- Marvin, J. S. and Hellinga, H. W. 1998. Engineering biosensors by introducing fluorescent allosteric signal transducers: construction of a novel glucose sensor. *Journal of the American Chemical Society*. **120**(1), pp.7-11.
- Mendoza, S. M., Arfaoui, I., Zanarini, S., Paolucci, F. and Rudolf, P. 2007. Improvements in the characterization of the crystalline structure of acid-terminated alkanethiol self-assembled monolayers on Au (111). *Langmuir*. **23**(2), pp.582-588.
- Microbewiki. 2010. *The Role of Antivirals in Influenza Treatment and Prevention*. [Online]. [Accessed 15 September 2013]. Available from: [https://microbewiki.kenyon.edu/index.php/The\\_Role\\_of\\_Antivirals\\_in\\_Influenza\\_Treatment\\_and\\_Prevention](https://microbewiki.kenyon.edu/index.php/The_Role_of_Antivirals_in_Influenza_Treatment_and_Prevention)
- Mizuguchi, H., Nakatsuji, M., Fujiwara, S., Takagi, M. and Imanaka, T. 1999. Characterization and application to hot start PCR of neutralizing monoclonal antibodies against KOD DNA polymerase. *Journal of Biochemistry*. **126**(4), pp.762-768.

- Moreno-Bondi, M. C., Wolfbeis, O. S., Leiner, M. J. and Schaffar, B. P. 1990. Oxygen optrode for use in a fiber-optic glucose biosensor. *Analytical Chemistry*. **62**(21), pp.2377-80.
- Mosavi, L. K., Cammett, T. J., Desrosiers, D. C. and Peng, Z. Y. 2004. The ankyrin repeat as molecular architecture for protein recognition. *Protein Science*. **13**(6), pp.1435-1448.
- Mrksich, M. and Whitesides G. M. 1997. Using self-assembled monolayers that present oligo(ethylene glycol) groups to control the interactions of proteins with surfaces. *American Chemical Society*. **680**, pp.361-373.
- Muyldermans, S. 2001. Single domain camel antibodies: current status. *Journal of Biotechnology*. **74**(4), pp.277-302.
- Nichols, M., Townsend, N., Luengo-Fernandez, R., Leal, J., Gray, A., Scarborough, P. and Rayner, M. 2012. European cardiovascular disease statistics 2012. *European Heart Network, Brussels, European Society of Cardiology, Sophia Antipolis*.
- Nilsson, B., Moks, T., Jansson, B., Abrahmsen, L., Elmlblad, A., Holmgren, E., Henrichson, C., Jones, T. A. and Uhlen, M. 1987. A synthetic IgG-binding domain based on staphylococcal protein A. *Protein Engineering Design and Selection*. **1**(2), pp.107-13.
- Nixon, A. E. and Wood, C. R. 2006. Engineered protein inhibitors of proteases. *Current Opinion in Drug Discovery & Development*. **9**(2), pp.261-8.
- Nord, K., Gunneriusson, E., Ringdahl, J., Stahl, S., Uhlen, M. and Nygren, P. A. 1997. Binding proteins selected from combinatorial libraries of an alpha-helical bacterial receptor domain. *Nature Biotechnology*. **15**(8), pp.772-7.
- Nord, K., Nilsson, J., Nilsson, B., Uhlen, M. and Nygren, P. A. 1995. A combinatorial library of an alpha-helical bacterial receptor domain. *Protein Engineering Design and Selection*. **8**(6), pp.601-8.
- Nuzzo, R. G. and Allara, D. L. 1983. Adsorption of bifunctional organic disulfides on gold surfaces. *Journal of the American Chemical Society*. **105**(13), pp.4481-4483.
- Orkin, S. H., Markham, A. F. and Kazazian Jr, H. H. 1983. Direct detection of the common Mediterranean beta-thalassemia gene with synthetic DNA probes. An alternative approach for prenatal diagnosis. *Journal of Clinical Investigation*. **71**(3), pp.775-9.
- Ostuni, E., Chapman, R. G., Holmlin, R. E., Takayama, S. and Whitesides, G. M. 2001. A survey of structure-property relationships of surfaces that resist the adsorption of protein. *Langmuir*. **17**(18), pp.5605-5620.
- Ostuni, E., Yan, L. and Whitesides, G. M. 1999. The interaction of proteins and cells with self-assembled monolayers of alkanethiolates on gold and silver. *Colloids and Surfaces B: Biointerfaces*. **15**(1), pp.3-30.

- Ozdemir, M. S., Marczak, M., Bohets, H., Bonroy, K., Roymans, D., Stuyver, L., Vanhoutte, K., Pawlak, M. and Bakker, E. 2013. A label-free potentiometric sensor principle for the detection of antibody-antigen interactions. *Analytical Chemistry*. **85**(9), pp.4770-4776.
- Pace, C. N., Shirley, B. A., McNutt, M. and Gajiwala, K. 1996. Forces contributing to the conformational stability of proteins. *The FASEB Journal*. **10**(1), pp.75-83.
- Pace, C. N., Vajdos, F., Fee, L., Grimsley, G. and Gray, T. 1995. How to measure and predict the molar absorption coefficient of a protein. *Protein Science*. **4**(11), pp.2411-2423.
- Patel, D. J., Suri, A. K., Jiang, F., Jiang, L., Fan, P., Kumar, R. A. and Nonin, S. 1997. Structure, recognition and adaptive binding in RNA aptamer complexes. *Journal of Molecular Biology*. **272**(5), pp.645-64.
- Pauling, L., Itano, H. A., Singer, S. J. and Wells, I. C. 1949. Sick cell anemia a molecular disease. *Science*. **110**(2865), pp.543-8.
- Plaxco, K. W. and Soh, H. T. 2011. Switch-based biosensors: a new approach towards real-time, *in vivo* molecular detection. *Trends in Biotechnology*. **29**(1), pp.1-5.
- Porter, M. D., Bright, T. B., Allara, D. L. and Chidsey, C. E. D. 1987. Spontaneously organized molecular assemblies. 4. Structural characterization of n-alkyl thiol monolayers on gold by optical ellipsometry, infrared spectroscopy, and electrochemistry. *Journal of the American Chemical Society*. **109**(12), pp.3559-3568.
- Porter, T. L., Eastman, M. P., Macomber, C., Delinger, W. G. and Zhine, R. 2003. An embedded polymer piezoresistive microcantilever sensor. *Ultramicroscopy*. **97**(1-4), pp.365-369.
- Ramachandran, N., Larson, D. N., Stark, P. R., Hainsworth, E. and LaBaer, J. 2005. Emerging tools for real-time label-free detection of interactions on functional protein microarrays. *Federation of European Biochemical Societies Journal*. **272**(21), pp.5412-25.
- Rickert, J., Göpel, W., Beck, W., Jung, G. and Heiduschka, P. 1996. A 'mixed' self-assembled monolayer for an impedimetric immunosensor. *Biosensors and Bioelectronics*. **11**(8), pp.757-768.
- Roberts, R. W. 1999. Totally *in vitro* protein selection using mRNA-protein fusions and ribosome display. *Current Opinion in Chemical Biology*. **3**(3), pp.268-73.
- Safo, M. K. and Abraham, D. J. 2005. The enigma of the liganded hemoglobin end state: a novel quaternary structure of human carbonmonoxy hemoglobin. *Biochemistry*. **44**(23), pp.8347-59.

- Sahalov, H., O'Brien, B., Stebe, K. J., Hristova, K. and Searson, P. C. 2007. Influence of applied potential on the impedance of alkanethiol SAMs. *Langmuir*. **23**(19), pp.9681-9685.
- Schasfoort, R. B. M., Bergveld, P., Kooyman, R. P. H. and Greve, J. 1990. Possibilities and limitations of direct detection of protein charges by means of an immunological field-effect transistor. *Analytica Chimica Acta*. **238**, pp.323-329.
- Schlehuber, S., Beste, G. and Skerra, A. 2000. A novel type of receptor protein, based on the lipocalin scaffold, with specificity for digoxigenin. *Journal of Molecular Biology*. **297**(5), pp.1105-20.
- Schlehuber, S. and Skerra, A. 2005. Lipocalins in drug discovery: from natural ligand-binding proteins to "anticalins". *Drug Discovery Today*. **10**(1), pp.23-33.
- Schreiber, F. 2000. Structure and growth of self-assembling monolayers. *Progress in surface science*. **65**(5), pp.151-257.
- Schulze-Gahmen, U., De Bondt, H. L. and Kim, S. H. 1996. High-resolution crystal structures of human cyclin-dependent kinase 2 with and without ATP: bound waters and natural ligand as guides for inhibitor design. *Journal of Medicinal Chemistry*. **39**(23), pp.4540-4546.
- Shahzad, A., Knapp, M., Lang, I. and Kohler, G. Interleukin 8 (IL-8) - a universal biomarker? *International Archives of Medicine*. **3**, pp.e11.
- Sharma, H. and Mutharasan, R. 2013. Half antibody fragments improve biosensor sensitivity without loss of selectivity. *Analytical Chemistry*. **85**(4), pp.2472-2477.
- Shin Ae, K., Kyung Min, B., Kyujung, K., Sung Min, J., Kyungjae, M., Youngjin, O., Donghyun, K., Sung Guk, K., Michael, L. S. and Sung June, K. 2010. Surface-enhanced localized surface plasmon resonance biosensing of avian influenza DNA hybridization using subwavelength metallic nanoarrays. *Nanotechnology*. **21**(35), pp.355503.
- Shinoda, K. 1977. "Iceberg" formation and solubility. *The Journal of Physical Chemistry*. **81**(13), pp.1300-1302.
- Skerra, A. 2008. Alternative binding proteins: anticalins - harnessing the structural plasticity of the lipocalin ligand pocket to engineer novel binding activities. *Federation of European Biochemical Societies Journal*. **275**(11), pp.2677-83.
- Smith, G. P. 1985. Filamentous fusion phage: novel expression vectors that display cloned antigens on the virion surface. *Science*. **228**(4705), pp.1315-7.
- Song, Q., Stadler, L. K. J., Peng, J. and Ferrigno, P. K. 2011. Peptide Aptamer Microarrays: Bridging the bio-detector interface. *Faraday discussions*. **149**, pp.79-92.

- Sreerama, N. and Woody, R. W. 2000. Estimation of protein secondary structure from circular dichroism spectra: Comparison of CONTIN, SELCON, and CDSSTR methods with an expanded reference set. *Analytical Biochemistry*. **287**(2), pp.252-260.
- Studier, F. W. 2005. Protein production by auto-induction in high-density shaking cultures. *Protein Expression and Purification*. **41**(1), pp.207-234.
- Stumpp, M. T., Binz, H. K. and Amstutz, P. 2008. DARPinS: A new generation of protein therapeutics. *Drug Discovery Today*. **13**(15-16), pp.695-701.
- Taylor, R. F., Marenchic, I. G. and Cook, E. J. 1988. An acetylcholine receptor-based biosensor for the detection of cholinergic agents. *Analytica Chimica Acta*. **213**(0), pp.131-138.
- Taylor, R. F., Marenchic, I. G. and Spencer, R. H. 1991. Antibody- and receptor-based biosensors for detection and process control. *Analytica Chimica Acta*. **249**(1), pp.67-70.
- Tiede, C., Tang, A. A. S., Deacon, S. E., Mandal, U., Nettleship, J. E., Owen, R. L., George, S. E., Harrison, D. J., Owens, R. J., Tomlinson, D. C. and McPherson, M. J. 2014. Adhiron: a stable and versatile peptide display scaffold for molecular recognition applications. *Protein Engineering Design and Selection*. **27**(5), pp.145-155.
- Tlili, C., Korri-Youssoufi, H., Ponsonnet, L., Martelet, C. and Jaffrezic-Renault, N. J. 2005. Electrochemical impedance probing of DNA hybridisation on oligonucleotide-functionalised polypyrrole. *Talanta*. **68**(1), pp.131-137.
- Trettnak, W. and Wolfbeis, O. S. 1990. A fiberoptic cholesterol biosensor with an oxygen optrode as the transducer. *Analytical Biochemistry*. **184**(1), pp.124-7.
- Tuerk, C. and Gold, L. 1990. Systematic evolution of ligands by exponential enrichment: RNA ligands to bacteriophage T4 DNA polymerase. *Science*. **249**(4968), pp.505-10.
- Ulman, A. 1996. Formation and structure of self-assembled monolayers. *Chemical Reviews*. **96**(4), pp.1533-1554.
- Van Holde, K. E., Johnson, W. C. and Ho, P. S. 2006. *Principles of Physical Biochemistry*. 2nd ed. United States of America: Prentice hall.
- Vanderah, D. J., Arsenault, J., La, H., Gates, R. S., Silin, V., Meuse, C. W. and Valincius, G. 2003. Structural variations and ordering conditions for the self-assembled monolayers of HS(CH<sub>2</sub>CH<sub>2</sub>O)<sub>3</sub>-6CH<sub>3</sub>. *Langmuir*. **19**(9), pp.3752-3756.
- Vasapollo, G., Sole, R. D., Mergola, L., Lazzoi, M. R., Scardino, A., Scorrano, S. and Mele, G. 2011. Molecularly imprinted polymers: present and future prospective *International Journal of Molecular Sciences* **12**(9), pp.5908-5945.

Venter, J. C., Adams, M. D., Myers, E. W., Li, P. W., Mural, R. J., Sutton, G. G., Smith, H. O., Yandell, M., Evans, C. A., Holt, R. A., Gocayne, J. D., Amanatides, P., Ballew, R. M., Huson, D., H., Wortman, J. R., Zhang, Q., Kodira, C. D., Zheng, X. H., Chen, L., Skupski, M., Subramanian, G., Thomas, P. D., Zhang, J., Gabor Miklos, G. L., Nelson, C., Broder, S., Clark, A. G., Nadeau, J., McKusick, V. A., Zinder, N., Levine, A. J., Roberts, R. J., Simon, M., Slayman, C., Hunkapiller, M., Bolanos, R., Delcher, A., Dew, I., Fasulo, D., Flanigan, M., Florea, L., Halpern, A., Hannenhalli, S., Kravitz, S., Levy, S., Mobarry, C., Reinert, K., Remington, K., Abu-Threideh, J., Beasley, E., Biddick, K., Bonazzi, V., Brandon, R., Cargill, M., Chandramouliswaran, I., Charlab, R., Chaturvedi, K., Deng, Z., Di Francesco, V., Dunn, P., Eilbeck, K., Evangelista, C., Gabrielian, A. E., Gan, W., Ge, W., Gong, F., Gu, Z., Guan, P., Heiman, T. J., Higgins, M. E., Ji, R. R., Ke, Z., Ketchum, K. A., Lai, Z., Lei, Y., Li, Z., Li, J., Liang, Y., Lin, X., Lu, F., Merkulov, G. V., Milshina, N., Moore, H. M., Naik, A. K., Narayan, V. A., Neelam, B., Nuskern, D., Rusch, D. B., Salzberg, S., Shao, W., Shue, B., Sun, J., Wang, Z., Wang, A., Wang, X., Wang, J., Wei, M., Wides, R., Xiao, C., Yan, C., Yao, A., Ye, J., Zhan, M., Zhang, W., Zhang, H., Zhao, Q., Zheng, L., Zhong, F., Zhong, W., Zhu, S., Zhao, S., Gilbert, D., Baumhueter, S., Spier, G., Carter, C., Cravchik, A., Woodage, T., Ali, F., An, H., Awe, A., Baldwin, D., Baden, H., Barnstead, M., Barrow, I., Beeson, K., Busam, D., Carver, A., Center, A., Cheng, M. L., Curry, L., Danaher, S., Davenport, L., Desilets, R., Dietz, S., Dodson, K., Doup, L., Ferreira, S., Garg, N., Gluecksmann, A., Hart, B., Haynes, J., Haynes, C., Heiner, C., Hladun, S., Hostin, D., Houck, J., Howland, T., Ibegwam, C., Johnson, J., Kalush, F., Kline, L., Koduru, S., Love, A., Mann, F., May, D., McCawley, S., McIntosh, T., McMullen, I., Moy, M., Moy, L., Murphy, B., Nelson, K., Pfannkoch, C., Pratts, E., Puri, V., Qureshi, H., Reardon, M., Rodriguez, R., Rogers, Y. H., Romblad, D., Ruhfel, B., Scott, R., Sitter, C., Smallwood, M., Stewart, E., Strong, R., Suh, E., Thomas, R., Tint, N. N., Tse, S., Vech, C., Wang, G., Wetter, J., Williams, S., Williams, M., Windsor, S., Winn-Deen, E., Wolfe, K., Zaveri, J., Zaveri, K., Abril, J. F., Guigo, R., Campbell, M. J., Sjolander, K. V., Karlak, B., Kejariwal, A., Mi, H., Lazareva, B., Hatton, T., Narechania, A., Diemer, K., Muruganujan, A., Guo, N., Sato, S., Bafna, V., Istrail, S., Lippert, R., Schwartz, R., Walenz, B., Yoosheph, S., Allen, D., Basu, A., Baxendale, J., Blick, L., Caminha, M., Carnes-Stine, J., Caulk, P., Chiang, Y. H., Coyne, M., Dahlke, C., Mays, A., Dombroski, M., Donnelly, M., Ely, D., Esparham, S., Fosler, C., Gire, H., Glanowski, S., Glasser, K., Glodek, A., Gorokhov, M., Graham, K., Gropman, B., Harris, M., Heil, J., Henderson, S., Hoover, J., Jennings, D., Jordan, C., Jordan, J., Kasha, J., Kagan, L., Kraft, C., Levitsky, A., Lewis, M., Liu, X., Lopez, J., Ma, D., Majoros, W., McDaniel, J., Murphy, S., Newman, M., Nguyen, T., Nguyen, N., Nodell, M., Pan, S., Peck, J., Peterson, M., Rowe, W., Sanders, R., Scott, J., Simpson, M., Smith, T., Sprague, A., Stockwell, T., Turner, R., Venter, E., Wang, M., Wen, M., Wu, D., Wu, M., Xia, A., Zandieh, A. and Zhu, X. 2001. The sequence of the human genome. *Science*. **291**(5507), pp.1304-51.

Venton, D. L. and Gudipati, E. 1995. Entrapment of enzymes using organo-functionalized polysiloxane copolymers. *Biochimica et Biophysica Acta (BBA) - Protein Structure and Molecular Enzymology*. **1250**(2), pp.117-125.

- Voet, D. and Voet, J. G. 1995. *Biochemistry*. 2nd ed. New Jersey: John Wiley & Sons.
- Wahlberg, E., Lendel, C., Helgstrand, M., Allard, P., Dincbas-Renqvist, V., Hedqvist, A., Berglund, H., Nygren, P. Å. and Härd, T. 2003. An affibody in complex with a target protein: Structure and coupled folding. *Proceedings of the National Academy of Sciences*. **100**(6), pp.3185-3190.
- Wang, R. L. C., Kreuzer, H. J. and Grunze, M. 1997. Molecular conformation and solvation of oligo(ethylene glycol)-terminated self-assembled monolayers and their resistance to protein adsorption. *The Journal of Physical Chemistry B*. **101**(47), pp.9767-9773.
- Wassermann, A. and Bruck, C. 1906. Experimentelle Studien über die Wirkung von Tuberkelbacillen-Präparaten auf den tuberculös erkrankten Organismus. *Deutsche medizinische Wochenschrift*. **32**(12), pp.449-454.
- Weaver, J. C. and Chizmadzhev, Y. A. 1996. Theory of electroporation: a review. *Bioelectrochemistry and Bioenergetics*. **41**(2), pp.135-160.
- Whitesides, G. M., Kriebel, J. K. and Love, J. C. 2005. Molecular engineering of surfaces using self-assembled monolayers. *Science progress*. **88**, pp.17-48.
- Whiting, D. R., Guariguata, L., Weil, C. and Shaw, J. 2011. IDF diabetes atlas: global estimates of the prevalence of diabetes for 2011 and 2030. *Diabetes research and clinical practice*. **94**(3), pp.311-321.
- Whitmore, L. and Wallace, B. A. 2004. DICHROWEB, an online server for protein secondary structure analyses from circular dichroism spectroscopic data. *Nucleic Acids Research*. **32**(suppl 2), pp.W668-W673.
- Wilson, K. and Walker, J. M. 2000. *Practical biochemistry: Principles and techniques*. Cambridge University Press.
- Wolfwikis. (no date). *Chimeric DNA*. [Online]. [Accessed March 2013]. Available from: <http://wikis.lib.ncsu.edu/images/5/5f/ChimericDNA.gif>.
- Woodman, R., Yeh, J. T. H., Laurenson, S. and Ferrigno, P. K. 2005. Design and validation of a neutral protein scaffold for the presentation of peptide aptamers. *Journal of Molecular Biology*. **352**(5), pp.1118-1133.
- Wörn, A. and Plückthun, A. 2001. Stability engineering of antibody single-chain Fv fragments. *Journal of Molecular Biology*. **305**(5), pp.989-1010.
- Wulff, G. 2002. Enzyme-like catalysis by molecularly imprinted polymers. *Chemical Reviews*. **102**(1), pp.1-28.
- Yamamoto, N., Nagasawa, Y., Shuto, S., Tsubomura, H., Sawai, M. and Okumura, H. 1980. Antigen-antibody reaction investigated with use of a chemically modified electrode. *Clinical Chemistry*. **26**(11), pp.1569-1572.
- Yang, K. and Zhang, C. Y. 2010. Improved sensitivity for the electrochemical biosensor with an adjunct probe. *Analytical Chemistry*. **82**(22), pp.9500-5.

- Yao, C., Zhu, T., Qi, Y., Zhao, Y., Xia, H. and Fu, W. 2010. Development of a quartz crystal microbalance biosensor with aptamers as bio-recognition element. *Sensors*. **10**(6), pp.5859-5871.
- Yao, T. and Rechnitz, G. A. 1987. Potentiometric biosensor for riboflavin based on the use of aporiboflavin-binding protein. *Analytical Chemistry*. **59**(17), pp.2115-2118.
- Yau, W. Y., Shih, H. C., Tsai, M. H., Sheu, J. C., Chen, C. H. and Chow, L. P. 2013. Autoantibody recognition of an N-terminal epitope of hnRNP L marks the risk for developing HBV-related hepatocellular carcinoma. *Journal of Proteomics*. **94**, pp.346-358.
- Zaccari, I., Catchpole, B. G., Laurenson, S. X., Davies, A. G. and Wälti, C. 2014. Improving the dielectric properties of ethylene-glycol alkanethiol self-assembled monolayers. *Langmuir*. **30**(5), pp.1321-1326.
- Zasadzinski, J. A., Viswanathan, R., Madsen, L., Garnaes, J. and Schwartz, D .K. 1994. Langmuir-Blodgett films. *Science-AAAS-Weekly Paper Edition-including Guide to Scientific Information*. **263**(5154), pp.1726-1738.
- Zhang, H., Ye, L. and Mosbach, K. 2006. Non-covalent molecular imprinting with emphasis on its application in separation and drug development. *Journal of Molecular Recognition*. **19**(4), pp.248-59.
- Zhang, X. Y., Zhou, L. Y., Luo, H. Q. and Li, N. B. 2013. A sensitive and label-free impedimetric biosensor based on an adjunct probe. *Analytica Chimica Acta*. **776**, pp.11-16.
- Zolk, M., Eisert, F., Pipper, J., Herrwerth, S., Eck, W., Buck, M. and Grunze, M. 2000. Solvation of oligo(ethylene glycol)-terminated self-assembled monolayers studied by vibrational sum frequency spectroscopy. *Langmuir*. **16**(14), pp.5849-5852.
- Zoski, C. G. ed. 2007. *Handbook of electrochemistry*. Amsterdam: Elsevier.

## Appendix

Component	g/L	% (w/v)
NaCl	10	1.0
Yeast extract	5	0.5
Bactotryptose (tryptone)	10	1.0

**Table 1. Composition of Luria-Burtani broth.**

The components were dissolved in  $\frac{3}{4}$  volume of deionised water and the pH was adjusted to 7.2 with 1 M sodium hydroxide (NaOH) solution. The final volume was made up using dd water. The media was autoclaved at 121 °C, 15 psi for 20 min to sterilise and stored at room temperature.

Component	g/L	Molarity (M)
NH <sub>4</sub> Cl	53.5g	1
Na <sub>2</sub> SO <sub>4</sub>	33.3g	0.5
KH <sub>2</sub> PO <sub>4</sub>	68.0g	0.5
Na <sub>2</sub> HPO <sub>4</sub>	471.0g	0.5

**Table 2. The composition of 20 X NPSC.**

The components were dissolved in  $\frac{3}{4}$  volume of deionised water and the pH was adjusted to 6.75 with 1 M sodium hydroxide (NaOH) solution. The final volume was made up using dd water. The media was autoclaved at 121 °C, 15 psi for 20 min to sterilise and stored at room temperature.

Component	g/L	Molarity (mM)
FeSO <sub>4</sub> .7H <sub>2</sub> O	1.001	3.6
ZnSO <sub>4</sub> .7H <sub>2</sub> O	8.626	30
CuSO <sub>4</sub> .5H <sub>2</sub> O	0.375	1.5
MnSO <sub>4</sub> .4H <sub>2</sub> O	0.118	0.7
Na <sub>2</sub> B <sub>4</sub> O <sub>7</sub> .10H <sub>2</sub> O	0.114	0.3
(NH <sub>4</sub> ) <sub>6</sub> MO <sub>7</sub> O <sub>24</sub> .4H <sub>2</sub> O	0.049	0.04

**Table 3. The composition of trace elements.**

Salts were added to 240 mL deionised water. 0.2 mL concentrated HCl was directly added on to the salt crystals to dissolve them. The volume was made up to 1 L using deionised water and the solution was filter sterilised through 0.22 µm filter.

Component	Volume (mL)
ZY component	930
1 M MgSO <sub>4</sub>	2
40 % glucose	20
20X NPSC	50
Trace elements	1
Total	1000

**Table 4. The composition ZYP-0.8G Media.**

Antibiotics	Concentration (mg/mL)	Storage	Working Concentration (µg/mL)
Carbenicilin	50	-20°C	50
Kanamycin	50	-20°C	50
Chloramphenicol	25	-20°C	50

**Table 5. Bacterial antibiotic selection.**

Component	
TRIS base	242 g
Glacial Acetic acid	57.1 mL
0.5 M EDTA	100 mL

**Table 6. Composition of TAE (50 X) stock solution.**

The components were dissolved in deionised water. The volume was made up to 1 L and the pH was ~8.1.

Component	g/100 mL (in deionised water)
0.15 % (w/v) Orange G	0.15
60 mM EDTA	2.23
Glycerol	60 % (w/v)
10 mM TRIS-HCl (pH 7.5)	0.12
0.02 % (w/v) SDS	0.02

**Table 7. Composition of 10 X gel loading buffer.**

Component	Volume ( $\mu$ l)
Buffer 4	2
1/10 BSA	2
Restriction enzyme 1	0.5
Restriction enzyme 2	0.5
DNA (Plasmid)	5
Sterile deionised water to final volume	40

**Table 8. Restriction enzyme double digestion mixture.**

The digestion mixture was incubated at 37 °C for 1 hr.

Component	Volume ( $\mu$ l)	Final concentration
10X buffer for KOD	5	1 X
25mM MgSO <sub>4</sub>	3	1.5 mM
dNTPs	5	0.2 mM
Template DNA	5	<250 ng
5' primer	1.5	0.3 $\mu$ M
3' primer	1.5	0.3 $\mu$ M
KOD Hot Start DNA Polymerase	1	0.02 U/ $\mu$ l
PCR grade water to final volume	50	

**Table 9. The KOD Hot Polymerase mix for PCR reaction.**

Component	Volume ( $\mu$ l)	Concentration
5 X Phusion buffer	10	1 X
10 mM dNTPs	1	200 $\mu$ M
Template DNA	0.5	<250 ng
5' primer (10 $\mu$ M)	2.5	0.5 $\mu$ M
3' primer (10 $\mu$ M)	2.5	0.5 $\mu$ M
DMSO	1.5	3 %
Phusion DNA polymerase	0.5	1 u/50 $\mu$ l
PCR grade water to final volume	50	

**Table 10. Composition of Phusion DNA polymerase mix.**

Step	Time	Temperature (°C)
Activation	2 min	95
Denature	30 sec	95
Annealing	30 sec	55
Extension	1 min/kb	72
Final extension	5 min	72
Hold	-	4

**Table 11. PCR amplification cycle using MJResearch Thermal Cycler.**

	Vector + Insert (µl) Experimental ligation	Vector alone (µl) Background ligation
10 X Ligase buffer	4	4
Insert	6	-
Vector	4	4
Ligase enzymes (1 U/µL)	1	1
Deionised water to final volume	20	20

**Table 12. Composition of ligation mixture using T7 DNA ligase.**

	Temperature	Time (min)
<i>Nde</i> I	65 °C	20
<i>Nhe</i> I-HF	80 °C	20
<i>Not</i> I-HF	65 °C	20
<i>Bam</i> HI-HF	-	-

**Table 13. Heat deactivation temperature for restriction enzymes.**

	Volume ( $\mu$ l)
PCR blunt vector	0.5
T4 DNA Ligase buffer	1
PCR product	5
Deionised water to final volume	10

**Table 14. The Zero blunt PCR cloning mixture.**

Component	Volume ( $\mu$ l)	Final concentration
5 X Green GoTaq Buffer	10	1 X
25mM MgCl <sub>2</sub>	10	1.5 mM
dNTPs	1	0.2 mM
Template DNA	5	<250 ng
5' primer (10 $\mu$ M)	1.5	0.3 $\mu$ M
3' primer (10 $\mu$ M)	1.5	0.3 $\mu$ M
GoTaq DNA Polymerase	0.25	1.25 u/50 $\mu$ l
PCR grade water to final volume	50	

**Table 15. Composition of GoTaq Green master mix for PCR.**

Step	Time	Temperature ( $^{\circ}$ C)
Activation	2 min	95
Denature	30 sec	95
Annealing	30 sec	55
Extension	1 min/kb	72
Final extension	5 min	72
Hold	-	4

**Table 16. Thermocycling conditions for PCR using GoTaq Green master mix.**

Component	
Sucrose	25 % (w/v)
MgCl <sub>2</sub>	5 mM
Triton X100	1% (v/v)
HEPES	50 mM

**Table 17. Composition of lysis buffer.**

The pH of the lysis buffer was adjusted to 8.0 with 5 M NaOH and filter sterilised through 0.2 µm filter. A 10 mg/ml stock of lysozyme was prepared, aliquoted and stored at -20 °C. 10 U/L of omnicleave endonuclease (Epicenter) and 0.1 mg/ml lysozyme were added to the lysis buffer just before use.

	g/L	Molarity (mM)
HEPES (pH 7.5)	11.92	50
NaCl	11.6	200
Imidazole	340.4	5

**Table 18. Composition of binding buffer.**

	g/L	Molarity (mM)
HEPES (pH 7.5)	11.92	50
NaCl	11.6	200
Imidazole	2.7	40

**Table 19. Composition of wash buffer.**

	g/L	Molarity (mM)
HEPES (pH 7.5)	11.92	50
NaCl	11.6	200
Imidazole	34.04	500

**Table 20. Composition of elution buffer.**

	g/l	Molarity (mM)
HEPES (pH 7.5)	11.92	50
NaCl	29.2	500
EDTA	18.6	50

**Table 21. Composition of stripping buffer.**

Component	Concentration (mM)
NaCl	136.8
KCl	2.7
Na <sub>2</sub> HPO <sub>4</sub>	10.1
KH <sub>2</sub> PO <sub>4</sub>	1.7

**Table 22. Composition of 1 X PBS (phosphate buffer saline).**

	Volume (mL)	Final concentration
20% SDS	2	2 %
1M Tris-HCl (pH7)	1	50 mM
Glycerol	1	5 %
Mercaptoethanol	1	5 %

**Table 23. Composition of 4 X Sample buffer used for loading proteins.**

Few grains of bromophenol blue were added to the prepared buffer. Before use, 1/3 sample volume of mercaptoethanol was added to each and boiled for 2 min.

	TRIS	SDS (0.4%)	pH
Gel buffer (GB) 100 ml	18.5 g (1.5 M)	0.4 g	8.9
Stacking gel buffer (SGB) 100 ml	5.1 g (0.4 M)	0.4 g	6.7

**Table 24. Composition of gel buffer and stacking gel.**

	Separating gel Volume (mL)	Stacking gel Volume (mL)
GB	1.2	-
SGB	-	0.6
30 % Acrylamide stock	2.6	0.4
H <sub>2</sub> O	1.2	1.4
APS (25 % w/v)	0.03	0.02
TEMED	0.003	0.002
Total	5	2.4

**Table 25. Gel composition used for polyacrylamide gel electrophoresis.**

	g/L	Final concentration
Tris	30	0.25 M
Glycine	144	1.91 M
SDS	10	1 %

**Table 26. Composition of 10 X running buffer.**

The pH was adjusted to 8.3 and the solution was stored at 4 °C.

Component	Volume (mL)	Final concentration (%)
Isopropanol	250	25
Acetic acid	100	10
Deionised water to final volume	1000	

**Table 27. Composition of Coomassie blue staining solution.**

2.5 g (0.25 %) Coomassie blue 250 was added to the above prepared solution and stirred on a stir plate.

Component	Volume (mL)	Final Concentration (%)
Ethanol	250	25
Acetic acid	75	7.5
Deionised water to final volume	1000	

**Table 28. Composition of Destaining solution.**

Component	g/ 100mL	Final concentration (M)
Tris	0.6	0.05
NaCl	1.75	0.3
GuHCl	76.43	8

**Table 29. Composition of Dot Blot Solubilisation buffer.**

The solutions were prepared in deionised water. The pH was adjusted to 8.0 with 5 M HCl. The solution was filter sterilised through 0.2  $\mu$ m filter and stored at room temperature.

Component	Concentration
Tris	0.1 M
Glycine	0.192 M
Methanol	20 % (w/v)

**Table 30. Composition of 1 X Transfer buffer.**

	Number of amino acids	Molecular weight (kDa)	Theoretical Isoelectric point (pI)	Extinction Coefficient ( $M^{-1}cm^{-1}$ )
Adhiron	107	12.109	6.75	1.278
Adhiron myc binder 1	122	13.8	5.77	0.720
Adhiron myc binder 2	122	14.08	6.25	1.098
Adhiron myc binder 4	122	14.05	6.25	0.709
Adhiron myc binder 5	122	13.9	7.21	1.502
Adhiron myc binder 7	122	14.07	6.49	0.920
Adhiron myc binder 11	122	14.02	6.54	1.220
Adhiron myc binder 13	122	14.2	6.8	1.193
Adhiron myc binder 17	122	14.02	6.87	0.817
Adhiron myc binder 18	122	14.2	6.75	1.293
Adhiron myc binder 20	122	14.2	6.58	1.342

**Table 31. Theoretical molecular weights of the Adhiron myc binders. (The values were obtained using online ExPaSy ProtParam tool).**

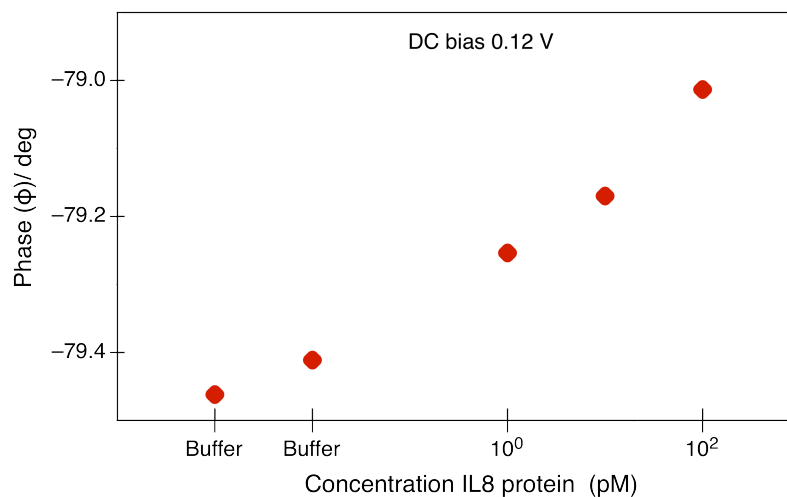


**Figure 1. Response of IL8 biosensor to IL8 protein on a surface subjected to 0.12 V.**

Shows the phase response of SAM derivatised gold surface immobilised with 10  $\mu\text{g/mL}$  Adhiron IL8 binder against different concentrations of IL8 protein. The measurements were done after incubating the surface in different concentration of IL8 protein (10-100 pM). The DC bias applied against reference Ag/AgCl was 0.12 V.